EXAMINING ISSUES IN PERCUTANEOUS TRANSPORT USING MATHEMATICAL MODELS

by

Micaela B. Reddy

ProQuest LLC.
789 East Eisenhower Parkway
P.O. Box 1346
Ann Arbor, MI 48106 – 1346

A thesis submitted to the Faculty of and the Board of Trustees of the Colorado School of Mines in partial fulfillment of the requirements for the degree of Doctor of Philosophy (Chemical and Petroleum-Refining Engineering).

Golden, Colorado

Date 6/2/2000

Signed: Micaela B Reddy

Micaela B. Reddy

Approved: Annette L Bunge

Dr. Annette L. Bunge
Thesis Advisor

Golden, Colorado

Date 5/30/00

Dr. Robert Baldwin
Professor and Head,
Department of Chemical
and Petroleum-Refining
Engineering

ABSTRACT

The outermost layer of skin, the stratum corneum (sc), is the primary barrier for mass transport of chemicals into the body. For highly lipophilic chemicals, the second skin layer, the viable epidermis (ve), can also contribute a significant resistance. In this thesis, mathematical models describing dermal absorption through one or two pseudo-homogenous membranes in series (i.e., representing the sc or both the sc and ve) were used to examine important issues of current debate in the dermal absorption literature.

In Chapter 2, four one-compartment models and a one-layer membrane model are combined with a one-compartment systemic pharmacokinetic (PK) model to clarify how differences between models affect the predicted systemic response. Because the models have different underlying assumptions, they do predict different results such as blood concentrations and percent of dose absorbed. Although the compartment models were derived by assuming that vehicle and blood concentrations are constant, for many exposure situations compartment models give acceptable results with most pronounced differences from the membrane model during short exposure times relative to the lag time for chemical to cross the sc, $t_{lag,sc}$.

In Chapter 3, a one-layer membrane model is used to study a potential problem with the tape strip (TS) experiment (i.e., that chemical in the sc when the exposure ends continues to diffuse during the time that it takes to apply and remove all of the TS's, t_{TS}). Experiments and mathematical models were used to assess the conditions where diffusion alters TS results. Calculations show that the chemical concentrations in TS's can differ significantly from that which existed when the tape stripping started, but if $t_{TS} < 0.2\ t_{lag,sc}$ and the exposure time, t_{exp}, is $> 0.3\ t_{lag,sc}$, TS experimental results are not significantly affected by t_{TS}. In Chapter 4, human, *in vivo* TS data of 4CP in a soil vehicle with $t_{TS} >$

0.2 $t_{lag,sc}$ were analyzed. Estimates of $t_{lag,sc}$ calculated with a mathematical model that did not include the effect of t_{TS} were 3-10 times higher than values from the literature, but data analysis including the effect of t_{TS} produced reasonable parameter estimates.

After its removal from the skin surface, chemical remaining within the skin can become systemically available. Growth of skin (i.e., epidermal turnover) and the subsequent sloughing of the outer layer (i.e., desquamation) can reduce percutaneous penetration. The fate of chemical within the skin following a dermal exposure was examined in Chapter 5 using a mathematical model representing turnover of and absorption into the sc and ve, including the effects of t_{exp} and penetrant lipophilicity. Except for highly lipophilic or large molecular weight chemicals, most of the chemical in the skin at the end of an exposure will enter the body regardless of t_{exp}.

Chapter 6 shows the analysis of *in vivo* dermal absorption data for 18 pesticides in the rat. Data included the moles of pesticide in the skin, m_{skin}, and absorbed systemically, m_{abs}, for six t_{exp} and three applied doses (AD's). Typically, m_{skin} reached a maximum in less than 4 hours, while m_{abs} increased with time up to 24 hours. For liquid pesticides, both m_{skin} and m_{abs} increased proportionally with AD. For solid pesticides, m_{skin} increased with AD, but m_{abs} was relatively independent of AD. For many of the studies, AD's were too small to completely cover the exposed area. Effects of spatial distribution on dermal absorption were studied theoretically in Chapter 7. A two-dimensional, steady-state, two-layer skin model was used to calculate the amount of chemical in the epi, M_{epi}^{ss}, and average flux through the epi, J^{ss}, from uniformly spaced, rectangular piles of chemical. For a constant AD, M_{epi}^{ss} and J^{ss} are larger from many small piles than a few large piles and can exhibit maximum values even when the skin surface is only partly covered. Consistent with results of the pesticide data analysis, J^{ss} can reach a maximum at smaller AD's than M_{epi}^{ss}.

TABLE OF CONTENTS

LIST OF FIGURES

LIST OF TABLES

ACKNOWLEDGEMENTS

This work was supported by the U. S. Environmental Protection Agency (Assistance Agreement Nos. CR822757 and CR824053), the U. S. Air Force Office of Scientific Research (F49620-95-1-021) and the National Institute of Environmental Health Sciences (ES06825).

I would like to thank my research advisor Dr. Annette Bunge. Her work ethic, intellect, dedication, presence, and support were an inspiration. My research committee, consisting of L. Figueroa, D. Macalady, S. Selim, D. Way, and V. Yesavage, has my gratitude. I would like also like to thank the members my research group including D. Macalady, K. McCarley, B. Vecchia, L. Choate, J. Ranville, S. Arnold, L. Sun and C.-P. Chen. The Department of Chemical Engineering provided a wonderful atmosphere for women in engineering. S. Selim's classes in transport phenomena captured my imagination and made mathematics fun. R. Zendzian, R. Guy, A. Stinchcomb, and G. Touraille provided discussion and experimental data. Their generous contribution is greatly appreciated.

M. Reddy and C. Reddy, for their unflagging encouragement and strength, H. Reddy, for her willingness to listen when I encountered a setback, and A. Reddy, J. Wiltshire and M. Wiltshire for their support and encouragement have my heartfelt thanks.

Chapter 1. DERMAL ABSORPTION AND MATHEMATICAL MODELS

Skin acts as a barrier between the body and the environment, preventing water loss and infection. However, the skin is an inferior barrier to many organic chemicals including pesticides and industrial solvents. Mechanistically sound mathematical models of dermal absorption, the process of chemical transferring across the skin, are critical in the areas of drug delivery and risk assessment, to name only a few. Transdermal drug delivery has many advantages over more traditional methods (e.g., oral administration), including the bypass of hepatic first-pass metabolism, controlled administration of drugs with a narrow therapeutic window for blood concentrations, and increased patient compliance (Moore and Chien, 1988). Improved understanding of the dermal absorption process could increase the viability of this advantageous drug delivery method. Of the three exposure routes included in risk assessment (i.e., inhalation, oral and dermal exposures) dermal absorption has been afforded the least attention, and has recently been called the "missing link" of risk assessment (Zartarian and Leckie, 1998). Percutaneous penetration contributes significantly to risk in situations such as household exposures to contaminated potable water (Brown *et al.*, 1984) and to indoor applications of pesticide (Fenske *et al.*, 1990). Clearly, society benefits from improved understanding of the dermal absorption process.

The goal of dermal absorption research at CSM is to develop methods for predicting the rate and extent of dermal absorption for a variety of exposure conditions. Mathematical models for predicting the amount absorbed under certain conditions have been developed, but so far these are only useful for simple situations such as exposures to aqueous solutions. Predicting percutaneous penetration for many realistic conditions

presents difficulties. An understanding of the physiology of skin allows for the development of more complicated of mathematical models.

Physiologically, skin is a multi-layered membrane (Kligman, 1964). For many chemicals, the outermost skin layer, the stratum corneum (sc), is the rate-limiting barrier for mass transfer into and through skin. For highly lipophilic chemicals, the second skin layer, the viable epidermis (ve), also contributes a significant resistance to percutaneous penetration. The sc is composed of dead, desiccated, keratinized cells, but the cells of the ve are alive and capable of metabolizing some chemicals. Together, the sc and ve form the epidermis (epi). The dermis, located beneath the epi, is a highly vascularized tissue that usually has sufficient blood flow to clear away all chemical passing through the epi (Scheuplein and Bronaugh, 1983).

Chemical on the skin surface, often present in a solution called a vehicle, can partition into and passively diffuse through skin. Both the vehicle and the absorbing chemical can interact with skin and alter its physiochemical properties. Often, dermal absorption of chemical is represented mathematically as passive diffusion through one or more membranes in series (Scheuplein, 1978; EPA, 1992; Cleek and Bunge, 1993). For describing dermal absorption of chemicals with a range of lipophilic properties, the sc and ve are included as separate membranes with distinct properties. The differential mass balance equations describing one-dimensional chemical transport by passive diffusion within the sc and ve are:

$$\frac{\partial C_{sc}}{\partial t} = D_{sc}\frac{\partial^2 C_{sc}}{\partial x^2} \qquad \text{for } 0 < x < L_{sc} \qquad (1\text{-}1)$$

$$\frac{\partial C_{ve}}{\partial t} = D_{ve}\frac{\partial^2 C_{ve}}{\partial x^2} \qquad \text{for } L_{sc} < x < L_{sc}+L_{ve} \qquad (1\text{-}2)$$

where x is the distance in the epi from the skin surface and t is time. In eqs 1-1 and 1-2, with j designating either the sc or ve, C_j is the concentration in membrane layer j and D_j is the effective diffusion coefficient of the absorbing chemical through layer j of apparent

thickness L_j. One-dimensional models of skin are reasonable when the dimensions of the area covered by the vehicle on the skin surface are larger than L_{sc}. Eqs 1-1 and 1-2 are written assuming that the properties of the skin are not a function of position (i.e., the sc and ve are pseudo-homogenous) or time (i.e., the absorbing chemical and vehicle do not alter skin properties) and that metabolism does not occur in the ve. For hydrophilic and moderately lipophilic chemicals, the ve does not provide a significant resistance to dermal absorption and a one-layer membrane model (i.e., eq 1-1 alone) is adequate. To estimate the concentration of a chemical in the blood or at a target organ resulting from a dermal exposure, a model for skin must be combined with a systemic pharmacokinetic (PK) model, which describes chemical distribution in the body.

Recently many scientists have used compartment models of the skin, in which skin is mathematically represented as a well-stirred tank, for estimating health risks (Rao and Brown, 1993) or for calculating dermal absorption parameters from experimental data (Shatkin and Brown, 1991; Chinery and Gleason, 1993). Physiologically skin is a membrane, and a well-stirred tank is not the most mechanistically accurate choice for a model. However, compartment models have the advantages of mathematical simplicity and compatibility with many PK models of the body. Chapter 2 examines four one-compartment models from the literature and a one-layer membrane model (i.e., all models were developed by assuming the sc controls the rate of dermal absorption). The four compartment models, developed assuming constant vehicle and blood concentrations, and the membrane model were combined with a vehicle model and a one-compartment PK model of the body. Compartment model results were compared with membrane model results to test if compartment models can provide good estimates of dermal absorption when vehicle and blood concentrations change in time and to determine if a compartment model combined with a PK model can reasonably predict systemic response. Also, differences between compartment models were analyzed.

In contrast to Chapter 2, which critically examines a popular type of dermal absorption model, Chapter 3 evaluates a common experimental technique. Tape stripping of the sc has been proposed as a fast and relatively noninvasive technique for measuring the rate and extent of dermal absorption (Dick *et al.*, 1997; Schwarb *et al.*, 1999; Stinchcomb *et al.*, 1999) and for estimating dermal absorption parameters *in vivo* (Tojo and Lee, 1989; Pirot *et al.*, 1997). A potential problem with the tape strip (TS) experiment is that chemical in the sc when the exposure ends will continue to diffuse during the time that it takes to apply and remove all of the TS's. Unless the TS procedure is fast, the concentration measured in each TS will be different than the concentration at that location in the sc when the chemical exposure ended. To mathematically model the tape stripping procedure, skin can be represented as a one-layer membrane that gets thinner with time as TS's are removed. In Chapter 3, experiments and mathematical models have been used to assess the conditions under which diffusion might affect TS results and the magnitude of this effect when it occurs.

The TS experiment is also the focus of Chapter 4. Tourailles (1998) performed a TS experiment studying *in vivo* dermal absorption of 4-cyanophenol from a soil vehicle in humans. The time to tape strip the sc was long relative to the lag time of 4CP through the sc, and it is likely that the data were affected by diffusion during the TS procedure. For meaningful dermal absorption parameter estimation from this data, a one-layer membrane model was developed which accounted for both diffusion during stripping and, as an additional complication, the resistance provided by the soil vehicle. The model incorporating these effects was used to interpret the data and estimate meaningful dermal absorption parameters for 4CP absorbing from a soil vehicle. The data were also analyzed using a model that did not include the diffusion during the TS procedure, and the results of the two data analysis methods were compared.

In Chapter 5, mathematical modeling is used to address another unusual issue in percutaneous penetration. Skin is continuously replaced through epidermal turnover, the

process by which new cells are generated at the base of the epidermis while the outermost surface flakes off (i.e., desquamates) at the same rate. The complete regeneration of the sc and the ve takes about 14 and 31 days, respectively (Bergstresser and Taylor, 1977). During an exposure, the skin acts as a reservoir for chemical, and so after an exposure ends chemical in the skin continues to absorb into the bloodstream. For brief chemical exposures, much of the systemic absorption can occur after the chemical has been removed from the skin surface. It has been suggested that epidermal turnover and desquamation could result in decreased systemic absorption because chemical trapped in desquamating cells could flake off before the chemical is systemically absorbed (Schaefer *et al.*, 1982). For highly lipophilic chemicals (e.g., many pesticides), which can build up in high concentrations in the sc, the effect of desquamation could be particularly important. Thus, a two-layer membrane model accounting for the resistances of both the sc and ve and including the effect of epidermal turnover was developed to examine the efficacy of desquamation as a mechanism for eliminating chemical from the skin.

Chapter 6 focuses on understanding the dermal absorption of pesticides, which is crucial for estimating the potential health risks associated with their use. In its role as regulator for pesticide use, the U. S. EPA is the repository of a large collection of studies on *in vivo* dermal absorption of pesticides in the rat. The database contains more than 263 dermal absorption studies of more than 160 different pesticides. Many of the studies used a uniform experimental procedure commonly called the Zendzian Protocol, which was formalized in 1994 (Zendzian, 1994). Chapter 6 presents dermal absorption measurements for 18 pesticides from the EPA collection. Most of the studies include data for six exposure times (i.e., 0.5, 1, 2, 4, 10 and 24 hours) and three doses (i.e., the high dose is typically the concentrated pesticide solution and lower doses are 10-fold dilutions). Many of the applied doses of pesticides in these studies, which ranged from about 0.0001 to 10 mg /cm^2, were too small to completely cover the skin. For this situation, dermal absorption is not well understood. The effects of exposure time and

applied dose on dermal absorption, as measured by the amount of chemical in the skin and systemically absorbed, were studied. Although the emphasis of Chapter 6 is data interpretation instead of mathematical modeling, it is the companion to Chapter 7, which involves mathematical modeling of dermal absorption when the applied dose is small.

Chapter 7 presents a mathematical model representing skin as a two-layer membrane for the situation where the skin is not completely covered by chemical (i.e., a two-dimensional model is used). The chemical on the skin surface was modeled as regularly spaced, rectangular piles of constant size. To offset the increased complexity caused by the two-dimensional treatment of skin, a steady-state solution was developed. The effects of the distribution of chemical on the skin surface and increasing the applied dose on steady-state dermal absorption (i.e., on the amount of chemical in the skin and the flux through the skin) were examined.

In the following chapters, applications of mathematical modeling in percutaneous penetration research have been illustrated by studying six important issues of recent debate in the dermal absorption research community. Mathematical models were used to test simpler models, study experimental protocols, interpret data, and examine the mechanism of dermal absorption. The following chapters present increasingly complex mathematical models which all represent dermal absorption as passive diffusion through a membrane. For example, Chapters 2 through 4 represent skin as a one-layer membrane, while Chapters 5 through 7 present skin as a two-layer membrane. This thesis contributes to the state of dermal absorption research both by answering key questions of current debate in the literature and by developing more complicated dermal absorption models than are currently available.

Notation

C_j	concentration of the absorbing chemical in membrane layer j as a function of both position and time
D_j	effective diffusion coefficient of the absorbing chemical in membrane layer j
epi	epidermis
j	variable denoting sc or ve
L_j	apparent thickness of membrane layer j
sc	stratum corneum
t	time
ve	viable epidermis
x	coordinate of position in the epi

References

Bergstresser, P. R. and J. R. Taylor (1977). "Epidermal 'turnover time' - a new examiniation." British Journal of Dermatology **96**:503-509.

Brown, H. S., D. R. Bishop and C. R. Rowan (1984). "The role of skin absorption as a route of exposure for volatile organic compounds (VOCs) in drinking water." American Journal of Public Health **74**:479-484.

Chinery, R. L. and K. A. Gleason (1993). "A compartment model for the prediction of breath concentration and absorbed dose of chloroform after exposure while showering." Risk Analysis: An Official Publication of the Society for Risk Analysis **13**:51-62.

Cleek, R. L. and A. L. Bunge (1993). "A new method for estimating dermal absorption from chemical exposure. 1. General approach." Pharmaceutical Research **10**:497-506.

Dick, I. P., P. G. Blain and F. M. Williams (1997). "The percutaneous absorption and skin distribution of lindane in man. I. *In vivo* studies." Human and Experimental Toxicology **16**:645-651.

EPA, U. S. (1992). Dermal Exposure Assessment: Principles and Applications, EPA/600/8-91/011B. Exposure Assessment Group, Office of Health and Environmental Assessment, Washington.

Fenske, R. A., K. G. Black, K. P. Elkner, C. Lee, M. M. Methner and R. Soto (1990). "Potential exposure and health risks of infants following indoor residential pesticide applications." American Journal of Public Health **80**:689-693.

Kligman, A. M. (1964). The biology of the stratum corneum. The Epidermis. W. Montagna and W. C. Lobitz, eds. New York, Academic.

Moore, L. and Y. W. Chien (1988). "Transdermal drug delivery: a review of pharmaceutics, pharmacokinetics, and pharmacodynamics." Critical Reviews in Therapeutic Drug Carrier Systems **4**:285-349.

Pirot, F., Y. N. Kalia, A. L. Stinchcomb, G. Keating, A. L. Bunge and R. H. Guy (1997). "Characterization of the permeability barrier of human skin *in vivo*." Proceedings of the National Academy of Sciences of the United States of America **94**:1562-1567.

Rao, H. V. and D. R. Brown (1993). "A physiologically based pharmacokinetic assessment of tetrachloroethylene in groundwater for a bathing and showering

determination." Risk Analysis: An Official Publication of the Society for Risk Analysis **13**:37-49.

Schaefer, H., A. Zesch and G. Stuttgen (1982). Skin Permeability. Berlin, Springer-Verlag.

Scheuplein, R. J. (1978). "Permeability of the skin: a reveiw of major concepts." Current Problems in Dermatology **7**:172-186.

Scheuplein, R. J. and R. L. Bronaugh (1983). Percutaneous absorption. Biochemistry and Physiology of the Skin. L. A. Goldsmith, ed. New York, Oxford University Press.

Schwarb, F. P., B. Gabard, T. Rufli and C. Surber (1999). "Percutaneous absorption of salicylic acid in man after topical administration of three different formulations." Dermatology **198**:44-51.

Shatkin, J. and H. S. Brown (1991). "Pharmacokinetics of the dermal route of exposure to volatile organic chemicals in water: a computer simulation model." Environmental Research **56**:90-108.

Stinchcomb, A. L., F. Pirot, G. D. Touraille, A. L. Bunge and R. H. Guy (1999). "Chemical uptake into human stratum corneum *in vivo* from volatile and non-volatile solvents." Pharmaceutical Research **16**:1288-1293.

Tojo, K. and AE-RI C. Lee (1989). "A method for predicting steady-state rate of skin penetration in vivo." Journal of Investigative Dermatology **92**:105-108.

Tourailles, G. D. (1998). Unpublished data, Personal communication.

Zartarian, V. G. and J. O. Leckie (1998). "Dermal exposure: the missing link." Environmental Science and Technology **32**:134-137.

Zendzian, R. P. (1994). Pesticide Assessment Guidelines. Subdivision F, Hazard Evaluation, Human and Domestic Animals: Dermal Absorption of Pesticides, Office of Pesticide Programs, US Environmental Protection Agency, Washington, DC.

Chapter 2. COMPARISON OF PHYSIOLOGICALLY RELEVANT ONE-COMPARTMENT MODELS FOR SKIN COMBINED WITH A SYSTEMIC PHARMACOKINETIC MODEL

Introduction

Estimating systemic distribution and kinetics of dermally absorbed chemicals is of interest for drug delivery and for assessing human health risk from occupational and environmental exposures to toxic chemicals. To estimate the concentration of a chemical in the blood or at a target organ from a dermal exposure, a model for skin must be combined with a systemic pharmacokinetic (PK) model. If the drug concentration in the solution in contact with the skin (i.e., the vehicle) changes as a result of dermal absorption or other processes (such as evaporation of the drug or the vehicle), a vehicle model is also required.

Physiologically, skin is a multi-layered membrane (Kligman, 1964). The top layer, called the stratum corneum (sc), is more permeable to lipophilic compounds than hydrophilic compounds because it is mainly composed of lipids. Beneath the sc is the viable epidermis (ve), which is composed of living cells with lipids in the cell membranes and has a higher water content than the sc. Accordingly, the ve is more hydrophilic and has a higher diffusivity than the sc. The dermis, found directly beneath the ve, contains a dense capillary network that transports chemical from the region of absorption to the rest of the body. Except for chemicals that are extremely lipophilic, the sc is often the rate-limiting barrier to transport of chemicals through the skin.

Many different mathematical models of skin exist, representing skin as a series of either membranes or well-stirred compartments. In physiologically relevant models,

input parameters are defined in terms of measurable properties of the skin. For one-membrane or one-compartment models, which assume the sc is the major barrier for chemical absorption into the body, input parameters include the permeability coefficient of chemical transport across the sc from a vehicle v ($P_{sc,v}$, cm/hr), the equilibrium partition coefficients between the sc and the vehicle ($K_{sc/v}$) and the sc and the blood ($K_{sc/b}$), the apparent sc thickness (L_{sc}, μm), and the specific cutaneous blood flow rate (q_b, $cm^3 / s / cm^2$).

Many investigators have used a membrane model to estimate dermal absorption and skin properties (e.g., Bunge et al. (1995), US EPA (1992), and Silcox et al. (1990) to name only a few). Membrane models of skin are physiologically more representative than compartment models because skin is a membrane (Scheuplein and Blank, 1971). However, membrane model solutions for realistic dermal absorption conditions are mathematically cumbersome. When combined with a systemic PK model, membrane models must be solved by numerical simulations which are computer-resource intensive and which require considerable mathematical skill.

Some investigators have used compartment models to estimate dermal absorption (e.g., McKone (1993), Rao and Brown (1993), and Brown and Hattis (1989)) and to analyze *in vivo* experimental data (e.g., Shatkin and Brown (1991) and Chinery and Gleason (1993)). Strictly speaking, compartment models for skin are not representative because skin is not a well-stirred compartment. However, they are easy to use even when the dermal absorption situation becomes complicated, as in repeated exposures or chemical loss from the vehicle by evaporation. Compartment models for skin combine easily with systemic PK models, which usually are also compartment-based models. These can be readily solved with standard computer packages for first-order ordinary differential equations (e.g., STELLA).

Background

Figure 2.1 illustrates a one-compartment model of skin attached to a well-stirred vehicle model and a one-compartment PK model representing the body. Chemical transfer between the sc and vehicle or blood compartments depends on four rate constants (k_1^A, k_{-1}^A, k_2^A, and k_{-2}^A, m^3/s), the concentrations of chemical in the vehicle and systemic blood (C_v, C_b), and the position-averaged concentration of chemical in the sc ($< C_{sc} >$). The superscript A denotes that these rate constants are defined for one-compartment models. The elimination rate constant from the systemic blood compartment, k_{el} (s^{-1}), specifies the rate at which chemicals are cleared from the blood via mechanisms such as biotransformation, exhalation, and excretion (Klaassen *et al.*, 1996). Although there are many possible choices for a systemic PK model, a one-compartment model was chosen for simplicity.

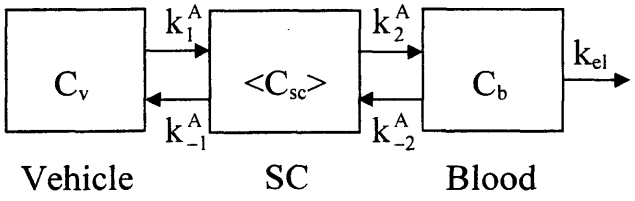

Figure 2.1 – A schematic diagram of the one-compartment model for skin combined with a vehicle model and a one-compartment PK model of the body.

One-compartment models for skin represent the position-averaged concentration of chemical in the sc, $< C_{sc} >$, as a function of time, t:

$$V_{sc}\frac{d < C_{sc} >}{dt} = k_1^A C_v + k_{-2}^A C_b - \left(k_{-1}^A + k_2^A\right) < C_{sc} > \qquad (2\text{-}1)$$

where V_{sc} is the volume of the sc exposed to the chemical, while membrane models represent the concentration in the sc, C_{sc}, as a function of position x and time as described by Fick's law:

$$\frac{\partial C_{sc}}{\partial t} = D_{sc} \frac{\partial^2 C_{sc}}{\partial x^2} \tag{2-2}$$

where D_{sc} is the effective diffusion coefficient of the absorbing chemical crossing the sc of apparent thickness L_{sc}.

Because the compartment model equation, eq 2-1, contains less information than the membrane model equation, eq 2-2, (i.e., the variation of concentration with position in the skin is unknown for compartment models), compartment model predictions can never exactly match membrane model predictions for all cases (McCarley and Bunge, 1997). For example, no compartment model can match the predictions of the membrane model at the limiting conditions of both steady state and equilibrium. As a result, it is possible to develop many different compartment models in which the relationships between the four rate constants and the sc properties are defined to match the membrane model predictions for different limiting cases. McCarley and Bunge (1997) illustrated this procedure by defining 11 different one-compartment models for skin from many more possibilities.

Rate constant expressions are listed in Table 2.1 for four selected compartment models, which were identified as the equilibrium (E), general time lag (G), simplified time lag (S), and traditional (T) models (which correspond respectively to models numbered 1, 4, 2a, and 5 in McCarley and Bunge (1997)). The rate constant expressions in Table 2.1, written assuming that the vehicle does not contribute a significant resistance to mass transfer, are functions of the parameter α_{sc}:

$$\alpha_{sc} = \frac{q_b K_{b/v}}{P_{sc,v}} \tag{2-3}$$

Table 2.1 - Rate constant expressions for four compartment models.[a]

Normalized Rate Constants	Equilibrium Model (E)	General Time Lag Model (G)	Simplified Time Lag Model (S)	Traditional Model (T)
$\hat{k}_1^A = \frac{k_1^A}{P_{sc,v} A}$	2	$\frac{3(2+\alpha_{sc})}{(3+\alpha_{sc})}$	$\frac{3(2+\alpha_{sc})}{(3+\alpha_{sc})}$	1
$\hat{k}_{-1}^A = \frac{k_{-1}^A K_{sc/v}}{P_{sc,v} A}$	2	$\frac{2\alpha_{sc}(3+\alpha_{sc})K_{sc/b}C_b + 4(3+3\alpha_{sc}+\alpha_{sc}^2)K_{sc/v}C_v}{(3+\alpha_{sc})(\alpha_{sc}K_{sc/b}C_b + (2+\alpha_{sc})K_{sc/v}C_v)}$	$\frac{4(3+3\alpha_{sc}+\alpha_{sc}^2)}{(2+\alpha_{sc})(3+\alpha_{sc})}$	1
$\hat{k}_2^A = \frac{k_2^A K_{sc/v}}{P_{sc,v} A}$	$\frac{2\alpha_{sc}}{(2+\alpha_{sc})}$	$\frac{2\alpha_{sc}(2\alpha_{sc}K_{sc/b}C_b + (3+\alpha_{sc})K_{sc/v}C_v)}{(3+\alpha_{sc})(\alpha_{sc}K_{sc/b}C_b + (2+\alpha_{sc})K_{sc/v}C_v)}$	$\frac{2\alpha_{sc}}{(2+\alpha_{sc})}$	α_{sc}
$\hat{k}_{-2}^A = \frac{k_{-2}^A K_{b/v}}{P_{sc,v} A}$	$\frac{2\alpha_{sc}}{(2+\alpha_{sc})}$	$\frac{3\alpha_{sc}}{(3+\alpha_{sc})}$	$\frac{3\alpha_{sc}}{(3+\alpha_{sc})}$	α_{sc}

[a] These equations are based on the assumption that mass transfer resistances in the vehicle are small relative to the penetration rate through the skin (i.e., equations are defined for $\alpha_v \rightarrow \infty$ as shown in Table 3 of McCarley and Bunge (1997)).

which is the ratio of the blood clearance rate ($q_b K_{b/v}$) to the rate of chemical penetration across the sc from a vehicle ($P_{sc,v}$). Here, $K_{b/v}$ is the partition coefficient of the chemical between the blood and the vehicle, and is equal to $K_{sc/v} / K_{sc/b}$ if the sc has not been altered by contact with the vehicle or absorbing chemical. The rate constant expressions for model G include concentrations for the absorbing chemical in the vehicle and blood.

The rate constant expressions listed in Table 2.1 are different for the four models because each model was developed by forcing the compartment model equations to match the membrane model solution in different respects as discussed in detail by McCarley and Bunge (1997). Table 2.2 identifies the conditions of the membrane model that were matched to develop each of the four compartment models. The matching conditions listed in Table 2.2 include the average steady-state sc concentration, the steady-state penetration rate, and the lag time. The lag time (t_{lag}) is the time intercept of the plot of the steady-state cumulative mass systemically absorbed as a function of time. The lag time approximately measures the time required for a chemical to transfer from the vehicle through the skin to enter the blood. These three matching conditions are defined at steady state, which can only occur when vehicle and blood concentrations do not change in time. In addition, the equations representing these conditions are different depending on the direction of the driving force for mass transfer (i.e., $K_{sc/v}C_v - K_{sc/b}C_b$). Consequently, Table 2.2 specifies values for $(K_{sc/v}C_v)/(K_{sc/b}C_b)$. Other conditions that can be matched are local equilibrium between the sc and vehicle and the sc and blood. Model T was developed using a criterion that is only a condition of the membrane model when the rate of chemical clearance to the blood is approximately zero.

To develop each compartment model, four matching conditions are required. For example, model E was developed by matching the membrane model steady-state average sc concentration and penetration rate for all blood and vehicle concentrations, and requiring local equilibrium at both the blood/sc and vehicle/sc interfaces. In this study,

Table 2.2 – Summary of conditions used to develop compartment models.

Matching Condition or Other Criteria	$\frac{K_{sc/v}C_v}{K_{sc/b}C_b}$	Model			
		E	G	S	T
Average steady-state skin concentration	any value	✓	✓		
	small value (<<1)		&[a]	✓	
	large value (>>1)		&[a]	✓	
Steady-state penetration rate	any value	✓	✓		
	small value (<<1)			✓	✓
Lag time	any value		✓		
	small value (<<1)		&[a]	✓	
Local equilibrium between sc and vehicle ($k_1^A/k_{-1}^A = K_{sc/v}$)	NA[b]	✓			✓
Local equilibrium between sc and blood ($k_2^A/k_{-2}^A = 1/K_{sc/b}$)	NA[b]	✓			✓
Skin clearance rate controlled by blood capacity ($k_2^A = \alpha_{sc} P_{sc,v} A/K_{sc/v}$)[c]	NA[b]				✓

[a] The symbol & is used when any one of several different matching conditions will result in the same rate constant expressions. [b] Not applicable. [c] This criterion represents a matching condition with the membrane model only when the rate of chemical clearance to the blood is approximately zero (i.e., $\alpha_{sc} \rightarrow 0$).

we compared the four compartment models listed in Table 2.1 with the membrane model when vehicle and blood concentrations were changing for three major reasons: to test if compartment models can provide good estimates of dermal absorption even when C_v and C_b change in time, to assess differences between models, and to determine if a compartment model combined with a PK model can reasonably predict systemic response.

Methods

Numerical simulations of dermal absorption scenarios were calculated using all five models. For the compartment model calculations, eq 2-1 was combined with equations for the vehicle and blood compartments,

$$V_v \frac{dC_v}{dt} = k_{-1}^A < C_{sc} > -k_1^A C_v \tag{2-4}$$

$$V_{dis} \frac{dC_b}{dt} = k_2^A < C_{sc} > -\left(k_{-2}^A + k_{el} V_{dis}\right) C_b \tag{2-5}$$

where V_v is the volume of the vehicle and V_{dis}, the apparent volume of chemical distribution, is equal to the total mass of chemical inside the body divided by the blood concentration and must be determined experimentally. To calculate V_{dis}, a known dose delivered by IV bolus is divided by the blood concentration measured soon after the dose is delivered. Because chemical distributes to tissues throughout the body, V_{dis} is not the same as the blood volume.

Equations 2-1, 2-4, and 2-5 were solved numerically using STELLA (a linear ordinary differential equation solver from High Performance Systems, Hanover, NH) assuming that:

$$C_v = C_v^o \qquad <C_{sc}> = 0 \qquad C_b = C_b^o \qquad \text{at } t = 0 \tag{2-6}$$

where C_v^o and C_b^o are the initial concentrations of the absorbing chemical in the vehicle and blood, respectively. The membrane-PK model equations were solved numerically using the finite difference technique described in Appendix 2A.

The membrane and compartment models were solved for identical vehicle and systemic conditions including the vehicle concentration, volume of the vehicle solution (V_v) and the PK constants (k_{el} and V_{dis}). Rate constants were calculated for the four skin compartment models using the same parameters as used by the membrane model (i.e., permeability coefficients, partition coefficients, sc thickness, and cutaneous blood flow rates). Because input parameters were identical for all models, differences in results reflect differences in the assumptions built into each model.

Results and Discussion

We have compared calculated results from the four compartment models with the membrane model for many different dermal absorption scenarios, presented in Appendix 2B. Five of these representing common yet widely different situations are presented here. In these exposure scenarios, C_v and C_b are time varying, and thus, these calculations will demonstrate how the four compartment models, which were developed assuming constant C_v and C_b, perform in more complex exposure situations. Table 2.3 summarizes the conditions of these five scenarios with respect to the length of time the vehicle remains on the skin, and whether the vehicle volume, blood volume, and blood flow rate are large or small. For V_v and V_{dis}, large or small is only meaningful when measured relative to the capacity of the skin to hold chemical (i.e., $K_{sc/v}\ V_{sc}$). The parameter Λ_{sc}, defined as

$$\Lambda_{sc} = \frac{V_v}{V_{sc} K_{sc/v}} \tag{2-7}$$

Table 2.3 – Summary of the five dermal absorption scenarios examined here.

Scenario Number	Scenario Description	Relative Vehicle Volume $[\Lambda_{sc}]^a$	$C_v(t)$	Relative Blood Volume $[\Gamma_{dis}]^a$	$C_b(t)$	Relative Blood Flow Rate $[\alpha_{sc}]^a$	Is Vehicle Removed? $[k_{el}\ t_{exp}]^a$	Preferred Model(s) Overall
1	Finite exposure time	large (infinite source) [>45]	$\approx C_v^o \neq 0$	large (infinite sink) [>15]	$\approx C_b^o = 0$	large [>20]	yes [0.3]	G,S
2	Decreasing vehicle concentration	small (finite source) [1]	$\leq C_v^o \neq 0$	large (infinite sink) [>15]	$\approx C_b^o = 0$	large [>20]	no $[\infty]^b$	G,S
3	Limited blood flow rate	large (infinite source) [>45]	$\approx C_v^o \neq 0$	large (infinite sink) [>15]	$\approx C_b^o = 0$	small [2]	no $[\infty]^b$	all
4	Increasing blood concentration	large (infinite source) [>45]	$\approx C_v^o \neq 0$	small (finite sink) [1]	$\geq C_b^o \neq 0$	large [>20]	no $[\infty]^b$	E,G
5	Absorption into skin from blood	large (infinite sink) [>45]	$\approx C_v^o = 0$	small (finite source) [1]	$\leq C_b^o \neq 0$ (from IV bolus)	large [>20]	no but $C_v \approx 0$ $[\infty]^b$	E

[a] Dimensionless group that defines the specified condition; when the value is reported as $> \gamma$, the effect on quantities calculated using the membrane model (e.g., C_v, C_b, C_{sc}, and % of dose absorbed and eliminated) is < 5% for $k_{el}t \leq 2$ as long as the value is $> \gamma$. [b] In this case, infinite exposure time means the exposure lasts longer than the maximum time in the calculation (i.e., plotted).

quantifies the capacity of the vehicle to hold chemical relative to the skin, while Γ_{dis}, defined as

$$\Gamma_{dis} = \frac{V_{dis} K_{b/v}}{V_{sc} K_{sc/v}} \tag{2-8}$$

represents the capacity of the blood to hold chemical relative to the sc. Similarly, the blood flow rate is large or small relative to the penetration rate as defined by the parameter α_{sc}, (eq 2-3). Table 2.3 reports the quantities of all parameters used in the calculations. In addition to the quantities listed in Table 2.3, the ratio $D_{sc} / (k_{el} L_{sc}^2)$ was set to 1 in all calculations.

Table 2.3 also describes how the vehicle and blood concentrations change during the time of the exposure. For example, when the relative vehicle volume is large (as it is for scenarios 1, 3, 4 and 5), the vehicle concentration change from the initial value (C_v^o) is too small to alter the rate of dermal penetration (i.e., $C_v(t) \approx C_v^o$ for the entire exposure). When the relative vehicle volume is small (as for scenario 2), dermal absorption reduces the vehicle concentration enough to decrease the rate of dermal absorption. Likewise, when the relative blood volume is large, the change in blood concentration from its initial value (C_b^o) is too small to affect the rate of dermal penetration.

Scenario 1 illustrates the situation in which the vehicle containing the absorbing chemical is removed (i.e., the exposure ends when $k_{el}\, t_{exp} = 0.3$). Chemical in the sc reservoir continues diffusing into the body (i.e., systemic compartment) after the exposure ends. In all other scenarios, the vehicle is not removed (i.e., the exposure does not end during the time of calculation). In scenario 2, the vehicle volume is small enough that dermal penetration causes the vehicle concentration to decrease significantly enough to affect the rate of dermal absorption. Scenario 3 represents the situation of chemical penetrating through the sc faster than the reduced blood flow rate can carry it away.

Scenario 4 portays the scenario of sufficient blood flow but a blood concentration that builds enough to reduce the skin penetration rate. In scenario 5, the direction of dermal absorption is reversed. That is, chemical absorbs into the skin from the blood, to which chemical has been abruptly added (e.g., by IV bolus). The penetrating chemical is then released into a vehicle, such as water during a shower or bath.

The calculated results for the average sc concentration, the systemic blood concentration, and the percent of dose eliminated are shown for each of the five scenarios in Figures 2.2 - 2.6. In addition, vehicle concentration is reported for those scenarios in which measurable changes in C_v occur. Each of these quantities is normalized as indicated in each figure. Concentrations for scenarios 1-4 are normalized by the initial vehicle concentration, C_v^o. In scenario 5, concentrations are normalized by C_b^o. The time scale of the plots is normalized by k_{el}, placing chemicals with different elimination rates on the same basis. The right-hand column of Table 2.3 indicates which of the four models most closely matches the membrane model overall for each of the five scenarios.

Calculated results for scenario 1, shown in Figure 2.2, illustrate the continued systemic absorption from the skin reservoir after the exposure has ended at $k_{el}t_{exp} = 0.3$. So that results are independent of the exact values of Λ_{sc} and Γ_{dis}, the blood concentration was normalized by Λ_{sc} and the percent of dose absorbed and eliminated were normalized by Γ_{dis}. The constants for this calculation were selected to insure that the blood concentration stays low and the vehicle concentration does not decrease while $k_{el}t \leq 2$.

As the average sc concentration indicates (Figure 2.2a), the membrane (M), equilibrium (E) and time lag (S, G) models all predict rapid absorption of chemical into the sc until the exposure ends, followed by a continued gradual release of chemical into the blood. Models S, G and E all underpredict the membrane model because the

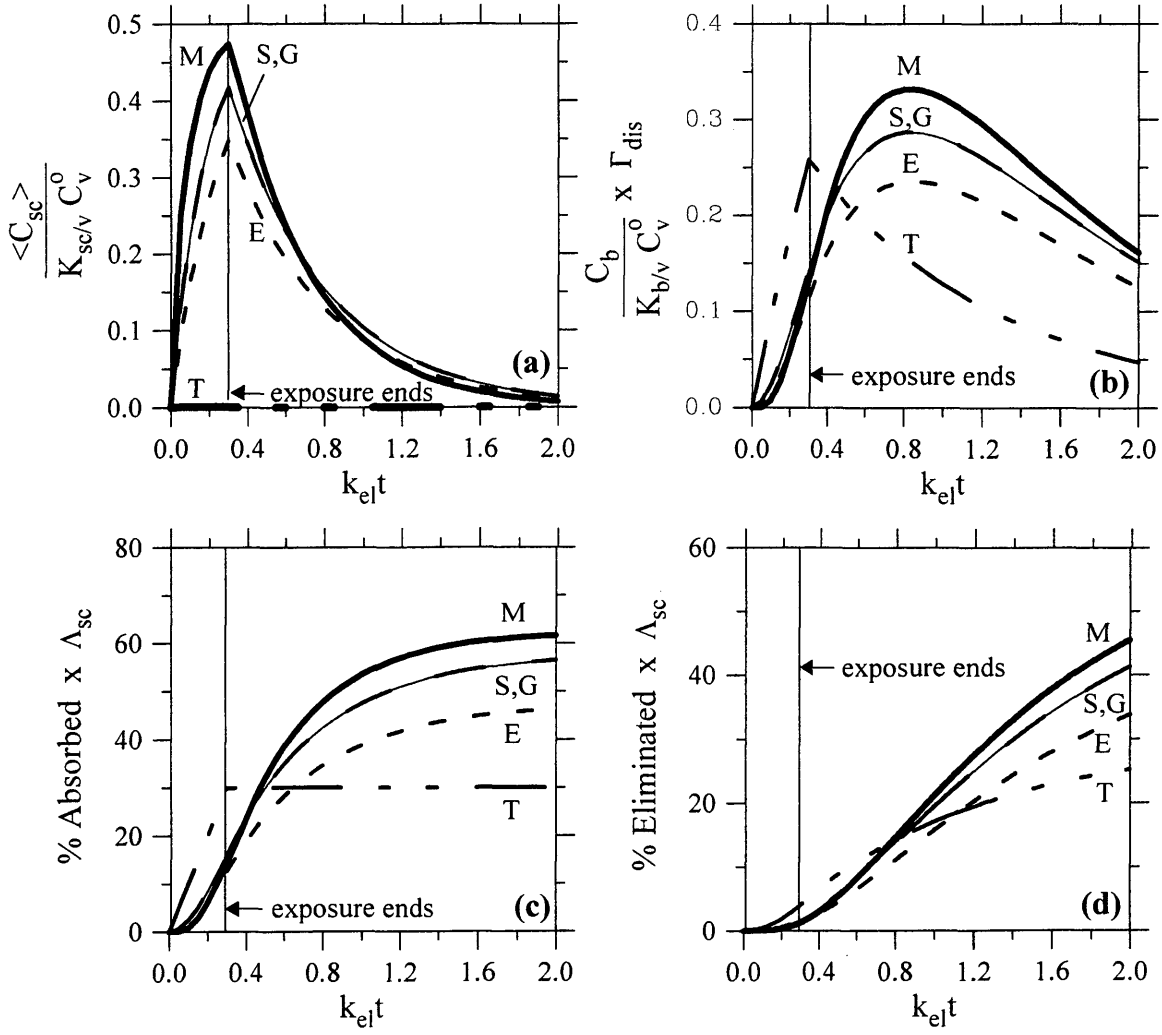

Figure 2.2 – Scenario 1 results: normalized a) $<C_{sc}>$, b) C_b, c) % of dose absorbed and d) % of dose eliminated.

exposure time ended before steady state was achieved. These three models would more closely match the membrane model if the exposure time were longer.

The traditional (T) model was developed assuming that clearance from the skin is controlled by the blood capacity for removal. Consequently, when the blood capacity for removal exceeds the rate at which chemical penetrates across the skin (as it does in this scenario), the traditional (T) model predicts that none of the penetrating chemical accumulates in the sc. As a result, model T predicts that the blood concentration (Figure 2.2b) increases faster than predicted by the membrane model M (i.e., model T predicts that all the chemical absorbed into the skin is immediately available to the cutaneous blood). Also, model T predicts that no chemical is left in the skin when the exposure ends, and consequently, the blood concentration declines more rapidly than for the other models because no chemical is systemically absorbed once the exposure ends. Because the other models account for slow release of chemical from the sc into the blood after the exposure ends, the maximum blood concentration is predicted to occur after the exposure ends.

Figure 2.2c shows the calculated percent of the dose that is absorbed systemically (i.e., the sum of the percent of dose in the blood and percent of the dose eliminated). Model T predicts no systemic absorption once the exposure ends, because, for the relative blood flow rate of this scenario, it does not allow for chemical storage in the skin (Figure 2.2a). With respect to the percent of dose eliminated (Figure 2.2d), model T predicts more elimination than model M while the skin is exposed to the vehicle, followed by less elimination once the exposure ends.

Figure 2.3 summarizes the calculations for scenario 2. In this scenario, the vehicle volume is small enough that vehicle concentration decreases as dermal absorption proceeds (Figure 2.3a). The average concentrations in the sc are shown in Figure 2.3b. As in scenario 1, the rate of chemical absorption into the blood is fast relative to the rate of penetration across the sc. Consequently, model T predicts that all chemical entering

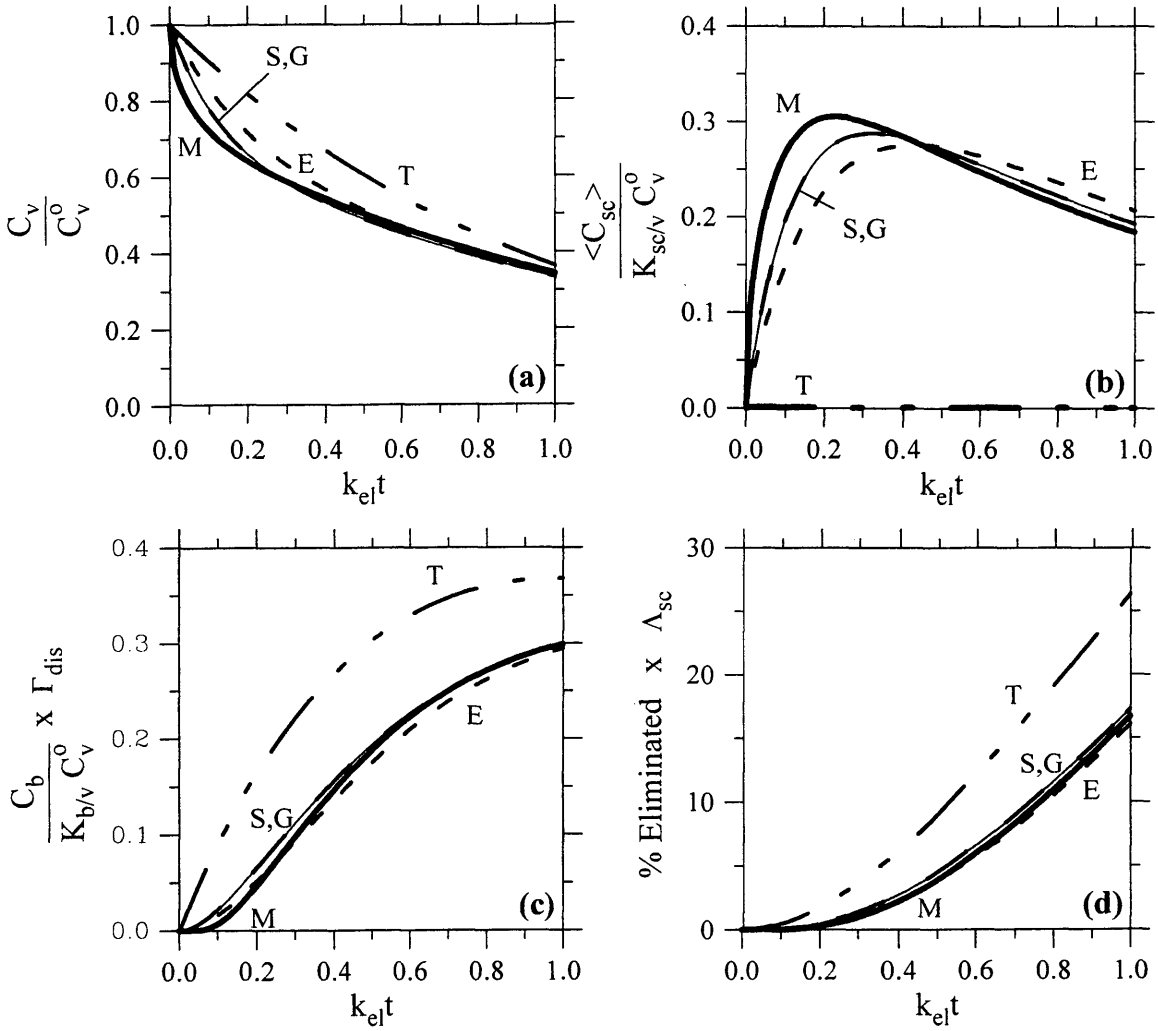

Figure 2.3 – Scenario 2 results: normalized a) C_v, b) $\langle C_{sc} \rangle$, c) C_b and d) % of dose eliminated.

the sc is immediately cleared by absorption into the blood (Figures 2.3c and 2.3d). Models S and G represent the model M results better than model E because models S and G were required to match the model M lag time.

The calculated results for scenario 3, showing the effects of a limited blood flow rate, are presented in Figure 2.4. Specifically, the rate of clearance into the blood is now only twice as fast as the rate of penetration across the skin (i.e., $\alpha_{sc} = 2$). Consequently, model T predicts that the chemical concentration in the sc is not negligible, but is still less than that predicted by the other models. Despite the differences in the predictions of sc concentration, all four compartment models closely match model M for blood concentration and the percent of dose eliminated, although models S and G are modestly better. For the scenario of restricted blood flow without vehicle removal, all four compartment models provide estimates of blood concentration and dose eliminated that are similar to model M.

The results of scenario 4, shown in Figure 2.5, illustrate the situation when dermal absorption is fast relative to the elimination rate, causing the chemical concentration in the blood to increase significantly (i.e., $K_{sc/b}\, C_b$ is no longer $<< K_{sc/v}\, C_v$). When the chemical concentration in the blood is no longer very small, the rate of chemical entering the blood from the sc is reduced, even at a high blood flow rate, because the driving force for transport (i.e., the concentration gradient) is decreased. Thus, as shown in Figure 2.5a, all five models predict that the skin clearance is slower than the penetration rate across the skin (i.e., models S, G, E and M predict that the steady-state $< C_{sc} > /(K_{sc/v}\, C_v^o) > 0.5$ and model T predicts that the steady-state $< C_{sc} > /(K_{sc/v}\, C_v^o) > 0$). Because equilibrium between the blood and sc limits clearance from the skin, model E, which contains equilibrium restrictions in its matching conditions, most closely matches model M. Neither models S nor G were required to match equilibrium conditions at the sc-blood interface, and consequently, predictions of sc concentrations for both deviate slightly

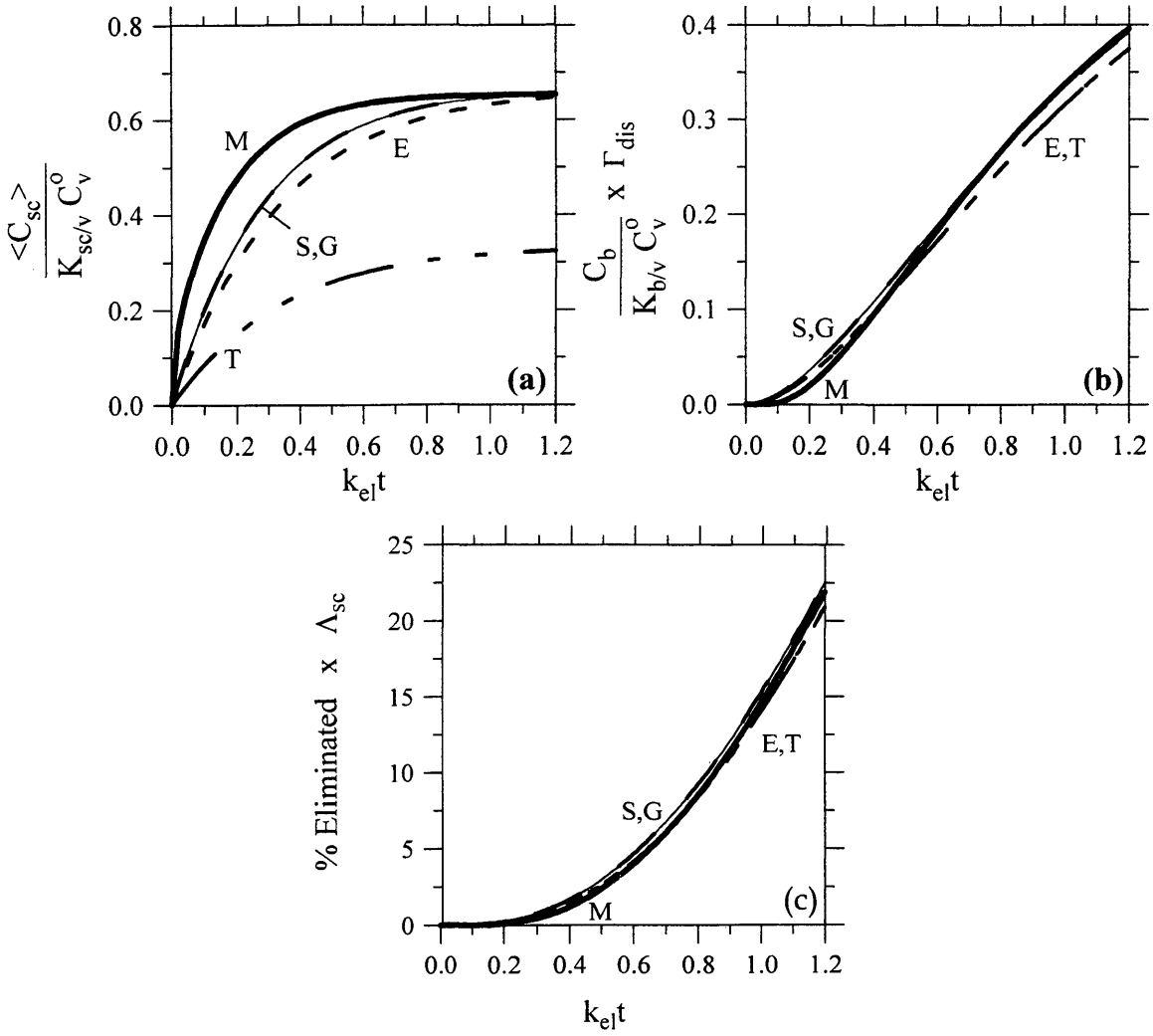

Figure 2.4 – Scenario 3 results: normalized a) $<C_{sc}>$, b) C_b and c) % of dose eliminated.

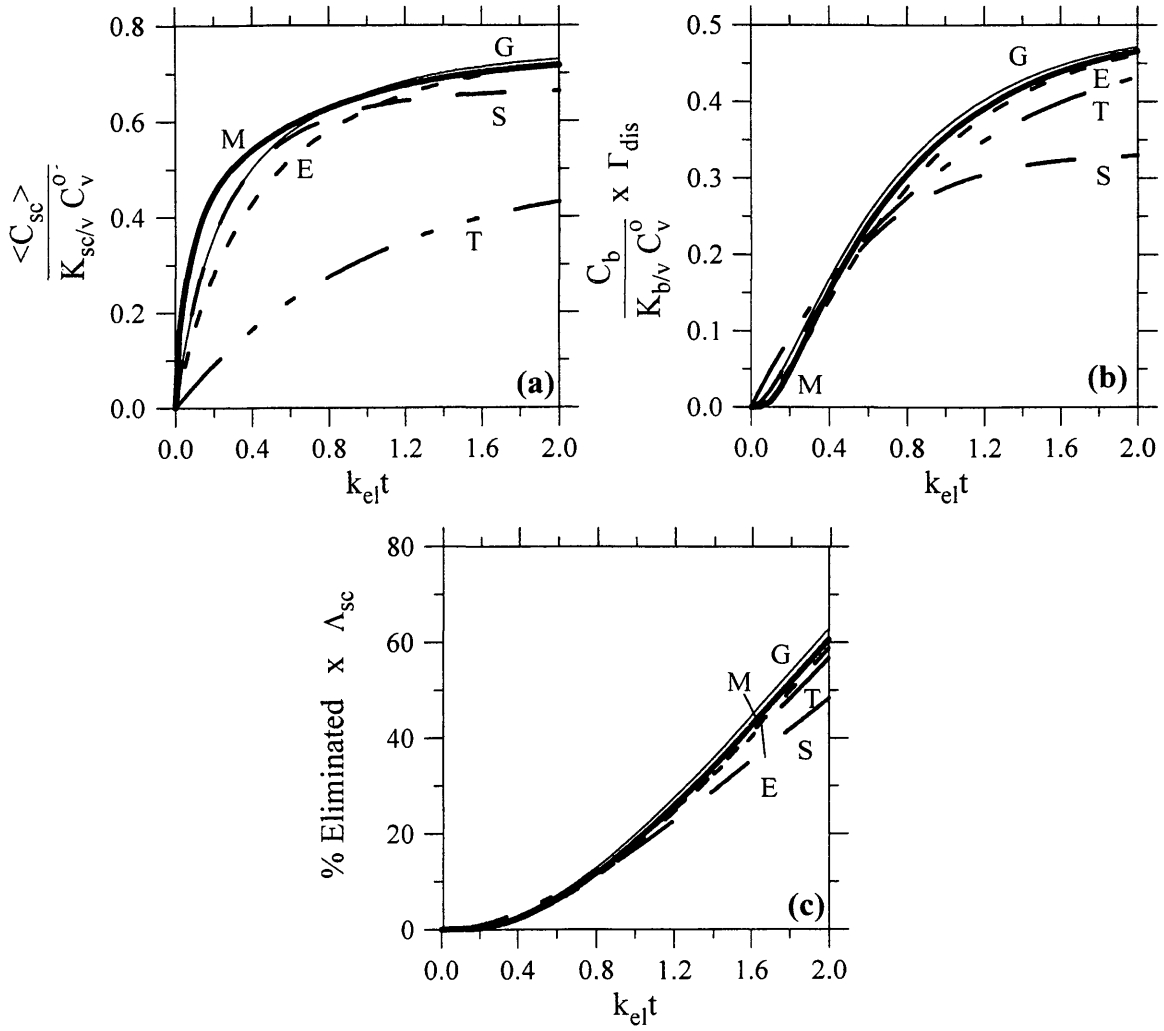

Figure 2.5 - Scenario 4 results: normalized a) $<C_{sc}>$, b) C_b and c) % of dose eliminated.

from model M. Model G deviates by less because it was required to match membrane model flux, sc concentration, and lag time for all blood concentrations (high and low).

With respect to the blood concentration and dose eliminated, models E and G provide the closest match to model M. Despite the underpredicted sc concentration, model T deviates only modestly from model M in predicting blood concentration and dose eliminated. It is not surprising that model S, which was developed assuming low blood concentrations, deviates most significantly from model M in predicting blood concentration.

Calculated results for the final scenario, representing the exposure of an individual in a large, chemical free water bath who is injected with an IV bolus, are shown in Figure 2.6. Results for this scenario are normalized using the initial blood concentration, C_b^o, instead of the vehicle concentration as for the other scenarios, because $C_v^o = 0$. For the calculations shown, the relative blood volume (i.e., Γ_{dis}) was assumed to be small (Table 2.3), and chemical concentration in the blood decreases as a result of both systemic elimination as well as dermal absorption. Consequently, chemical concentration in the blood and the percent of dose eliminated are different for the different dermal absorption models (Figures 2.6c and 2.6d). (If the blood capacity for the chemical was significantly larger than the capacity of the skin, then only the rate of systemic elimination would affect the blood concentration and all five skin models would predict the same blood concentrations and percent of dose eliminated.)

For all models, the chemical concentration in the sc increases initially as dermal absorption from the blood occurs and then decreases as the blood concentration declines. Model T predicts an immediate increase in the average sc concentration at $t = 0$ and a corresponding decrease in blood concentration. This occurs because, at the high blood flow rates assumed in this calculation, model T assumes that the sc immediately

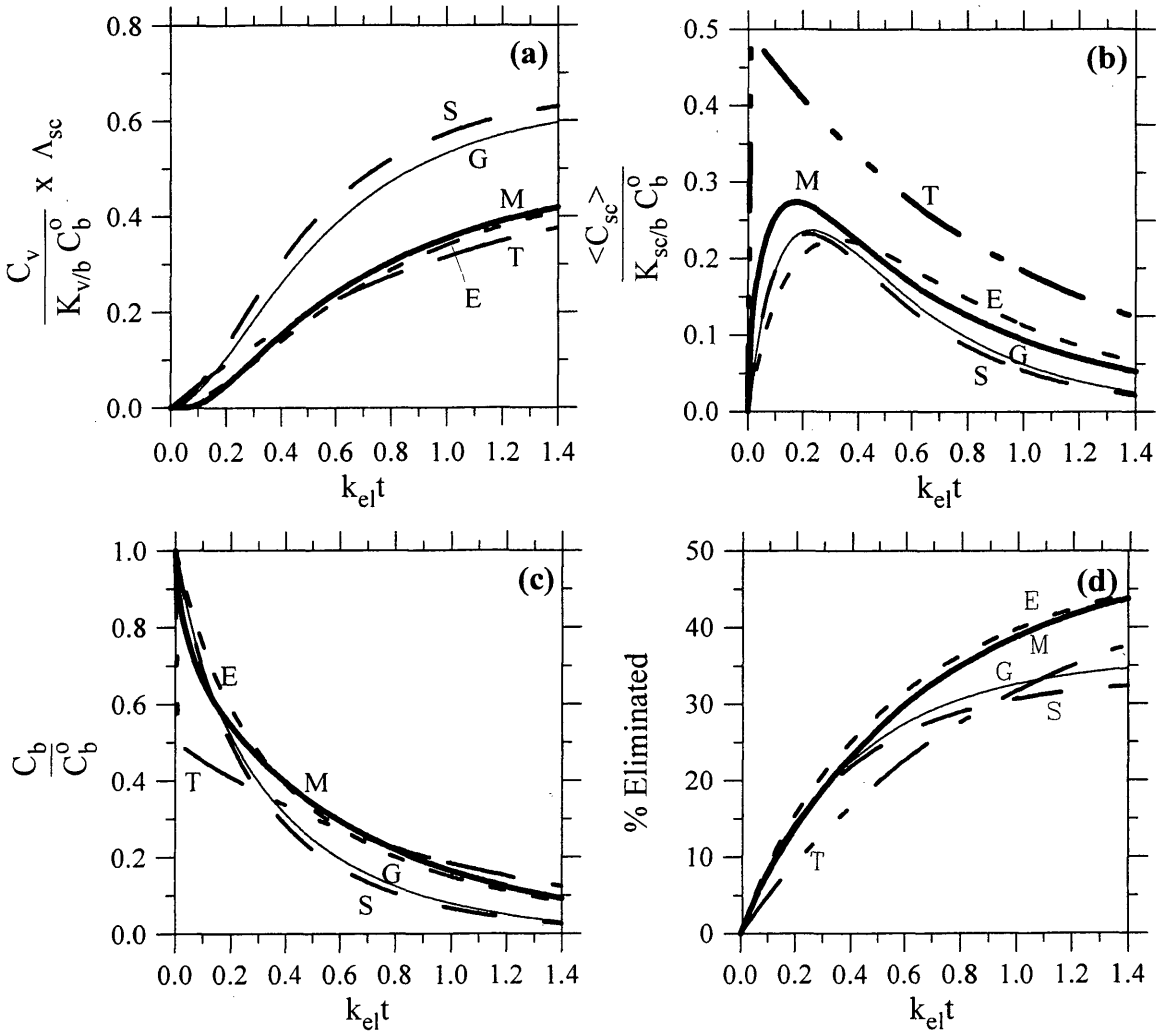

Figure 2.6 - Scenario 5 results: a) normalized C_v, b) normalized $\langle C_{sc} \rangle$, c) normalized C_b, d) % of dose eliminated.

equilibrates with the cutaneous blood. Predictions of chemical concentration in the sc by the other models consider the rate of chemical penetration. The average sc concentration (Figure 2.6b) at shorter times is predicted most closely by models S and G, and at later times by model E. However, the model E prediction of chemical concentration in the vehicle (Figure 2.6a) most closely matches model M, while models S and G significantly deviating from model M. This is an expected result because model E was required to match equilibrium conditions at the blood-sc interface while models S and G were not. Overall, model E most closely matches the membrane model in this scenario.

Typically, the differences between compartment models and the membrane model decrease as the time of exposure increases. This is illustrated in Figure 2.7 which shows the relative difference of the total cumulative mass absorbing into and transferring through the sc as predicted by the membrane (M_m) and compartment (M_c) models, defined as:

$$\text{Relative Percent Difference} = \left[\frac{M_m - M_c}{M_m}\right] \times 100 \tag{2-9}$$

for all 5 scenarios. Thus, for scenarios 1 - 4, M_m and M_c represent the total mass in the sc, the blood, and eliminated, while, for scenario 5, M_m and M_c are the total mass in the sc and the vehicle. The results are plotted as a function of time normalized by the lag time for the sc, defined as:

$$t_{lag,sc} = \frac{L_{sc}^2}{6 D_{sc}} = \frac{K_{sc/v} L_{sc}}{6 P_{sc,v}} \tag{2-10}$$

which approximately measures the time required for a chemical to penetrate across only the sc (i.e., delays caused by mass transfer resistances in the vehicle or blood are not included).

Except for model T in scenario 5, the membrane model always predicted much more dermal absorption than the compartment models at early times relative to the lag

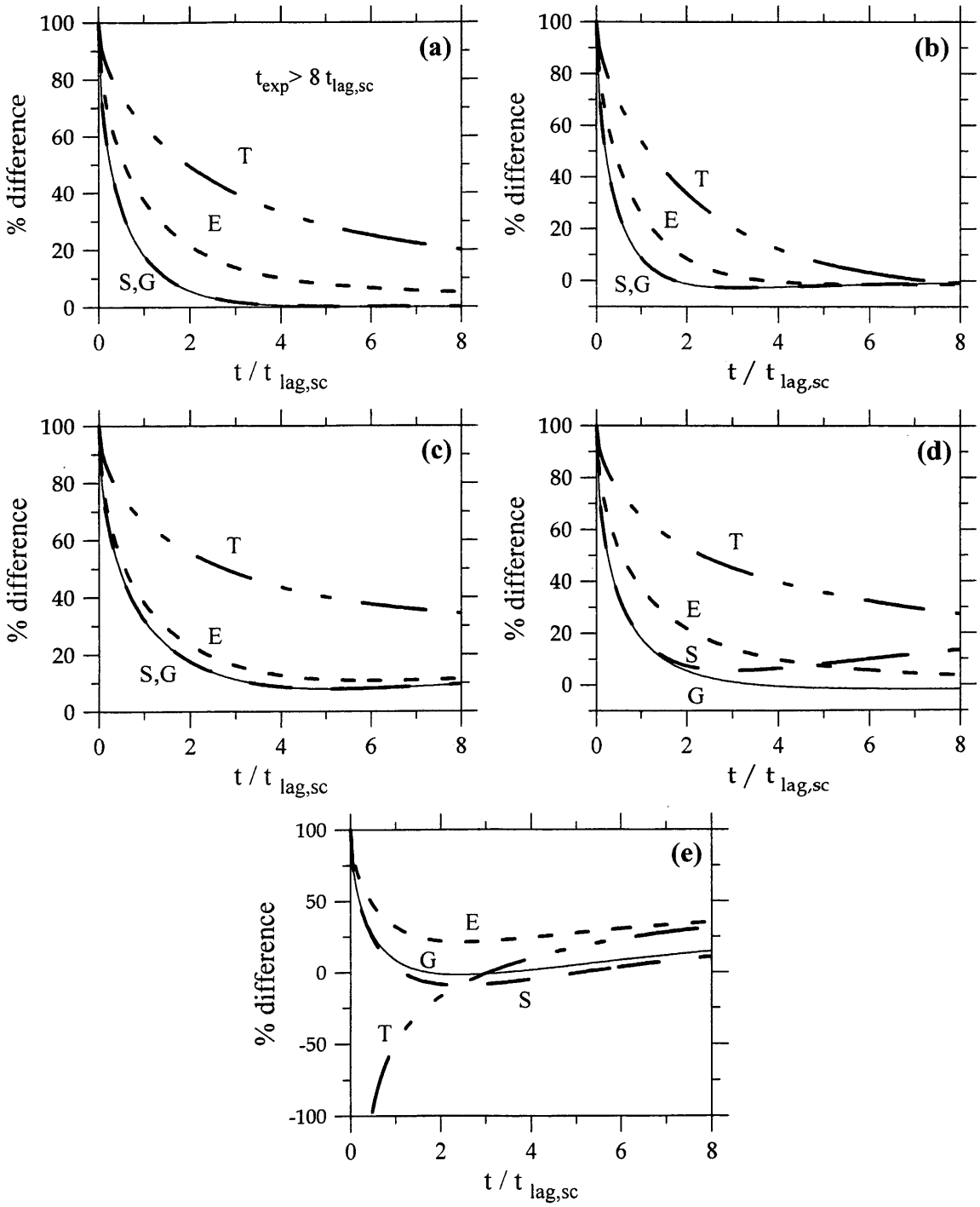

Figure 2.7 - Percent difference of cumulative mass entering and passing through the sc as a function of $t/t_{lag,sc}$ for scenarios: a) 1, b) 2, c) 3, d) 4, and e) 5.

time. Eventually, for scenarios 1 - 4, all models reach steady state (at $t \approx 3\ t_{lag,sc}$) and the relative differences between model M and each of the compartment models approach a constant. Because C_b continues to change in scenario 5, steady state is never reached (until all chemical is removed from the blood compartment), and the differences between model M and the compartment models continue to change although more slowly. Clearly, compartment model representations of model M are poorest when $t < t_{lag,sc}$ and usually underpredict the dermally absorbed mass.

When choosing a skin compartment model to estimate dermal absorption, the model that most closely predicts the membrane model is preferred. The preferred compartment model contains rate constants that force it to match the membrane model for the conditions most critical to the particular set of dermal absorption circumstances. The critical conditions for each of the five dermal absorption scenarios examined here were different, and consequently, different compartment models were preferred for different scenarios, as shown in Table 2.3. For each of the scenarios, at least one of the compartment models adequately represented the blood concentration and percent of dose absorbed except for the scenario when t_{exp} was short relative to $t_{lag,sc}$ (scenario 1). Even though the rate constant expressions for the compartment models were developed assuming constant blood and vehicle concentrations, the results appear to be adequately robust for describing more complicated exposure scenarios or physical conditions (i.e., situations in which C_v or C_b varies in time).

Model T, the model most frequently used in the literature, is typically a poor choice among the compartment models presented here for predicting membrane model results. However, the long time (relative to $t_{lag,sc}$) penetration rates predicted by model T are often correct. This can be seen in the plots of percent of dose absorbed, where model T results typically have approximately the same slope as model M results. Consequently, model T may be appropriate if only the steady-state dermal penetration rate is required.

Conclusions

For many chemicals, transport through skin is best modeled as passive diffusion through a membrane. Under many conditions, a compartment model is an acceptable, easy alternative to the membrane model even when C_v or C_b varies in time. However, the choice of which compartment model to use is critical. Different compartment models have been developed by matching different limiting characteristics of the membrane model, but no skin compartment model can match membrane model predictions for all cases. These different compartment models do predict different results.

If carefully chosen, a skin compartment model will do an acceptable job predicting blood concentrations and percent of dose absorbed and eliminated resulting from dermal penetration. A new model (model G) developed by McCarley and Bunge (1997) reasonably matched the membrane model predictions except when chemical was absorbed into the skin from the blood. Significantly, a model commonly described in the literature, model T, was not preferred in any of the scenarios studied, but typically predicted the correct long time (relative to $t_{lag,sc}$) rate of dermal absorption. Differences between the membrane model and all of the compartment models examined decrease as the time for dermal absorption increases. Compartment models provide acceptable results when chemicals have a small $t_{lag,sc}$ relative to the exposure time, or when the physical parameters used as input for the models are not known precisely.

Notation

A	surface area of chemical exposure
C_b	average concentration of the absorbing chemical in the blood plasma
C_b^o	initial concentration of the absorbing chemical in the blood plasma
C_{sc}	concentration of the absorbing chemical in the sc as a function of both position and time
$< C_{sc} >$	average concentration of absorbing chemical in the sc as a function of time
C_v	average concentration of the absorbing chemical in the vehicle
C_v^o	initial concentration of the absorbing chemical in the vehicle
D_{sc}	effective diffusion coefficient of the absorbing chemical in the sc
k_{el}	pharmacokinetic elimination rate constant
k_n^A	compartment model rate constants (n = 1, -1, 2, -2)
$\hat{k}_n^A$	normalized compartment model rate constants as defined in Table 2.1 (n = 1, -1, 2, -2)
$K_{b/v}$	equilibrium partition coefficient between the blood and the vehicle for the absorbing chemical
$K_{sc/b}$	equilibrium partition coefficient between the sc and the blood for the absorbing chemical
$K_{sc/v}$	equilibrium partition coefficient between the sc and the vehicle for the absorbing chemical
L_{sc}	effective thickness of the sc
M_c	cumulative mass of chemical which has passed into and through the sc as predicted by a compartment model
M_m	cumulative mass of chemical which has passed into and through the sc as predicted by the membrane model

N	number of nodes in the sc for the finite difference solution
$P_{sc,v}$	steady-state permeability coefficient of the absorbing chemical through the sc from the vehicle
q_b	specific cutaneous blood flow rate
sc	stratum corneum
t	time
t_{exp}	duration of the dermal exposure
t_{lag}	lag time for chemical to go from the vehicle through the sc and into the blood
$t_{lag,sc}$	lag time for chemical penetrating through the sc
V_{dis}	pharmacokinetic volume of distribution
ve	viable epidermis
V_{sc}	volume of the sc
V_v	volume of the vehicle
x	position in the sc

Greek

α_{sc}	ratio of the blood clearance rate ($q_{b\ Kb/v}$) to the rate of chemical penetration across the sc from a vehicle ($P_{sc,v}$)
α_v	ratio of the rate of transfer of the absorbing chemical from a vehicle to the rate of chemical penetration across the sc
Γ_{dis}	ratio of the capacity of the blood to hold chemical ($V_{dis}K_{b/v}$) relative to the sc ($V_{sc}K_{sc/v}$)
Λ_{sc}	ratio of the capacity of the vehicle to hold chemical (V_v) relative to the sc ($V_{sc}K_{sc/v}$)

References

Brown, H. S. and D. Hattis (1989). "The role of skin absorption as a route of exposure to volatile organic compounds in household tap water: a simulated kinetic approach." Journal of the American College of Toxicology **8**:839-851.

Bunge, A. L. and K. D. McCarley (1995). An improved physiologically relevant pharmacokinetic model for skin. Prediction of Percutaneous Penetration: Methods, Measurements, and Modeling, vol. 4b. K. R. Brain, V. J. James and K. A. Walters, eds. Cardiff, Wales, UK, STS Publishing, 190-194.

Chinery, R. L. and K. A. Gleason (1993). "A compartment model for the prediction of breath concentration and absorbed dose of chloroform after exposure while showering." Risk Analysis: An Official Publication of the Society for Risk Analysis **13**:51-62.

EPA, U. S. (1992). Dermal Exposure Assessment: Principles and Applications, EPA/600/8-91/011B. Exposure Assessment Group, Office of Health and Environmental Assessment, Washington.

Klaassen, C. D., M. O. Amdur and J. Doull, Eds. (1996). Casarett & Doull's Toxicology The Basic Science of Poisons. New York, NY, McGraw-Hill.

Kligman, A. M. (1964). The biology of the stratum corneum. The Epidermis. W. Montagna and W. C. Lobitz, eds. New York and London, Academic Press, 387-433.

McCarley, K. D. and A. L. Bunge (1997). "Physiologically relevant one-compartment pharmacokinetic models for skin. 1. Development of models." Journal of Pharmaceutical Sciences **4**:470-481.

McKone, T. E. (1993). "Linking a PBPK model for chloroform with measured breath concentrations in showers: implications for dermal exposure models." Journal of Exposure Analysis and Environmental Epidemiology **3**:339-365.

Rao, H. V. and D. R. Brown (1993). "A physiologically based pharmacokinetic assessment of tetrachloroethylene in groundwater for a bathing and showering determination." Risk Analysis: An Official Publication of the Society for Risk Analysis **13**:37-49.

Scheuplein, R. J. and I. H. Blank (1971). "Permeability of the skin." Physiological Reviews **51**:702-747.

Shatkin, J. and H. S. Brown (1991). "Pharmacokinetics of the dermal route of exposure to volatile organic chemicals in water: a computer simulation model." Environmental Research **56**:90-108.

Silcox, G. D., G. E. Parry, A. L. Bunge, L. K. Pershing and D. W. Pershing (1990). "Percutaneous absorption of benzoic acid across human skin. II. Prediction of an in vivo, skin-flap system using in vitro parameters." Pharmaceutical Research **7**:352-358.

Appendix 2A – Membrane Model Equations and Solution

Differential mass balances of the amount of absorbing chemical in the vehicle, membrane, and body (i.e., the PK compartment model) result in the following system of partial differential equations:

$$V_v \frac{dC_v}{dt} = AD_{sc}\left[\frac{\partial C_{sc}}{\partial x}\right]_{x=0} \tag{2A-1}$$

$$\frac{\partial C_{sc}}{\partial t} = D_{sc}\frac{\partial^2 C_{sc}}{\partial x^2} \tag{2A-2}$$

$$V_{dis}\frac{dC_b}{dt} = -k_{el}V_{dis}C_b - AD_{sc}\left[\frac{\partial C_{sc}}{\partial x}\right]_{x=L_{sc}} \tag{2A-3}$$

with the restricting conditions:

$$\text{at } t = 0 \qquad C_v = C_v^o \qquad C_{sc} = 0 \qquad C_b = C_b^o \tag{2A-4}$$

$$\text{at } x = 0 \qquad C_{sc} = K_{sc/v}C_v \qquad \text{for } t \le t_{exp} \tag{2A-5}$$

$$\frac{\partial C_{sc}}{\partial x} = 0 \qquad \text{for } t > t_{exp} \tag{2A-6}$$

$$\text{at } x = L_{sc} \qquad -D_{sc}\frac{\partial C_{sc}}{\partial x} = q_b\left[\frac{C_{sc}}{K_{sc/b}} - C_b\right] \tag{2A-7}$$

where all parameters have been defined previously. In eq 2A-1 the rate of penetration into the membrane is assumed to control the rate of loss from the vehicle. The concentration of absorbing chemical in the systemic blood (C_b) depends on the rate of systemic elimination relative to the rate of dermal penetration, eq 2A-3. The sc is assumed to be initially chemical free, although either C_v^o or C_b^o can be non-zero, eq 2A-4. The outermost layer of the skin is in local equilibrium with the vehicle until chemical is removed at a specified exposure time (t_{exp}), eq 2A-5. After this, chemical flux across the vehicle-sc interface becomes zero, eq 2A-6. Cutaneous blood sweeps chemical from the

skin into the systemic circulation as specified by eq 2A-7, which allows inadequate blood flow to restrict penetration through the sc.

Equations 2A-1 through 2A-7 were solved with a finite difference scheme transforming the system of partial differential equations of t and x into a system of ordinary differential equations of t alone. The sc is split into N nodes and the equations are approximated using the following finite differencing formulas:

$$\frac{\partial^2 C_{sc}}{\partial x^2} = \frac{C_{sc,i-1} - C_{sc,i} + C_{sc,i+1}}{(\Delta x)^2} \tag{2A-8}$$

$$\left(\frac{\partial C}{\partial x}\right)_{x=0} = \frac{-3C_{sc,1} + 4C_{sc,2} - C_{sc,3}}{2\Delta x} \tag{2A-9}$$

$$\left(\frac{\partial C}{\partial x}\right)_{x=L_{sc}} = \frac{C_{sc,N-2} - 4C_{sc,N-1} + 3C_{sc,N}}{2\Delta x} \tag{2A-10}$$

where

$$\Delta x = L_{sc} / (N-1) \tag{2A-11}$$

Eqs 2A-9 to 2A-10 are second-order accurate in x. The resulting equations were solved for N = 99 with the FORTRAN computer program shown in Appendix 2C, which uses the IVPAG routine from the IMSL library to solve initial-value ordinary differential equation problems.

Several checks were done to insure the stability and accuracy of the numerical solution. The numerical solution was checked using the analytical sotutions for several more simple limiting cases, including: 1) $C_v = C_v^o$ for all t, $C_b = 0$ for all t, $\alpha_{sc} \rightarrow \infty$, and finite t_{exp}; 2) $C_v \neq C_v^o$ for all t, $C_b = 0$ for all t, $\alpha_{sc} \rightarrow \infty$, and large t_{exp}; 3) $C_v = C_v^o$ for all t, $C_b \geq 0$ for all t, $\alpha_{sc} \rightarrow \infty$, and large t_{exp}; and 4) $C_v = C_v^o$ for all t, $C_b = 0$ for all t, finite α_{sc}, and large t_{exp}. Stability of the numerical solution with respect to the number of nodes was confirmed by increasing the number of nodes with no change in the answer. Finally,

all solutions included a mass balance to demonstrate that the mass of chemical in the membrane, M_{sc}, calculated using Simpson's rule,

$$\begin{aligned} M_{sc} &= \frac{V_{sc}}{L_{sc}} \int_0^{L_{sc}} C_{sc}(x)dx \\ &= \frac{V_{sc}}{N-1}\left[C_{sc,1} + 4C_{sc,2} + 2C_{sc,3} + \cdots + 2C_{sc,N-2} + 4C_{sc,N-1} + C_{sc,N}\right] \end{aligned} \tag{2A-12}$$

when added to the mass of chemical in the vehicle, blood, and eliminated, was always within 0.02% of 100%.

Appendix 2B – Complete Calculation Results

The exposure scenarios presented in the Results and Discussion of Chapter 2 were selected from the 31 cases documented here. These cases examine absorption into the skin in three types of situations: 1) a single exposure to chemical on the skin surface, 2) exposure to chemical in the bloodstream, and 3) repeated exposures to chemical on the skin surface.

Table 2B.1 summarizes the cases used to study the first type of situation. The various parameters reported in Table 2B.1 are discussed in detail in the Results and Discussion section, with the exception of the relative skin penetration rate. The calculations presented in the main body of Chapter 2 were completed assuming $D_{sc} / (k_{el} L_{sc}^2) \sim 1$. Other values of $D_{sc} / (k_{el} L_{sc}^2)$ were examined, as shown in Table 2B.1. Because for our results time was normalized with respect to the elimination rate constant, varying the parameter $D_{sc} / (k_{el} L_{sc}^2)$ simulates exposures to chemicals with different $t_{lag,sc}$. For example, a high value of $D_{sc} / (k_{el} L_{sc}^2)$ simulates an exposure to a chemical with a short lag time, which would be expected to penetrate the skin rapidly. The ratio $D_{sc} / (k_{el} L_{sc}^2)$ can also be represented as a relationship between $t_{lag,sc}$ and the half life for chemical elimination ($t_{1/2}$), defined as

$$t_{1/2} = 0.693 / k_{el} \qquad (2B\text{-}1)$$

where $t_{1/2}$ is the time it takes the blood plasma concentration to decrease to half of its original value after an IV bolus is injected into the bloodstream. The relationship between $t_{lag,sc}$ and $t_{1/2}$ used for the calculations is also listed in Table 2B.1.

Four of the cases described in Table 2B.1 are presented in the Results and Discussion section. Exposure scenarios 1, 2, and 4 correspond to cases 2, 6, and 9. Exposure scenario 3 is the same as cases 11 and 14, except that $\alpha_{sc} = 2$ in Exposure Scenario 3.

Table 2B.1 – Summary of dermal absorption cases involving a single exposure.

Case	Scenario Description	Relative Vehicle Volume $[\Lambda_{sc}]^a$	$C_v(t)$	Relative Blood Volume $[\Gamma_{dis}]^a$	$C_b(t)$	Relative Blood Flow Rate $[\alpha_{sc}]^a$	Relative Skin Penetration Rate $[D_{sc} / (k_{el} L_{sc}^2)]^a$	Is Vehicle Removed? $[k_{el}\, t_{exp}]^a$
1		large (infinite source) [>45]	$\approx C_v^o \neq 0$	large (infinite sink) [>15]	$\approx C_b^o = 0$	large [>20]	$t_{lag,sc} = 0.24\ t_{1/2}$ [1]	no $[\infty]^b$
2	finite exposure time	large (infinite source) [>45]	$\approx C_v^o \neq 0$	large (infinite sink) [>15]	$\approx C_b^o = 0$	large [>20]	$t_{lag,sc} = 0.24\ t_{1/2}$ [1]	yes [0.3]
3	slowly absorbing chemical, finite exposure time	large (infinite source) [>45]	$\approx C_v^o \neq 0$	large (infinite sink) [>15]	$\approx C_b^o = 0$	large [>20]	$t_{lag,sc} = 2.4\ t_{1/2}$ [0.1]	yes [0.3]
4	rapidly absorbing chemical, finite exposure time	large (infinite source) [>45]	$\approx C_v^o \neq 0$	large (infinite sink) [>15]	$\approx C_b^o = 0$	large [>20]	$t_{lag,sc} = 0.024\ t_{1/2}$ [10]	yes [0.3]
5	shorter finite exposure time	large (infinite source) [>45]	$\approx C_v^o \neq 0$	large (infinite sink) [>15]	$\approx C_b^o = 0$	large [>20]	$t_{lag,sc} = 0.24\ t_{1/2}$ [1]	yes [0.15]

(continued)

Table 2B.1 (continued)

Case	Scenario Description	Relative Vehicle Volume $[\Lambda_{sc}]^a$	$C_v(t)$	Relative Blood Volume $[\Gamma_{dis}]^a$	$C_b(t)$	Relative Blood Flow Rate $[\alpha_{sc}]^a$	Relative Skin Penetration Rate $[D_{sc} / (k_{el} L_{sc}^2)]^a$	Is Vehicle Removed? $[k_{el}\, t_{exp}]^a$
6	decreasing vehicle concentration	small (finite source) [1]	$\leq C_v^o \neq 0$	large (infinite sink) [>15]	$\approx C_b^o = 0$	large [>20]	$t_{lag,sc} = 0.24\, t_{1/2}$ [1]	no $[\infty]^b$
7	decreasing vehicle concentration, finite exposure time	small (finite source) [1]	$\leq C_v^o \neq 0$	large (infinite sink) [>15]	$\approx C_b^o = 0$	large [>20]	$t_{lag,sc} = 0.24\, t_{1/2}$ [1]	yes [0.3]
8	decreasing vehicle concentration, finite exposure time	small (finite source) [1]	$\leq C_v^o \neq 0$	large (infinite sink) [>15]	$\approx C_b^o = 0$	large [>20]	$t_{lag,sc} = 0.24\, t_{1/2}$ [1]	yes [0.5]
9	increasing blood concentration	large (infinite source) [>45]	$\approx C_v^o \neq 0$	small (finite sink) [1]	$\geq C_b^o \neq 0$	large [>20]	$t_{lag,sc} = 0.24\, t_{1/2}$ [1]	no $[\infty]^b$
10	increasing blood concentration, finite exposure time	large (infinite source) [>45]	$\approx C_v^o \neq 0$	small (finite sink) [1]	$\geq C_b^o \neq 0$	large [>20]	$t_{lag,sc} = 0.24\, t_{1/2}$ [1]	yes [1]

(continued)

Table 2B.1 (continued)

Case	Scenario Description	Relative Vehicle Volume $[\Lambda_{sc}]^a$	$C_v(t)$	Relative Blood Volume $[\Gamma_{dis}]^a$	$C_b(t)$	Relative Blood Flow Rate $[\alpha_{sc}]^a$	Relative Skin Penetration Rate $[D_{sc} / (k_{el} L_{sc}^2)]^a$	Is Vehicle Removed? $[k_{el}\, t_{exp}]^a$
11	limited blood flow rate	large (infinite source) [>45]	$\approx C_v^o \neq 0$	large (infinite sink) [>15]	$\approx C_b^o = 0$	medium [10]	$t_{lag,sc} = 0.24\, t_{1/2}$ [1]	no $[\infty]^b$
12	limited blood flow rate, finite exposure time	large (infinite source) [>45]	$\approx C_v^o \neq 0$	large (infinite sink) [>15]	$\approx C_b^o = 0$	medium [10]	$t_{lag,sc} = 0.24\, t_{1/2}$ [1]	yes [0.3]
13	slowly absorption, limited blood flow rate, finite exposure time	large (infinite source) [>45]	$\approx C_v^o \neq 0$	large (infinite sink) [>15]	$\approx C_b^o = 0$	medium [10]	$t_{lag,sc} = 2.4\, t_{1/2}$ [0.1]	yes [0.3]
14	very limited blood flow rate	large (infinite source) [>45]	$\approx C_v^o \neq 0$	large (infinite sink) [>15]	$\approx C_b^o = 0$	small [1]	$t_{lag,sc} = 0.24\, t_{1/2}$ [1]	no $[\infty]^b$
15	very limited blood flow rate, finite exposure time	large (infinite source) [>45]	$\approx C_v^o \neq 0$	large (infinite sink) [>15]	$\approx C_b^o = 0$	small [1]	$t_{lag,sc} = 0.24\, t_{1/2}$ [1]	yes [0.3]

[a] Dimensionless group defining the specified condition; when the value is reported as $> \gamma$, the effect on quantities calculated using model M (e.g., C_v, C_b, C_{sc}, and % of dose absorbed and eliminated) is < 5% for $(k_{el}\, t) \leq 2$ as long as the value is $> \gamma$. [b] Here, infinite exposure time means the exposure lasts longer than the maximum time in the calculation (i.e., plotted).

Cases 1 through 5 represent exposures to a constant-concentration vehicle when the blood concentration remains low and the blood can absorb chemical as quickly as chemical reaches the inside of the sc. For case 1, the vehicle is not removed from the skin. Cases 2 through 5 explore the effects of different lengths of exposure ($k_{el}\ t_{exp}$) and different rates of penetration relative to the elimination rate (i.e., $D_{sc} / (k_{el} L_{sc}^2)$). Examining situations in which the vehicle is removed pertains to many exposures because the skin is often exposed to a chemical and then washed.

Cases 6 through 8 examine exposures where the concentration of absorbing chemical in the vehicle decreases quickly enough to affect the rate of dermal absorption. These cases are relevant to situations with a small vehicle volume (e.g., a thin layer of ointment applied to the skin for a therapeutic effect). For case 6, the vehicle is not removed from the skin. For cases 7 and 8, the vehicle is removed from the skin at different values of $k_{el}\ t_{exp}$.

The situation in which blood concentration increases enough to decrease the rate of dermal absorption is examined in cases 9 and 10. This might occur if a rapidly absorbed chemical is eliminated very slowly or if the volume of distribution is small.

Cases 11 to 15 examine the effect of the blood being incapable of absorbing chemical as quickly as chemical penetrates the sc. Cases 14 and 15 examine larger blood flow limitations than cases 11 to 13. Blood flow limitations are not typically encountered unless cutaneous blood flow is reduced in some way (e.g., by reducing the skin temperature or by applying a pharmaceutical vasoconstrictor).

The results in this appendix include a plot not found in the results and discussion. Plots of the concentration profile (i.e., normalized C_{sc} as a function of dimensionless position) calculated using model M are included in results for cases 1 to 15. The curves for these plots represent different exposure times relative to $t_{lag,sc}$. The plot of the concentration profile in the membrane was included to provide insight into model M results and emphasize the difference between model M and the compartment models,

which treat the sc like a well-stirred tank. Also, calculation results for cases 1 to 15 include plots of the normalized $<C_{sc}>$, C_b, percent of dose absorbed, and percent of dose eliminated as a function of dimensionless time. Cases 6 through 8 include plots of the normalized vehicle concentration as a function of dimensionless time, because for those cases the vehicle is not acting as an infinite source. The normalization is discussed in detail in the Results and Discussion. Table 2B.2 presents a legend showing the symbol and style of curve used to identify the results of each model, which are the same as found in the rest of the chapter. Results for cases 1 to 15 are shown in Figures 2B.1 to 2B.15.

Table 2B.2 – Legend for plots of normalized C_v, $<C_{sc}>$, C_b and percent of dose absorbed and eliminated for all cases.

Model	Abbreviation	Curve
equilibrium	E	- - - - -
general time lag	G	———
membrane	M	———
simplified time lag	S	— —
traditional	T	—— - -

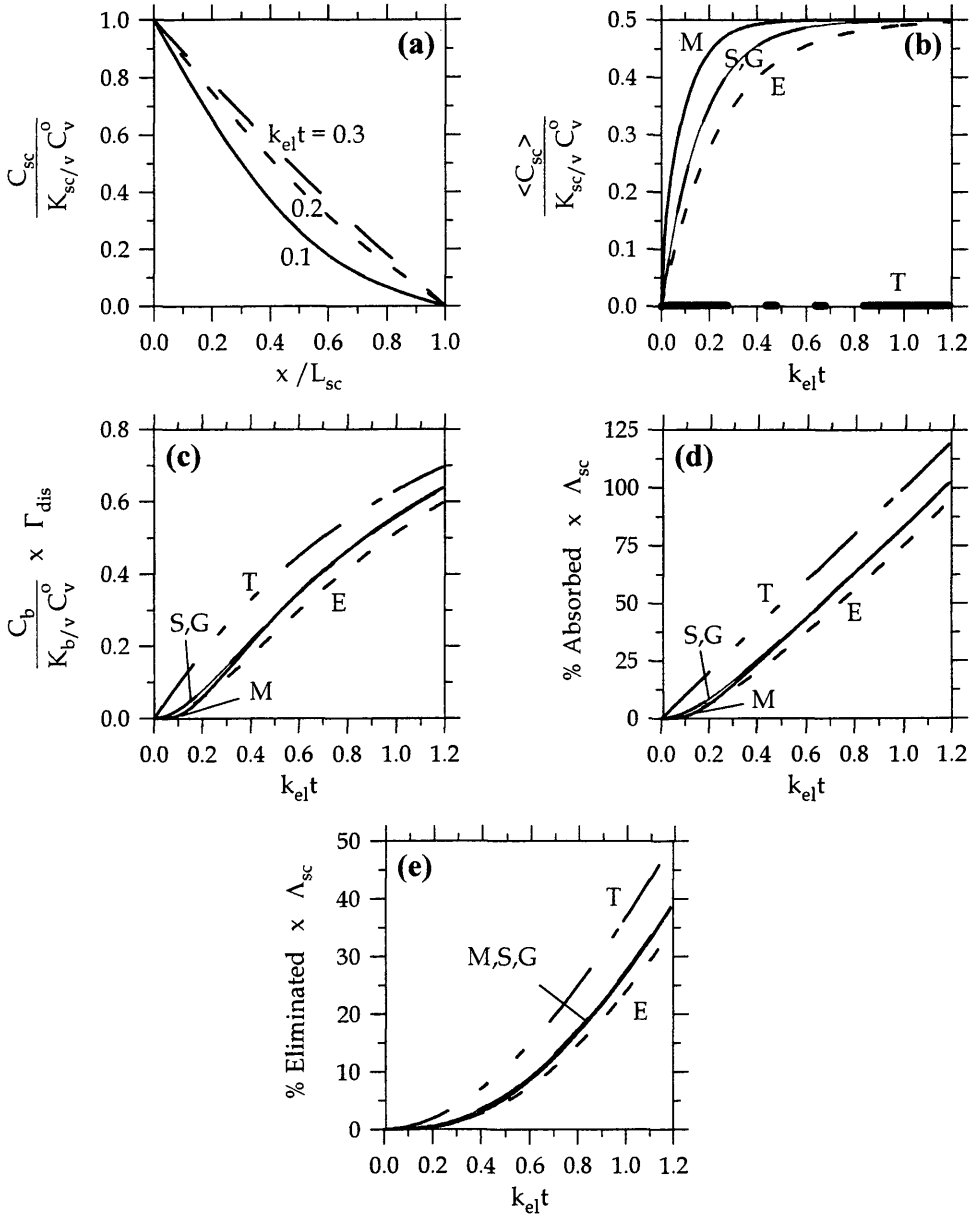

Figure 2B.1 – Case 1 results: normalized a) C_{sc} as a function of position in the sc for several $k_{el}t$, and b) $<C_{sc}>$, c) C_b, d) % of dose absorbed, and e) % of dose eliminated as a function of dimensionless time.

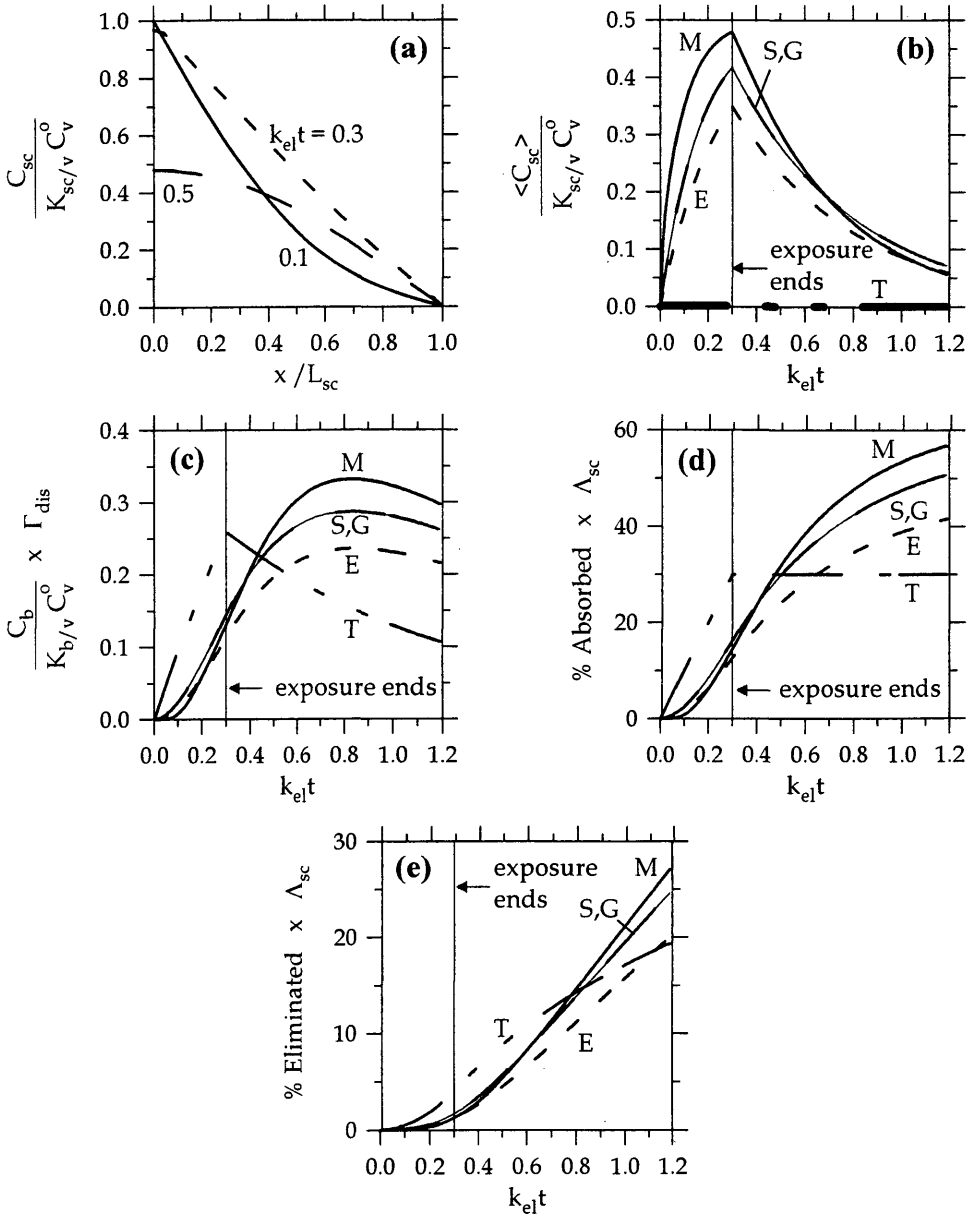

Figure 2B.2 – Case 2 results: normalized a) C_{sc} as a function of position in the sc for several $k_{el}t$, and b) $<C_{sc}>$, c) C_b, d) % of dose absorbed, and e) % of dose eliminated as a function of dimensionless time.

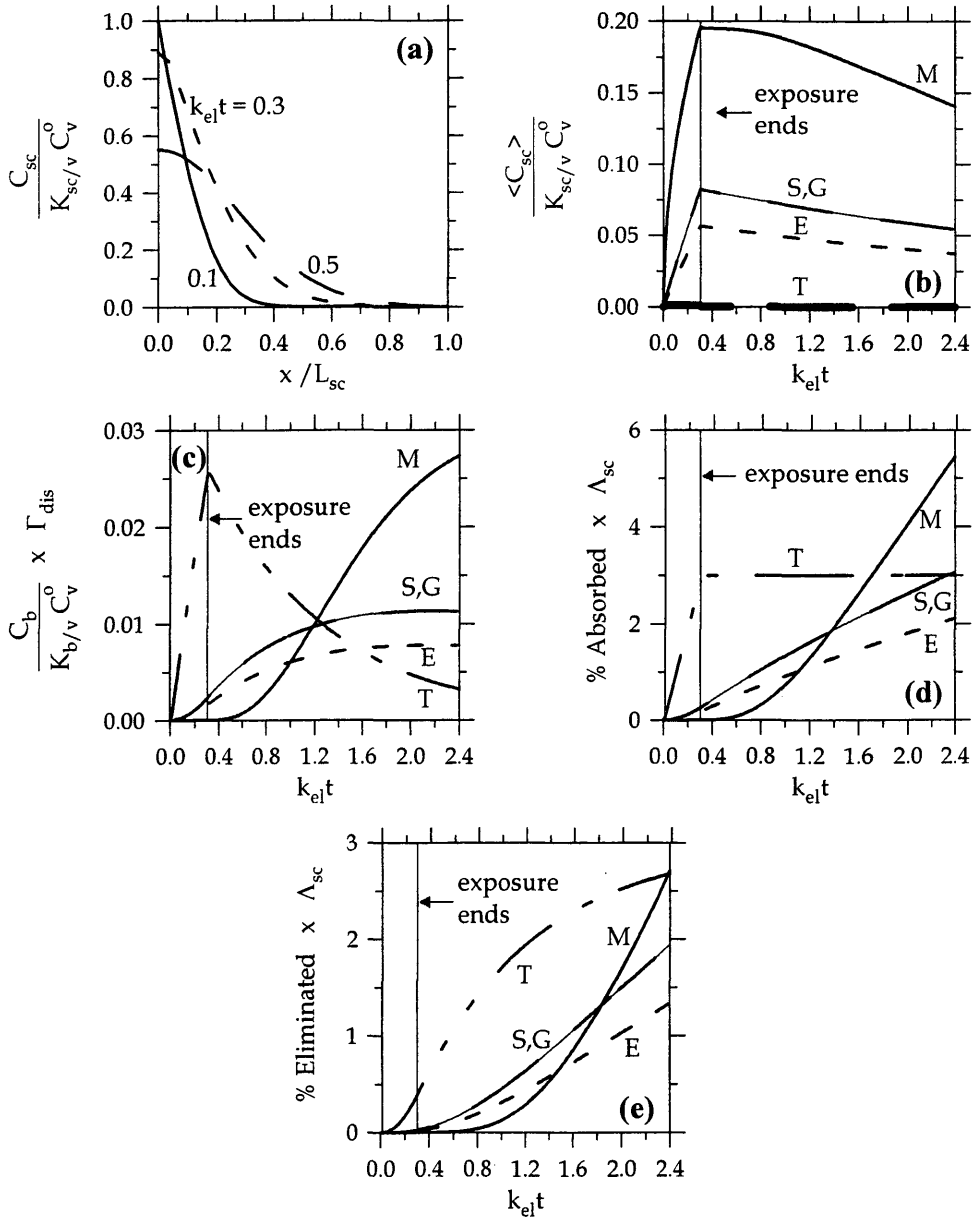

Figure 2B.3 – Case 3 results: normalized a) C_{sc} as a function of position in the sc for several $k_{el}t$, and b) $<C_{sc}>$, c) C_b, d) % of dose absorbed, and e) % of dose eliminated as a function of dimensionless time.

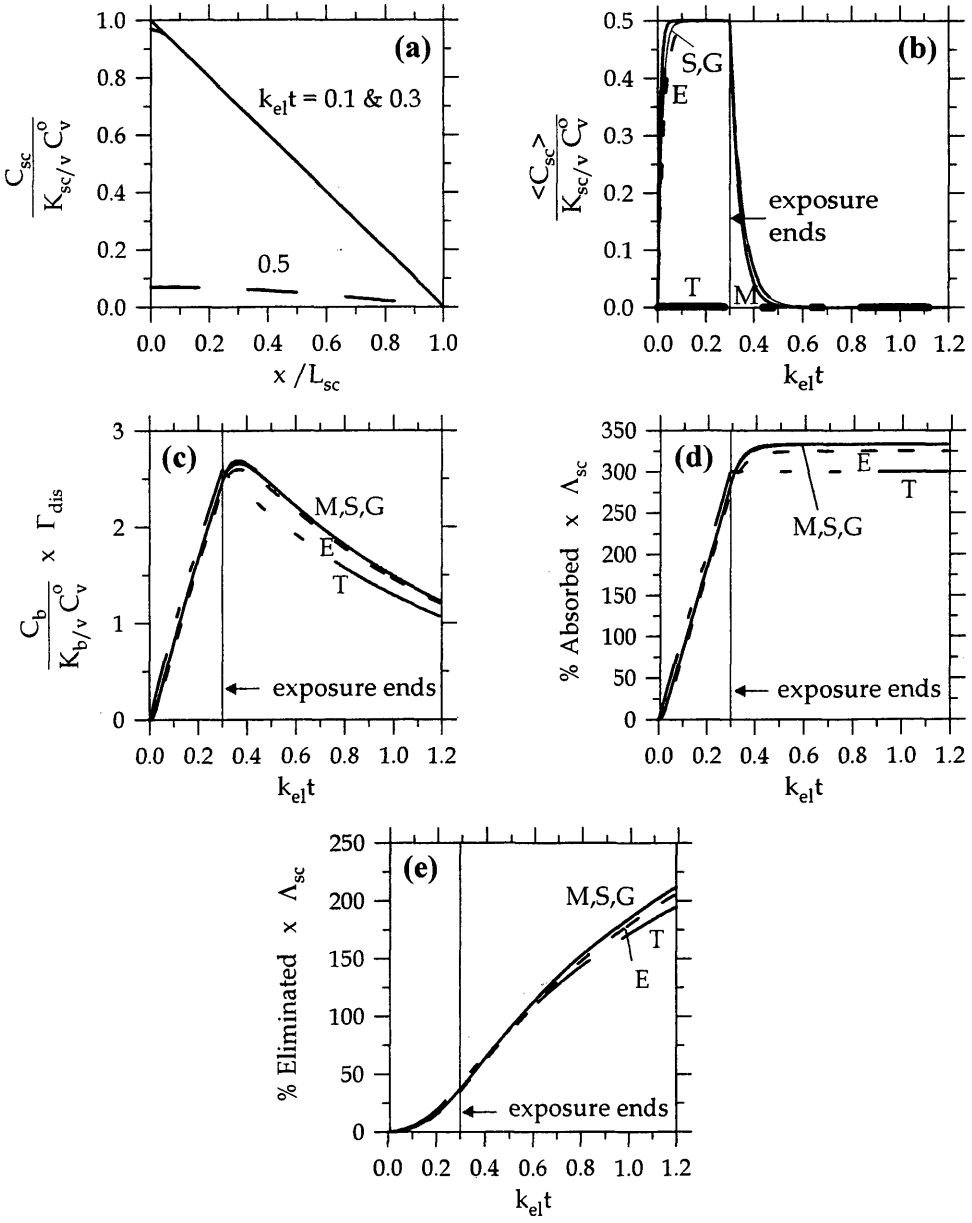

Figure 2B.4 – Case 4 results: normalized a) C_{sc} as a function of position in the sc for several $k_{el}t$, and b) $<C_{sc}>$, c) C_b, d) % of dose absorbed, and e) % of dose eliminated as a function of dimensionless time.

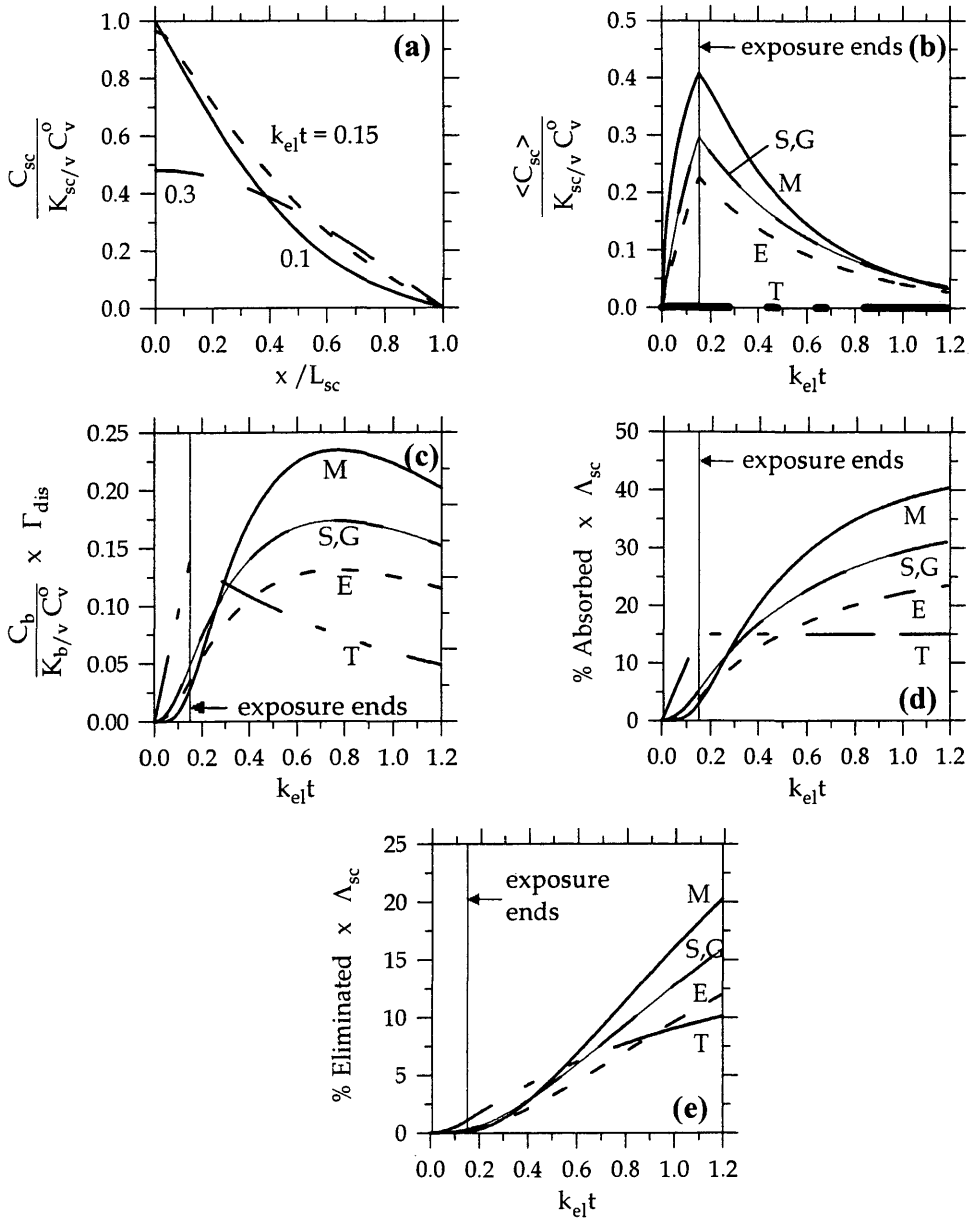

Figure 2B.5 – Case 5 results: normalized a) C_{sc} as a function of position in the sc for several $k_{el}t$, and b) $<C_{sc}>$, c) C_b, d) % of dose absorbed, and e) % of dose eliminated as a function of dimensionless time.

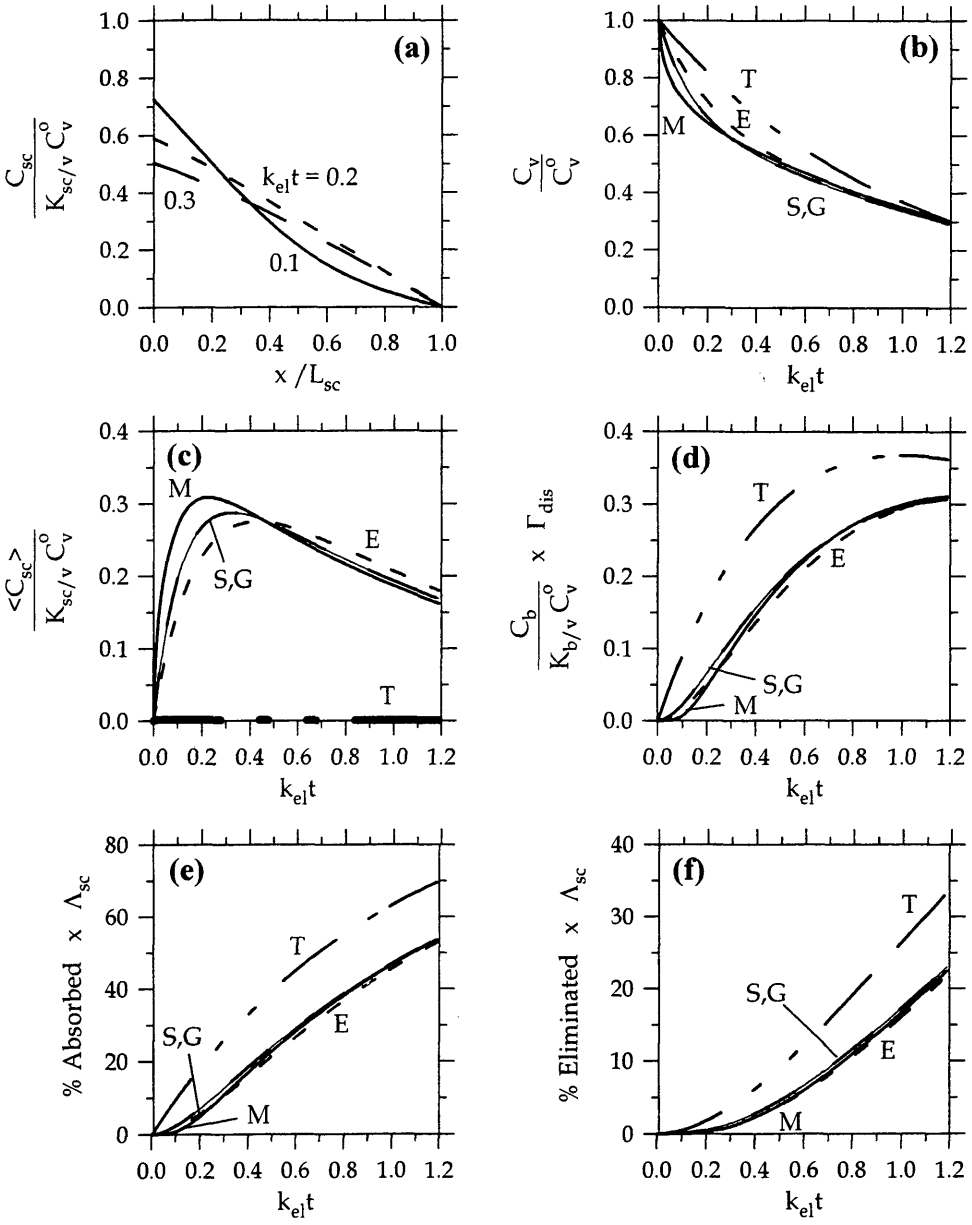

Figure 2B.6 – Case 6 results: normalized a) C_{sc} as a function of position in the sc for several $k_{el}t$, and b) C_v, c) $<C_{sc}>$, d) C_b, e) % of dose absorbed, and f) % of dose eliminated as a function of dimensionless time.

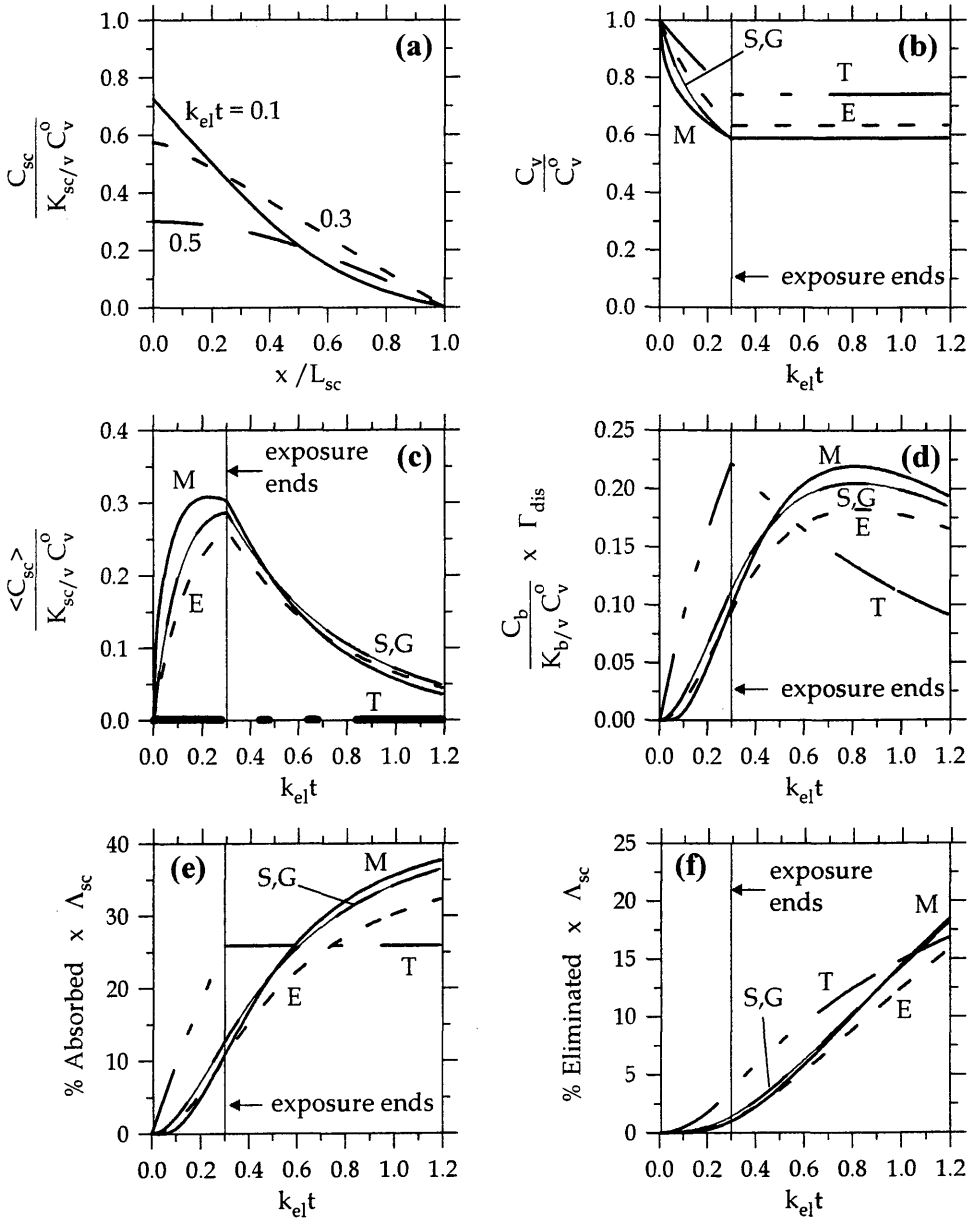

Figure 2B.7 – Case 7 results: normalized a) C_{sc} as a function of position in the sc for several $k_{el}t$, and b) C_v, c) $<C_{sc}>$, d) C_b, e) % of dose absorbed, and f) % of dose eliminated as a function of dimensionless time.

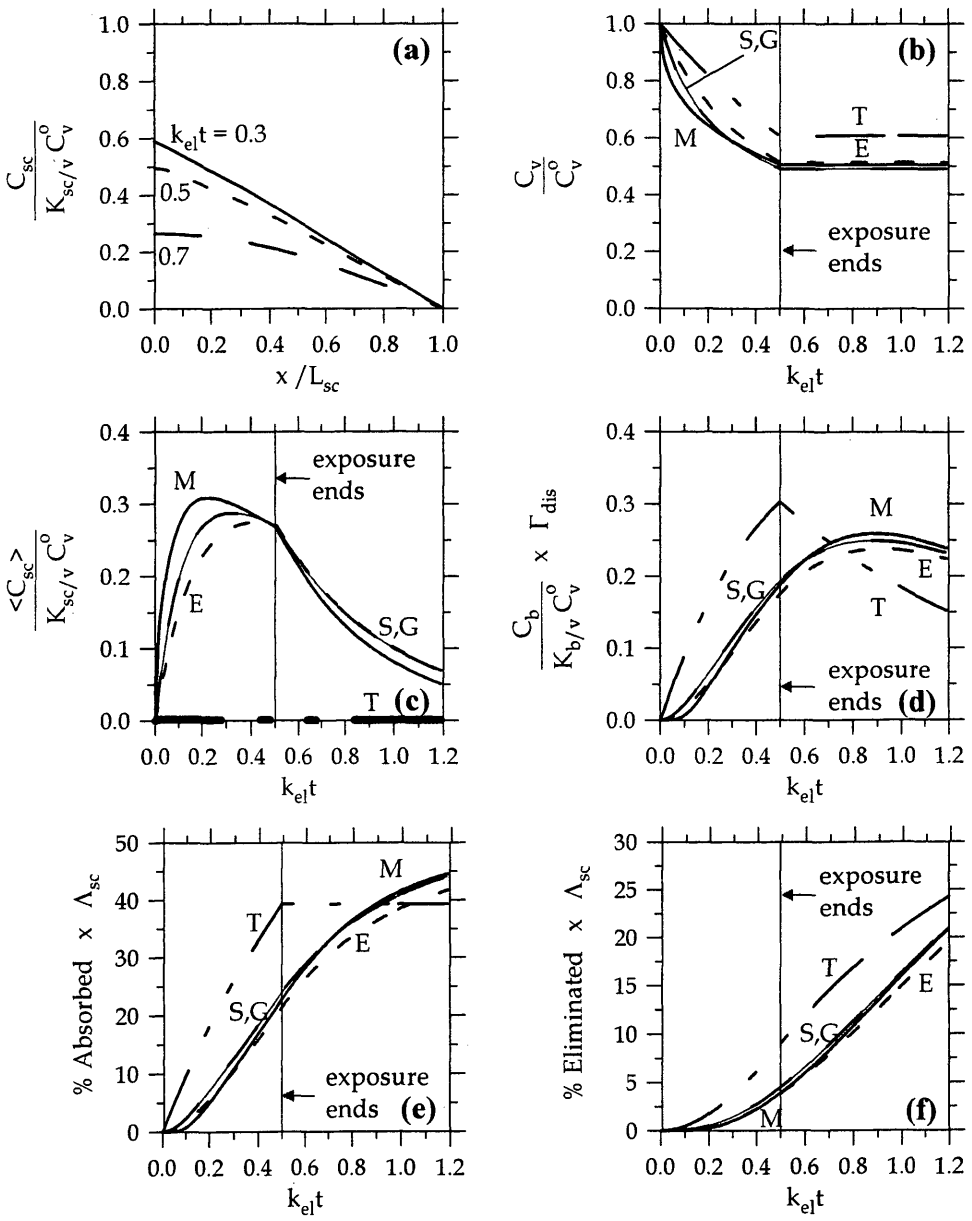

Figure 2B.8 – Case 8 results: normalized a) C_{sc} as a function of position in the sc for several $k_{el}t$, and b) C_v, c) $<C_{sc}>$, d) C_b, e) % of dose absorbed, and f) % of dose eliminated as a function of dimensionless time.

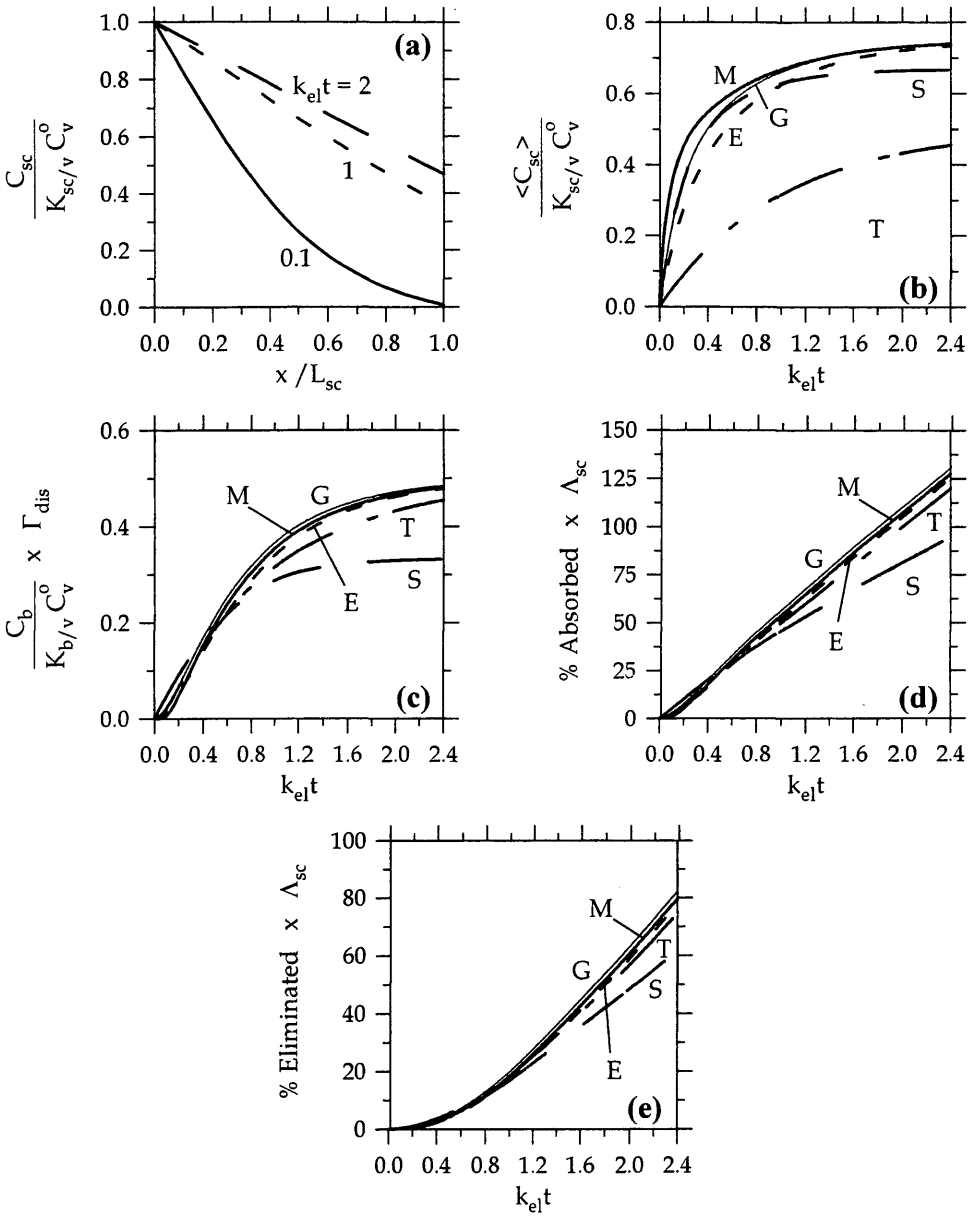

Figure 2B.9 – Case 9 results: normalized a) C_{sc} as a function of position in the sc for several $k_{el}t$, and b) $<C_{sc}>$, c) C_b, d) % of dose absorbed, and e) % of dose eliminated as a function of dimensionless time.

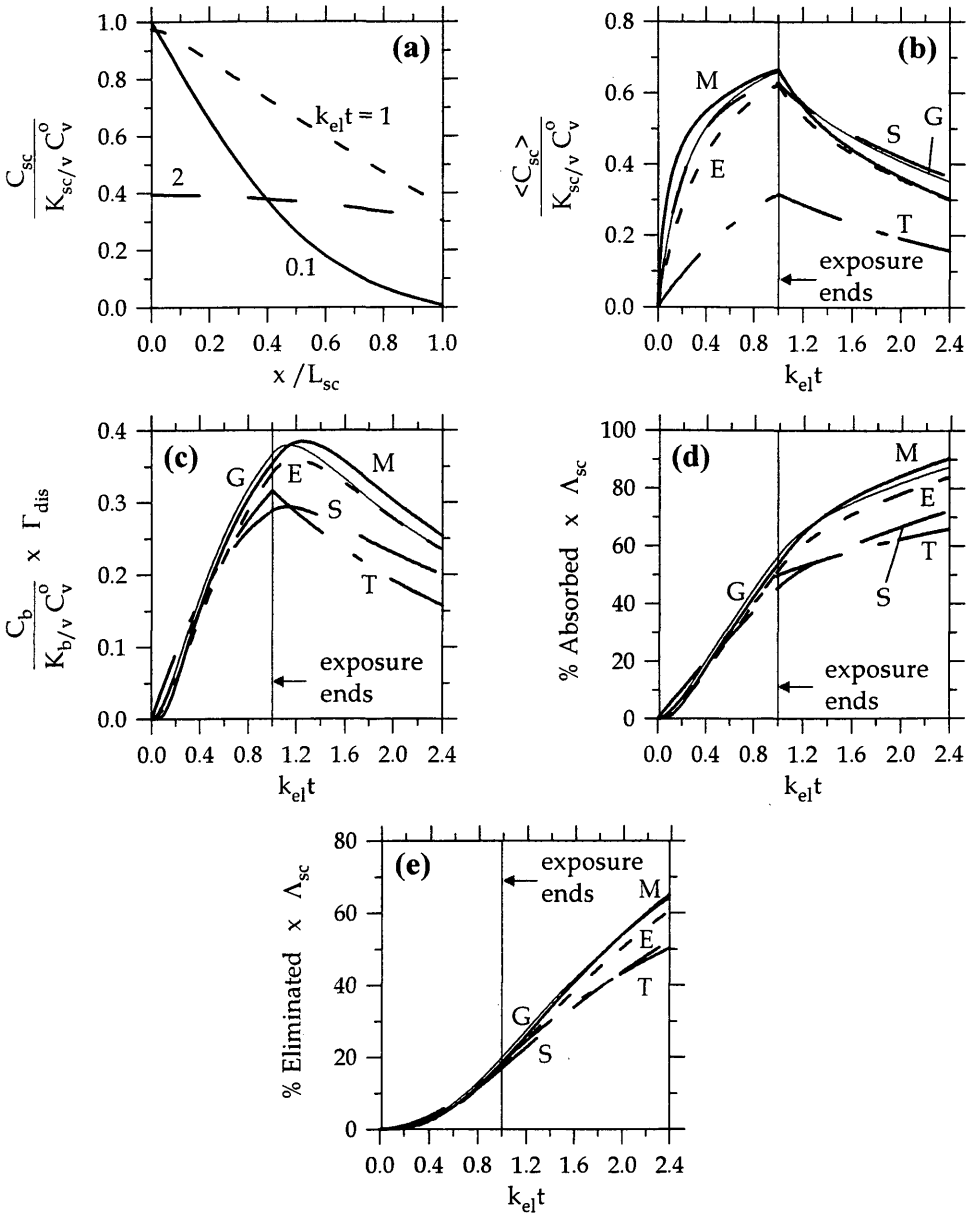

Figure 2B.10 – Case 10 results: normalized a) C_{sc} as a function of position in the sc for several $k_{el}t$, and b) $<C_{sc}>$, c) C_b, d) % of dose absorbed, and e) % of dose eliminated as a function of dimensionless time.

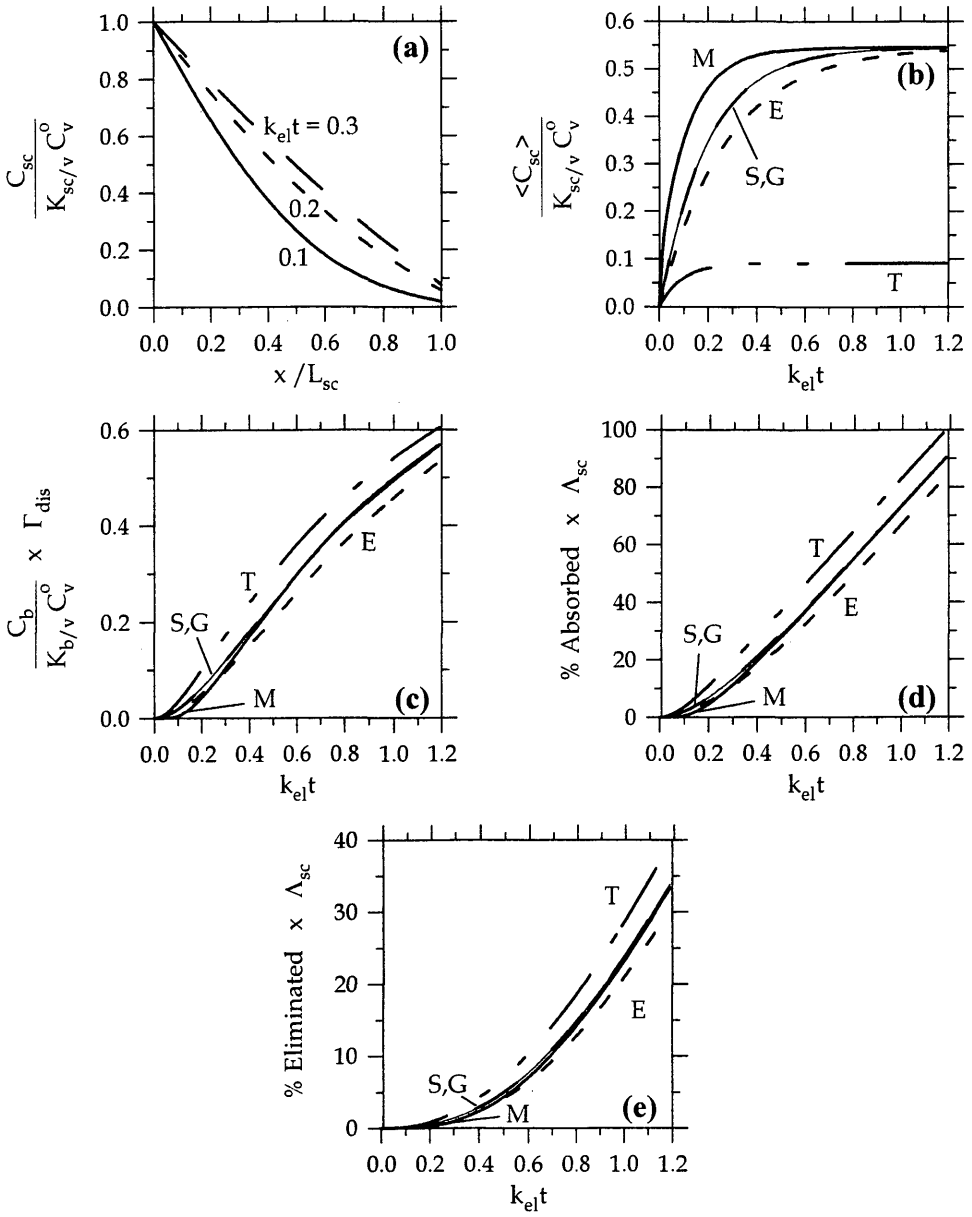

Figure 2B.11 – Case 11 results: normalized a) C_{sc} as a function of position in the sc for several $k_{el}t$, and b) $<C_{sc}>$, c) C_b, d) % of dose absorbed, and e) % of dose eliminated as a function of dimensionless time.

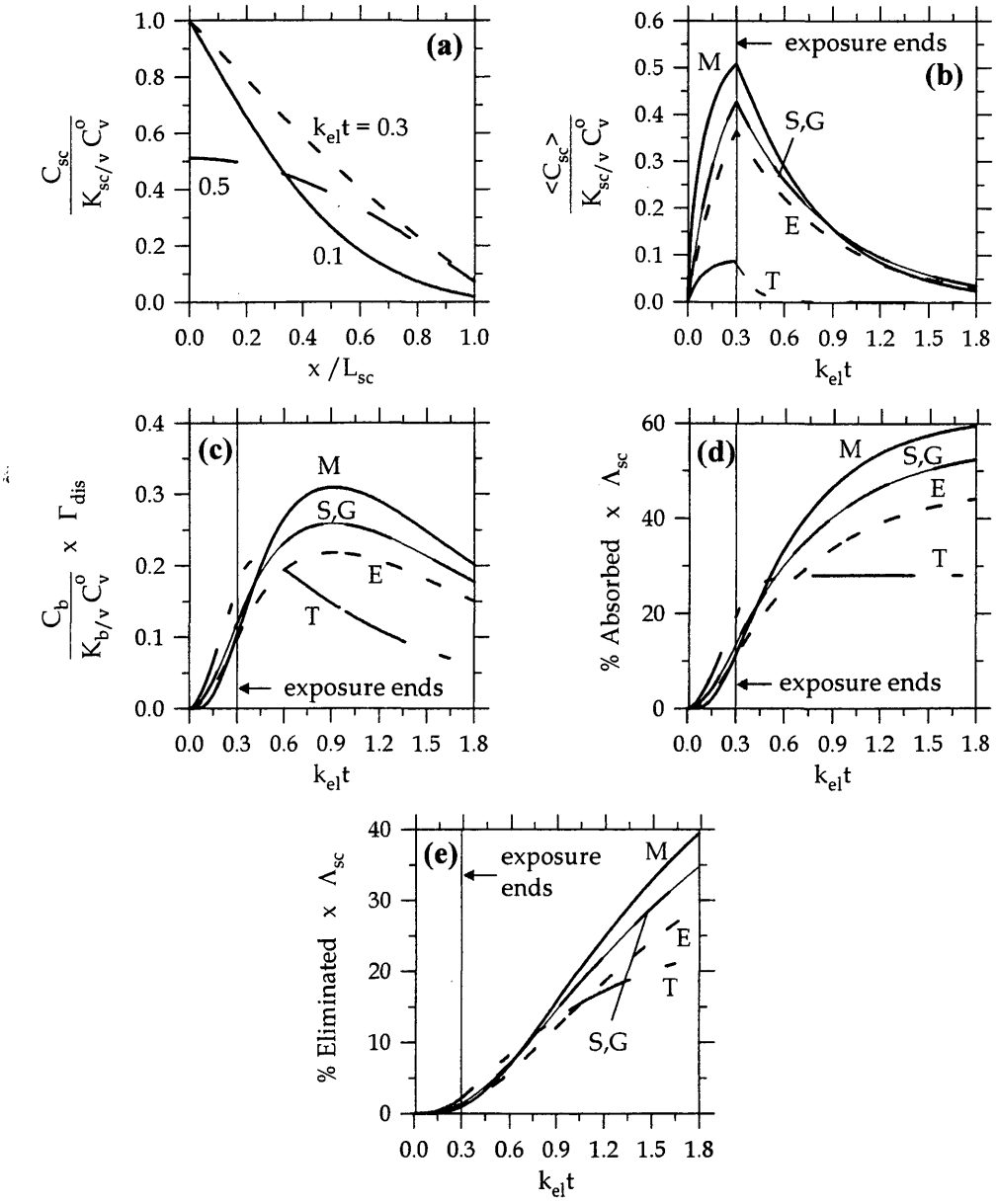

Figure 2B.12 – Case 12 results: normalized a) C_{sc} as a function of position in the sc for several $k_{el}t$, and b) $<C_{sc}>$, c) C_b, d) % of dose absorbed, and e) % of dose eliminated as a function of dimensionless time.

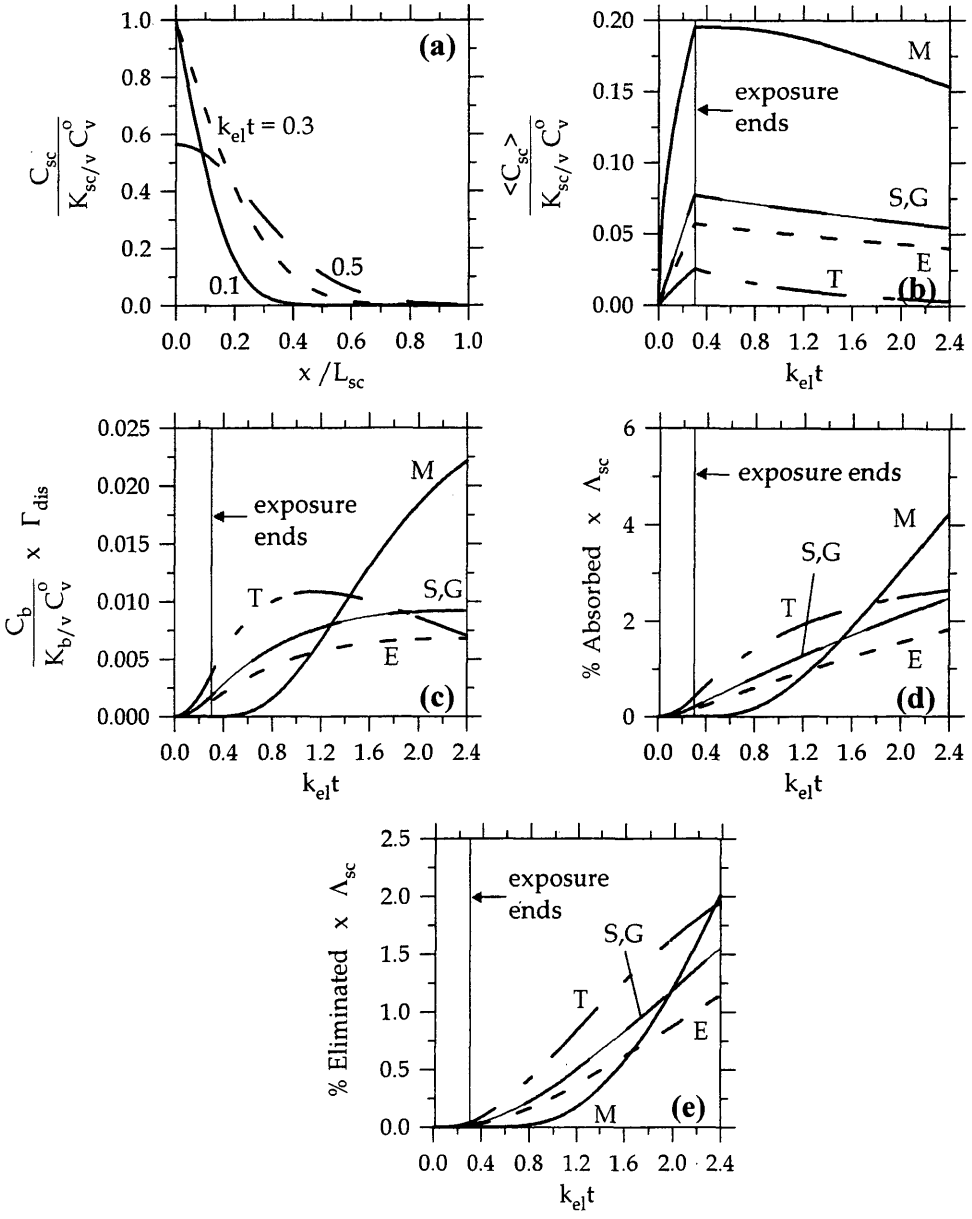

Figure 2B.13 – Case 13 results: normalized a) C_{sc} as a function of position in the sc for several $k_{el}t$, and b) $<C_{sc}>$, c) C_b, d) % of dose absorbed, and e) % of dose eliminated as a function of dimensionless time.

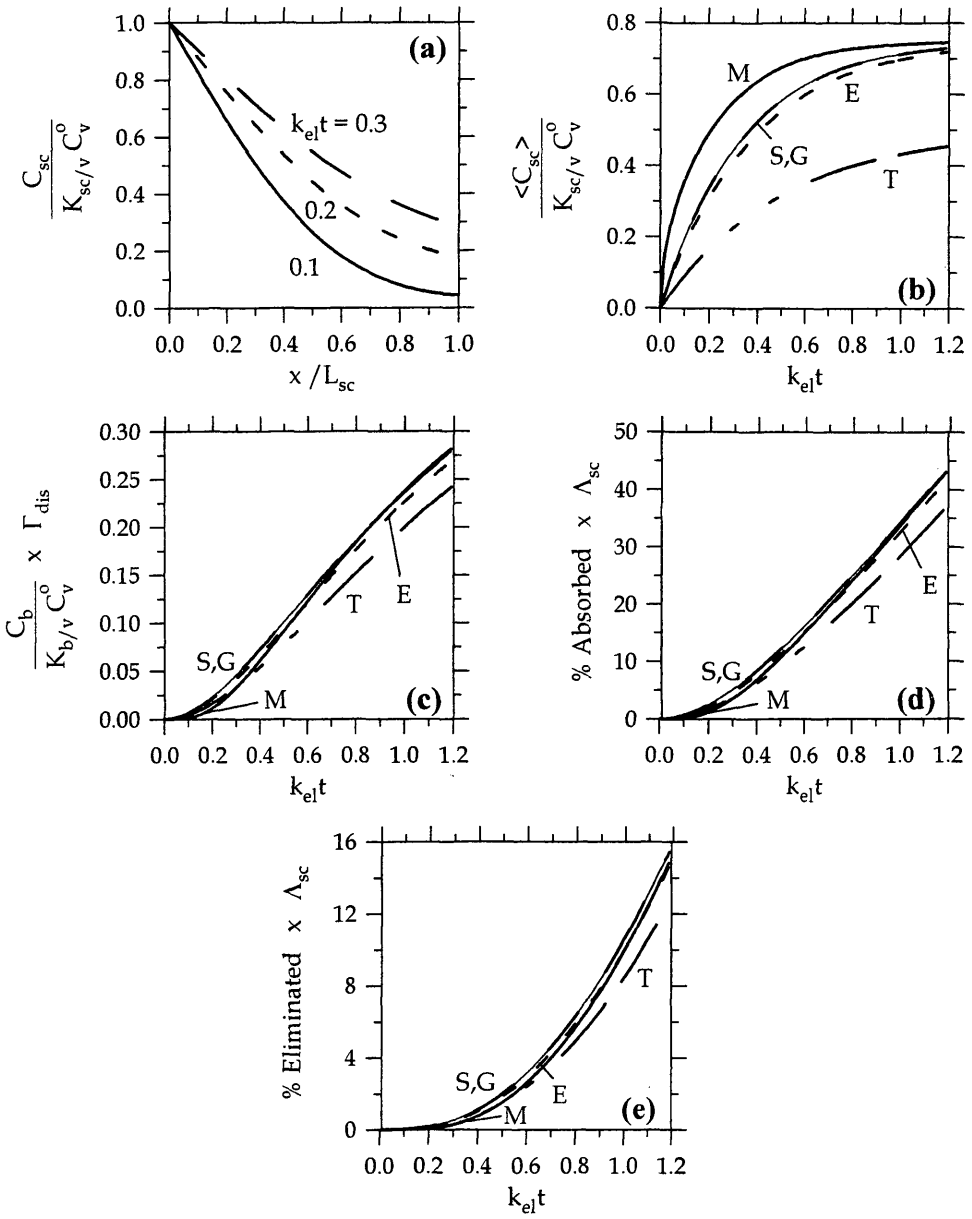

Figure 2B.14 – Case 14 results: normalized a) C_{sc} as a function of position in the sc for several $k_{el}t$, and b) $<C_{sc}>$, c) C_b, d) % of dose absorbed, and e) % of dose eliminated as a function of dimensionless time.

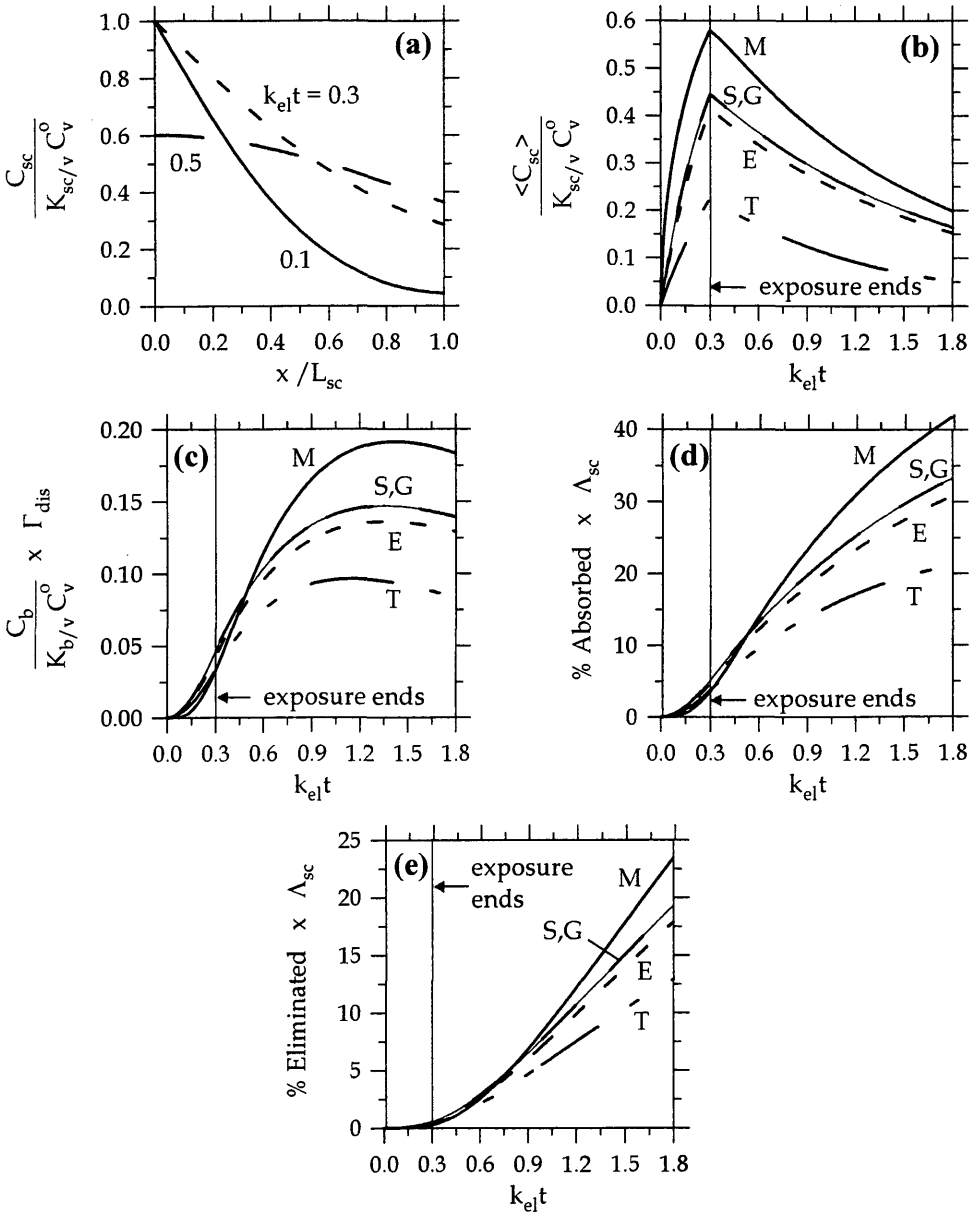

Figure 2B.15 – Case 15 results: normalized a) C_{sc} as a function of position in the sc for several $k_{el}t$, and b) $<C_{sc}>$, c) C_b, d) % of dose absorbed, and e) % of dose eliminated as a function of dimensionless time.

In cases 16 to 25, summarized in Table 2B.3, we examine the situation of chemical absorption into the skin from the blood following IV bolus delivery. The results also pertain to rapid absorption of chemical into the bloodstream from ingestion. Some of the cases have the skin exposed to an initially chemical-free vehicle (e.g., a bath), allowing chemical to pass through the skin into the vehicle. Exposure scenario 5 from the Results and Discussion, reported here as case 20, is an example of this situation. In other cases, the skin does not contact a vehicle and we assumed that the absorbing chemical was not volatile (i.e., there was no flux from the outside skin surface).

For cases 16 to 25, because chemical absorbs into the skin from the blood the relative blood volume (i.e., Γ_{dis}) has a different effect on dermal absorption than it has for cases 1 through 15. If the relative blood volume is large (e.g., case 16), the skin's capacity to hold chemical is small enough that the amount absorbed into the skin does not effect the blood concentration and decreases in the blood concentration are primarily due to elimination. In such a situation, all models predict the same blood concentration and rate of elimination because all models used the same pharmacokinetic model. In contrast, if the relative blood volume is small (e.g., case 17) the transfer of chemical into the skin can significantly reduce the amount of chemical in the blood, and thus the blood concentration and rate of elimination will depend on the model.

Cases 18 and 19 show the effects of limited blood flow rates when the relative blood volume is small. For these cases, as well as cases 16 and 17, we assumed that the skin was not in contact with a vehicle. Cases 20 and 22 through 25, however, examine situations in which chemical can transfer from the skin into a vehicle that is initially chemical free. Cases 20 and 22 to 24 have the skin in contact with a vehicle of large capacity. Cases 21 through 23 examine the effects of fast and slow rates of dermal absorption relative to the rate of elimination.

Table 2B.3 – Summary of dermal absorption cases involving absorption into skin from blood.

Case	Scenario Description	Relative Vehicle Volume $[\Lambda_{sc}]^a$	$C_v(t)$	Relative Blood Volume $[\Gamma_{dis}]^a$	$C_b(t)$	Relative Blood Flow Rate $[\alpha_{sc}]^a$	Relative Skin Penetration Rate $[D_{sc} / (k_{el} L_{sc}^2)]^a$	Is Vehicle Removed? $[k_{el}\, t_{exp}]^a$
16	absorption into skin does not affect blood concentration	no vehicle	not applicable	large (infinite source) [>15]	$\leq C_b^o \neq 0$	large [>20]	$t_{lag,sc} = 0.24\, t_{1/2}$ [1]	not applicable
17	absorption into skin affects blood concentration	no vehicle	not applicable	small (finite source) [1]	$\leq C_b^o \neq 0$	large [>20]	$t_{lag,sc} = 0.24\, t_{1/2}$ [1]	not applicable
18	limited blood flow rate	no vehicle	not applicable	small (finite source) [1]	$\leq C_b^o \neq 0$	medium [10]	$t_{lag,sc} = 0.24\, t_{1/2}$ [1]	not applicable
19	very limited blood flow rate	no vehicle	not applicable	small (finite source) [1]	$\leq C_b^o \neq 0$	small [1]	$t_{lag,sc} = 0.24\, t_{1/2}$ [1]	not applicable
20	chemical passes through skin into vehicle	large (infinite sink) [>45]	$\approx C_v^o = 0$	small (finite source) [1]	$\leq C_b^o \neq 0$	large [>20]	$t_{lag,sc} = 0.24\, t_{1/2}$ [1]	no, but $C_v \approx 0$ $[\infty]^b$

(continued)

Table 2B.2 (continued)

Case	Scenario Description	Relative Vehicle Volume $[\Lambda_{sc}]^a$	$C_v(t)$	Relative Blood Volume $[\Gamma_{dis}]^a$	$C_b(t)$	Relative Blood Flow Rate $[\alpha_{sc}]^a$	Relative Skin Penetration Rate $[D_{sc}/(k_{el}L_{sc}^2)]^a$	Is Vehicle Removed? $[k_{el}\, t_{exp}]^a$
21	slowly absorbing chemical	no vehicle	not applicable	small (finite source) [1]	$\leq C_b^o \neq 0$	large [>20]	$t_{lag,sc} = 2.4\, t_{1/2}$ [0.1]	not applicable
22	rapidly absorbing chemical passes from skin into vehicle	large (infinite sink) [>45]	$\approx C_v^o = 0$	small (finite source) [1]	$\leq C_b^o \neq 0$	large [>20]	$t_{lag,sc} = 0.024\, t_{1/2}$ [10]	no, but $C_v \approx 0$ $[\infty]^b$
23	slowly absorbing chemical passes from skin into vehicle	large (infinite sink) [>45]	$\approx C_v^o = 0$	small (finite source) [1]	$\leq C_b^o \neq 0$	large [>20]	$t_{lag,sc} = 2.4\, t_{1/2}$ [0.1]	no, but $C_v \approx 0$ $[\infty]^b$
24	chemical passes through skin into vehicle	large (infinite sink) [>45]	$\approx C_v^o = 0$	large (infinite source) [>15]	$\leq C_b^o \neq 0$	large [>20]	$t_{lag,sc} = 0.24\, t_{1/2}$ [1]	no, but $C_v \approx 0$ $[\infty]^b$
25	chemical passes through skin into vehicle	small (finite sink) [1]	$\geq C_v^o \neq 0$	large (infinite source) [>15]	$\leq C_b^o \neq 0$	large [>20]	$t_{lag,sc} = 0.24\, t_{1/2}$ [1]	no $[\infty]^b$

[a] Dimensionless group defining specified condition; when the value is reported as $> \gamma$, the effect on quantities calculated using model M (e.g., C_v, C_b, C_{sc}, and % of dose absorbed and eliminated) is < 5% for $(k_{el}t) \leq 2$ when the value is $> \gamma$.
[b] Infinite exposure time means the exposure lasts longer than the maximum time in the calculation (i.e., plotted).

Results for cases 16 through 25 include plots of the normalized average sc concentration, blood concentration, and percent of dose eliminated as a function of dimensionless time. For these cases, concentrations are normalized by C_b^o instead of C_v^o because the vehicle, if present, initially has a concentration of zero. Normalizing C_b by Γ_{dis} and the percent of dose eliminated by Λ_{sc} is not appropriate for these cases because chemical is absorbing from the blood. For cases where a vehicle was present (i.e., cases 20 and 22 through 25), a plot of the normalized vehicle concentration as a function of dimensionless time was also included. When the relative vehicle volume (i.e., Λ_{sc}) is large, the vehicle concentration remains very low (i.e., ~ 0), but normalizing by Λ_{sc} allows changes in C_v to be seen. Results for cases 16 through 25 are found in Figures 2B.16 through 2B.25. The legend shown in Table 2B.2 describes the curves and symbols corresponding to results for each model.

Several plots that were included for cases 1 through 15 were not included for cases 16 through 25. Plots of the concentration profile of chemical in the sc calculated using model M were not generated, but would have been different from those presented with cases 1 to 15 (i.e., initially C_{sc} would be zero at $x = 0$ and in local equilibrium with C_b at $x = L_{sc}$). Also, plots of the percent of dose absorbed were not included because the skin is exposed to chemical in the bloodstream.

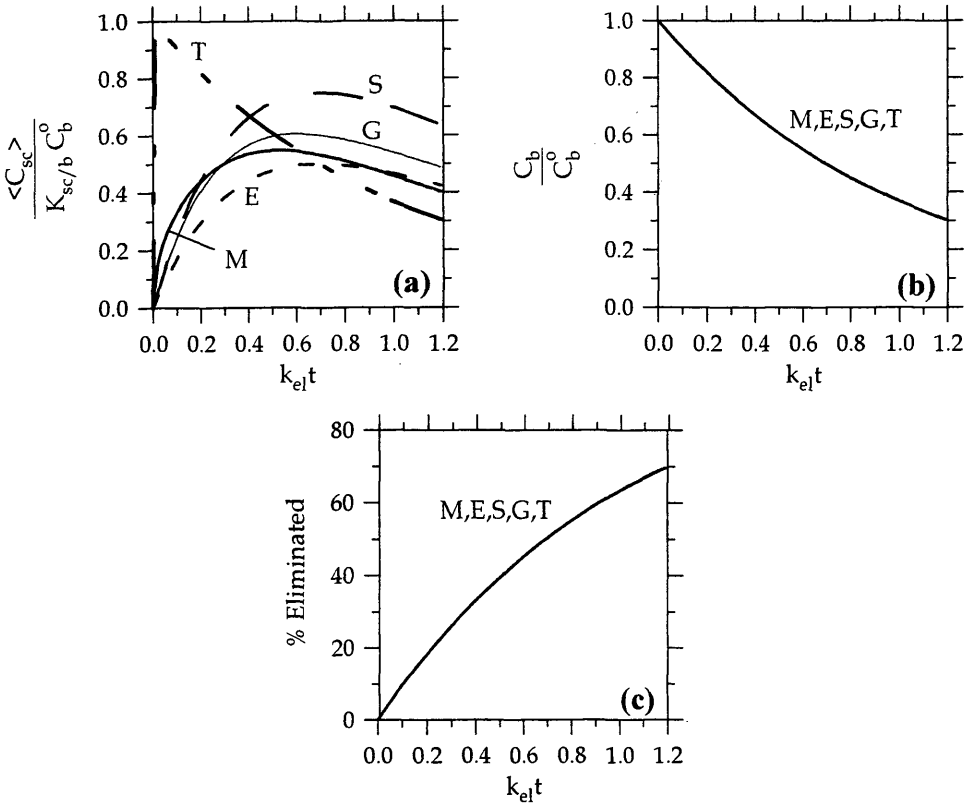

Figure 2B.16 – Case 16 results: normalized a) $<C_{sc}>$, b) C_b, and c) % of dose eliminated as a function of dimensionless time.

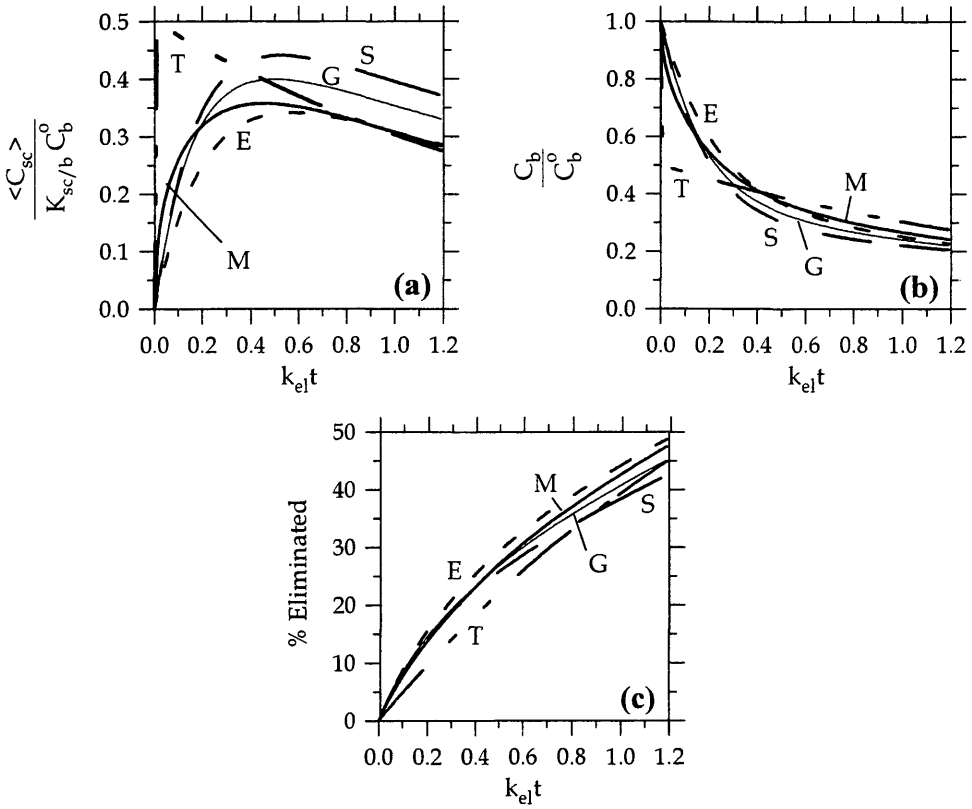

Figure 2B.17 – Case 17 results: normalized a) $<C_{sc}>$, b) C_b, and c) % of dose eliminated as a function of dimensionless time.

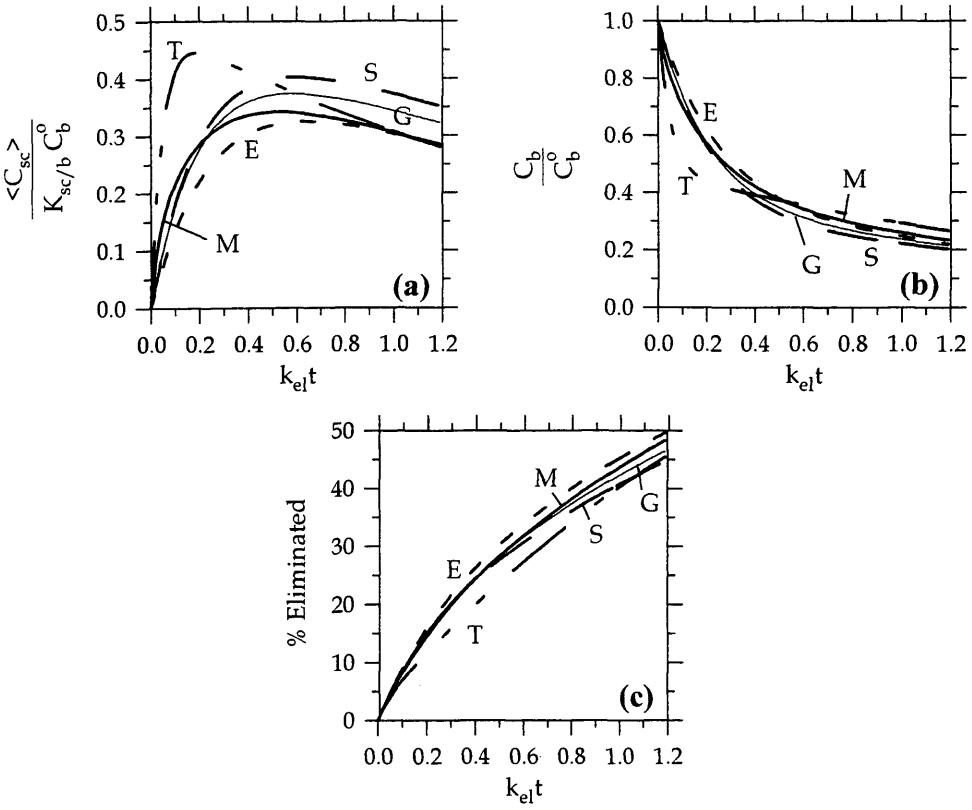

Figure 2B.18 – Case 218 results: normalized a) $<C_{sc}>$, b) C_b, and c) % of dose eliminated as a function of dimensionless time.

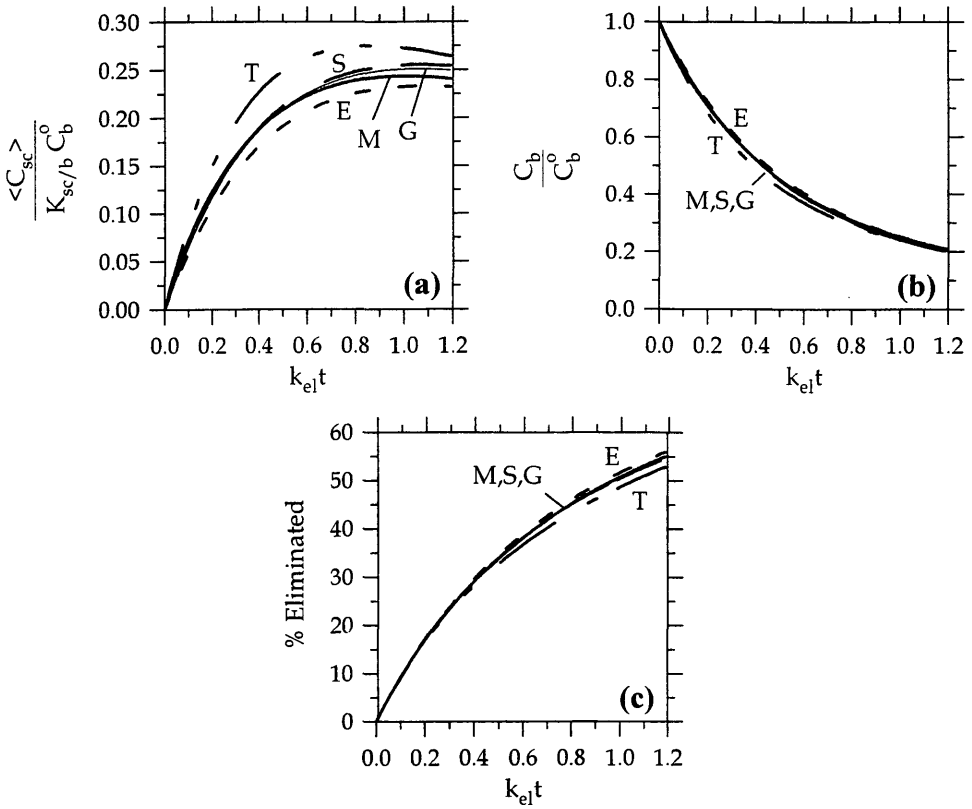

Figure 2B.19 – Case 19 results: normalized a) $<C_{sc}>$, b) C_b, and c) % of dose eliminated as a function of dimensionless time.

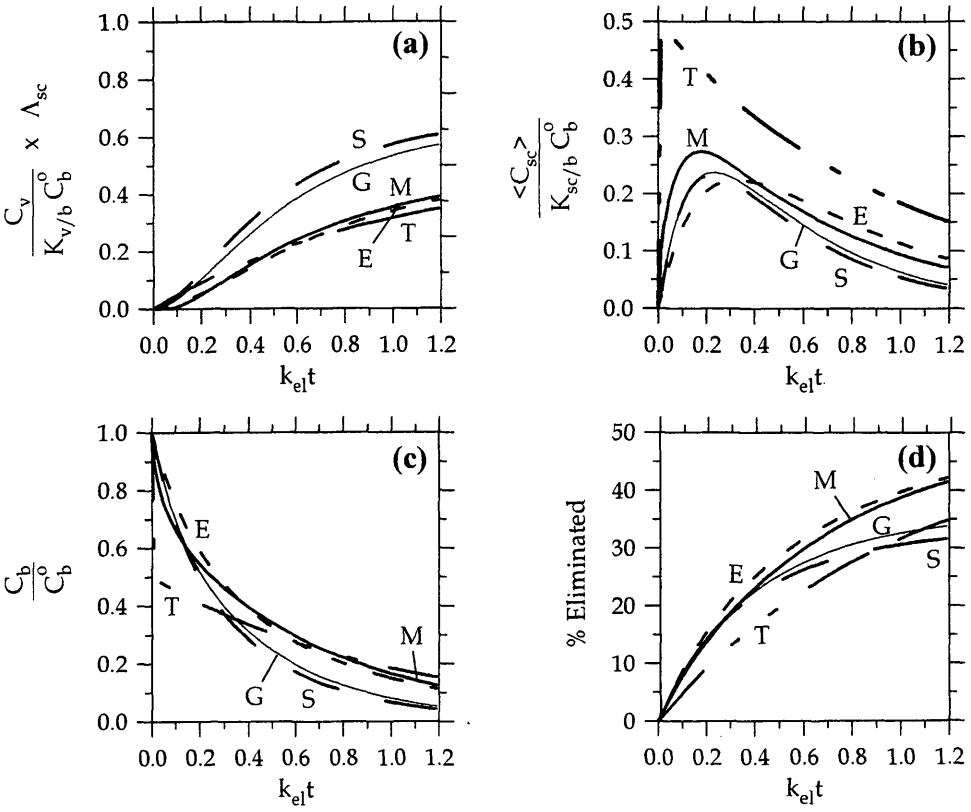

Figure 2B.20 – Case 20 results: normalized a) C_v, b) $<C_{sc}>$, c) C_b, and d) % of dose eliminated as a function of dimensionless time.

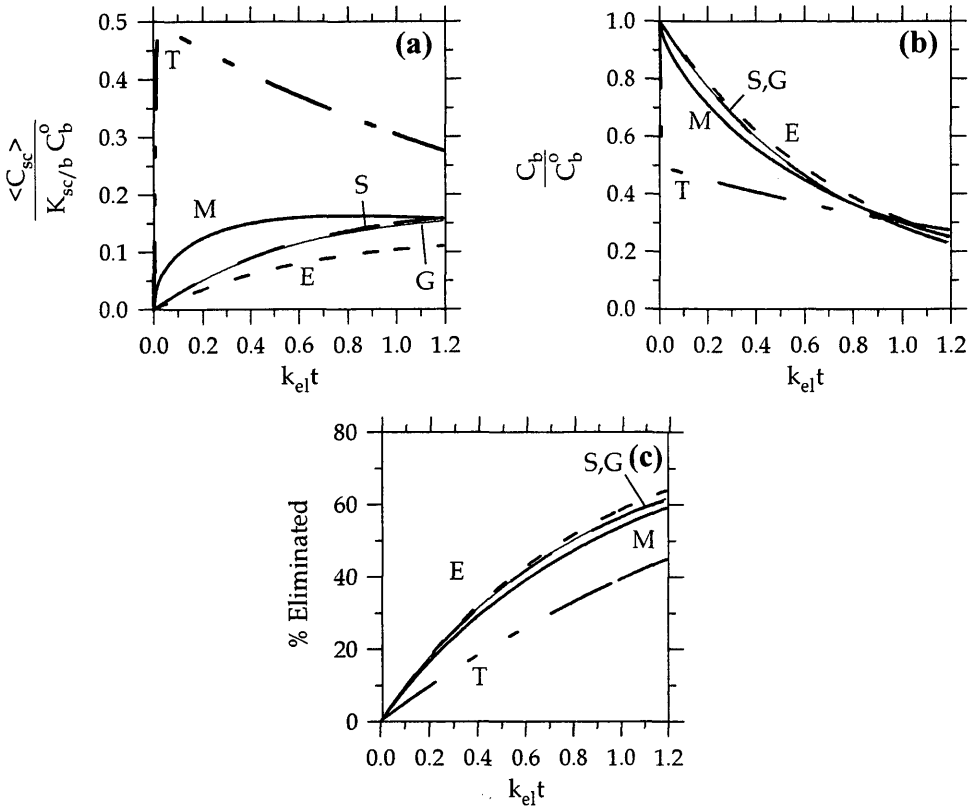

Figure 2B.21 – Case 21 results: normalized a) $<C_{sc}>$, b) C_b, and c) % of dose eliminated as a function of dimensionless time.

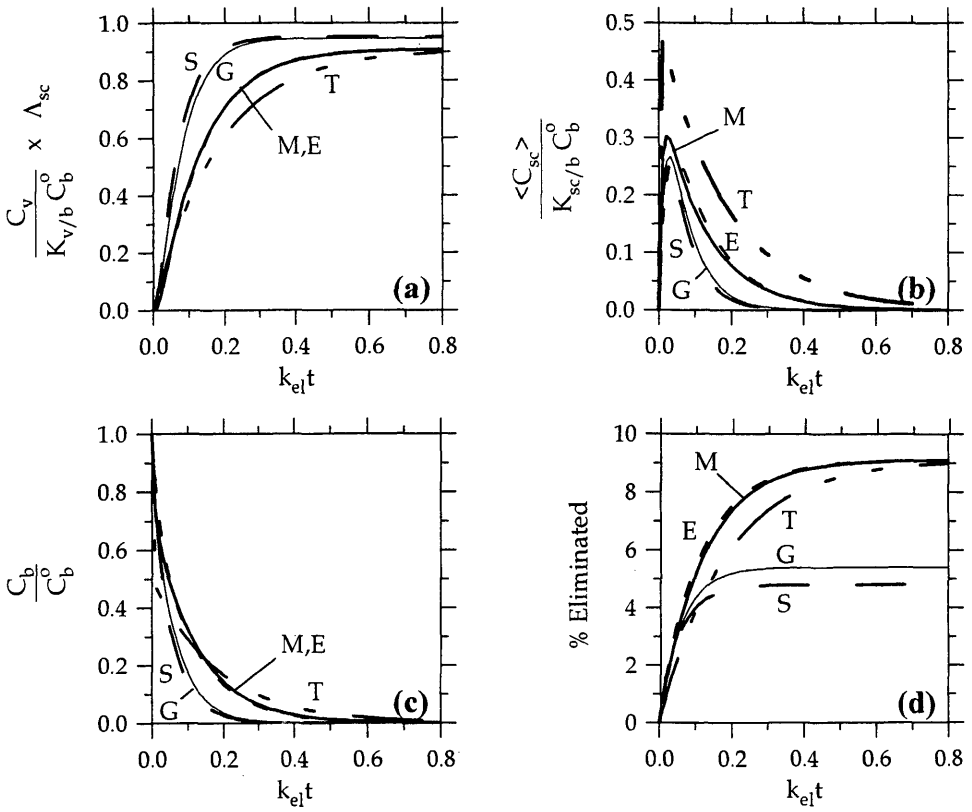

Figure 2B.22 – Case 22 results: normalized a) C_v, b) $<C_{sc}>$, c) C_b, and d) % of dose eliminated as a function of dimensionless time.

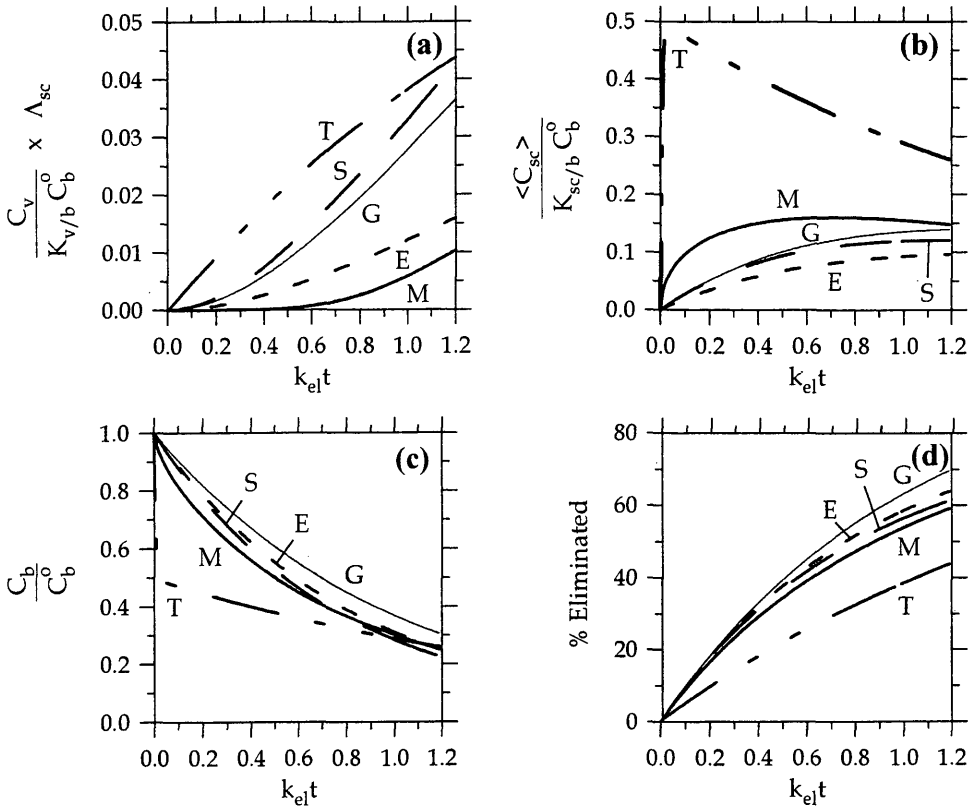

Figure 2B.23 – Case 23 results: normalized a) C_v, b) $<C_{sc}>$, c) C_b, and d) % of dose eliminated as a function of dimensionless time.

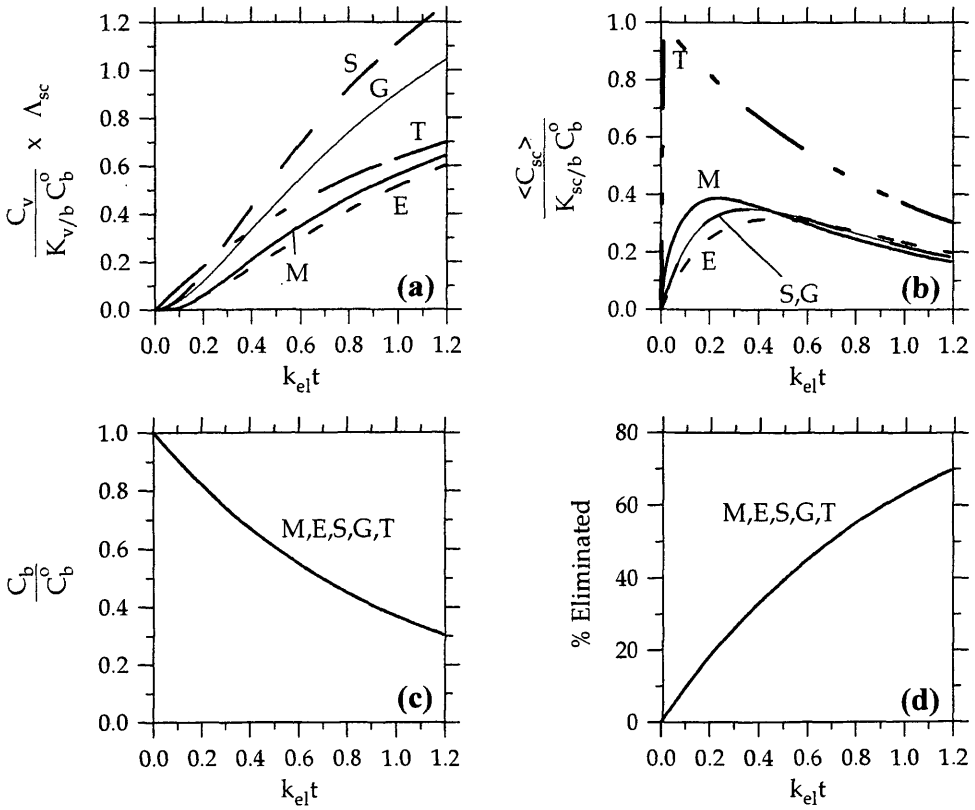

Figure 2B.24 – Case 24 results: normalized a) C_v, b) $<C_{sc}>$, c) C_b, and d) % of dose eliminated as a function of dimensionless time.

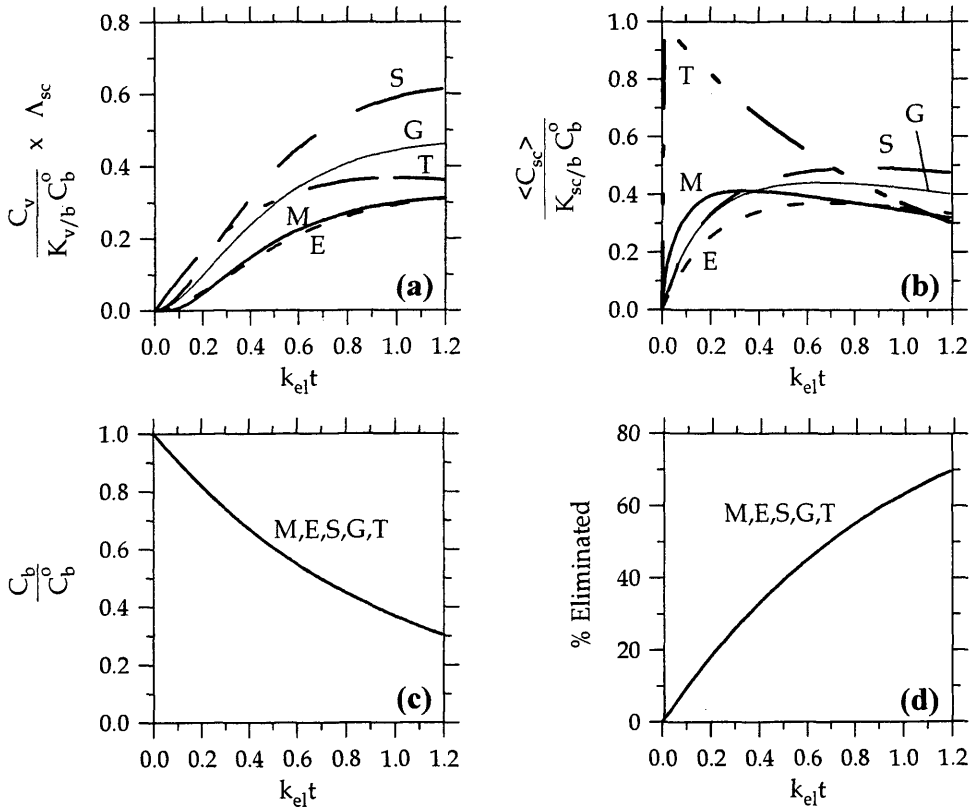

Figure 2B.25 – Case 25 results: normalized a) C_v, b) $<C_{sc}>$, c) C_b, and d) % of dose eliminated as a function of dimensionless time.

In the last type of situation, repeated dermal exposures were examined. Specifically, cases 26 through 31, summarized in Table 2B.4, illustrate the situation in which a vehicle is applied to and removed from the skin three times. The exposure times and the interval between exposures are held constant. Cases 26 through 29 demonstrate the effects of different exposure times. Cases 30 and 31 examine chemicals that penetrate rapidly or slowly relative to the rate of elimination.

Results for cases 26 through 31, shown in Figures 2B.26 through 2B.31, include plots of normalized average sc concentration, blood concentration, and percent of dose absorbed and eliminated as functions of dimensionless time. Plots for the concentration profile in the membrane for model M were not generated. Results for models S and G were the closest to model M results for cases 26 through 31 because these calculations were performed using assumptions consistent with those used for the development of model S and G. Model T results deviated the most from model M results for all these case, because when exposures end the chemical in the sc continues to penetrate, but Model T does not correctly represent the capacity of the sc to hold chemical.

For cases 26, 27, 29 and 31, at least one compartment model can adequately represent model M. For cases 26 and 27, models S and G reasonably predicted model M results. For case 29, with long exposures, and case 31, with a rapidly absorbing chemical, differences between results for model M and all compartment models were small. For short times relative to $t_{lag,sc}$, compartment model predictions of model M are the most different. For repeat exposures that period occurs several times, compounding the effect. Case 28 demonstrates that for short repeated exposures, compartment models can significantly deviate from membrane model predictions. Likewise, case 30 illustrates that compartment models might not be a good choice to represent model M response for exposures to slowly penetrating chemicals. For chemicals with a large $t_{lag,sc}$ relative to t_{exp}, a membrane model is a better choice for approximating dermal absorption than a compartment model.

Table 2B.4 – Summary of dermal absorption cases involving repeated exposures.[a]

Case	Scenario Description	Relative Skin Penetration Rate $[D_{sc} / (k_{el} L_{sc}^2)]^b$	Description of Exposure[c]	
			δ $[k_{el} t]^b$	Δ $[k_{el} t]^b$
26	repeated exposures	$t_{lag,sc} = 0.24\ t_{1/2}$ [1]	[0.3]	[0.6]
27	period of time between exposures is shortened	$t_{lag,sc} = 0.24\ t_{1/2}$ [1]	[0.3]	[0.3]
28	exposures are shorter	$t_{lag,sc} = 0.24\ t_{1/2}$ [1]	[0.15]	[0.45]
29	exposures are longer	$t_{lag,sc} = 0.24\ t_{1/2}$ [1]	[0.7]	[0.6]
30	slowly absorbing chemical	$t_{lag,sc} = 2.4\ t_{1/2}$ [0.1]	[0.3]	[0.6]
31	rapidly absorbing chemical	$t_{lag,sc} = 0.024\ t_{1/2}$ [10]	[0.3]	[0.6]

[a] For case 26 through 31 calculations, we assumed the vehicle is an infinite source (i.e., $\Lambda_{sc} > 45$), the blood is an infinite sink (i.e., $\Gamma_{dis} > 15$) and there are no mass transfer limitations due to inadequate blood flow (i.e., $\alpha_{sc} > 20$). [b] Dimensionless group defining the specified condition. [c]

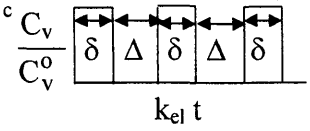

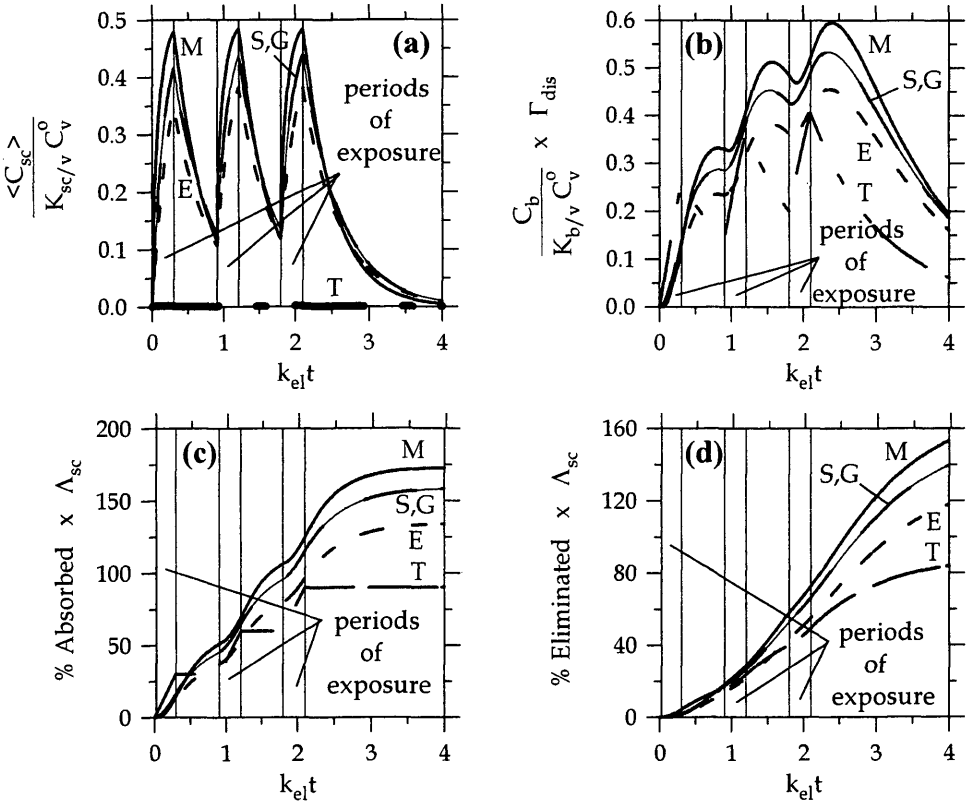

Figure 2B.26 – Case 26 results: normalized a) $<C_{sc}>$, b) C_b, c) % of dose absorbed, and d) % of dose eliminated as a function of dimensionless time.

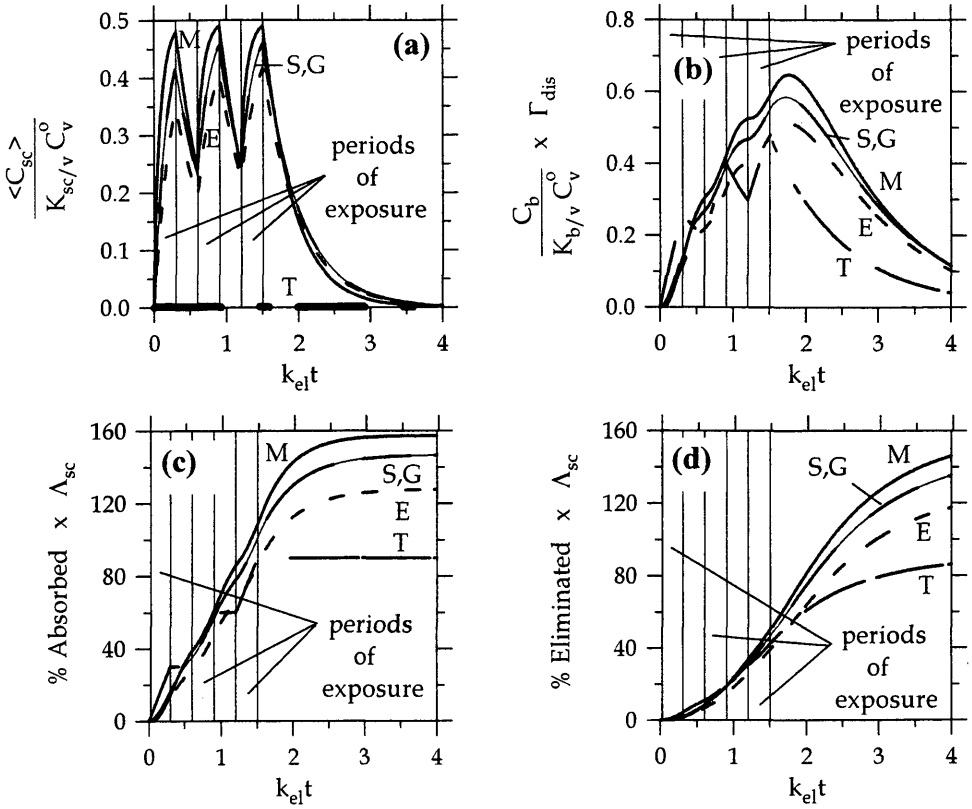

Figure 2B.27 – Case 27 results: normalized a) $<C_{sc}>$, b) C_b, c) % of dose absorbed, and d) % of dose eliminated as a function of dimensionless time.

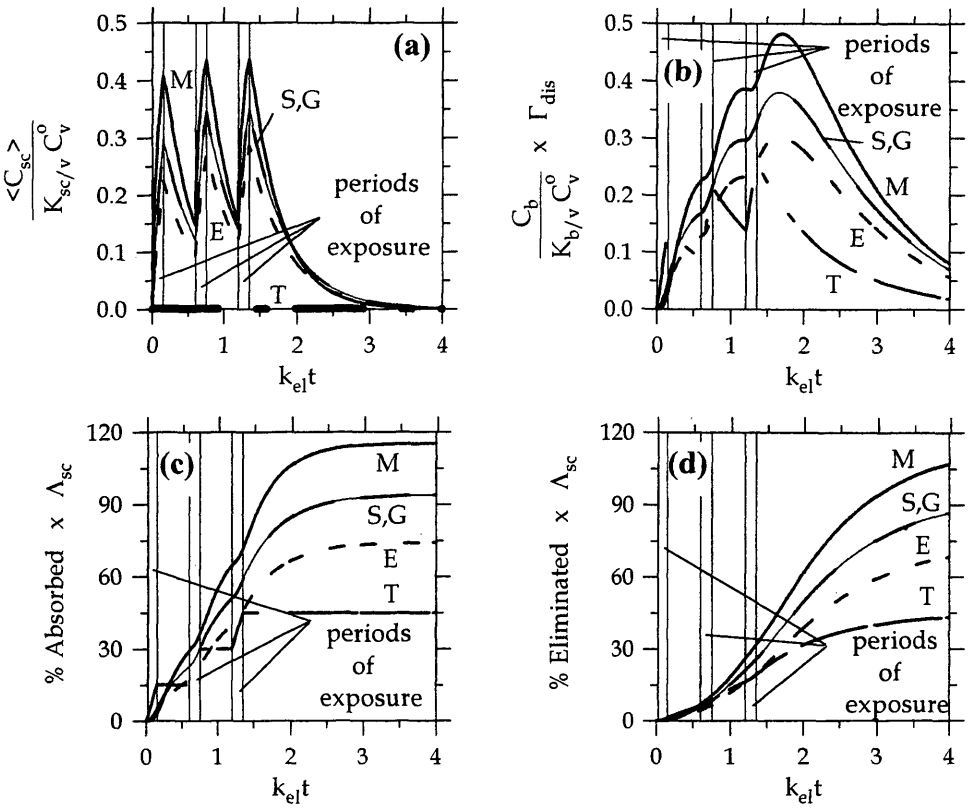

Figure 2B.28 – Case 28 results: normalized a) $<C_{sc}>$, b) C_b, c) % of dose absorbed, and d) % of dose eliminated as a function of dimensionless time.

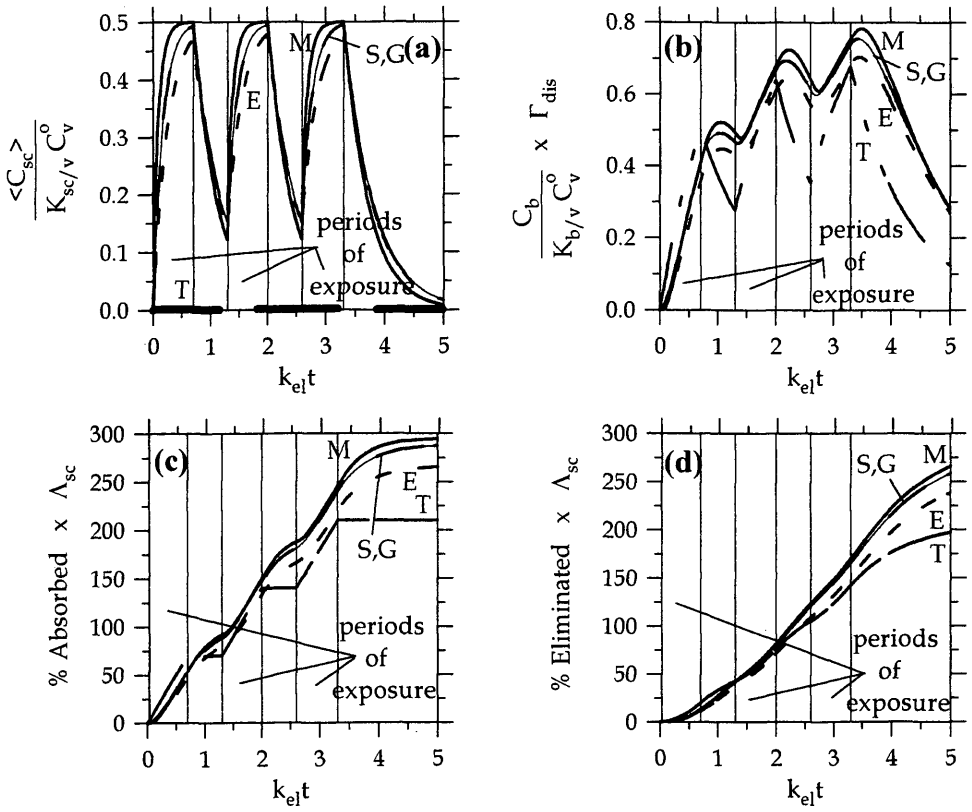

Figure 2B.29 – Case 29 results: normalized a) $<C_{sc}>$, b) C_b, c) % of dose absorbed, and d) % of dose eliminated as a function of dimensionless time.

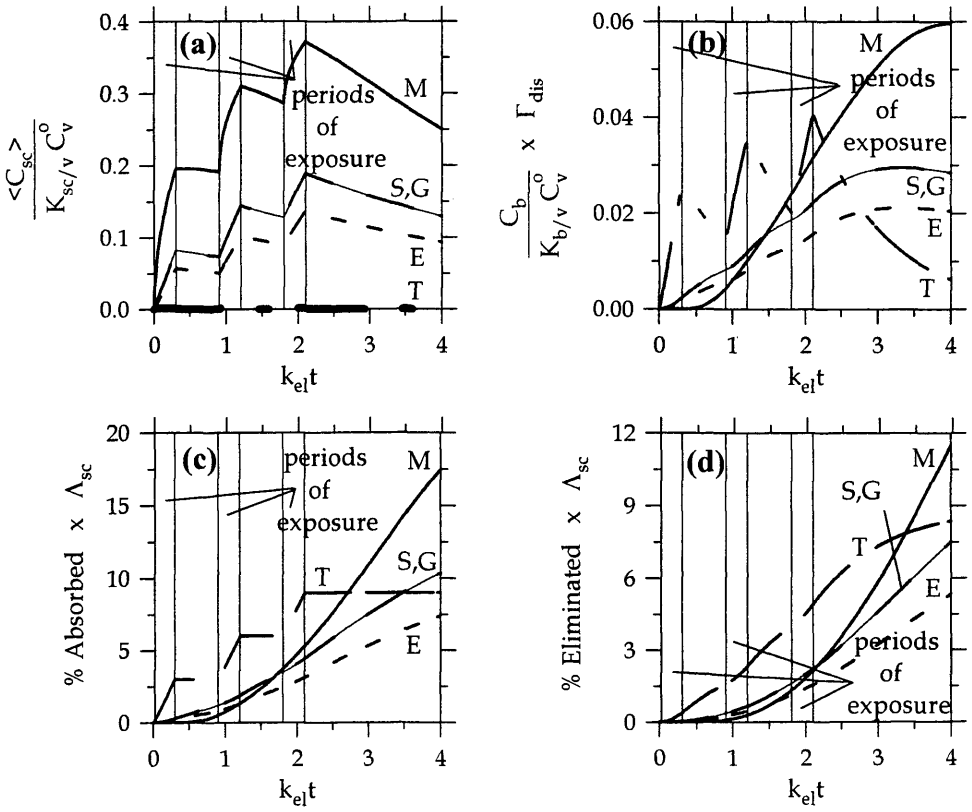

Figure 2B.30 – Case 30 results: normalized a) $<C_{sc}>$, b) C_b, c) % of dose absorbed, and d) % of dose eliminated as a function of dimensionless time.

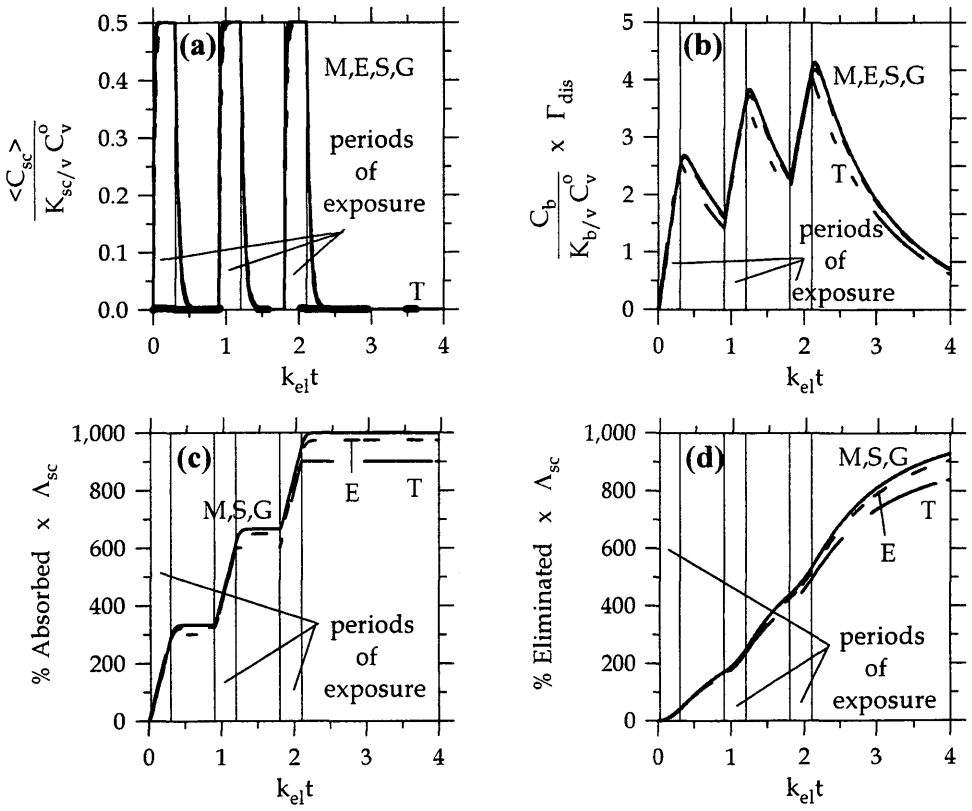

Figure 2B.31 – Case 31 results: normalized a) $<C_{sc}>$, b) C_b, c) % of dose absorbed, and d) % of dose eliminated as a function of dimensionless time.

Appendix 2C – FORTRAN Program

Table 2C.1 lists the names of variables in the following program. The program needs to be compiled so that the IVPAG subroutine in the IMSL library can be accessed.

Table 2C.1 – Variable names in the FORTRAN program.

variable in program	variable in chapter
T	$k_{el}\, t$
N	N + 3 (i.e., the number of nodes in the sc plus three)
Y(1)	C_v / C_v^o
Y(i), i = 2 to N-2	$C_{sc} / (K_{sc/v} C_v^o)$ at node position i
Y(N-1)	$C_b / (K_{b/v} C_v^o)$
Y(N)	variable to keep track of cumulative mass eliminated
YPRIME(N)	spatial derivative of Y calculated with finite differencing
AVESC	$< C_{sc} > /(K_{sc/v} C_v^o)$
LAMBDA1	Λ_{sc}
RATIO	$1 / \Gamma_{dis}$
AL	α_{sc}
TFINAL	dimensionless time ($k_{el}\, t$) that simulation ends
TCON	$k_{el}\, t_{exp}$ (if TCON > TFINAL, exposure does not end)
PDA	percent of dose absorbed
PDE	percent of dose eliminated
PDSC	percent of dose in the sc
OM	$D_{sc} / (k_{el} L_{sc}^2)$
DZ	dimensionless distance between nodes
MB	variable for mass balance (remains ~ 0 for adequate solution)

```
      PROGRAM CHAP2
```

```
      INTEGER NPARAM, N
C ********** N = number of sc nodes plus 3 and must be even.
      PARAMETER (NPARAM = 50, N = 102)
      INTEGER IDO, NOUT
      REAL PARAM(NPARAM),T,TEND,TOL,Y(N),A(1,1),IEND,MB
      REAL TFINAL,AVESC,LAMBDA1,RATIO,PDA,PDE,PDSC,PDTOT

C ********** SPECIFICATIONS FOR SUBROUTINES
      EXTERNAL IVPAG, SSET, UMACH
      EXTERNAL FCN, FCNJ
      CALL SSET(NPARAM, 0.0, PARAM, 1)

      OPEN (1, FILE='data.dat', STATUS = 'NEW')
      OPEN (2, FILE='data2.dat', STATUS = 'NEW')

C ********** SETTINGS FOR THE IVPAG SUBROUTINE
      PARAM(4) = 5000000
      PARAM(12) = 2
      PARAM(10) = 1.

C ********** SETTING INITIAL CONDITIONS
      IDO = 1
      T = 0.0
      Y(1) = 1.0
      Y(2) = Y(1)
      DO 111, I = 3,(N)
  111 Y(I) = 0.0

C ********** SETTING ERROR TOLERANCE
      TOL = 1.0E-6
      CALL UMACH (2, NOUT)
      WRITE (NOUT,99998)

C ********** SET LAMBDA1 (Λ_SC) AND RATIO (1/Γ_DIS)
      LAMBDA1 = 100000.
      RATIO = 0.1
      TFINAL = 1.0001
      IEND = 0.0
 10   CONTINUE
C ********** NUMBER ADDED TO IEND SETS HOW OFTEN VALUES ARE REPORTED
      IEND = IEND + 0.01
      TEND = IEND
      CALL IVPAG (IDO,N,FCN,FCNJ,A,T,TEND,TOL,PARAM,Y)
      PDA = 0.
      AVESC = 0.
      AVESC = Y(2) + Y(N-2)
      DO 65 J = 2, ((N-4)/2)
 65      AVESC = AVESC + (2.0*Y(2*J))
      DO 75 J = 1, ((N-4)/2)
 75      AVESC = AVESC + (4.0*Y(2*J+1))
      AVESC = AVESC * 1.0/3.0/REAL(N-4)
      PDA = (Y(N-1)+Y(N))/RATIO/LAMBDA1*100.
      PDE = Y(N)/RATIO/LAMBDA1*100.
      PDSC = AVESC / LAMBDA1 * 100.
```

```
      PDTOT = PDSC + PDA
      MB = Y(1)+(AVESC + (Y(N-1)+Y(N))/RATIO)/LAMBDA1
      MB = 1.0 - MB
      IF (IEND .LE. TFINAL) THEN
          WRITE (1,99999) T,PDTOT,Y(N-1)
          WRITE (2,99999) T,Y(1),Y(N-1),AVESC,PDA,PDE,MB
          IF (IEND .GE. TFINAL) IDO = 3
          GO TO 10
      END IF
99998 FORMAT(11X, 'T', 14X, 'Y')
99999 FORMAT(7E10.4)
99997 FORMAT(2E10.4)
      END

      SUBROUTINE FCN (N, T, Y, YPRIME)
      INTEGER N
      REAL X,Y(N),YPRIME(N),AL,OM,LAM1,RAT,DZ,DZS,TCON

C ********** SET LAM1 AND RAT TO MATCH LAMBDA1 AND RATIO
      AL = 1000.0
      OM = 1.0
      LAM1 = 100000.0
      TCON = 10.3
      RAT = 0.1
      DZ = 1. / (REAL(N) - 4.)
      DZS = DZ * DZ

      YPRIME(1) = 0
      IF (T .LT. TCON) THEN
         YPRIME(1)=OM/LAM1*(-3.*Y(2)+4.*Y(3)-Y(4))/2./DZ
      END IF
      DO 222, J = 3,(N-3)
  222 YPRIME(J) = OM*(Y(J-1)-2.*Y(J)+Y(J+1))/DZS
      IF (T .LT. TCON) YPRIME(2) = YPRIME(1)
      IF (T .GE. TCON) THEN
         Y(2) = -1.0/3.0*(Y(4)-4.0*Y(3))
         YPRIME(2) = 0
      END IF
      YPRIME(N-1)=-1.*Y(N-1) -OM*RAT*(Y(N-4)-4.*Y(N-3)+3.*Y(N-2))/2./DZ
      YPRIME(N-2) = ((-1.*YPRIME(N-4)+4.*YPRIME(N-3))
     '    /2./AL/DZ + YPRIME(N-1))/(1.+1.5/AL/DZ)
      YPRIME(N) = Y(N-1)
      RETURN
      END

      SUBROUTINE FCNJ(N, X, Y, DYPDY)
      INTEGER N
      REAL X, Y(N), DYPDY(N,*)
      RETURN
      END
```

Chapter 3. DETERMINING DERMAL ABSORPTION PARAMETERS *IN VIVO* FROM TAPE STRIPPING DATA

Introduction

Many *in vivo* methods for measuring dermal absorption of drugs or other chemicals are invasive (e.g., blood samples are collected) or slow (e.g., urine samples are collected for extended periods after the exposure ends). Tape stripping of the outermost skin layer, the stratum corneum (sc), has been proposed as a fast and relatively noninvasive technique for measuring the rate and extent of dermal absorption (Dick *et al.*, 1997; Schwarb *et al.*, 1999; Stinchcomb *et al.*, 1999). Tape strip (TS) data have been used to estimate steady-state permeability coefficients and partition coefficients from *in vivo*, short dermal exposures (Tojo and Lee, 1989; Pirot *et al.*, 1997). Tape stripping has also been proposed as a method for evaluating bioequivalence of topical dermatological dosage forms (Shah *et al.*, 1998).

In a TS experiment, an area of skin is exposed to a chemical for a set exposure time and then cleaned. Between 10 and 30 pieces of adhesive tape are applied to and removed from the exposed area in sequence. The mass of chemical in each TS is determined by an appropriate analytical technique. When analytical sensitivity is low, or to reduce the number of analyses required, TS's are sometimes combined for analysis into one or a few groups (e.g., Thiele and Packer (1999)).

Background

Although the TS procedure is relatively simple to execute, there are many opportunities for experimental artifacts to develop. For example, if each TS is not applied to exactly the same site, chemical from adjacent, previously unstripped sc could be removed by a later TS. Using TS's that are larger than the exposed area is one solution to this problem. Another limitation of the TS technique is that samples are small making accurate chemical analysis difficult. Consequently, chemicals with high analytical sensitivity must be chosen and applied to the skin in high concentrations. Also, TS samples have high surface-to-volume ratios, and losses by evaporation can be significant even for chemicals with relatively low volatility. Generally, the TS experiment is unsuitable for volatile chemicals, and for all other chemicals appropriate steps (e.g., chemical extraction or chemical analysis) should be completed soon after the tape is removed from the skin surface. The special difficulties of working with volatile chemicals are evident in the study of chloroform by Islam *et al.* (1995).

Many studies report results as the mass of absorbing chemical in each TS based on order of application, referred to as the TS number. However, the amount of sc removed on each TS varies, generally decreasing with increasing depth (Higo *et al.*, 1993; Islam *et al.*, 1999). To estimate dermal absorption parameters (e.g., permeability coefficients and partition coefficients) or to compare data from different experiments, the amount of chemical in each TS must be normalized by the amount of sc (Higo *et al.*, 1993; Pirot *et al.*, 1997). Methods for measuring the amount of sc on each tape include gravimetric analysis (Higo *et al.*, 1993) and optical spectroscopy in the visible range (Weigmann *et al.*, 1999).

When the mass of sc in the n^{th} TS, $m_{sc,n}$, is determined gravimetrically, the concentration of chemical in the n^{th} TS, C_n, is

$$C_n = m_n \rho_{sc} / m_{sc,n} \qquad (3\text{-}1)$$

where m_n is the mass of absorbing chemical in the n^{th} TS and ρ_{sc} is the density of the sc (~ 1 g/cm^3 (Pirot *et al.*, 1997)). To report C_n as a function of depth in the sc, the location of the center of $m_{sc,n}$ from the skin surface, x_n, is:

$$x_n = \frac{1}{A\rho_{sc}}\left\{\frac{m_{sc,n}}{2} + \sum_{i=1}^{n-1} m_{sc,i}\right\} \qquad (3\text{-}2)$$

where A is the area being tape stripped (which could be different from the area exposed to chemical).

Pirot *et al.* (1997) determined diffusion coefficients and partition coefficients for 4-cyanophenol (4CP) by comparing C_n and x_n data to theoretical equations describing dermal absorption as diffusion through a pseudo-homogeneous membrane. A potential problem with this approach is that chemical in the sc when the exposure ends will continue to diffuse during the time that it takes to apply and remove all of the TS's. Consequently, unless the TS procedure is fast, the concentration measured in each TS will be different than the concentration at that location in the sc when the chemical exposure ended. If the measured concentration is significantly different from the concentration at the end of the exposure, this will affect estimated values for diffusion coefficients and partition coefficients. Experiments and mathematical models have been used to assess the conditions under which diffusion might affect TS results and the magnitude of this effect when it occurs.

Experimental Methods

For all experiments, saturated aqueous solutions of 4CP (reagent grade from Aldrich Chemical Company, Milwaukee, WI) prepared with deionized water (approximately 0.11 M) were applied to the forearms of human volunteers at the Albany College of Pharmacy with approval of the Albany College Institutional Review Board. A

gauze pad (2.5 x 8 cm, CVS, Woonsocket, RI) soaked with 4CP solution was placed on the application area. The gauze pad was held in place by a nonocclusive transparent dressing (2 x 4.75 in, Tegaderm, 3M, St. Paul, MN). At the end of the exposure period after the gauze pad was removed, the four corners of the treated area were marked with a Sharpie pen. The skin surface was quickly cleaned with cotton balls soaked with deionized water and dried with more cotton balls. Pre-weighed adhesive tapes (2.5 x 8 cm, 3M Book Tape 845) were then applied to and removed from the application site sequentially. Twenty-five TS's were sufficient to reach glistening, red tissue (i.e., to remove essentially all of the sc). Each TS was weighed after application to the skin surface to determine the mass of sc removed. The mass of 4CP on each TS was determined using attenuated total reflectance Fourier transform infrared spectroscopy (ATR-FTIR) as described by Pirot *et al.* (1997) and Stinchcomb *et al.* (1999).

Two types of experiments were conducted. In both experiments, two sites on the subject's forearm were exposed to 4CP solution for 1 h and then one site was tape stripped rapidly, taking less than 6 min. In the type one experiment, the second site was tape stripped slowly at regular time intervals over 60 min. In the type two experiment, chemical concentration in the sc at the second site was measured after a period of clearance. Specifically, after the exposed sites were cleaned, the second site was occluded for one hour using a 2-mm thick polyethylene layer (2.5 x 8 cm, Fisher Scientific, Pittsburg, PA) secured with Tegaderm to prevent evaporation and then tape stripped rapidly.

In both types of experiments, the chemical concentration in and the location of each TS were calculated using eqs 3-1 and 3-2, respectively. To locate x_n relative to the total thickness of the sc, x_n / L_{sc}, it was assumed that the sc was completely removed by tape stripping. That is,

$$\frac{x_n}{L_{sc}} = \left\{ \frac{m_{sc,n}}{2} + \sum_{i=1}^{n-1} m_{sc,i} \right\} \Bigg/ \sum_{j=1}^{N_{TS}} m_{sc,j} \qquad (3\text{-}3)$$

where N_{TS} is the total number of TS's.

Experimental Results

Experimental results, listed in Appendix 3A, were provided by Stinchcomb (1999). Type one experimental results for one subject are presented in Figure 3.1. 4CP TS concentrations calculated with eq 3-1 are shown as a function of relative position in the SC calculated with eq 3-3. The use of eq 3-3 approximates the apparent value of L_{sc}, L_{sc}^{app}, as:

$$L_{sc}^{app} = \frac{1}{A\,\rho_{sc}} \sum_{n=1}^{N_{TS}} m_{sc,n} = \frac{M_{sc}}{A\,\rho_{sc}} \tag{3-4}$$

were M_{sc} is the total mass of sc removed by tape stripping. In this experiment, values of L_{sc}^{app} were 7.4 and 9.2 μm, respectively, for the areas that were rapidly and slowly tape stripped. The concentration in TS's collected over 60 min are clearly smaller than concentrations in TS's collected in less than 6 min at a similar position. This observation is consistent with chemical diffusion while TS's are collected, and was expected based on experimental results of Pirot *et al.* (1997), who found that significant amounts of 4CP entered the sc within 15 minutes. If chemical enters the skin quickly, it is reasonable that it leaves the skin quickly.

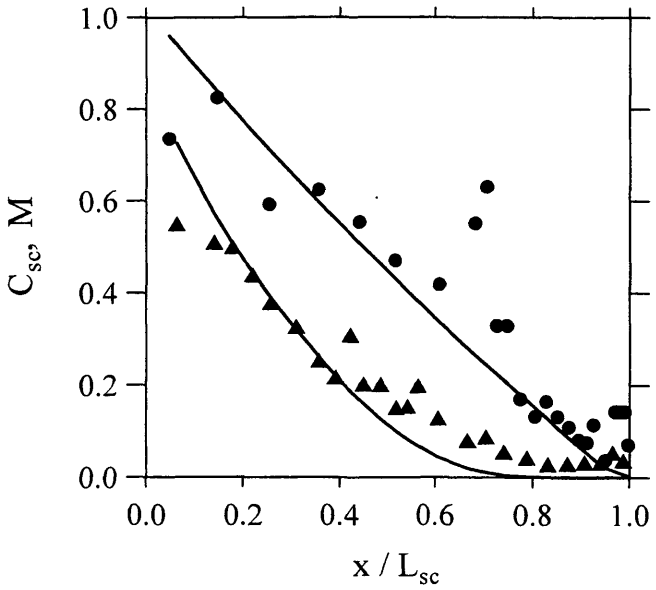

Figure 3.1 – Experimental and calculated 4CP concentrations in the sc (C_{sc}) as a function of x / L_{sc} for fast (●, < 6 min) and slow (▲, 60 min) tape stripping following a one-hour exposure to a saturated aqueous 4CP solution.

Type two experimental results are shown in Figure 3.2 for three subjects. In these experiments, values of L_{sc}^{app} calculated using eq 3-4 were 11.0 and 11.8 μm for subject A, 8.5 and 8.6 μm for subject B, and 10.2 and 10.8 μm for subject C. Consistent with the type one experiments, concentrations in TS's collected after a one-hour delay are smaller than those collected immediately after the exposure ends.

For subjects B and C the 4CP concentration at x / L_{sc} = 1 was not zero. That could indicate that the sc was not completely removed by tape stripping. Values of L_{sc}^{app} were lower than the average value of 12 μm reported by Pirot *et al.* (1998). Another possible explanation arises from the last several TS's removing increasingly smaller

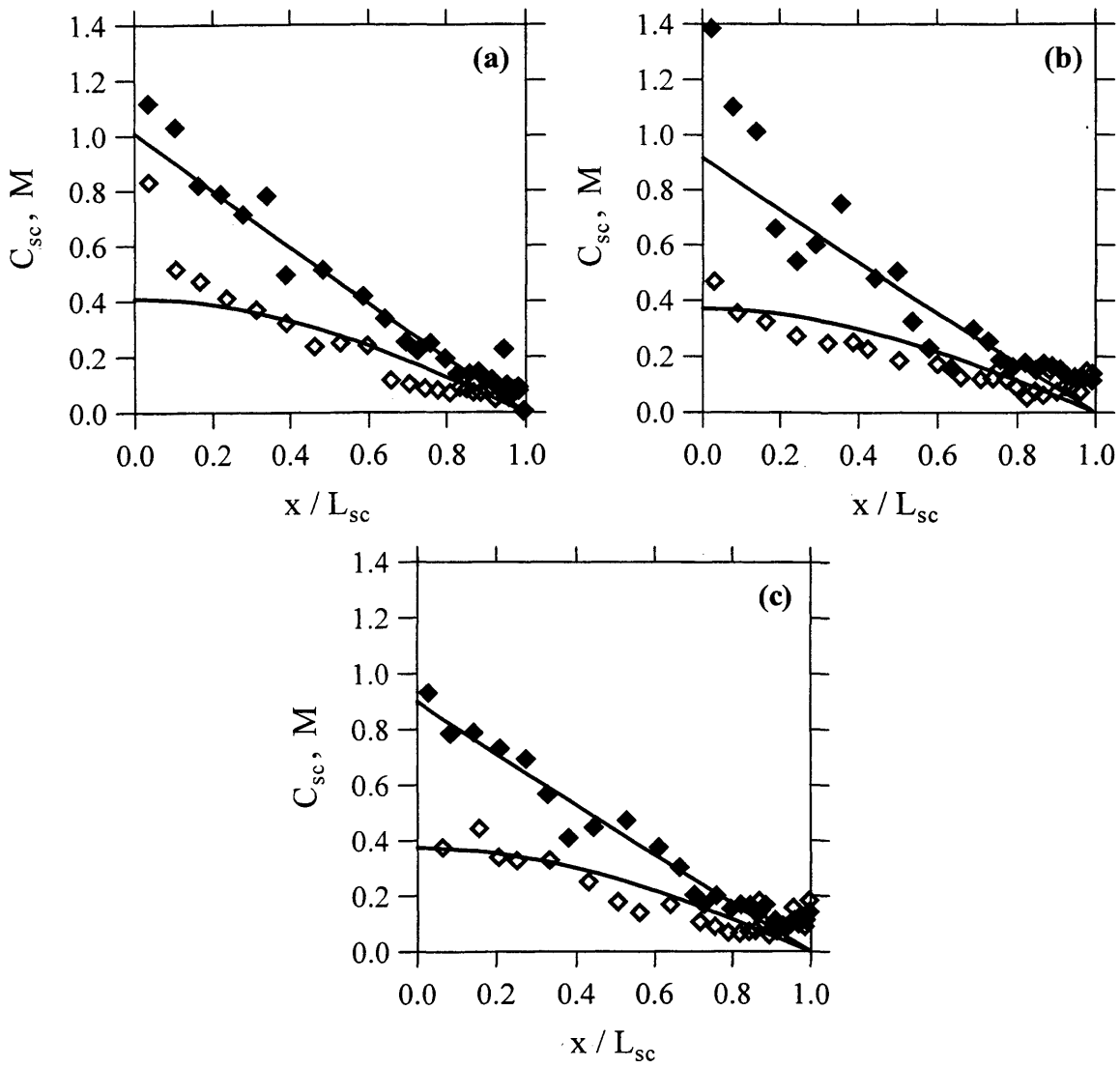

Figure 3.2 – Experimental and calculated 4CP concentrations in the sc (C_{sc}) without (closed symbols) and with (open symbols) a one-hour delay before tape stripping as a function of x / L_{sc} following a one-hour exposure to a saturated aqueous 4CP solution for subjects A (a), B (b) and C (c).

amounts of sc. If it takes two or more TS's to remove a layer of cells, the same average concentration could be measured in subsequent TS's, making it appear that the concentration at $x / L_{sc} = 1$ is not zero.

Theory

Mathematical models were developed to describe the diffusion of chemicals during the TS procedure. Two types of models were developed. In the first type, equations were developed describing chemical concentration as a function of position in the sc, assuming that the TS procedure could be completed instantaneously (i.e., diffusion of chemical did not occur while the TS's were being collected). In the second type of model, the concentration within the sc was calculated allowing for diffusion during the TS procedure.

Although skin is a multi-layered membrane, the two outside layers, the sc and the viable epidermis (ve), are the principle barriers to dermal absorption of chemicals. While the ve can contribute a significant barrier to extremely lipophilic chemicals, the sc is the rate-limiting barrier to dermal absorption for many chemicals (Scheuplein and Bronaugh, 1983). Because of this and to simplify calculations, the equations presented here were derived assuming that the sc controls the rate of dermal absorption.

Assuming dermal absorption is passive diffusion through a single, pseudo-homogenous membrane (i.e., the sc), the concentration of chemical in the sc (C_{sc}) at the end of an exposure ($t = t_{exp}$) to a constant-concentration vehicle can be estimated by the following equation (Crank, 1975):

$$\frac{C_{sc}}{K_{sc/v}C_v^o} = 1 - \frac{x}{L_{sc}} - \frac{2}{\pi}\sum_{n=1}^{\infty}\frac{1}{n}\exp\left(-n^2\pi^2\frac{t_{exp}}{6t_{lag,sc}}\right)\sin\left(\frac{n\pi x}{L_{sc}}\right) \qquad (3\text{-}5)$$

in which C_v^o is the initial concentration of the vehicle, x is the position in the sc, $K_{sc/v}$ is the equilibrium partition coefficient of the absorbing chemical between the sc and the vehicle, and $t_{lag,sc}$ is the lag time for chemical to penetrate the sc, defined as $L_{sc}^2/(6D_{sc})$, where D_{sc} is the effective diffusion coefficient in the sc. Eq 3-5 was developed assuming: (1) the sc was initially free of chemical (i.e., $C_{sc} = 0$ at $t = 0$ for $0 < x < L_{sc}$), (2) the outer surface of the sc was in local equilibrium with the vehicle (i.e., $C_{sc} = K_{sc/v}C_v^o$ at $x = 0$), and (3) the concentration of absorbing chemical at the sc / ve interface was zero (i.e., $C_{sc} = 0$ at $x = L_{sc}$). The mass of chemical in the sc at $t = t_{exp}$, M^o, can be calculated as:

$$\frac{M^o}{AL_{sc}K_{sc/v}C_v^o} = \frac{1}{2} - \frac{4}{\pi^2}\sum_{n=0}^{\infty}\frac{\exp\left[-(2n+1)^2\pi^2 t_{exp}/\left(6t_{lag,sc}\right)\right]}{(2n+1)^2} \qquad (3\text{-}6)$$

which was derived by integrating C_{sc} as a function of x for $0 \le x \le L_{sc}$. The average concentration of absorbing chemical in the sc at $t = t_{exp}$, $< C_{sc}^o >$, is calculated as $< C_{sc}^o >= M^o/(A\,L_{sc})$.

If t_{exp} is long, steady state will be established and eqs 3-5 and 3-6 become simply

$$C_{sc} = K_{sc/v}C_v^o(1 - x / L_{sc}) \qquad (3\text{-}7)$$

$$M^o = A\,L_{sc}K_{sc/v}C_v^o/2 \qquad (3\text{-}8)$$

As indicated in eqs 3-5 and 3-7, C_{sc} depends on both $K_{sc/v}$ and $t_{lag,sc}$ prior to steady state, but on only $K_{sc/v}$ after steady state is established. Since the permeability coefficient through the sc from a vehicle v, $P_{sc,v}$, is defined as $D_{sc}\,K_{sc/v} / L_{sc}$ ($= 6\,K_{sc/v}\,L_{sc} / t_{lag,sc}$), it is impossible to determine $P_{sc,v}$ from only a steady-state concentration profile.

For short exposure times (i.e., for t_{exp} < about $0.05\ t_{lag,sc}$), chemical penetrates only a short distance in the sc. In this situation C_{sc} and M^o can be accurately estimated using the following equations (Crank, 1975; Cleek and Bunge, 1993):

$$\frac{C_{sc}}{K_{sc/v}C_v^o} = \text{erfc}\left(\frac{x/L_{sc}}{2\sqrt{t_{exp}/(6t_{lag,sc})}}\right) \tag{3-9}$$

$$\frac{M^o}{AL_{sc}K_{sc/v}C_v^o} = 2\sqrt{\frac{t_{exp}}{\pi 6 t_{lag,sc}}} \tag{3-10}$$

in which erfc is the complimentary error function. Eqs 3-9 and 3-10 were derived for conditions similar to those for eqs 3-5 and 3-6, except that the sc was assumed to be semi-infinite.

Figure 3.3 presents concentration profiles calculated using eq 3-5 for values of the ratio t_{exp} / $t_{lag,sc}$. When $t_{exp} > 1.7\ t_{lag,sc}$ the concentration is essentially linear with position and the total mass of chemical in the sc, M^o, will increase by less than 5% if the exposure time is increased further.

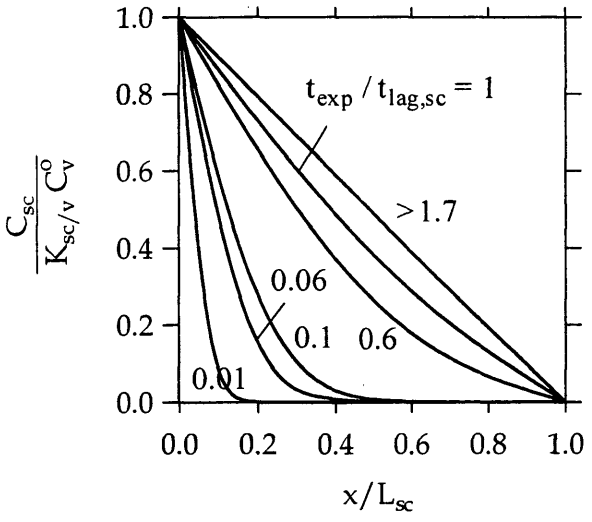

Figure 3.3 – C_{sc} as a function of x / L_{sc} for several values of t_{exp} / $t_{lag,sc}$.

If sc removal by serial tape stripping occurred immediately at the end of a chemical exposure, then the chemical concentration measured in each TS (i.e., C_n) should be described by eq 3-5. However, if after the chemical is removed there is a delay, t_{delay}, before the sc is tape stripped, then the concentration of chemical in the sc decreases as diffusion proceeds. Consistent with the development of eqs 3-5 and 3-6, we assumed Fickian diffusion through a single pseudo-homogeneous membrane to obtain the following differential mass balance:

$$\frac{\partial C_{sc}}{\partial t} = D_{sc}\frac{\partial^2 C_{sc}}{\partial x^2} \qquad \text{for } 0 \le x \le L_{sc} \qquad (3\text{-}11)$$

In the general case, eq 3-11 is solved for the following boundary conditions:

$$\text{at } x = 0 \qquad \frac{\partial C_{sc}}{\partial x} = 0 \qquad \text{for } t - t_{exp} > 0 \qquad (3\text{-}12)$$

$$\text{at } x = L_{sc} \qquad C_{sc} = 0 \qquad \text{for } t - t_{exp} > 0 \qquad (3\text{-}13)$$

where C_{sc} is given by eq 3-5 for $t - t_{exp} = 0$. Eq 3-12 states that flux from the outermost surface of the sc is zero, which is expected for non-volatile chemicals. As in the development of eq 3-5, the concentration at the sc – ve interface is assumed to be zero (eq 3-13). When an exposure ends after steady state is established, C_{sc} at $t - t_{exp} = 0$ is described by eq 3-7 and the solution of eqs 3-11 through 3-13 is then:

$$\frac{C_{sc}}{K_{sc/v}C_v^o} = \sum_{n=0}^{\infty}\frac{8}{(2n+1)\pi}\cos\left(\frac{(2n+1)\pi}{2}\frac{x}{L_{sc}}\right)\exp\left(\frac{-(2n+1)^2\pi^2}{24}\frac{t-t_{exp}}{t_{lag,sc}}\right) \qquad (3\text{-}14)$$

Eq 3-14 represents C_{sc} some time after the exposure has ended (i.e., $t_{delay} = t - t_{exp}$) when the sc is the rate-controlling barrier to dermal absorption for $t_{exp} > 1.7\ t_{lag,sc}$.

Because chemical will diffuse across the remaining sc while the tape stripping procedure is completed, eq 3-5 could represent C_n poorly if the time to TS was slow compared to the rate that chemical penetrates the sc. In this case, eq 3-11 describes the diffusion of chemical for $x_{TS} \le x \le L_{sc}$, the part of the sc remaining after a portion has been removed by the TS procedure, with the outside of the sc located at x_{TS}. As each TS

is removed, the position of the outside edge of the sc moves inward (i.e., x_{TS} increases) until all of the sc is removed (i.e., until $x_{TS} = L_{sc}$), as illustrated schematically in Figure 3.4. To simplify the mathematical analysis, we assumed that the time required to clean the skin is insignificant, that TS's are removed at the end of even time intervals (i.e., the time between TS applications is constant), and that the same amount of sc is removed by each TS. Consequently, the location of x_{TS} relative to L_{sc} is described by:

$$\frac{x_{TS}}{L_{sc}} = \frac{1}{N_{TS}} \sum_{j=1}^{N_{TS}} u\left[t - t_{exp} - j\frac{t_{TS}}{N_{TS}}\right] \qquad (3\text{-}15)$$

in which N_{TS} is the number of individual TS's required to completely remove the sc and t_{TS} is the total time to complete the TS process. The unit step function, u[t-a], is defined as 0 for $t \leq a$ and 1 for $t > a$.

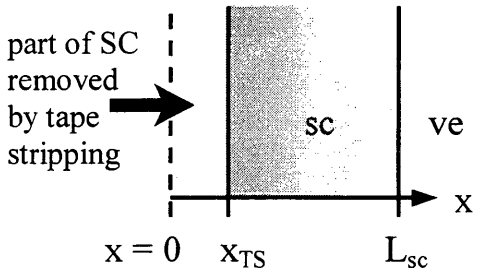

Figure 3.4 – Schematic diagram of the sc during a TS experiment.

For the model including diffusion during stripping, eq 3-11 was solved numerically by finite difference with C_{sc} given by eq 3-5 at $t - t_{exp} = 0$, restricted by eq 3-13 and the following condition:

$$\text{at } x = x_{TS} \qquad \frac{\partial C_{sc}}{\partial x} = 0 \qquad \text{for } t - t_{exp} > 0 \qquad (3\text{-}16)$$

Eq 3-16 states that flux is zero from the outer sc surface after each TS is removed, implying that the absorbing chemical is not volatile. These equations were solved numerically as described in Appendix 3B. Once C_n is calculated, the total mass of chemical in all TS's, M_{TS}, is given by:

$$M_{TS} = \frac{A L_{sc}}{N_{TS}} \sum_{n=1}^{N_{TS}} C_n \qquad (3\text{-}17)$$

which should be less than or equal to M^o.

Discussion

Figure 3.5 presents model calculations comparing the concentration in TS's (represented by data points) as a function of x / L_{sc} for three values of the total time to tape strip, t_{TS}, relative to how rapidly the chemical can penetrate the sc, represented by $t_{lag,sc}$. The concentration profile in the sc at the end of the exposure is represented by the solid curve. In these calculations and all others shown here, $N_{TS} = 30$. Figure 3.5a presents results for $t_{exp} = 0.3\ t_{lag,sc}$. Figure 3.5b shows results when the exposure ended after steady state was established (i.e., $t_{exp} > 1.7\ t_{lag,sc}$).

As shown in Figure 3.5, diffusion can alter TS experimental results if tape stripping takes a long time relative to the time required for chemical to diffuse across the sc. Significantly, when $t_{TS} > t_{lag,sc}$ the concentration profile measured by tape stripping can be nonlinear even if the exposure time was long enough to achieve steady state. These theoretical calculations are consistent with the experimental results presented in Figure 3.1. In addition, the calculations shown in Figure 3.5 may explain the 4CP data reported by Higo *et al.* (1993), which were nonlinear even for long exposure times (t_{exp} was as long as 3 h). In these experiments, subjects placed their tape-stripped forearms

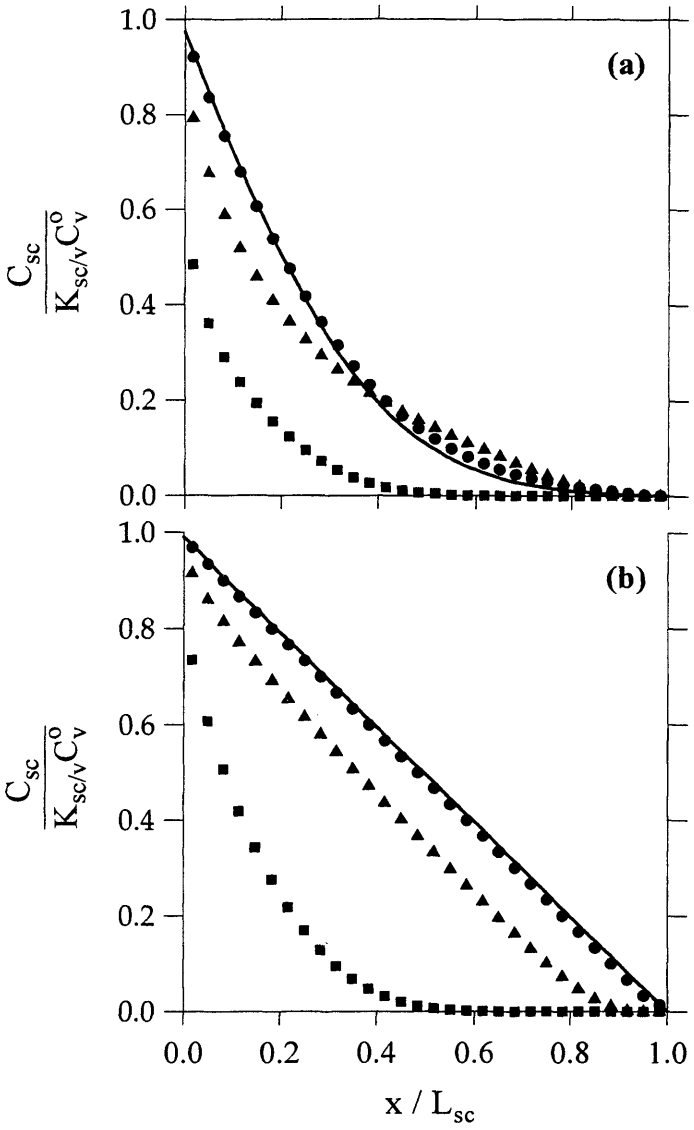

Figure 3.5 – The concentration in the sc at t = t_{exp} (curves) compared to calculated concentrations in 30 TS's as a function of x / L_{sc} when t_{TS} = (●) 0.1 $t_{lag,sc}$, (▲) 1 $t_{lag,sc}$, and (■) 10 $t_{lag,sc}$ for t_{exp} (a) = 0.3 $t_{lag,sc}$ and (b) > 1.7 $t_{lag,sc}$.

directly onto the ATR crystal of the FTIR after each TS was applied and removed. Based on experimental results in Figures 3.1 and 3.2 and theoretical calculations in Figure 3.5, we suspect that t_{TS} was greater than $t_{lag,sc}$ for this procedure.

Figure 3.6 quantitatively presents the calculated differences between the chemical concentration in each TS at the end of the exposure (C_n^o, calculated using eq 3-5) and at the time of tape stripping (i.e., C_n) as a function of t_{TS} / $t_{lag,sc}$ for the same conditions as in Figure 3.5. To simplify viewing, the individual data points representing 30 TS's are shown as curves in Figure 3.6. In Figure 3.6a, $t_{exp} = 0.3\ t_{lag,sc}$, and in Figure 3.6b, t_{exp} is longer than the time required for steady state. When the exposure time is long enough for steady state to be reached, $\left(C_n^o - C_n\right)$ is always > 0 (Figure 3.6b). However, if steady state was not reached during the exposure, then $\left(C_n^o - C_n\right)$ can be negative for interior TS's (see Figure 3.6a), because larger chemical concentrations from the outside sc layers have moved into regions that previously had little chemical. Whether or not steady state was achieved during the exposure, the magnitude of $\left(C_n^o - C_n\right)$ increases with increasing values of t_{TS} / $t_{lag,sc}$.

Figure 3.7 shows the average value of $\left|\left(C_n^o - C_n\right)\right|$ for all TS's calculated as

$$< \left|C_n^o - C_n\right| > = \frac{1}{N_{TS}} \sum_{i=1}^{N_{TS}} \left|C_n^o - C_n\right| \qquad (3\text{-}18)$$

and normalized by $< C_{sc}^o >$. Based on the calculations shown in Figure 3.7, the average change in the concentration profile during t_{TS} is less than about 10% when $t_{exp} > 0.3\ t_{lag,sc}$ if $t_{TS} < 0.2\ t_{lag,sc}$. If $0.03 < t_{exp} / t_{lag,sc} < 0.3$, then the average change in the concentration profile is < 10% if $t_{TS} < 0.05\ t_{lag,sc}$.

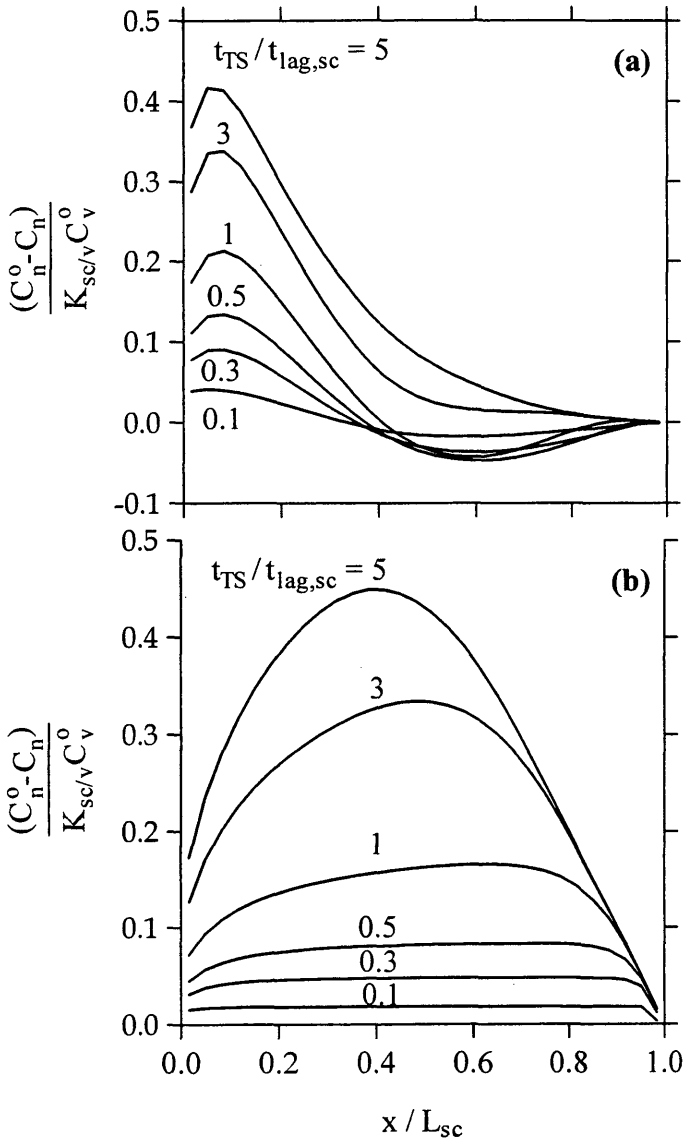

Figure 3.6 – Normalized $\left(C_n^o - C_n\right)$ as a function of x / L_{sc} for t_{exp} (a) = 0.3 $t_{lag,sc}$ and (b) > 1.7 $t_{lag,sc}$ for several values of $t_{TS} / t_{lag,sc}$.

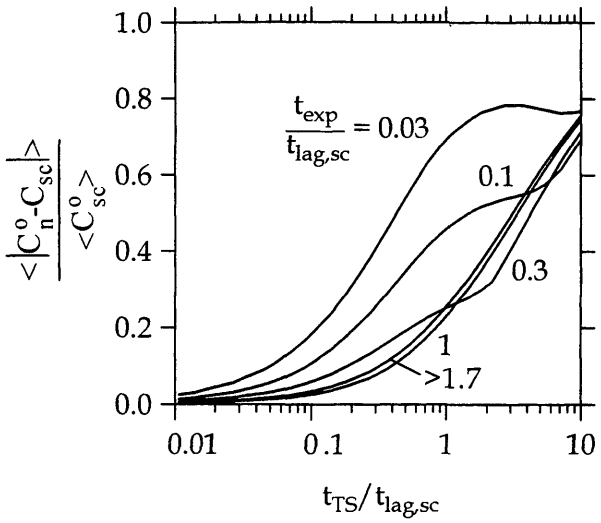

Figure 3.7 – Normalized $<|C_n^o - C_n|>$ as a function of t_{TS} / $t_{lag,sc}$ for varying values of t_{exp} / $t_{lag,sc}$.

Sometimes TS data are used to calculate the total mass of chemical in the sc, which could also be reduced by diffusion during the TS procedure. Figure 3.8 presents model calculations for M_{TS}/M^o as a function of t_{TS} / $t_{lag,sc}$ for various values of t_{exp} / $t_{lag,sc}$. The dashed curve represents M_{TS}/M^o for t_{exp} longer than the time required to establish steady state (i.e., $t_{exp} > 1.7\ t_{lag,sc}$). As t_{TS} increases relative to $t_{lag,sc}$, M_{TS}/M^o decreases. The effect of exposure time on M_{TS}/M^o is less than 15% for any value of t_{TS} / $t_{lag,sc}$. As long as $t_{TS} < 0.3\ t_{lag,sc}$, $M_{TS} > 0.9\ M^o$ for any t_{exp}. If t_{TS} and $t_{lag,sc}$ were equal, as they might have been for chloroform in the measurements by Islam *et al.* (1999), then the mass measured by tape stripping could have been 10 – 25% smaller than the amount in the sc at the end of the exposure, even if no chloroform were lost from the TS's by evaporation.

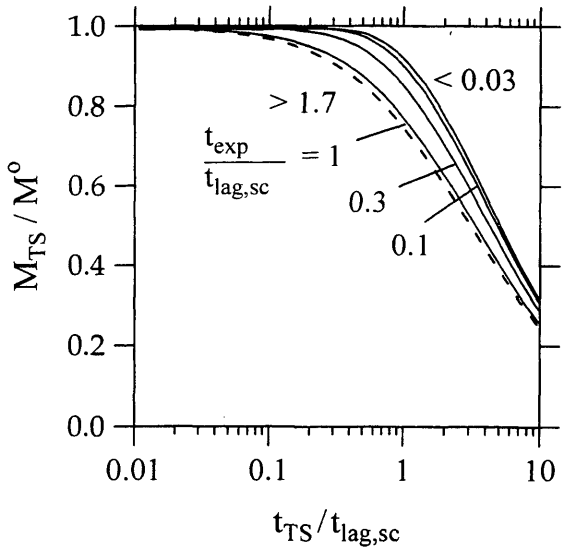

Figure 3.8 – M_{TS}/ M^o as a function of $t_{TS} / t_{lag,sc}$ for several values of $t_{exp} / t_{lag,sc}$.

Estimating Dermal Absorption Parameters

As shown in the theory section, when the sc is the controlling mass transfer barrier, dermal absorption of chemicals depends on three parameters: L_{sc}, $K_{sc/v}$ and $t_{lag,sc}$. Consequently, apparent values of the parameters L_{sc}^{app}, $K_{sc/v}^{app}$ and $t_{lag,sc}^{app}$ can be estimated by comparing TS data with mathematical model equations.

Values for L_{sc}^{app} are needed to locate x within the sc (i.e., to specify x / L_{sc}) and to calculate the permeability coefficient from estimates of $K_{sc/v}^{app}$ and $t_{lag,sc}^{app}$. Often in estimating x / L_{sc}^{app}, it is assumed (as in Figures 3.1 and 3.2) that the sc is completely removed by tape stripping and L_{sc}^{app} is calculated using eq 3-4 (e.g., Pirot *et al.* (1997) and Stinchcomb *et al.* (1999)). Recently, Kalia *et al.* (1996) proposed a method for estimating L_{sc}^{app} by combining $m_{sc,n}$ with measurements of transepidermal water loss (TEWL). A similar technique requiring fewer experimental measurements of TEWL has

since been proposed by Pirot *et al.* (1998). The TEWL technique has some significant limitations. First, it cannot be used at the exposed site if the chemical exposure has affected skin hydration (e.g., aqueous vehicles hydrate the skin). The TEWL method could be applied to a site adjacent to the exposed site. However, if the chemical exposure alters skin hydration, then $m_{sc,n}$ from the site exposed to chemical can be different from the site of the TEWL measurements. When estimates of permeability coefficients have been calculated, sometimes L_{sc}^{app} was assumed to be 15 μm even when L_{sc}^{app} for calculating x / L_{sc} was derived from eq 3-4 (e.g., see Pirot *et al.* (1997)).

If TS data were collected after steady state was established (i.e., $t_{exp} > 1.7\ t_{lag,sc}$), then $K_{sc/v}^{app}$ but not $t_{lag,sc}^{app}$ can be estimated. As shown in eq 3-8, $K_{sc/v}^{app}$ can be calculated from steady-state TS data as follows:

$$K_{sc/v}^{app} = \frac{2}{L_{sc}^{app} A C_v^o} \sum_{i=1}^{N_{TS}} m_i \tag{3-19}$$

assuming that the sc is the primary barrier to dermal absorption. If a chemical is lipophilic enough that the ve contributes a significant resistance, then the concentration at the sc / ve barrier for a steady-state exposure will not be zero. In this situation, $K_{sc/v}^{app}$ can be calculated using eq 3-20:

$$K_{sc/v}^{app} = \frac{2(B+1)}{L_{sc}^{app} A C_v^o (2B+1)} \sum_{i=1}^{N_{TS}} m_i \tag{3-20}$$

in which B, the ratio of permeability coefficients of the absorbing chemical in the sc, $P_{sc,v}$, to the ve, $P_{ve,v}$, from the same vehicle, can be estimated as:

$$B = C_{sc}\big|_{x/L_{sc}=1} \Big/ \left(C_{sc}\big|_{x/L_{sc}=0} - C_{sc}\big|_{x/L_{sc}=1}\right) \tag{3-21}$$

Values for C_{sc} at $x / L_{sc} = 0$ and 1 can be estimated from a linear regression of C_n as a function of x_n / L_{sc}. Although a non-zero concentration at the sc / ve interface (i.e., at $x / L_{sc} = 1$) can indicate that the ve is contributing a resistance to mass transport, it is equally

likely that not all the sc was removed by tape stripping. When the ve does contribute a significant mass transfer resistance, it takes longer to reach steady state and $t_{exp} > 1.7\ t_{lag,sc}$ may not be a sufficient criterion (Cleek and Bunge, 1993).

If TS's are collected rapidly, then diffusion during TS collection will be insignificant and the concentration profile represented by the TS's should fairly represent the concentration profile in the sc at the time the TS's were collected. If the concentration profile was not at steady state (e.g., t_{exp} was less than $t_{lag,sc}$, or t_{delay} after the exposure ended was $\neq 0$), then both $K_{sc/v}^{app}$ and $t_{lag,sc}^{app}$ can be estimated by comparing C_n and x_n / L_{sc} with the appropriate theoretical equation (e.g., eq 3-5, 3-9 or 3-14). Alternatively, if $K_{sc/v}^{app}$ is known from a steady-state experiment, then $t_{lag,sc}^{app}$ can be estimated from the unsteady state data. Often more than one pair of values for $K_{sc/v}^{app}$ and $t_{lag,sc}^{app}$ will provide an acceptable fit of unsteady TS data. This difficulty is avoided if a steady-state experiment can provide a separate estimate for $K_{sc/v}^{app}$. However, steady-state measurements will not always be possible, particularly for chemicals with large $t_{lag,sc}$. Finally, equations developed assuming that the sc is the controlling mass transfer resistance (e.g., eq 3-5, 3-9 or 3-14), can be used for short exposures to highly lipophilic chemicals (for which the ve contributes a significant resistance), because when $t_{exp} < t_{lag,sc}$, the ve has not affected C_{sc}.

In experiments used to estimate $t_{lag,sc}^{app}$, ideally $0.06 < t_{exp} / t_{lag,sc} < 0.6$. As illustrated in Figure 3.3, the concentration profile is almost insensitive to $t_{lag,sc}^{app}$ when $t_{exp} > t_{lag,sc}$. At the other extreme, when $t_{exp} < 0.06\ t_{lag,sc}$, the concentration profile is too sensitive to $t_{lag,sc}^{app}$ and small changes in TS data would produce large variations in estimates for $t_{lag,sc}^{app}$.

Data Analysis

The data from the type one experiment shown in Figure 3.1 were analyzed in two ways. In the first analysis, data from both the rapid and slow TS experiments were used. After a 60-min exposure, the 4CP concentration in TS's that were removed rapidly vary linearly with position in the sc, suggesting that 60 min was long enough to achieve steady state. The value of $K_{sc/v}^{app}$ was estimated as 9.1 using these data as specified in eq 3-19. Using this value of $K_{sc/v}^{app}$, the lag time ($t_{lag,sc}^{app}$ = 40 min) was determined by minimizing the sum of the squared residuals between the slow TS data and the mathematical model calculations that included the TS time for C_n (i.e., the numerical solution of eqs 3-11, 3-13 and 3-16 combined with eq 3B-3). The curves in Figure 3.1 represent model calculations based on these values of $K_{sc/v}^{app}$ and $t_{lag,sc}^{app}$. As shown in Table 3.1, the values of $K_{sc/v}^{app}$ and $t_{lag,sc}^{app}$ derived in this analysis of the type one experiment are consistent with results from tape stripping experiments reported by Pirot *et al.* (1997).

Notably, for the fast TS experiment, t_{TS} / $t_{lag,sc}^{app} \cong$ 6 min / 40 min = 0.15, which meets the criteria developed from Figure 3.7 for neglecting diffusion in the TS results. By comparison, t_{TS} / $t_{lag,sc}^{app} \cong$ 1.5 for the slow TS data, clearly indicating that diffusion during the TS procedure would be significant. Furthermore, t_{exp} / $t_{lag,sc}^{app}$ = 60 min / 40 min = 1.5, which is almost enough time to establish a steady-state concentration profile (i.e., for steady state, $t_{exp} > 1.7\ t_{lag,sc}$).

If only the slow TS data in Figure 3.1 had been collected, then there would be no evidence that chemical had diffused during the tape stripping procedure. If, assuming that diffusion during the TS procedure was insignificant, eq 3-5 was regressed to only the

Table 3.1 – Description of TS experiments and summary of parameter estimation results.

Exper-iment	Experimental Details				Estimated Parameters			
	Sub-ject	t_{exp}	t_{delay}	t_{TS}	$L_{sc/v}^{app}$	$K_{sc/v}^{app}$	$t_{lag,sc}^{app}$	$P_{sc,v}^{app}$
		min	min	min	μm		min	cm / h
Type 1	A	60	0	< 6	7.4[c]	9.1[e]	—	0.0019[h]
			0	60	9.2[c]	—	40[f]	
Type 1	A	60	0	60	9.2[c]	6.1[d]	95[d]	0.00059[h]
Type 2	A	60	0	< 6	11.0[c]	9.5[e]	—	0.0032[h]
			60	< 6	11.8[c]	—	34[g]	
Type 2	B	60	0	< 6	8.5[c]	9.1[e]	—	0.0030[h]
			60	< 6	8.6[c]	—	26[g]	
Type 2	C	60	0	< 6	10.2[c]	8.2[e]	—	0.0026[h]
			60	< 6	10.8[c]	—	34[g]	
Type 2	A, B & C	60	0 & 60	< 6	10.1 ± 1.5[i]	9.0 ± 0.7[i]	31 ± 5[i]	0.0029 ± 0.0003[i]
Pirot *et al.* (1997)	3 sub-jects	15	0	NA[a]	NA[a]	8.4 ± 3.6	32.5 ± 6.2	0.0037 ± 0.0009[b]

[a] NA = not available. [b] Calculated using $L_{sc}^{app} = 15$ μm. [c] Calculated using eq 3-4. [d] Calculated using eq 3-5. [e] Calculated using eq 3-19. [f] Calculated using the model that accounted for diffusion during tape stripping (i.e., eqs 3-11, 3-13 and 3-16). [g] Calcuated using eq 3-14. [h] Calculated as $P_{sc,v}^{app} = K_{sc/v}^{app} L_{sc}^{app} / \left(6 t_{lag,sc}^{app}\right)$. When two values of L_{sc}^{app} were available a mean value was used. [i] Mean value for subjects A, B and C ± one standard deviation.

slow TS data, then $K_{sc/v}^{app}$ and $t_{lag,sc}^{app}$ are calculated to be 6.1 and 95 min, respectively. Compared to the data analysis using both fast and slow TS data, $K_{sc/v}^{app}$ is 30% smaller, $t_{lag,sc}^{app}$ is almost 140% larger, and the resulting estimate for the permeability coefficient is 70% smaller. The slow TS data and calculations made using eq 3-5 based on these values of $K_{sc/v}^{app}$ and $t_{lag,sc}^{app}$ are shown in Figure 3.9. Significantly, nothing in Figure 3.9 suggests that regression to eq 3-5 is not appropriate in this case. However, even using an inappropriate estimate for $t_{lag,sc}^{app}$, t_{TS} / $t_{lag,sc}^{app}$ = 60 min / 95 min = 0.6, indicating that diffusion probably affected the TS results.

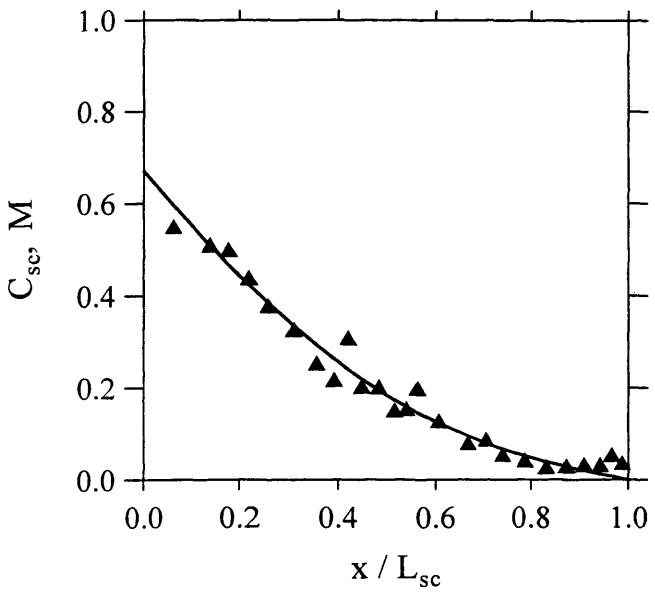

Figure 3.9 – Experimental and calculated (eq 3-5) 4CP concentrations from slowly stripped TS experiment (t_{TS} = 60 min) as a function of x / L_{sc} following a 1-hour exposure to a saturated aqueous 4CP solution.

The type two clearance experiments were analyzed assuming that $t_{TS} < 6$ min was fast enough that diffusion was insignificant during tape stripping. Specifically, eq 3-19 was used to calculate $K_{sc/v}^{app}$ with the TS data collected immediately after chemical was removed from the skin surface. Using this value of $K_{sc/v}^{app}$, $t_{lag,sc}^{app}$ was determined by minimizing the sum of the squared residuals between eq 3-14 and the TS data collected 1 h after the chemical was removed. Model calculations for all three subjects are shown as the curves in Figure 3.2 and the results are summarized in Table 3.1. Calculated values for $K_{sc/v}^{app}$ and $t_{lag,sc}^{app}$ in these clearance experiments are consistent with the type one experiment analysis that included diffusion during the TS procedure and with results reported by Pirot *et al.* (1997). As already presented in the discussion of the type one experiments, $t_{TS} = 6$ min was fast enough that diffusion should not have affected the data and $t_{exp} = 60$ min was long enough for C_{sc} to be linear with position in the sc (i.e., $t_{TS} / t_{lag,sc}^{app} < 0.2$ and $t_{exp} / t_{lag,sc}^{app} > 1.7$)

It is worth noting that during clearance time after a chemical exposure ends, C_{sc} decreases thereby reducing the concentration gradient for diffusion (e.g., see the data in Figure 3.2 collected 1 h after the end of the exposure). Consequently, TS data some time after the exposure are less affected by diffusion than data collected immediately after the end of the exposure. Thus, the criteria that $t_{TS} < 0.2\ t_{lag,sc}$ if $t_{exp} > 0.3\ t_{lag,sc}$ and $t_{TS} < 0.05\ t_{lag,sc}$ if $0.03\ t_{lag,sc} < t_{exp} < 0.3\ t_{lag,sc}$ should be more than adequate for analyzing data after a period of clearance.

Simulated TS Experiments

One way to do TS experiments is to perform a steady-state experiment to calculate $K_{sc/v}^{app}$ and a short-exposure experiment to calculate $t_{lag,sc}^{app}$. Figure 3.10 illustrates the effect of t_{TS} / $t_{lag,sc}$ on parameter estimation for this experimental method. The data used to create Figure 3.10 were simulated using the model that accounted for diffusion during stripping for N_{TS} = 30 and t_{TS} values ranging from 0.01 to 1 $t_{lag,sc}$. Based on the calculations shown in Figure 3.5, TS data for a steady-state exposure with $t_{TS} \leq t_{lag,sc}$ would appear linear with position especially if the sc was not completely removed by stripping, which often happens in TS experiments. For $t_{TS} > t_{lag,sc}$, the data would appear curved and the analysis would be done differently.

The effect of t_{TS} on estimates of $K_{sc/v}^{app}$ was examined using the formula

$$\frac{K_{sc/v}^{app}}{K_{sc/v}} = \frac{M_{TS}}{M^{o}} \tag{3-22}$$

on simulated data for a steady-state exposure. The calculation in Figure 3.10 was performed assuming $L_{sc} = L_{sc}^{app}$ to examine the effect of t_{TS} on $K_{sc/v}^{app}$ and $t_{lag,sc}^{app}$. Next, data for unsteady-state exposures (i.e., for exposures with t_{exp} = 0.03, 0.1, 0.3, 0.6 and 1 $t_{lag,sc}$) were simulated. Using the value of $K_{sc/v}^{app}/K_{sc/v}$ estimated from the steady-state exposure data with a corresponding value of t_{TS} / $t_{lag,sc}$, $t_{lag,sc}^{app}$ was estimated by minimizing the residuals between the simulated TS concentrations for short t_{exp} and C_{sc} calculated using eq 3-5. Finally, Figure 3.10c shows $P_{sc,v}^{app}$ calculated using $K_{sc/v}^{app}$ and $t_{lag,sc}^{app}$ from Figures 3.10a and b and again assuming $L_{sc} = L_{sc}^{app}$. For the t_{exp} examined in Figure 3.10, when $t_{TS} < 0.2\ t_{lag,sc}$ t_{TS} has less than a 10% effect on $K_{sc/v}^{app}$, $t_{lag,sc}^{app}$ and $P_{sc,v}^{app}$.

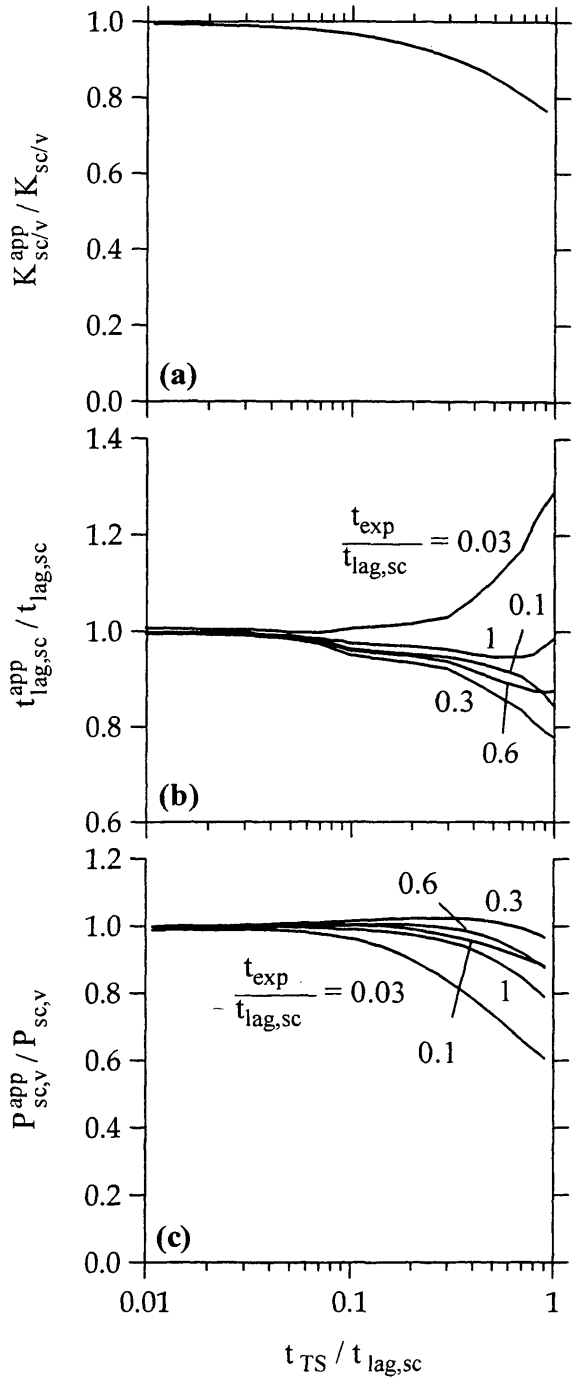

Figure 3.10 –Estimates of a) $K^{app}_{sc/v}$, b) $t^{app}_{lag,sc}$, and c) $P^{app}_{sc,v}$ as a function of $t_{TS} / t_{lag,sc}$ for exposures with $t_{exp} < t_{lag,sc}$.

Figure 3.11 illustrates the magnitude of the deviation between apparent and actual values for $K_{sc/v}$, $t_{lag,sc}$ and $P_{sc,v}$ that could arise for $t_{TS} > t_{lag,sc}$. In these calculations, TS concentrations were simulated using the TS model accounting for diffusion during stripping for two exposure times assuming $N_{TS} = 30$ and $t_{TS} / t_{lag,sc} = 10$. For the short exposure, $t_{exp} / t_{lag,sc}$ was 0.3, and the long t_{exp} was set to be 5-fold longer (i.e., 1.5 t_{exp}). In Figure 3.11, the data with $t_{exp} = 1.5\ t_{lag,sc}$ TS concentrations are not linear with x / L_{sc} because the tape stripping procedure took a long time relative to $t_{lag,sc}$. The data were regressed using eq 3-5. Resulting estimations of parameters were significantly different from the actual values uses to simulate the TS data ($K^{app}_{sc/v}/K_{sc/v}$ =0.70, $t^{app}_{lag,sc}/t_{lag,sc}$ =8.53, and $P^{app}_{sc,v}/P_{sc,v}$ = 0.081). Although it was possible to use eq 3-5 to analyze the data, it was impossible to fit the data well (i.e., the residuals are large).

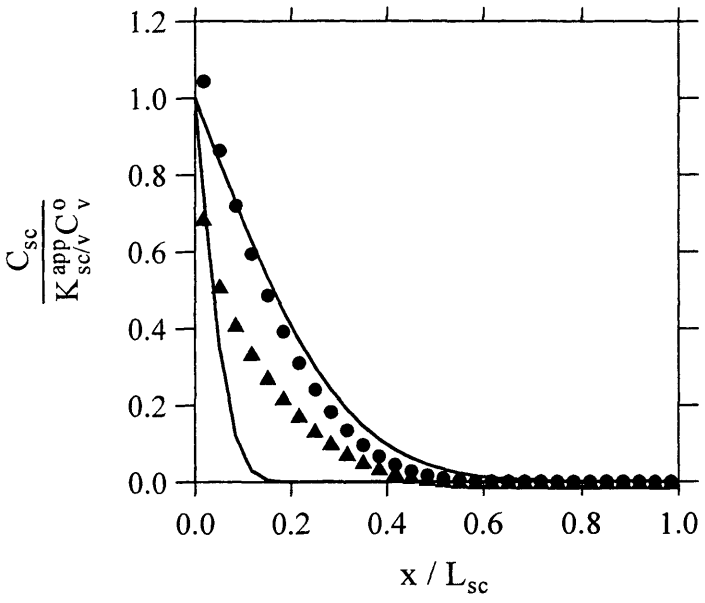

Figure 3.11 –Calculated concentrations in 30 TS's when $t_{TS} = 10\ t_{lag,sc}$ for t_{exp} = (▲) 0.3 $t_{lag,sc}$ and (●) 1.5 $t_{lag,sc}$ as a function of x / L_{sc} and best-fit curves calculated with eq 3-5 .

Recommendations

Based on experimental results and model calculations presented in Figures 3.1 through 3.11 and summarized in Table 3.1, several precautions should improve the outcome of the TS procedure. If TS data are collected immediately following the end of an exposure, experiments should be conducted at two different exposure times. At least one of these must be an unsteady-state experiment in which $0.06 \leq t_{exp} / t_{lag,sc} \leq 0.6$. If possible, the second experiment should be conducted at an exposure time sufficient to establish steady state (i.e., $t_{exp} > 1.7\ t_{lag,sc}$). The TS procedure should be completed as rapidly as possible. If $t_{TS} < 0.2\ t_{lag,sc}$ for $t_{exp} > 0.3\ t_{lag,sc}$ or if $t_{TS} < 0.05\ t_{lag,sc}$ for $0.03\ t_{lag,sc} < t_{exp} < 0.3\ t_{lag,sc}$, then diffusion during the TS procedure should not significantly affect the TS concentrations. A complication in this procedure could arise for vehicles that significantly alter the skin (e.g., those that hydrate the sc). If the sc permeability is different for the long and short exposures, then an analysis assuming that $t_{lag,sc}$ and $K_{sc/v}$ are independent of the exposure time would be incorrect.

The clearance type experiment would provide an alternative strategy in which two TS experiments are conducted, one with and one without a delay after the exposure has ended. For the simplest data analysis, t_{exp} should be selected to establish steady state. At the least, t_{exp} should be $> 0.3\ t_{lag,sc}$. The delay time after the exposure has ended should be long enough for the concentration profile to change appreciably (t_{delay} greater than about $0.3\ t_{lag,sc}$), but not so long that the analytical errors become significant relative to C_n. As before, if $t_{TS} < 0.2\ t_{lag,sc}$ when $t_{exp} > 0.3\ t_{lag,sc}$ TS results should not be affected by the time required for tape stripping.

Conclusions

Results from experiments and mathematical models show that the time required to tape strip the sc can affect concentrations in TS's. Parameter estimates from experimental TS data for which $t_{TS} > t_{lag,sc}$ were consistent with other measurements in the literature when diffusion during tape stripping was included in the data analysis. However, if diffusion during tape stripping was not included in the data analysis, parameter estimates were affected significantly. For example, the permeability coefficient estimated without considering diffusion, 0.00059 cm/hr, was 70% smaller than the value calculated including the effect of t_{TS} in the data analysis, 0.0019 cm/hr.

Recommended procedures for TS experiments include collecting data for two exposure situations. Experiments can be performed at two values of t_{exp}, or two experiments with one value of t_{exp} can be performed with and without a delay after the exposure ends. For concentrations in the TS's to be unaffected by diffusion during the TS collection procedure, $t_{TS} < 0.2\ t_{lag,sc}$ if $t_{exp} > 0.3\ t_{lag,sc}$ and $t_{ts} < 0.05\ t_{lag,sc}$ if $0.03\ t_{lag,sc} < t_{exp} < 0.3\ t_{lag,sc}$.

Notation

A	surface area of chemical exposure (area being tape stripped)
B	ratio of the sc and ve permeability coefficients of chemical from the same vehicle, $P_{sc,v} / P_{ve,v}$
C_n	average concentration of the absorbing chemical in the n^{th} TS
C_n^o	average concentration of the absorbing chemical in the n^{th} TS at $t = t_{exp}$
C_{sc}	concentration of chemical in the sc as a function of position and time
$< C_{sc}^o >$	position-averaged concentration of absorbing chemical in the sc at $t = t_{exp}$
C_v^o	initial concentration of the absorbing chemical in the vehicle
D_{sc}	effective diffusion coefficient of the absorbing chemical in the sc
$K_{sc/v}$	partition coefficient of the absorbing chemical between the sc and the vehicle
$K_{sc/v}^{app}$	apparent partition coefficient of chemical between the sc and the vehicle
L_{sc}	effective thickness of the sc
$L_{sc/v}^{app}$	apparent effective thickness of the sc
L_{TS}	thickness of sc removed by each TS
M^o	mass of absorbing chemical in the sc at $t = t_{exp}$
m_n	mass of absorbing chemical in the n^{th} tape strip
M_{sc}	total amount of sc removed by all TS's
$m_{sc,n}$	mass of sc removed in the n^{th} tape strip
M_{TS}	mass of absorbing chemical in the sc as measured by tape stripping
N	number of nodes in the sc for the finite-difference solution
N_{TS}	number of TS's used to completely remove the sc by tape stripping
$P_{sc,v}$	permeability coefficient of chemical through the sc from the vehicle
$P_{sc,v}^{app}$	apparent permeability coefficient of chemical through the sc from the vehicle

$P_{ve,v}$	permeability coefficient of chemical through the ve from the vehicle
sc	stratum corneum
t	time
t_{delay}	period of delay before the sc is tape stripped
t_{exp}	duration of the exposure
$t_{lag,sc}$	lag time for chemical penetrating through the sc, $L_{sc}^2/(6D_{sc})$
$t_{lag,sc}^{app}$	apparent lag time for chemical penetrating through the sc
t_{TS}	period of time required to completely remove the sc by tape stripping
u[t-a]	unit step function defined as 0 for $t \leq a$ and 1 for $t > a$
ve	viable epidermis
x	position in the sc
x_n	location of the center of the n^{th} TS
x_{TS}	location of the outside of the sc which moves inward as TS's are removed

Greek

ρ_{sc}	density of the sc

References

Cleek, R. L. and A. L. Bunge (1993). "A new method for estimating dermal absorption from chemical exposure. 1. General approach." Pharmaceutical Research **10**:497-506.

Crank, J. (1975). The mathematics of diffusion, 2nd ed. Oxford, Clarendon Press.

Dick, I. P., P. G. Blain and F. M. Williams (1997). "The percutaneous absorption and skin distribution of lindane in man. I. *In vivo* studies." Human and Experimental Toxicology **16**:645-651.

Higo, N., A. Naik, D. B. Bommannan, R. O. Potts and R. H. Guy (1993). "Validation of reflectance infrared spectroscopy as a quantitative method to measure percutaneous absorption *in vivo*." Pharmaceutical Research **10**:1500-1506.

Islam, M. S., L. Zhao, J. N. McDougal and G. L. Flynn (1995). "Uptake of chloroform by skin during short exposures to contaminated water." Risk Analysis: An Official Publication of the Society for Risk Analysis **15**:343-352.

Islam, M. S., L. Zhao, J. N. McDougal and G. L. Flynn (1999). "Uptake of chloroform by skin on brief exposures to the neat liquid." American Industrial Hygiene Association Journal **60**:5-15.

Kalia, Y. N., F. Pirot and R. H. Guy (1996). "Homogenous transport in a heterogeneous membrane: water diffusion across human stratum corneum *in vivo*." Biophysical Journal **71**:2692-2700.

Pirot, F., E. Berardesca, Y. N. Kalia, M. Singh, H. I. Maibach and R. H. Guy (1998). "Stratum corneum thickness and apparent water diffusivity: facile and noninvasive quantitation *in vivo*." Pharmaceutical Research **15**:492-494.

Pirot, F., Y. N. Kalia, A. L. Stinchcomb, G. Keating, A. L. Bunge and R. H. Guy (1997). "Characterization of the permeability barrier of human skin *in vivo*." Proceedings of the National Academy of Sciences of the United States of America **94**:1562-1567.

Scheuplein, R. J. and R. L. Bronaugh (1983). Percutaneous absorption. Biochemistry and Physiology of the Skin. L. A. Goldsmith, ed. New York, Oxford University Press.

Schwarb, F. P., B. Gabard, T. Rufli and C. Surber (1999). "Percutaneous absorption of salicylic acid in man after topical administration of three different formulations." Dermatology **198**:44-51.

Shah, V. P., G. L. Flynn, A. Yacobi, H. I. Maibach, C. Bon, N. M. Fleischer, T. J. Frantz, S. A. Kaplan, J. Kawamoto, L. J. Lesko, J. P. Marty, L. K. Pershing, H. Schaefer, J. A. Sequeira, S. P. Shrivastava, J. Wilkin and R. L. Williams (1998). "Bioequivalence of topical dermatological dosage forms-- methods of evaluation of bioequivalence." Pharmaceutical Research **15**:167-171.

Stinchcomb, A. L. (1999). Unpublished data, Personal communication.

Stinchcomb, A. L., F. Pirot, G. D. Touraille, A. L. Bunge and R. H. Guy (1999). "Chemical uptake into human stratum corneum *in vivo* from volatile and non-volatile solvents." Pharmaceutical Research **16**:1288-1293.

Thiele, J. J. and L. Packer (1999). "Noninvasive measurement of α-tocopherol gradients in human stratum corneum by high-performance liquid chromatography analysis of sequential tape strippings." Methods in Enzymology **300**:413-419.

Tojo, K. and AE-RI C. Lee (1989). "A method for predicting steady-state rate of skin penetration *in vivo*." Journal of Investigative Dermatology **92**:105-108.

Weigmann, H., J. Lademann, H. Meffert, H. Schaefer and W. Sterry (1999). "Determination of the horny layer profile by tape stripping in combination with optical spectroscopy in the visible range as a prerequisite to quantify percutaneous absorption." Skin Pharmacology and Applied Skin Physiology **12**:34-45.

Appendix 3A – Experimental Data

Table 3A.1 – Data for the type one experiment performed on subject A.

Rapid tape stripping (t_{TS} < 6 min)		Slow tape stripping (t_{TS} = 60 min)	
x_n / L_{sc}	C_n, M	x_n / L_{sc}	C_n, M
0.0473	0.736	0.0628	0.551
0.145	0.826	0.139	0.511
0.253	0.593	0.178	0.501
0.355	0.624	0.219	0.440
0.439	0.553	0.257	0.379
0.514	0.470	0.309	0.327
0.608	0.418	0.355	0.254
0.682	0.551	0.391	0.218
0.706	0.631	0.421	0.309
0.726	0.329	0.448	0.203
0.747	0.329	0.484	0.202
0.774	0.170	0.516	0.151
0.804	0.132	0.541	0.154
0.828	0.164	0.563	0.198
0.851	0.132	0.607	0.129
0.875	0.110	0.667	0.0806
0.895	0.0822	0.705	0.0882
0.912	0.0767	0.740	0.0556
0.926	0.115	0.787	0.0438
0.949	0.0378	0.831	0.0292
0.970	0.143	0.872	0.0311
0.976	0.143	0.907	0.0338
0.983	0.143	0.940	0.0338
0.990	0.143	0.964	0.0548
0.997	0.0715	0.986	0.0378

Table 3A.2 – Data for the type two experiment performed on subject A.

No delay		60-minute delay	
x_n / L_{sc}	C_n, M	x_n / L_{sc}	C_n, M
0.0347	1.12	0.0358	0.832
0.103	1.03	0.103	0.516
0.163	0.820	0.166	0.472
0.220	0.789	0.236	0.411
0.278	0.715	0.314	0.370
0.340	0.782	0.391	0.322
0.388	0.496	0.462	0.238
0.483	0.513	0.528	0.250
0.586	0.418	0.596	0.240
0.643	0.337	0.658	0.116
0.695	0.253	0.705	0.102
0.726	0.221	0.744	0.0857
0.758	0.248	0.777	0.0798
0.796	0.194	0.807	0.0697
0.827	0.138	0.832	0.0897
0.857	0.139	0.850	0.0845
0.880	0.145	0.867	0.0725
0.896	0.120	0.886	0.0714
0.914	0.118	0.903	0.0770
0.933	0.0825	0.922	0.0483
0.944	0.227	0.941	0.0705
0.952	0.0994	0.956	0.0539
0.966	0.0730	0.970	0.0826
0.981	0.0925	0.981	0.0806
0.994	0.00710	0.993	0.00587

Table 3A.3 – Data for the type two experiment performed on subject B.

No delay		60-minute delay	
x_n / L_{sc}	C_n, M	x_n / L_{sc}	C_n, M
0.0233	1.38	0.0293	0.470
0.0788	1.10	0.0908	0.356
0.140	1.01	0.164	0.325
0.188	0.660	0.241	0.274
0.242	0.542	0.322	0.249
0.291	0.604	0.387	0.253
0.356	0.752	0.424	0.228
0.443	0.482	0.505	0.186
0.499	0.506	0.600	0.175
0.539	0.327	0.657	0.127
0.579	0.232	0.708	0.121
0.634	0.161	0.739	0.123
0.689	0.300	0.755	0.158
0.727	0.255	0.772	0.120
0.758	0.190	0.797	0.0915
0.788	0.164	0.823	0.0539
0.819	0.179	0.844	0.0764
0.847	0.153	0.865	0.0622
0.867	0.175	0.882	0.150
0.888	0.167	0.899	0.0750
0.908	0.156	0.920	0.0949
0.925	0.129	0.939	0.0935
0.946	0.127	0.961	0.0740
0.969	0.121	0.977	0.148
0.990	0.115	0.991	0.139

Table 3A.4 – Data for the type two experiment performed on subject C.

No delay		60-minute delay	
x_n / L_{sc}	C_n, M	x_n / L_{sc}	C_n, M
0.0280	0.932	0.0648	0.376
0.0840	0.785	0.157	0.444
0.143	0.790	0.206	0.340
0.209	0.732	0.251	0.328
0.274	0.695	0.332	0.331
0.328	0.568	0.431	0.252
0.380	0.410	0.505	0.179
0.444	0.448	0.561	0.140
0.528	0.474	0.640	0.169
0.610	0.376	0.714	0.106
0.663	0.304	0.753	0.0904
0.701	0.203	0.788	0.0692
0.725	0.170	0.817	0.0657
0.758	0.201	0.841	0.0725
0.795	0.153	0.858	0.0759
0.821	0.169	0.869	0.183
0.845	0.167	0.878	0.106
0.864	0.135	0.894	0.0600
0.885	0.168	0.913	0.0746
0.910	0.112	0.928	0.0940
0.935	0.0813	0.944	0.0976
0.958	0.113	0.956	0.157
0.974	0.120	0.968	0.0998
0.986	0.114	0.984	0.0899
0.996	0.143	0.996	0.184

Appendix 3B – Numerical Solution

Eqs 3-11, 3-13 and 3-16 were solved using a finite difference scheme that transformed a partial differential equation of t and x into a system of ordinary differential equations of t alone. The concentration in the sc was represented by N nodes equally spaced in x and the derivatives were approximated using the following formulas:

$$\frac{\partial^2 C_{sc,i}}{\partial x^2} = \frac{C_{sc,i-1} - C_{sc,i} + C_{sc,i+1}}{(\Delta x)^2} \tag{3B-1}$$

$$\left.\frac{\partial C_{sc,i}}{\partial x}\right|_{x=x_{ts}} = \frac{-3C_{sc,i} + 4C_{sc,i+1} - C_{sc,i+2}}{2\Delta x} \tag{3B-2}$$

where $\Delta x = L_{sc} / (N-1)$. Eqs 3B-1 and 3B-2 are second-order accurate in x. The ordinary differential equations were solved using the FORTRAN computer program in Appendix 3C, which uses the IVPAG routine from the IMSL library to solve the ordinary differential equations. In all calculations shown in this chapter, N_{TS} was 30 and N was either 121 or 301. Consequently, each TS was represented by either 5 or 11 nodes. The chemical concentration in the n^{th} TS, C_n, was calculated by numerically averaging C_{sc} using Simpson's Rule over the thickness removed by each TS, L_{TS}, as follows:

$$C_n = \frac{1}{L_{TS}} \int_{(n-1)L_{TS}}^{nL_{TS}} C_{sc} dx \tag{3B-3}$$

where L_{TS} is L_{sc} / N_{TS}. Eq 3B-3 was derived for even TS thickness, but for experimental data a different amount of sc is removed with every TS. To use the TS concentrations predicted by eq 3B-3 to analyze data, values of the concentration between the TS's which correspond to the x_n / L_{sc} position of the data can be interpolated (i.e., treating C_n as a curve instead of as N_{TS} discrete values).

Stability of the numerical solution with respect to the number of nodes was confirmed (i.e., increasing the number of nodes did not change the results). Also, at the

end of each simulation it was determined that the sum of the mass of chemical removed by tape stripping, M_{TS}, and that had diffused through the sc was within 0.4% the mass of chemical in the sc at the end of the exposure (i.e., M^0).

Appendix 3C – FORTRAN Program

Table 3B.1 lists the names of variables in the following program. The program needs to be compiled so that the IVPAG subroutine in the IMSL library can be accessed.

Table 3C.1 – Variable names in the FORTRAN program.

variable in program	variable in chapter
T	$D_{sc}\left(t - t_{exp}\right) / L_{sc}^2$
N	N
Y(i), i = 1 to N	$C_{sc} / (K_{sc/v} C_v^o)$ at node position i
YPRIME(N)	spatial derivative of Y calculated with finite differencing
AVESC(30)	$C_n / (K_{sc/v} C_v^o)$, the concentration in the 30 TS's
AVE2(30)	$C_n^o / (K_{sc/v} C_v^o)$, the concentration in the 30 TS's at $t = t_{exp}$
MSC	$M^o / \left(A\, L_{sc} K_{sc/v} C_v^o\right)$, normalized mass in the sc at $t = t_{exp}$
MTS	$M_{TS} / \left(A\, L_{sc} K_{sc/v} C_v^o\right)$, normalized mass removed by TS's
XL	x / L_{sc}, normalized position in the sc
EXPRAT	$t_{exp} / t_{lag,sc}$
TEXP	$D_{sc}\, t_{exp} / L_{sc}^2$
STEP2	$t_{TS} / t_{lag,sc}$
RD1	$(C_n^o - C_n) / (K_{sc/v} C_v^o)$
NSR2	$\sum_{n=1}^{N_{TS}} \lvert C_o - C_n \rvert / \left(N_{TS} < C_{sc}^o >\right)$
DZ	$\Delta x / L_{sc}$
MB	$\left(M_{TS} + M_{abs}\right) / M^o$ (~ 1 for adequate solution)

```
PROGRAM TAPE5

C Program is used to examine effects of time on tapestripping results
      INTEGER NPARAM, N

C 30 tape strips, represented by 121 nodes, are removed.
      PARAMETER (NPARAM=50, N=121)

C SPECIFICATIONS FOR LOCAL VARIABLES
      INTEGER IDO, NOUT,II,MMM,MM,I2,I1,I3,I22
      REAL PARAM(NPARAM),T,TEND,A(1,1),IEND,MRAT,STEP2,EXPRAT
      REAL XL,TEXP,Q,QQ,TFINAL,NSR2,RD1,P,AVE2(30),SUMRS
      REAL YD(N),Y(N),AVESC(30),RRR,TOL,STEP,MTS,MSC,MEL,MB
      COMMON/SKIN/II,MEL

C SPECIFICATIONS FOR SUBROUTINES
      EXTERNAL IVPAG, SSET, UMACH
      EXTERNAL FCN, FCNJ
      CALL SSET(NPARAM, 0.0, PARAM, 1)

      OPEN (1, FILE='data.dat', STATUS = 'NEW')
      OPEN (2, FILE='data2.dat', STATUS = 'NEW')
      OPEN (3, FILE='strip.dat', STATUS = 'OLD')
      OPEN (4, FILE='data3.dat', STATUS = 'NEW')
      OPEN (6, FILE='data6.dat', STATUS = 'NEW')

C CHOOSING GEAR'S BDF METHOD
      PARAM(12) = 2

      READ(3,*) I22,EXPRAT
      TEXP = EXPRAT/6.
      I2 = 0
      P = 3.14159

C SETTING INITIAL CONDITIONS
      DO 2,I3 = 1,30
  2   AVE2(I3) = 0.
      MEL = 0.
C THE INITIAL CONCENTRATION PROFILE IS ENTERED WITH A FORMULA
      DO 112, I = 1,N-1
        XL = REAL(I-1)/REAL(N-1)
        RRR = 0.
        DO 113, I1 = 1,20
          Q = EXP(-1.*TEXP*(REAL(I1)*P)**2)
          QQ = SIN(REAL(I1)*P*XL)
  113     RRR=RRR+Q*QQ/REAL(I1)
  112 YD(I) = 1.-XL-2.*RRR/P

      MSC = 0.
      DO 437,I=1,N-1
  437 MSC=MSC+(YD(I)+YD(I+1))/2./(REAL(N)-1.)

C AVE2 is the average conc in TS for tts = 0
      DO 431,I=1,30
```

```
      AVE2(I)=YD(4*(I-1)+1)+4.*YD(4*(I-1)+2)
      AVE2(I)=AVE2(I)+2.*YD(4*(I-1)+3)+4.*YD(4*(I-1)+4)
 431  AVE2(I)=(AVE2(I)+YD(4*(I-1)+5))/12.

      DO 6,I3= 1,N
 6    Y(I3) = YD(I3)

 194  CONTINUE
      I2 = I2+1
      SUMRS = 0.
      NSR2 = 0.
      DO 4,I3 = 1,30
 4    AVESC(I3) = 0.

C STEP represents the time to remove 1 tape strip
      READ(3,*) STEP

C SETTING INITIAL CONDITIONS.  T = DSC(T-Texp)/LSC2
      IDO = 1
      T = 0.
      TEND = 0.
      IEND = 0.

C SETTING ERROR TOLERANCE AND ABSOLUTE ERROR CONTROL
      TOL = 1.0E-6
      CALL UMACH (2, NOUT)
      WRITE (NOUT,99998)
      PARAM(10) = 1.

C II is the number of TS's that have been removed.
      II = 0
      MM = 0
      MMM = 0
 10   CONTINUE
      IEND = IEND + STEP
      TEND = IEND
      MMM = MMM + 1
      IF (MMM .EQ. 30) IDO = 3
      CALL IVPAG (IDO, N, FCN, FCNJ, A, T, TEND, TOL, PARAM, Y)

C       IF (MMM .GT. 3) MM=1
      IF (MMM .GT. 0) MM = 1
      IF (MM .EQ. 1) THEN
      II = II+1
C AVESC is the average conc. in each tape strip
      AVESC(II)=Y(4*(II-1)+1)+4.*Y(4*(II-1)+2)+2.*Y(4*(II-1)+3)
      AVESC(II)=AVESC(II)+4.*Y(4*(II-1)+4)+Y(4*(II-1)+5)
      AVESC(II)=AVESC(II)/12.
      RD1 = AVE2(II) - AVESC(II)
      WRITE(6,99997) RD1
      MM = 0
      END IF
      IF (MMM .LE. 29) GO TO 10
```

```
      MTS = 0.
      DO 439, I=1,30
  439 MTS = MTS + AVESC(I)/30.

      MRAT=MTS/MSC
      STEP2 = 30.*6.*STEP
C MEL is the normalized mass absorbed systemically
      MB = (MTS + MEL)/MSC
      WRITE(4,*) STEP2,MRAT,MB
      SUMRS = 0.
      DO 441,I=1,30
      NSR2=NSR2+SQRT(((AVE2(I)-AVESC(I))/MSC)**2.)/30.
  441 SUMRS=SUMRS+SQRT((AVE2(I)-AVESC(I))**2.)/30.
      WRITE(1,*) STEP,STEP2,SUMRS,NSR2
      WRITE(2,*) STEP2,AVESC
      WRITE(2,*)
      DO 5,I3= 1,N
  5   Y(I3) = YD(I3)
      IF (I2 .LT. I22) GO TO 194

99998 FORMAT(11X, 'T', 14X, 'Y')
99999 FORMAT(33E13.7)
99997 FORMAT(E13.7)
      END

      SUBROUTINE FCN (N, T, Y, YPRIME)

      INTEGER N, II
      REAL DZ, DZS, X, Y(N), YPRIME(N), MEL, T2
      COMMON/SKIN/II,MEL
      SAVE T2

      DZ = 1. / (REAL(N) - 1.)
      DZS = DZ * DZ

      DO 111, J = 1, 4*II+1
  111 YPRIME(J) = 0.
      Y(4*II+1) = -1./3.*(Y(4*II+3)-4.*Y(4*II+2))
      DO 222, J = 4*II+2,(N-1)
  222 YPRIME(J) = (Y(J-1)-2.*Y(J)+Y(J+1))/DZS
      YPRIME(N) = 0.
      MEL = MEL - (Y(N-2)-4.*Y(N-1)+3.*Y(N))/2./DZ*(T-T2)
      T2 = T

      RETURN
      END

      SUBROUTINE FCNJ(N, X, Y, DYPDY)
      INTEGER N
      REAL X, Y(N), DYPDY(N,*)
      RETURN
      END
```

Chapter 4. ESTIMATING DERMAL ABSORPTION PARAMETERS FOR 4-CYANOPHENOL FROM SOIL USING TAPE STRIP DATA

Introduction

The tape strip (TS) experiment is a minimally invasive technique for measuring dermal absorption into humans *in vivo*. In a TS experiment, adhesive tapes (10 to 30) are sequentially applied to and removed from a site that was exposed to chemical. The skin adhering to the TS's is then analyzed for the absorbing chemical and the concentration in each TS is calculated. Dermal absorption parameters (e.g., lag time, partition coefficient and permeability coefficient) can be estimated by comparing concentrations in these TS's with theoretical representations of the dermal absorption process. However, if the TS procedure takes longer than about 0.2 times the lag time for the chemical to diffuse through the outermost layer of skin, the stratum corneum (sc), then concentration in the TS's can be affected significantly by diffusion during the TS procedure (see Chapter 3). TS studies reported by Islam *et al.* (1999) and Higo *et al.* (1993) are two examples in which diffusion probably affected the experimental results. As shown in Chapter 3, dermal absorption parameters calculated from experiments like these can deviate substantially from their actual values. It was demonstrated in Chapter 3 that meaningful dermal absorption parameters could be deduced from such data if the mathematical model used in the data analysis allowed for diffusion during the TS procedure.

Recently, Touraille (1998) studied the *in vivo* dermal absorption of 4-cyanophenol, 4CP, in humans from a soil vehicle using a TS technique that took about 35 minutes to complete. As shown in Chapter 3 and by Pirot *et al.* (1997), the *in vivo* lag

time ($t_{lag,sc}$) for 4CP through human sc is about 33 minutes. Based on this value for $t_{lag,sc}$, it is likely that diffusion during the TS procedure affected Touraille's experimental results. In this chapter, Touraille's data are analyzed using two different mathematical models describing dermal absorption from a soil vehicle. One of the models accounted for 4CP diffusion during the TS procedure and the other did not.

Experimental Methods

The experiment was performed at the University of California at San Francisco with approval of the UCSF Committee on Human Research. The soil was collected from the Colorado State University (CSU) Agricultural Field Station and prepared and characterized at the Colorado School of Mines. For all experiments described here, the soil fraction particle size was < 250 μm and the organic carbon content of this fraction was 0.7%. The soil was contaminated by mixing it with an unsaturated solution of 4CP (reagent grade from Aldrich Biochemicals, Brea, CA) in ethanol and then allowing the soil to dry overnight. The amount of 4CP in the soil, determined by exhaustive extraction with acetonitrile followed by UV analysis, was 0.045 g 4CP / g soil, which was large enough that a white residue of 4CP was visible on the soil particles. The load of soil on the skin surface was greater than the mass required to provide a single layer of particles. Soil was applied to a 20 cm^2 area on each forearm of three healthy human volunteers and held in place using a nonocclusive transparent dressing (Tegaderm 1626 3M). One forearm was exposed for 45 minutes and the other for 180 minutes.

At the end of the exposure, the soil was cleaned from the skin and then pre-weighed adhesive tapes (3M Book Tape 845) were applied and removed sequentially on the application site. Approximately 30 TS's were required to reach glistening, pink tissue (i.e., to remove essentially all of the sc). Measurements of transepidermal water loss

(TEWL) performed after cleaning and after every fourth TS strip were used to estimate the thickness of the sc, L_{sc}, as described by Kalia *et al.* (1996). Cleaning the skin with water after the exposure would have altered the TEWL measurements and so compressed air was used to blow the soil off instead. Each TS was weighed after application to the skin to determine the mass of sc removed. The mass of 4CP on each TS was determined using attenuated total reflectance Fourier transform infrared spectroscopy (ATR-FTIR) as described by Pirot *et al.* (1997) and Stinchcomb *et al.* (1999).

The TS analysis using ATR-FTIR provided the mass of 4CP on the n^{th} TS, m_n, per exposed area, A. However, the amount of sc removed by each TS varies, generally decreasing with depth (Higo *et al.*, 1993). To estimate dermal absorption parameters or to compare different experiments, the amount of chemical in each TS must be normalized by the amount of sc (e.g., as done by Pirot *et al.* (1997)). The concentration of 4CP in the sc, C_n (i.e., the mass of 4CP/volume of sc) from each TS can be calculated as follows:

$$C_n = \left(m_n / A\right) \rho_{sc} \Big/ \left(m_{sc,n} / A\right) \tag{4-1}$$

where ρ_{sc} is the density of the sc (~ 1 g/cm^3), and $(m_{sc,n} / A)$ is the mass of sc on the n^{th} TS per area. The location of the center of the n^{th} TS from the skin surface, x_n, was calculated as:

$$x_n = \frac{1}{A \rho_{sc}} \left\{ \frac{m_{sc,n}}{2} + \sum_{i=1}^{n-1} m_{sc,i} \right\} \tag{4-2}$$

When C_n is reported as a function of relative depth in the sc (i.e., x_n / L_{sc}), L_{sc} was estimated using TEWL measurements.

Experimental Results

Experimental results, which were provided by Touraille (1998), are listed in Appendix 4A. Although L_{sc} was calculated for both arms, only the average values (17.8, 8.3, and 16.2 μm for subjects A, B, and C, respectively) were reported. Figure 4.1 shows C_n as a function of x_n / L_{sc} for the 45 and 180-minute exposures. Touraille (1998) did not provide data for TS's with 4CP values below the detection limit. Concentrations in TS's from the 180-minute experiment were larger than on TS's from the 45-minute experiment.

The first data points in Figure 4.1 (i.e., closest to the outside edge of the sc) are marked with an open symbol. For subjects A and B the first data points were larger than expected, perhaps due to incomplete cleaning. It is common for the first few TS's to be more variable than later TS's, and some investigators exclude the first one or few TS's in their data analysis (Shah *et al.*, 1998). Like these previous studies, the following data analysis does not include data from the first TS.

Theory

The sc constitutes the major skin barrier to percutaneous transport of 4CP, which is moderately lipophilic (i.e., the octanol – water partition coefficient is approximately 40 (Hansch *et al.*, 1995)). In addition, the release rate from soil could affect the rate of dermal absorption. This contribution is included in the following model by a first-order mass transfer coefficient, k_o. The concentration profile of the absorbing chemical in the sc (C_{sc}) at the end of an exposure time (t_{exp}) can be estimated by assuming that chemical passively diffuses through a one-layer pseudo-homogenous membrane with an effective diffusion coefficient D_{sc} and apparent thickness L_{sc}. That is:

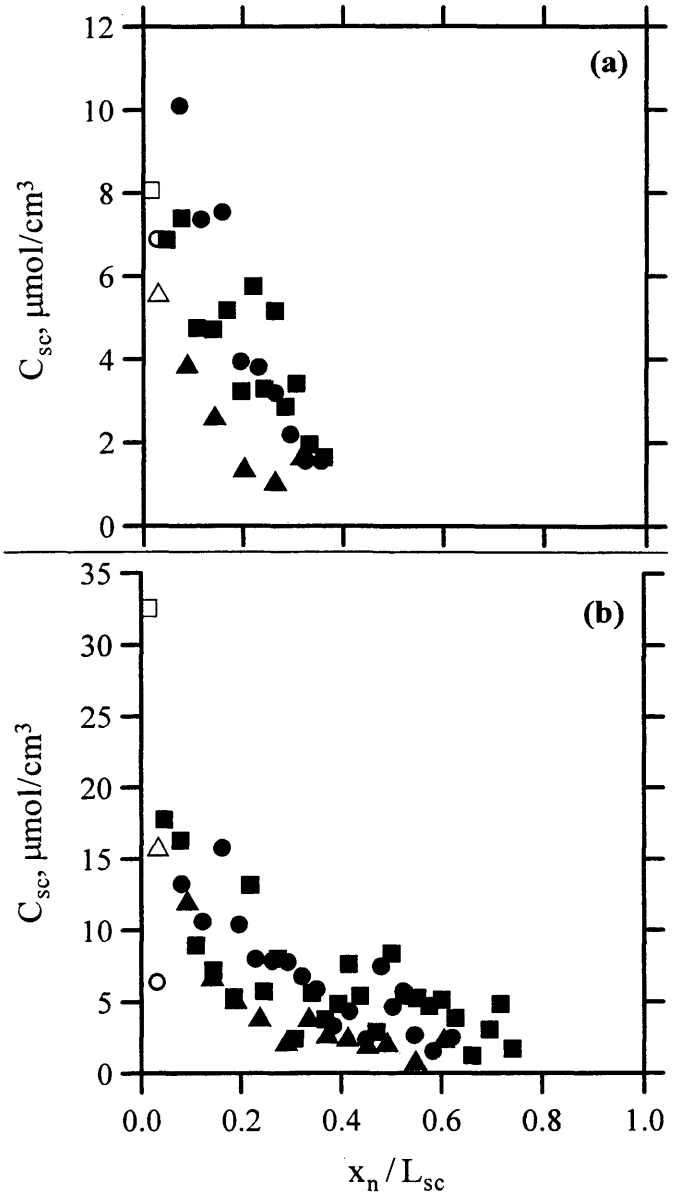

Figure 4.1 – TS experimental results for a) 45-min and b) 180-min exposures to soil contaminated with 4CP for subjects A (■), B (▲) and C (●). The first TS for each subject is indicated by an open symbol.

$$\frac{C_{sc}}{C_{sc}^*} = \frac{\alpha_v}{1+\alpha_v}\left(1-\frac{x}{L_{sc}}\right) - 2\alpha_v \sum_{n=1}^{\infty} e^{-\left\{\frac{\lambda_n^2 t_{exp}}{6 t_{lag,sc}}\right\}} \left[\frac{\frac{\alpha_v}{\lambda_n}\sin\left(\frac{\lambda_n x}{L_{sc}}\right)+\cos\left(\frac{\lambda_n x}{L_{sc}}\right)}{\left(\alpha_n^2+\alpha_v+\lambda_n^2\right)}\right] \qquad (4\text{-}3)$$

where $t_{lag,sc}$ is defined as $L_{sc}^2/(6\,D_{sc})$, C_{sc}^* is the concentration of absorbing chemical in the sc if the sc was in equilibrium with the soil vehicle, x is the coordinate of position in the sc, λ_n are eigenvalues defined as

$$\alpha_v \tan(\lambda_n) + \lambda_n = 0 \qquad (4\text{-}4)$$

and the parameter α_v

$$\alpha_v = \frac{6 k_o / L_{sc}}{t_{lag,sc}} \qquad (4\text{-}5)$$

is the ratio of the mass transfer rate from the soil to the rate of chemical penetration across the sc. Eq 4-3 was developed assuming: (1) the sc is initially free of chemical (i.e., $C_{sc} = 0$ at $t = 0$ for $0 < x < L_{sc}$), (2) transport of chemical from the soil vehicle into the sc is described by a first-order mass transfer coefficient (i.e., $D_{sc}\frac{\partial C_{sc}}{\partial x} = -k_o\left(C_{sc}^* - C_{sc}\right)$ at $x = 0$), and (3) the concentration of absorbing chemical at the innermost layer of the sc is zero (i.e., $C_{sc} = 0$ at $x = L_{sc}$).

If the sc is rapidly removed by serial tape stripping immediately after the contaminated soil is cleaned from the skin surface, then eq 4-3 would describe the concentration of chemical in each TS. However, if the TS procedure is slow relative to chemical diffusion, then the concentration of chemical in the sc will continue to change as specified by Fick's second law:

$$\frac{\partial C_{sc}}{\partial t} = D_{sc}\frac{\partial^2 C_{sc}}{\partial x^2} \qquad \text{for } x_{TS} \le x \le L_{sc} \qquad (4\text{-}6)$$

where x_{TS} is the thickness of the sc that has been removed by tape stripping (see Figure 4.2) at some time after the exposure has ended (i.e., $t > t_{exp}$). If the absorbing chemical is

not volatile, then the flux will be zero at the outermost surface of the remaining sc. That is,

$$\text{at } x = x_{TS} \qquad \frac{\partial C_{sc}}{\partial x} = 0 \qquad \text{for } t > t_{exp} \tag{4-7}$$

As TS's are removed, x_{TS} increases until $x_{TS} = L_{sc}$ and all of the sc is removed. Also,

$$\text{at } x = L_{sc} \qquad C_{sc} = 0 \qquad \text{for } t > 0 \tag{4-8}$$

because the concentration of chemical at the inside edge of the sc is still assumed to be zero.

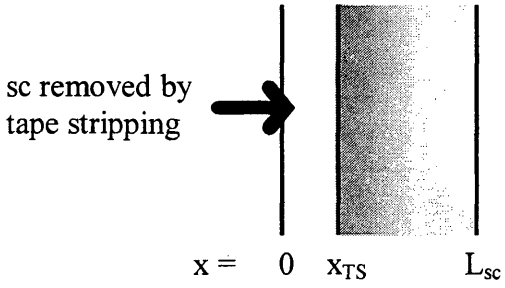

Figure 4.2 – A schematic diagram depicting the TS procedure.

In mathematically simulating Touraille's *in vivo* soil experiments, we assumed that it took 20 seconds to apply and remove each TS. In addition, we assumed that cleaning the sc surface after the exposure ended took one minute, and that TEWL measurements (3 min each) were completed after the surface was cleaned and after every fourth TS. The time to complete the tape strip procedure, t_{TS}, was about 35 min. The TS's were assumed to remove uniform layers of sc of varying thickness. The concentration of chemical in the sc on each TS was calculated by solving eqs 4-6 through 4-8, using eq 4-3 as the initial condition, numerically with the finite difference scheme described in Appendix 4B. To represent the different thicknesses of sc removed, each TS

was assumed to remove an appropriate number of nodes as described in Appendix 4B. Three parameters were required in the calculation: k_o, $t_{lag,sc}$ and C^*_{sc}.

Methods

Best-fit values for k_o, $t_{lag,sc}$ and C^*_{sc} were calculated by minimizing the normalized sum of residual squared (SRS) between the experimental and model-simulated TS concentrations for each subject, defined as

$$SRS = \frac{1}{N_{dp,45}} \sum_{i=1}^{N_{dp,45}} \left[C_{i,45} - C_{sc,i}\right]^2 + \frac{1}{N_{dp,180}} \sum_{i=1}^{N_{dp,180}} \left[C_{i,180} - C_{sc,i}\right]^2 \qquad (4\text{-}9)$$

in which $C_{i,j}$ is the experimental concentration in TS i for exposure time j (j = 45 or 180 min), and $C_{sc,i}$ is the model-calculated concentration for TS i. The data for each exposure time were normalized by the number of data points, $N_{dp,j}$, at that exposure time so that the 45 and 180-minute experiments were weighted equally in the calculation of SRS. Because k_o is a property of soil, it was assumed to be the same for all experiments. The parameters $t_{lag,sc}$ and C^*_{sc} could be different for each subject.

Discussion

Examination of eq 4-3 shows that at steady state, the concentration at the outer edge of the sc, $\hat{C}^*_{sc}$, is $C^*_{sc}\left[\alpha_v/(1+\alpha_v)\right]$. When α_v is large, $\hat{C}^*_{sc}$ equals C^*_{sc}. If transfer from the soil to the skin surface (k_o) contributes a significant resistance, then the concentration of chemical in the outermost layer of the sc (i.e., C_{sc} at x = 0) is not equal to

$\hat{C}^*_{sc}$ immediately. The time required for $C_{sc}(x = 0)$ to reach $\hat{C}^*_{sc}$ is longer when k_o is smaller (i.e., when the soil contributes a larger resistance). This is illustrated in Figure 4.3, which was constructed using eq 4-3 and shows the concentration at the outer edge of the sc normalized by $\hat{C}^*_{sc}$ as a function of $t / t_{lag,sc}$ for several values of α_v. For example, if $\alpha_v < 0.1$, then t_{exp} must be $\geq 6\ t_{lag,sc}$ for $C_{sc}(x = 0) \geq 0.95\ \hat{C}^*_{sc}$. If the soil contributes no resistance (i.e., α_v is very large), then $C_{sc}(x = 0) = \hat{C}^*_{sc}$ from the beginning of the exposure. As shown in Figure 4.1, 4CP concentrations at $x / L_{sc} = 0$ were larger after 180 minutes than after 45 minutes (about 20 compared to 10 $\mu m/cm^3$, respectively), suggesting that soil did contribute a significant resistance to mass transport.

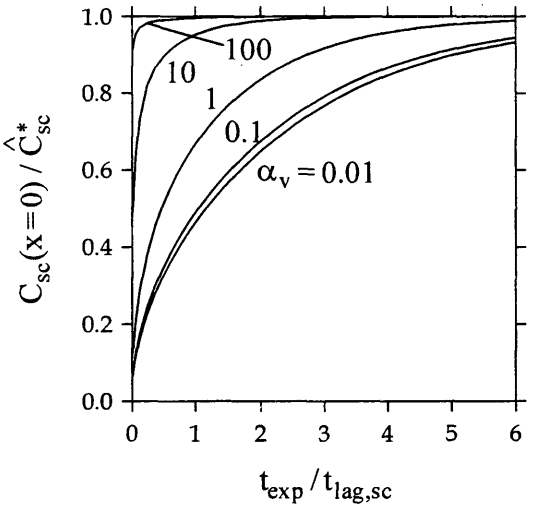

Figure 4.3 – Normalized sc concentration at x = 0 as a function of $t_{exp} / t_{lag,sc}$ when the vehicle adds a significant resistance to mass transport.

Table 4.1 lists values for k_o, $t_{lag,sc}$ and C^*_{sc} determined by minimizing SRS without considering diffusion during the TS procedure (i.e., using eq 4-3). Figure 4.4

compares the TS data to theoretical estimates of the TS concentrations for all three subjects calculated using eq 4-3. The values of $t_{lag,sc}$ (i.e., 130, 430 and 280 min for subjects A, B and C, respectively) were significantly longer than those reported by Pirot *et al.* and in Chapter 3 (i.e., 26-40 min) for exposures to 4CP in aqueous solutions. Although water does alter the sc, previous studies indicate that hydration has a minimal effect on lag time through the sc (Scheuplein and Blank, 1973). It is unlikely that $t_{lag,sc}$ from soil should be 3 to 10 times slower than from an aqueous solution.

Table 4.1 also shows calculated values for the steady-state flux (J^{ss}) through the sc estimated from the fitted parameters. For the parameters determined by regression to eq 4-3, J^{ss} was 0.24, 0.024, and 0.14 $\mu g/cm^2/h$, for subjects A, B, and C, respectively. These values are all smaller than expected. In other experiments, Touraille *et al.* (2000) measured penetration of 4CP through hairless mouse skin (HMS) *in vitro* from the same CSU soil contaminated with a similar amount of 4CP (i.e., 0.038 g 4CP/g soil) and from pure 4CP powder. In the contaminated soil experiments, J^{ss} was 5.6 $\mu g/cm^2/hr$, which is 23 to 230 times larger than the *in vivo* J^{ss}, which was calculated without considering diffusion during the TS procedure. For the *in vitro* experiments from pure 4CP powder, J^{ss} was 20 $\mu g/cm^2/hr$, which, as expected, is the same order of magnitude as the *in vitro* results from a heavily contaminated soil. While penetration rates through HMS are usually more rapid than through human skin, this difference is almost always less than one order of magnitude (Vecchia, 1997). So, although the theoretical calculations shown in Figure 4.4 appear to fit the TS data satisfactorily, estimated values for J^{ss} seem unreasonably small compared to related *in vitro* measurements, and values for $t_{lag,sc}$ seem unreasonably long compared to other *in vivo* measurements.

The lower half of Table 4.1 lists values for k_o, $t_{lag,sc}$ and C^*_{sc} calculated using eqs 4-6 through 4-8, which account for 4CP diffusion during the TS procedure. Consistent with measurements by Pirot *et al.* (1997) and in Chapter 3, $t_{lag,sc}$ was 35 min when $t_{lag,sc}$

Table 4.1 – Parameter estimation results.

Eqs Fit	Subject	k_o[a] cm/s	L_{sc}[b] μm	C^*_{sc} μmol/cm^3	$t_{lag,sc}$ min	J^{ss}[c] μg/cm^2/h	α_v	t_{TS} / $t_{lag,sc}$
4-3	A	1E-7	17.8	20	130	0.24	2.6	0.27
	B	1E-7	8.3	11	430	0.024	18	0.081
	C	1E-7	16.2	23	280	0.14	6.2	0.13
	A, B and C[d]	1E-7	14.1 ± 5.1	18 ± 6	280 ± 150	0.13 ± 0.11	8.9 ± 8.5	0.16 ± 0.10
4-6 through 4-8	A	7E-9	17.8	337	35[a]	0.97	0.05	1
	B	7E-9	8.3	85	35[a]	0.22	0.1	1
	C	7E-9	16.2	314	35[a]	0.82	0.05	1
	A, B and C[d]	7E-9	14.1 ± 5.1	250 ± 140	35[a]	0.67 ± 0.40	0.07 ± 0.03	1

[a] Forced to be the same for all subjects. [b] Calculated by Touraille (1998) using TEWL measurements as described by Kalia *et al.* (1996). [c] $J^{ss} = \hat{C}^*_{sc} L_{sc} / \left(6 t_{lag,sc}\right)$ where $\hat{C}^*_{sc} = C^*_{sc}\left[\alpha_v / (1+\alpha_v)\right]$. [d] Mean value for subjects A, B and C ± one standard deviation where appropriate.

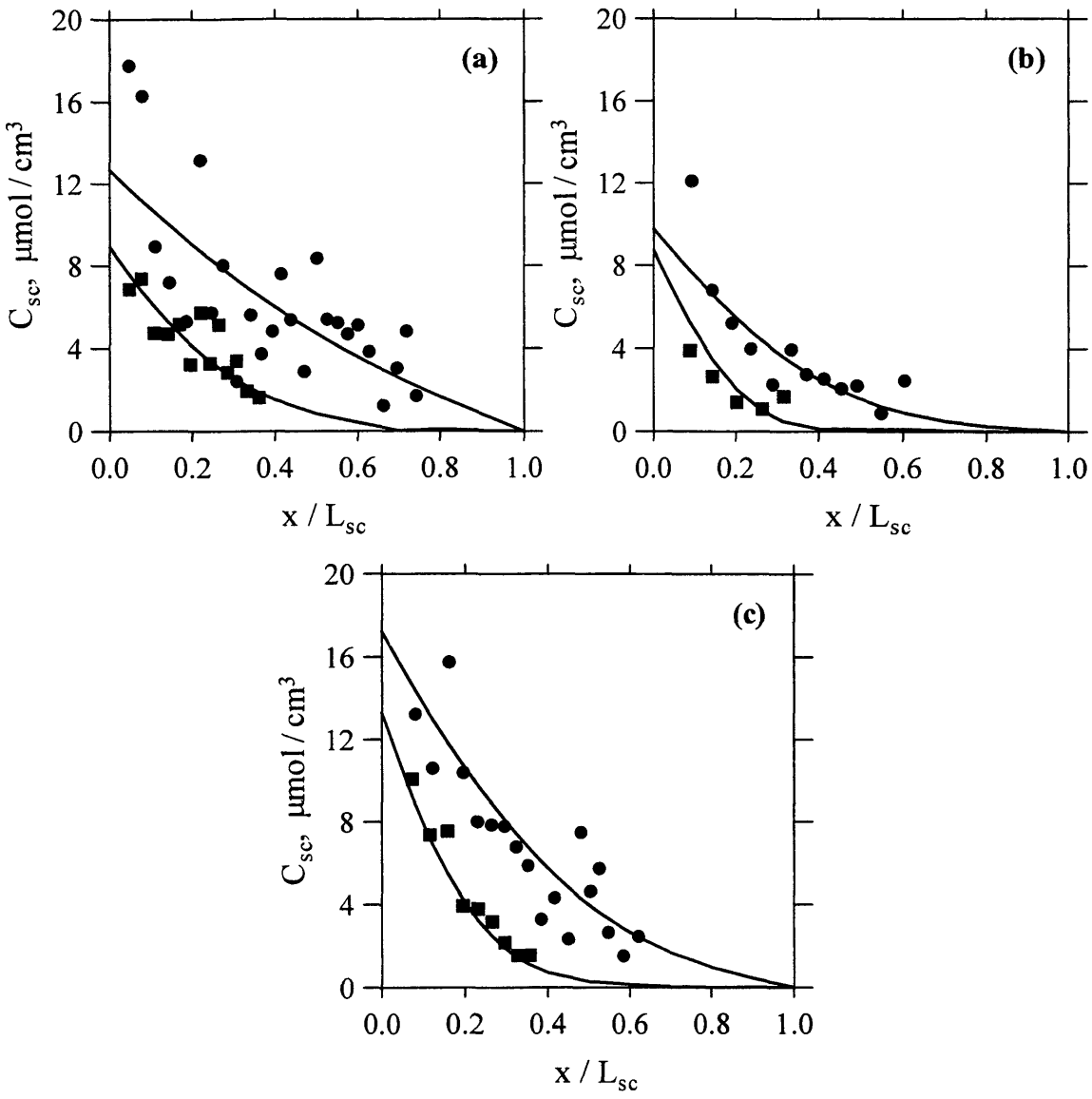

Figure 4.4 – TS data for 45-min (■) and 180-min (●) exposures and curve-fitting results calculated using eq 4-3 for subjects a) A, b) B, and c) C.

was forced to be the same for all subjects and restricted to a reasonable value (i.e., less than 45 min). In this case, calculated values of J^{ss} (0.97, 0.22 and 0.82 $\mu g/cm^2/h$ for subjects A, B and C, respectively) compare more closely with the values reported by Touraille *et al.* for steady-state flux of 4CP through HMS from contaminated CSU soil and from a powder vehicle.

If $t_{lag,sc}$ was allowed to be different for each subject, $t_{lag,sc}$ determined by minimizing SRS for eqs 4-6 through 4-8 was < 30 min for subject C, but > 45 min for subjects A and B. As already discussed, $t_{lag,sc}$ > 45 min was larger than previously reported. When $t_{lag,sc}$ was forced to be the same for all subjects, data regressions to eqs 4-6 through 4-8 produced SRS that were slightly larger (by about 30%) than from data regressions to eq 4-3. Despite this, dermal absorption parameters estimated using eqs 4-6 through 4-8 are reasonable compared to other experimental studies while parameters derived using eq 4-3 do not seem reasonable. Given the scatter in the TS data, the mathematical model (i.e., regression to eq 4-3 compared with regression to eqs 4-6 through 4-8) producing the minimum value of SRS might not correctly indicate the physical reality, particularly when differences between SRS from the two regressions are not very different.

Figure 4.5 compares the TS data (solid symbols) to theoretical results (open symbols) for all three subjects when 4CP diffusion during the tape stripping is included in the calculations. The solid curves represent the theoretical concentration profiles at the end of the 45 and 180-minute exposures. The differences between the curves and the open symbols indicate that diffusion during the time to tape strip does significantly affect experimental results if $t_{lag,sc}$ = 35 min. Figure 4.5 shows that curvature in the sc concentration profile measured by tape stripping can result from diffusion during the TS procedure as well as short exposures.

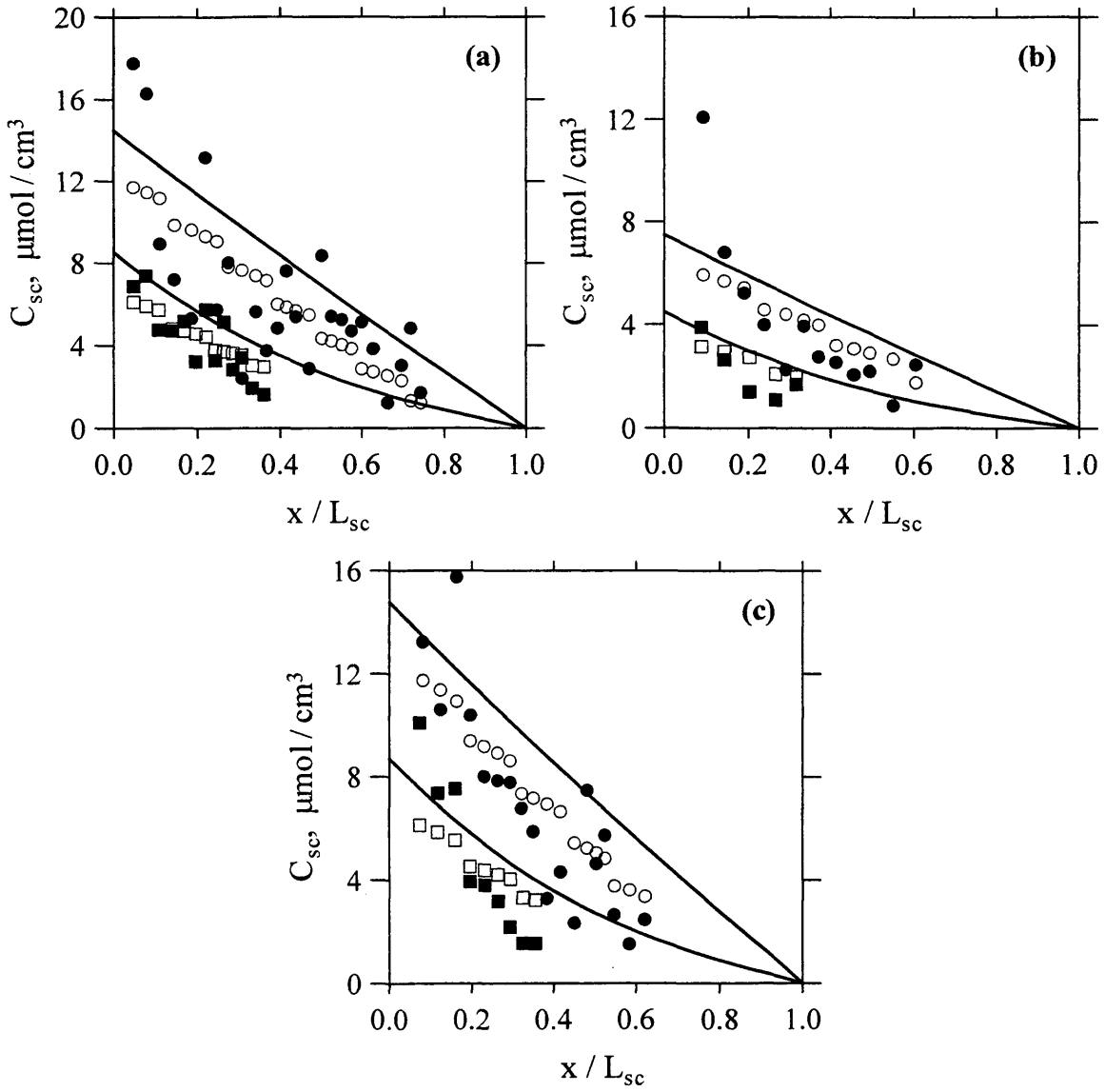

Figure 4.5 – TS data for 45-min (■) and 180-min (●) exposures (closed symbols) and curve-fitting results (open symbols) for subjects a) A, b) B, and c) C. The curves show the approximated TS concentrations at t = t_{exp}.

When t_{TS} was accounted for in the data analysis, the values of α_v were 0.05, 0.1, and 0.05 for subjects A, B and C, respectively. This indicates that the rate of dermal absorption was controlled by the mass transfer resistance from the soil. Tourailles *et al.* (2000) found that J^{ss} of 4CP from the contaminated CSU soil through HMS *in vitro* (soil contamination was 0.038 g 4CP/g soil) and through a polymeric membrane of mixed (acetate/nitrate) cellulose esters (soil contamination was 0.03 g 4CP/g soil) were 5.6 and 3.6 $\mu g/cm^2/hr$, respectively. The similar values of J^{ss} for absorption through these two very different membranes suggest that penetration rates were controlled by the soil.

Touraille measured TEWL after cleaning the skin surface and after every fourth TS for the purpose of estimating L_{sc}. According to mathematical simulations of 4CP diffusion shown above, these TEWL measurements slowed the TS procedure enough that concentrations in the TS's were altered by diffusion after the exposure had ended. Recently, Pirot *et al.* (1998) demonstrated that L_{sc} could be estimated using only two TEWL measurements. If only two TEWL measurements were used, then the TS procedure could be completed in about 17 min (i.e., 1 min to clean the surface, 10 min for application of 30 TS's, and 6 min for two TEWL measurements), which would give $t_{TS}/t_{lag,sc} \approx 0.5$ if $t_{lag,sc} = 35$ min. Theoretical calculations described in Chapter 3 demonstrated that diffusion will affect TS results minimally if $t_{TS}/t_{lag,sc} < 0.2$ (i.e., $t_{TS} < 7$ min if $t_{lag,sc} = 35$ min). Thus, the procedure with two TEWL measurements would greatly reduce but not completely remove the effect of diffusion on TS results of 4CP absorption from soil vehicles.

Conclusions

A mathematical model accounting for diffusion during the time to tape strip, t_{TS}, was developed and used to analyze *in vivo* dermal absorption data of 4CP in humans from

a soil vehicle. Dermal absorption parameters estimated by best-fit regression (J^{ss} and $t_{lag,sc}$) neglecting the effect of stripping time were significantly different than those reported previously in the literature. When the time required to tape strip the sc was included in the model used to analyze the data, then estimated values of J^{ss} were consistent with J^{ss} measured through HMS *in vitro* from the same soil contaminated with 4CP and from powdered 4CP. Dermal absorption parameters estimated allowing for diffusion during the TS procedure indicate that the mass transfer resistance of the soil controlled the rate of dermal absorption.

Notation

A	surface area of chemical exposure
C_{sc}	concentration of the absorbing chemical in the sc
$C_{sc,n}$	model-calculated concentration of the absorbing chemical in the n^{th} TS
C_{sc}^{*}	the concentration of absorbing chemical in the sc if the sc were in equilibrium with the soil vehicle
$\hat{C}_{sc}^{*}$	the steady-state concentration of absorbing chemical at the outer edge of the sc $(= C_{sc}^{*}[\alpha_v/(1+\alpha_v)])$
C_n	concentration of the absorbing chemical in the n^{th} TS
$C_{n,j}$	concentration of the absorbing chemical in the n^{th} TS at exposure time j (j = 45 or 180 min)
D_{sc}	effective diffusion coefficient of the absorbing chemical in the sc
J^{ss}	steady-state flux through the sc
k_o	first-order mass transfer coefficient in the soil
L_{sc}	apparent thickness of the sc
m_n	mass of absorbing chemical on the n^{th} TS
$m_{sc,n}$	mass of sc on the n^{th} TS
N	number of nodes in the sc for the finite-difference solution
$N_{dp,j}$	number of experimental data points collected in the j^{th} exposure time (j = 45 or 180 min)
sc	stratum corneum
t	time
t_{exp}	duration of the dermal exposure
$t_{lag,sc}$	lag time for chemical penetrating through the sc, $L_{sc}^2/(6D_{sc})$
t_{TS}	time required to completely remove the sc by tape stripping

x	position in the sc
Δx	distance between nodes of the finite difference solution
x_n	location of the center of the n^{th} TS
Δx_n	thickness of sc removed by the n^{th} TS
x_{TS}	location of the sc edge which moves inward as TS's are removed

Greek

α_v	ratio of the rate of transfer of the absorbing chemical from the soil to the rate of chemical penetration across the sc
ρ_{sc}	density of the sc

References

Hansch, C., A. Leo and D. Hoekman (1995). Exploring QSAR. Hydrophobic, electronic, and steric constants. Washington, DC, American Chemical Society.

Higo, N., A. Naik, D. B. Bommannan, R. O. Potts and R. H. Guy (1993). "Validation of reflectance infrared spectroscopy as a quantitative method to measure percutaneous absorption *in vivo*." Pharmaceutical Research **10**:1500-1506.

Islam, M. S., L. Zhao, J. N. McDougal and G. L. Flynn (1999). "Uptake of chloroform by skin on brief exposures to the neat liquid." American Industrial Hygiene Association Journal **60**:5-15.

Kalia, Y. N., F. Pirot and R. H. Guy (1996). "Homogenous transport in a heterogeneous membrane: water diffusion across human stratum corneum *in vivo*." Biophysical Journal **71**:2692-2700.

Pirot, F., E. Berardesca, Y. N. Kalia, M. Singh, H. I. Maibach and R. H. Guy (1998). "Stratum corneum thickness and apparent water diffusivity: facile and noninvasive quantitation *in vivo*." Pharmaceutical Research **15**:492-494.

Pirot, F., Y. N. Kalia, A. L. Stinchcomb, G. Keating, A. L. Bunge and R. H. Guy (1997). "Characterization of the permeability barrier of human skin *in vivo*." Proceedings of the National Academy of Sciences of the United States of America **94**:1562-1567.

Scheuplein, R. J. and I. H. Blank (1973). "Mechanism of percutaneous absorption. IV. Penetration of nonelectrolytes (alcohols) from aqueous solutions and from pure liquids." Journal of Investigative Dermatology **60**:286-296.

Shah, V. P., G. L. Flynn, A. Yacobi, H. I. Maibach, C. Bon, N. M. Fleischer, T. J. Frantz, S. A. Kaplan, J. Kawamoto, L. J. Lesko, J. P. Marty, L. K. Pershing, H. Schaefer, J. A. Sequeira, S. P. Shrivastava, J. Wilkin and R. L. Williams (1998). "Bioequivalence of topical dermatological dosage forms-- methods of evaluation of bioequivalence." Pharmaceutical Research **15**:167-171.

Stinchcomb, A. L., F. Pirot, G. D. Touraille, A. L. Bunge and R. H. Guy (1999). "Chemical uptake into human stratum corneum *in vivo* from volatile and non-volatile solvents." Pharmaceutical Research **16**:1288-1293.

Touraille, G. D. (1998). Unpublished data, Personal communication.

Touraille, G. D., S. M. Arnold, A. L. Bunge, J. P. Marty and R. H. Guy (2000). "Uptake of 4-cyanophenol from soils, water and pure solids." Perspectives in Percutaneous Penetration **vol. 6B**, in press.

Vecchia, B. (1997). Estimating the Dermally Absorbed Dose from Chemical Exposure: Data Analysis, Parameter Estimation, and Sensitivity to Parameter Uncertainties. M.S. thesis, Department of Chemical Engineering and Petrolium Refining, Colorado School of Mines, Golden, CO.

Appendix 4A – Experimental Data

Table 4A.1 – Dermal absorption study results for a 45-min exposure to 4CP in a soil vehicle (Touraille, 1998).

Subject A		Subject B		Subject C	
x_n / L_{sc}	C_n, μmol/cm^3	x_n / L_{sc}	C_n, μmol/cm^3	x_n / L_{sc}	C_n, μmol/cm^3
0.016	8.07	0.031	5.61	0.027	6.89
0.047	6.88	0.089	3.91	0.073	10.10
0.077	7.39	0.143	2.65	0.117	7.36
0.108	4.75	0.203	1.41	0.159	7.54
0.140	4.72	0.264	1.09	0.195	3.94
0.168	5.17	0.317	1.69	0.231	3.81
0.196	3.23			0.264	3.19
0.221	5.75			0.294	2.19
0.242	3.28			0.325	1.56
0.264	5.16			0.356	1.55
0.284	2.86				
0.307	3.41				
0.332	1.95				
0.361	1.64				

Table 4A.2 – Dermal absorption study results for a 180-min exposure to 4CP in a soil vehicle (Touraille, 1998).

Subject A		Subject B		Subject C	
x_n / L_{sc}	C_n, μmol/cm^3	x_n / L_{sc}	C_n, μmol/cm^3	x_n / L_{sc}	C_n, μmol/cm^3
0.014	32.6	0.034	15.9	0.031	6.40
0.046	17.8	0.093	12.1	0.081	13.2
0.079	16.3	0.143	6.82	0.123	10.6
0.110	8.95	0.190	5.23	0.162	15.8
0.145	7.20	0.237	3.99	0.196	10.4
0.186	5.32	0.290	2.26	0.229	8.01
0.219	13.2	0.335	3.95	0.262	7.86
0.246	5.75	0.371	2.76	0.293	7.79
0.274	8.04	0.413	2.55	0.322	6.78
0.307	2.42	0.454	2.06	0.350	5.88
0.341	5.64	0.491	2.20	0.383	3.30
0.367	3.75	0.549	0.89	0.416	4.32
0.394	4.85	0.605	2.46	0.450	2.35
0.415	7.62			0.481	7.48
0.438	5.40			0.503	4.64
0.471	2.89			0.524	5.74
0.501	8.37			0.546	2.66
0.525	5.42			0.584	1.53
0.551	5.26			0.621	2.48
0.575	4.71				
0.600	5.14				
0.628	3.85				
0.662	1.23				
0.696	3.05				
0.718	4.84				
0.742	1.72				

Appendix 4B – Numerical Solution

Eqs 4-6 through 4-8 were solved using a finite difference scheme that transformed the partial differential equation of t and x (eq 4-6) into a system of ordinary differential equations of t alone. The concentration in the sc was represented by N nodes equally spaced in x and the derivatives were approximated using the following formulas:

$$\frac{\partial^2 C_{sc,i}}{\partial x^2} = \frac{C_{sc,i-1} - C_{sc,i} + C_{sc,i+1}}{(\Delta x)^2} \tag{4B-1}$$

$$\left(\frac{\partial C_{sc,i}}{\partial x}\right)_{x=x_{TS}} = \frac{-3C_{sc,i} + 4C_{sc,i+1} - C_{sc,i+2}}{2\Delta x} \tag{4B-2}$$

where $\Delta x = L_{sc} / (N-1)$. For the calculations in this chapter, N = 200. Eqs 4B-1 and 4B-2 are second-order accurate in x. The resulting ordinary differential equations were solved using the FORTRAN computer program listed in Appendix 4C, which uses the IVPAG routine from the IMSL library to solve the ordinary differential equations. In the calculations shown in this chapter, the thickness of sc removed by the n^{th} TS, Δx_n, was calculated as

$$\Delta x_n = m_{sc,n} / (A \rho_{sc}) \tag{4B-3}$$

and the number of nodes used to represent each TS were estimated as $(\Delta x_n / \Delta x) + 1$ rounded to the nearest integer. The TS removing the smallest amount of sc required three nodes and had an error of less than 17% in the thickness of sc removed. On average, sc thickness on TS's were represented by 7 nodes, and had an error of less than 7.1%. The chemical concentration in the n^{th} TS was calculated by averaging the value of C_{sc} in the mass of sc removed by each TS as follows:

$$C_n = \frac{1}{\Delta x_n} \int_{x_{TS}-\Delta x_n}^{x_{TS}} C_{sc} dx \tag{4B-4}$$

which was calculated by numerical integration.

Stability of the numerical solution with respect to the number of nodes was confirmed (i.e., increasing the number of nodes did not change the results). Also, at the end of each simulation the sum of the mass of chemical that had been removed by TS's, diffused through the sc, and remained in the sc was within 0.3% of the mass of chemical in the sc at the end of the exposure.

Appendix 4C – FORTRAN Program

Table 4C.1 lists the names of variables in the following program. The program needs to be compiled so that the IVPAG subroutine can be accessed.

Table 4C.1 – Variable names in the FORTRAN program.

variable in program	variable in chapter
T	$D_{sc}\left(t - t_{exp}\right) / L_{sc}^2$
N	N
Y(i), i = 1 to N	C_{sc} / C_{sc}^* at node position i
YPRIME(N)	spatial derivative of Y calculated with finite differencing
NTS	$N_{dp,j}$
AVESC(NTS)	C_n / C_{sc}^*, an array containing the concentration of each TS
E(20)	array with 20 λ_n's calculated with NEWTR subroutine
MSC	$M^o / \left(A\, L_{sc}\, C_{sc}^*\right)$, normalized mass in the sc (M^o) at $t = t_{exp}$
MTS	$M_{TS} / \left(A\, L_{sc}\, C_{sc}^*\right)$, normalized mass removed by TS's (M_{TS})
XL	x / L_{sc}, normalized position in the sc
EXPRAT	$t_{exp} / t_{lag,sc}$
TEXP	$D_{sc}\, t_{exp} / L_{sc}^2$
STEP	dimensionless time to remove one TS (corresponds to 20 secs)
DZ	Δz
MB	$\left(M_{TS} + M_{abs}\right) / M^o$ (remains ~ 1 for adequate solution)

```
      PROGRAM TAPE5

C This program simulates the TS experiment for a combination of ko,
C tlag,sc and Csc* to compare with TS data for subject A at 45 min.
      INTEGER NPARAM, N, NTS

C 30 tape strips are removed during an experiment. NTS
C is the number of TS's not below the detection limit.
      PARAMETER (NPARAM=50, N=201, NTS=14)

C SPECIFICATIONS FOR LOCAL VARIABLES
      INTEGER IDO, NOUT,II,MMM,I2,I1,I22,I,IO
      REAL PARAM(NPARAM),T,TEND,A(1,1),IEND
      REAL XL,TEXP,ALV,E(20),Q,QQ,TFINAL,TLAG,MEL,MB
      REAL Y(N),AVESC(NTS),RRR,TOL,STEP,MTS,MSC,LSC,KO
      COMMON/SKIN/II,MEL

C SPECIFICATIONS FOR SUBROUTINES
      EXTERNAL IVPAG, SSET, UMACH
      EXTERNAL FCN, FCNJ
      CALL SSET(NPARAM, 0.0, PARAM, 1)

      OPEN (1, FILE='data.dat', STATUS = 'NEW')
      OPEN (3, FILE='strip.dat', STATUS = 'OLD')

C CHOOSING GEAR'S BDF METHOD
      PARAM(12) = 2

C Units on Lsc are cm, TEXP are min, and KO is cm/s.
      READ(3,*) I22
      LSC = 0.00178
      I2 = 0
      TEXP = 45.

 194  CONTINUE
      I2 = I2+1

C STEP represents the time to remove 1 tape strip (20s)
C Units on TLAG are min.
      READ(3,*) STEP,KO
      TLAG = 1./3./6./STEP
      ALV = 360.*KO*TLAG/LSC
      TFINAL = 105.*STEP+STEP/10.
      MEL = 0.

C SETTING INITIAL CONDITIONS.  T = DSC(T-Texp)/LSC2
      IDO = 1
      T = 0.
      DO 3,I=1,N
  3   Y(I) = 0.

      DO 2,I=1,NTS
  2   AVESC(I) = 0.
      TEND = 0.
```

```
      IEND = 0.

C Calling a subroutine to calculate the eigenvalues needed
C for the concentration profile with vehicle resistance
      CALL NEWTR(ALV,E)

      IO = 1
      II = 1
C THE INITIAL CONCENTRATION PROFILE IS ENTERED WITH A FORMULA
      DO 112, I = 1,N-1
        XL = REAL(I-1)/REAL(N-1)
        RRR = 0.
        DO 113, I1 = 1,8
          Q = EXP(-1.*TEXP/6./TLAG*E(I1)**2)
          QQ = ALV*SIN(E(I1)*XL)+E(I1)*COS(E(I1)*XL)
  113     RRR=RRR+Q*QQ/(E(I1)*(ALV**2+ALV+E(I1)**2))
  112 Y(I) = ALV/(1.+ALV)*(1.-XL)-2.*ALV*RRR

C This calculates the mass in the sc at the end of the exposure
      MSC = 0.
      DO 437,I=1,N-1
  437 MSC=MSC+(Y(I)+Y(I+1))/2./(REAL(N)-1.)

C SETTING ERROR TOLERANCE
      TOL = 1.0E-6
      CALL UMACH (2, NOUT)
      WRITE (NOUT,99998)

C SELECTING ABSOLUTE ERROR CONTROL
      PARAM(10) = 1.

C II is the number of tape strips that have been removed.
      MMM = 0

 10   CONTINUE
      IEND = IEND + STEP
      TEND = IEND
C After MMM goes up by 1, 20 seconds pass in the simulation.
      MMM = MMM + 1
      CALL IVPAG (IDO, N, FCN, FCNJ, A, T, TEND, TOL, PARAM, Y)

C This calculates the average concentration in each TS.
       IO = II
       IF (MMM .EQ. 13) THEN
         II = 6
         AVESC(1) = CALC1(Y,5,IO,II)
       END IF
       IF (MMM .EQ. 14) THEN
         II = 13
         AVESC(2) = CALC1(Y,7,IO,II)
       END IF
       IF (MMM .EQ. 15) THEN
         II = 18
         AVESC(3) = CALC1(Y,5,IO,II)
```

```
          END IF
          IF (MMM .EQ. 16) THEN
            II = 25
            AVESC(4) = CALC1(Y,7,IO,II)
          END IF
          IF (MMM .EQ. 26) THEN
            II = 31
            AVESC(5) = CALC1(Y,6,IO,II)
          END IF
          IF (MMM .EQ. 27) THEN
            II = 36
            AVESC(6) = CALC1(Y,5,IO,II)
          END IF
          IF (MMM .EQ. 28) THEN
            II = 42
            AVESC(7) = CALC1(Y,6,IO,II)
          END IF
          IF (MMM .EQ. 29) THEN
            II = 46
            AVESC(8) = CALC1(Y,4,IO,II)
          END IF
          IF (MMM .EQ. 39) THEN
            II = 51
            AVESC(9) = CALC1(Y,5,IO,II)
          END IF
          IF (MMM .EQ. 40) THEN
            II = 54
            AVESC(10) = CALC1(Y,3,IO,II)
          END IF
          IF (MMM .EQ. 41) THEN
            II = 59
            AVESC(11) = CALC1(Y,5,IO,II)
          END IF
          IF (MMM .EQ. 42) THEN
            II = 63
            AVESC(12) = CALC1(Y,4,IO,II)
          END IF
          IF (MMM .EQ. 52) THEN
            II = 69
            AVESC(13) = CALC1(Y,6,IO,II)
          END IF
          IF (MMM .EQ. 53) THEN
            II = 75
            AVESC(14) = CALC1(Y,6,IO,II)
          END IF

        IF (MMM .LE. 105) THEN
           IF (MMM .EQ. 105) IDO = 3
C           WRITE(1,*) MMM,IDO
           GO TO 10
        END IF

C This calculates the amount total mass removed by tape stripping
        MTS = 0.
```

```
      MTS = MTS + AVESC(1)*5.+AVESC(2)*7.+AVESC(3)*5.
      MTS = MTS + AVESC(4)*7.+AVESC(5)*6.+AVESC(6)*5.
      MTS = MTS + AVESC(7)*6.+AVESC(8)*6.+AVESC(9)*5.
      MTS = MTS + AVESC(10)*3.+AVESC(11)*5.+AVESC(12)*4.
      MTS = MTS + AVESC(13)*6.+AVESC(14)*6.
      MTS = MTS / REAL(N-1)

C The mass balance includes chemical removed by tape stripping,
C chemical absorbed systemically, and chemical in sc that is
C not removed by stripping (there is no need to simulate all
C 30 TS's, so I just had simulation run until last TS needed!)
      MB = 0.
      MB = (MTS+MEL)/MSC
      DO 882, I = 75,N-1
  882 MB = MB + (Y(I)+Y(I+1))/2./REAL(N-1)/MSC

      WRITE(1,99997) ALV,MB,TLAG,KO,AVESC
      WRITE(1,*)

      IF (I2 .LT. I22) GO TO 194

99998 FORMAT(11X, 'T', 14X, 'Y')
99999 FORMAT(33E13.7)
99997 FORMAT(E13.7)
      END

      SUBROUTINE FCN (N, T, Y, YPRIME)

      INTEGER N, II
      REAL DZ, DZS, MEL
      REAL X, Y(N), YPRIME(N)

      COMMON/SKIN/II,MEL
      SAVE T2

      DZ = 1. / (REAL(N) - 1.)
      DZS = DZ * DZ

      DO 111, J = 1, II
  111 YPRIME(J) = 0.
      Y(II) = -1./3.*(Y(II+2)-4.*Y(II+1))
      DO 222, J = II+1,(N-1)
  222 YPRIME(J) = (Y(J-1)-2.*Y(J)+Y(J+1))/DZS
      YPRIME(N) = 0.

      MEL = MEL - (Y(N-2)-4.*Y(N-1)+3.*Y(N))/2./DZ*(T-T2)
      T2 = T

      RETURN
      END

      SUBROUTINE FCNJ(N, X, Y, DYPDY)
      INTEGER N
      REAL X, Y(N), DYPDY(N,*)
```

```
      RETURN
      END

      SUBROUTINE NEWTR(ALV, EIG)

      INTEGER NN
      REAL P1,P2,TT
      REAL ALV,F,FP,EIG(20)

      P1 = 0.
      P2 = -3.14159/4.

      DO 4, NN = 1,20
      P1 = P2 + 3.14159
      TT = 1.
    7 IF (TT .LT. 0.00001) GOTO 8
      F = ALV * SIN(P1) + P1*COS(P1)
      FP = ALV*COS(P1) - P1*SIN(P1)
      P2 = P1 - F/FP
      TT = ABS(P2-P1)/ABS(P2)
      P1 = P2
      GOTO 7

    8 EIG(NN) = P2
    4 TT = 1.

      RETURN
      END

      FUNCTION CALC1(Y,IN,IO,II)
      REAL Y(201)
      INTEGER IN,IO,II,I

      CALC1 = 0.
      DO 192, I = IO,II-1
  192 CALC1 = CALC1 + (Y(I)+Y(I+1))/2.
      CALC1 = CALC1 / REAL(IN)

      RETURN
      END
```

Chapter 5. DOES EPIDERMAL TURNOVER REDUCE PERCUTANEOUS PENETRATION?

Introduction

The skin can be an important exposure route to chemicals from a variety of pharmaceutical, cosmetic, household, agricultural, or industrial products. For organic chemicals of moderate size, penetration through the skin membrane is a solution-diffusion process (Scheuplein, 1978; EPA, 1992; Potts and Guy, 1992; Vecchia, 1997). Once chemical is removed from the skin's surface, chemical within the skin can continue to diffuse through the skin and enter the bloodstream. As a result, for brief chemical exposures, much of the systemic chemical absorption can occur after the chemical has been removed from the skin surface.

Skin is continuously replaced through epidermal turnover, the process by which new cells are generated at the base of the epidermis while the outermost surface flakes off (i.e., desquamates) at the same rate. Chemical in desquamated skin cannot be absorbed systemically. Some investigators have suggested that desquamation will significantly reduce systemic exposure to dermally absorbed chemicals (e.g., Schaefer *et al.* (1982) and Auton *et al.* (1994)). A mathematical model describing chemical absorption into the epidermis allowing for epidermal turnover is used to examine that claim quantitatively.

Background

Physiologically, skin is a multi-layered membrane. For many chemicals, the outermost skin layer, the stratum corneum (sc), is the rate-limiting barrier for mass transfer into and through skin. For highly lipophilic chemicals, the second skin layer, the viable epidermis (ve), also contributes a significant resistance to mass transfer across the skin. Together, the sc and ve comprise the epidermis (epi). The dermis, located beneath the epi, is a highly vascularized tissue that usually has sufficient blood flow to clear away all chemical passing through the epi (Scheuplein and Bronaugh, 1983).

New cells continually form in the proliferating basal layer of the ve to replace cells lost from the sc surface by desquamation. The typical time required to completely replace the sc (i.e., the turnover time for the sc, $t_{t,sc}$) is approximately 14 days, but varies with physiological location (Finlay *et al.*, 1982) and age (Grove, 1986). The turnover time for the ve, $t_{t,ve}$, has been reported as 38 – 61 days (Halprin, 1972), 31 days (Bergstresser and Taylor, 1977), 33 – 34 days (Iizuka, 1994), and 25 days (Weinstein *et al.*, 1984). The variations in reported values of $t_{t,ve}$ arise because in each of the references cited, $t_{t,ve}$ was calculated using different methods, models, and assumptions. Also, turnover times can be shorter for diseased skin (Weinstein *et al.*, 1984). While the rate of desquamation can be changed by chemically or mechanically forcing desquamation or by protecting a site, the rate of cell proliferation does not change (Kligman, 1964; Roberts and Marks, 1980).

Although the potential contribution of desquamation to chemical elimination from the skin has been mentioned in many papers, quantitative mathematical modeling of the process has been limited. The model described by Auton *et al.* (1994) did include desquamation and sc turnover. However, their model did not include ve turnover and did not clearly relate sc turnover and chemical loss from the surface layer.

Theory

Typically, dermal absorption models account for chemical transport through the skin by passive diffusion alone (Silcox *et al.*, 1990; Cleek and Bunge, 1993; Reddy *et al.*, 1998). However, cell proliferation at the basal layer of the ve along with desquamation of the outer surface of the sc cause the epi to move slowly outward, carrying chemical dissolved in the sc along with it. Most dermal absorption models neglect this convective transport of absorbed chemical because cell growth is frequently much slower than diffusion. By including the epi turnover velocity in the model presented here, we are able to examine theoretically the effect of desquamation on dermal absorption.

In the ve, cells are released from the basal layer and move upward in a random manner (Halprin, 1972). However, many cells in the differentiating layers of the ve move in tandem as a front (Weinstein *et al.*, 1984). Once the cells reach the sc, they are tightly attached to each other and travel in unison (Halprin, 1972). Consequently, we assume that the sc and ve move at the constant velocities u_{sc} and u_{ve}, respectively. These velocities are estimated as the constant apparent thickness of the sc (L_{sc}) or ve (L_{ve}) divided by the turnover time for each layer (i.e., $u_{sc} = L_{sc} / t_{t,sc}$ and $u_{ve} = L_{ve} / t_{t,ve}$).

We describe dermal absorption as mass transport through two pseudohomogenous membranes in series, including both the sc and ve. The differential mass balance equations describing one-dimensional chemical transport by passive diffusion and epidermal turnover within the sc and ve are:

$$\frac{\partial C_{sc}}{\partial t} = D_{sc}\frac{\partial^2 C_{sc}}{\partial x^2} + u_{sc}\frac{\partial C_{sc}}{\partial x} \qquad \text{for } 0 < x < L_{sc} \tag{5-1}$$

$$\frac{\partial C_{ve}}{\partial t} = D_{ve}\frac{\partial^2 C_{ve}}{\partial x^2} + u_{ve}\frac{\partial C_{ve}}{\partial x} \qquad \text{for } L_{sc} < x < L_{sc}+L_{ve} \tag{5-2}$$

where x is the distance in the epi from the skin surface and t is time. In eqs 5-1 and 5-2, with j designating either the sc or ve, C_j is the concentration in membrane layer j and D_j is

the effective diffusion coefficient of the absorbing chemical through layer j of apparent thickness L_j. Eqs 5-1 and 5-2 are written assuming that the epi moves outward (i.e., the sc and ve velocities are negative). The assumption of one-dimensional transport is reasonable when the width of the exposed area of the skin is much larger than the thickness of the sc.

In the general case, eqs 5-1 and 5-2 are solved assuming the skin is initially chemical free, and then is exposed to a vehicle at a constant concentration C_v^o for a period of time t_{exp}, with sink conditions at the ve-dermis interface. In addition, local equilibrium is assumed between the vehicle and the skin surface and at the sc-ve interface, flux is conserved at the sc-ve interface, and the absorbing chemical is not volatile (i.e., the flux from the outer surface of the sc is zero once the chemical has been removed). Stated mathematically, the boundary conditions are:

$$\text{at } t = 0 \qquad C_{sc} = 0 \quad \text{for } 0 < x < L_{sc} \quad \text{and} \quad C_{ve} = 0 \quad \text{for } L_{sc} < x < L_{sc} + L_{ve} \tag{5-3}$$

$$\text{at } x = 0 \qquad C_{sc} = K_{sc/v}\, C_v^o \qquad \text{for } 0 < t < t_{exp} \tag{5-4}$$

$$\text{and} \qquad \frac{\partial C_{sc}}{\partial x} = 0 \qquad \text{for } t > t_{exp} \tag{5-5}$$

$$\text{at } x = L_{sc} \qquad C_{sc} = \frac{K_{sc/v}}{K_{ve/v}} C_{ve} \tag{5-6}$$

$$\text{and} \qquad D_{ve}\frac{\partial C_{ve}}{\partial x} + u_{ve}C_{ve} = D_{sc}\frac{\partial C_{sc}}{\partial x} + u_{sc}C_{sc} \quad \text{for } t > 0 \tag{5-7}$$

$$\text{at } x = L_{sc} + L_{ve} \quad C_{ve} = 0 \qquad \text{for } t > 0 \tag{5-8}$$

where $K_{sc/v}$ is the equilibrium partition coefficient of absorbing chemical between the sc and the vehicle and $K_{ve/v}$ is the equilibrium partition coefficient between the ve and the vehicle. Eqs 5-1 through 5-8 must be solved numerically during and following a chemical exposure. However, simplifying assumptions representing special physical situations can be applied to eqs 5-1 through 5-8 to make analytical solutions for $t < t_{exp}$ possible, resulting in algebraic equations describing C_{sc} and C_{ve} at $t = t_{exp}$. In these

situations, numerical solutions are only required for $t > t_{exp}$. Solutions for two such cases are presented next.

In the first case, only the sc contributes a significant resistance to mass transport (i.e., the ve presents almost no barrier to chemical absorption). This case is relevant for chemicals with low to moderate lipophilicity, or for exposures that are short enough that chemical has not reached the ve. In such a situation, the concentration in the ve remains approximately zero. The following algebraic equation for C_{sc} as a function of position (x / L_{sc}) after an exposure time t_{exp} was derived by solving eq 5-1 for conditions 5-3, and 5-4 when $C_{sc} = 0$ at $x = L_{sc}$.

$$\frac{C_{sc}}{K_{sc/v}C_v^o} = \frac{\exp\left(\frac{-6t_{lag,sc}}{t_{t,sc}}\frac{x}{L_{sc}}\right) - \exp\left(\frac{-6t_{lag,sc}}{t_{t,sc}}\right)}{1-\exp\left(\frac{-6t_{lag,sc}}{t_{t,sc}}\right)} - 2\pi\sum_{n=1}^{\infty}\frac{n}{\lambda_n^2}\exp\left(\frac{-3t_{lag,sc}}{t_{t,sc}}\frac{x}{L_{sc}} - \frac{\lambda_n^2 t_{exp}}{6t_{lag,sc}}\right)\sin\left(\frac{n\pi x}{L_{sc}}\right) \tag{5-9}$$

In eq 5-9, $t_{lag,sc}$ is the lag time for a chemical to cross the sc, defined as $L_{sc}^2 / (6D_{sc})$, and λ_n are eigenvalues that satisfy eq 5-10.

$$\lambda_n^2 = n^2\pi^2 + 9\left(\frac{t_{lag,sc}}{t_{t,sc}}\right)^2 \tag{5-10}$$

As indicated in eq 5-9, C_{sc} depends on only two dimensionless groups: $t_{exp} / t_{lag,sc}$ and $t_{t,sc} / t_{lag,sc}$. Thus, for a dermal exposure, time is only meaningful relative to $t_{lag,sc}$, which characterizes how long a specific chemical takes to cross the sc. When only the sc contributes a resistance to mass transport across the epi and $u_{sc} \sim 0$, C_{sc} reaches steady state when $t_{exp} \approx 1.7\ t_{lag,sc}$, meaning that the mass of chemical in the sc changes by less than 5% if $t_{exp} > 1.7\ t_{lag,sc}$. When $u_{sc} \neq 0$, it takes even less time to reach steady state.

In the second special case, dermal absorption through the epi has reached steady state. The following algebraic equations for C_{sc} and C_{ve} as functions of position (x / L_{sc}) were derived by solving eqs 5-1 and 5-2 when $\partial C_{sc} / \partial t$ and $\partial C_{ve} / \partial t$ are both zero for conditions 5-4 and 5-6 through 5-8:

$$\frac{C_{sc}}{K_{sc/v}C_v^o} = \frac{\exp\left(\frac{-6t_{lag,sc}}{t_{t,sc}}\frac{x}{L_{sc}}\right)\left[\frac{\gamma}{BG} - 1 + \exp\left(\frac{\gamma}{G}\frac{6t_{lag,sc}}{t_{t,sc}}\right)\right] - \frac{\gamma}{BG}\exp\left(\frac{-6t_{lag,sc}}{t_{t,sc}}\right)}{\frac{\gamma}{BG} - \frac{\gamma}{BG}\exp\left(\frac{-6t_{lag,sc}}{t_{t,sc}}\right) + \exp\left(\frac{\gamma}{G}\frac{6t_{lag,sc}}{t_{t,sc}}\right) - 1} \quad (5\text{-}11)$$

$$\frac{C_{ve}}{K_{ve/v}C_v^o} = \frac{\exp\left[\frac{\gamma}{\eta_{ve}G}\frac{6t_{lag,sc}}{t_{t,sc}}\left(1 + \eta_{ve} - \frac{x}{L_{sc}}\right)\right] - 1}{\frac{\gamma}{BG}\left[\exp\left(\frac{6t_{lag,sc}}{t_{t,sc}}\right) - 1\right] + \exp\left(\frac{6t_{lag,sc}}{t_{t,sc}}\right)\left[\exp\left(\frac{\gamma}{G}\frac{6t_{lag,sc}}{t_{t,sc}}\right) - 1\right]} \quad (5\text{-}12)$$

To use these equations, five groups of parameters must be specified: (1) $t_{t,sc} / t_{lag,sc}$; (2) $\gamma = t_{t,sc} / t_{t,ve}$, the ratio of the sc and ve turnover times; (3) $\eta_{ve} = L_{ve} / L_{sc}$, the ratio of the ve and sc thicknesses; (4) B, the ratio of permeability coefficients of the absorbing chemical in the sc, $P_{sc,v}$, to the ve, $P_{ve,v}$, from the same vehicle,

$$B = \frac{P_{sc,v}}{P_{ve,v}} = \frac{K_{sc/v}D_{sc}L_{ve}}{K_{ve/v}D_{ve}L_{sc}} \quad (5\text{-}13)$$

and (5) G, the ratio of the lag time through the sc, $t_{lag,sc}$, to the lag time through the ve, $t_{lag,ve}$,

$$G = \frac{t_{lag,sc}}{t_{lag,ve}} = \frac{L_{sc}^2/(6D_{sc})}{L_{ve}^2/(6D_{ve})} \quad (5\text{-}14)$$

The parameters γ and η_{ve} are properties of the skin alone while $t_{t,sc} / t_{lag,sc}$, B and G will vary with the absorbing chemical.

The mass of chemical in the epi, M_{epi}, at any time t is calculated by integrating the concentration of absorbing chemical in the sc and ve as follows:

$$M_{epi} = A\int_0^{L_{sc}} C_{sc}dx + A\int_{L_{sc}}^{L_{sc}+L_{ve}} C_{ve}dx \tag{5-15}$$

where A is the surface area exposed to the absorbing chemical. The mass of chemical in the skin at the end of an exposure, M_{epi}^{o}, is defined as M_{epi} at $t = t_{exp}$. The flux, J, through any position x in the epi (j denotes either the sc or the ve) due to convection and diffusion is calculated as:

$$J = -D_j\frac{\partial C_j}{\partial x} - u_j C_j \tag{5-16}$$

For nonvolatile chemicals, the mass of chemical removed from the sc by desquamation after an exposure ends, M_{desq}, is calculated by integrating the convective term in eq 5-16 at the outside edge of the sc with respect to time, to yield

$$M_{desq} = u_{sc}A\int_{t_{exp}}^{\infty} C_{sc}\big|_{x=0}dt \tag{5-17}$$

The total mass of chemical absorbed systemically through the epi after an exposure ends, M_{abs}, is calculated by integrating the diffusive term in eq 5-16 at the inside edge of the ve with respect to time as follows:

$$M_{abs} = -AD_{ve}\int_{t_{exp}}^{\infty} \left.\frac{\partial C_{ve}}{\partial x}\right|_{x=L_{sc}+L_{ve}} dt \tag{5-18}$$

When the ve contributes little resistance to mass transport compared to the sc,

$$\left.\frac{\partial C_{ve}}{\partial x}\right|_{x=L_{sc}+L_{ve}} \approx \left.\frac{\partial C_{sc}}{\partial x}\right|_{x=L_{sc}} \tag{5-19}$$

In the model, chemical in the skin at $t = t_{exp}$ is either systemically absorbed or removed from the skin by desquamation, and thus,

$$M_{epi}^{o} = M_{abs} + M_{desq} \tag{5-20}$$

For convenience, we define

$$FA = M_{abs}/M_{epi}^{o} \tag{5-21}$$

which represents the fraction of chemical in the skin at the end of an exposure that systemically absorbs.

Methods

The mathematical model described in eqs 5-1 through 5-8 was used to quantitatively examine the effect of exposure time, chemical lipophilicity, and epidermal turnover rate on chemical elimination from the skin by desquamation. Eqs 5-1 and 5-2 were solved numerically for $t > t_{exp}$ using the finite difference scheme described in the Appendix. To simplify the computational strategy, the effect of varying t_{exp} was examined when the sc limits the rate of mass transport through the skin (i.e., B is small). Under these circumstances, the ve is an infinite sink (i.e., $C_{ve} = 0$) and model results do not depend on lipophilicity of the absorbing chemical. For this calculation, eqs 5-9 and 5-10 were used to describe C_{sc} at $t = t_{exp}$.

Since the ve can present a significant barrier to highly lipophilic chemicals, both the sc and ve were included in the general form of the model. The resulting increase in computational complexity was partially reduced by assuming the chemical penetration rate had reached steady state before the exposure ended, allowing eqs 5-11 and 5-12 to describe C_{sc} and C_{ve} at $t = t_{exp}$. For this calculation, four ratios of sc and ve parameters must be specified: the sc – ve ratios of (1) turnover times ($\gamma = t_{t,sc}/t_{t,ve}$), (2) membrane thicknesses ($\eta_{ve} = L_{ve}/L_{sc}$), (3) lag times ($G = t_{lag,sc} / t_{lag,ve}$) and (4) permeability coefficients ($B = P_{sc,v} / P_{ve,v}$). In all calculations presented here, we assumed $\gamma = 0.5$, $\eta_{ve} = 10$, and $G > 10$, which are all based on typical values for normal human skin (i.e., $L_{sc} \sim 10$ - 40 μm, and $L_{ve} \sim 100$-200 μm and $D_{sc} / D_{ve} < 10^{-3}$) (Scheuplein, 1972). When $G > 10$, C_{sc} and C_{ve} are insensitive to changes in G (Scheuplein, 1976). The amount of chemical removed by desquamation was calculated as a function of B and $t_{t,sc} / t_{lag,sc}$.

Results and Discussion

Figure 5.1 shows the fraction of chemical in the skin that would be systemically absorbed, FA, as a function of the sc turnover time for short and long (i.e., relative to the time required to reach steady state) values of the exposure time, t_{exp}. Both t_{exp} and $t_{t,sc}$ are examined relative to $t_{lag,sc}$. To provide perspective, the upper axis of Figure 5.1 specifies values of $t_{lag,sc}$ if $t_{t,sc}$ = 14 days. As $t_{lag,sc}$ increases relative to $t_{t,sc}$, the effect of desquamation on dermal absorption increases (i.e., FA approaches 0). However, FA > 0.8 if $t_{lag,sc}$ is less than 5% of the time for the sc to be completely replaced (i.e., $t_{lag,sc}$ < 0.05 $t_{t,sc}$). This corresponds to $t_{lag,sc}$ < about 17 hours for $t_{t,sc}$ = 14 days. Many chemicals penetrate the sc with lag times less than 17 hours. For example, $t_{lag,sc}$ for benzoic acid and 4-cyanophenol (molecular weights, MW's, of 122.1 and 119.4, respectively) are less than 1 hour (Parry *et al.*, 1990; Pirot *et al.*, 1997). Lag times are affected by molecular size, and larger molecules will have longer $t_{lag,sc}$ values. One would expect that for non-volatile chemicals with up to moderate lipophilicity and modest molecular size (i.e., MW less than about 300 daltons), almost all of the chemical in the sc at the end of an exposure would eventually be absorbed systemically.

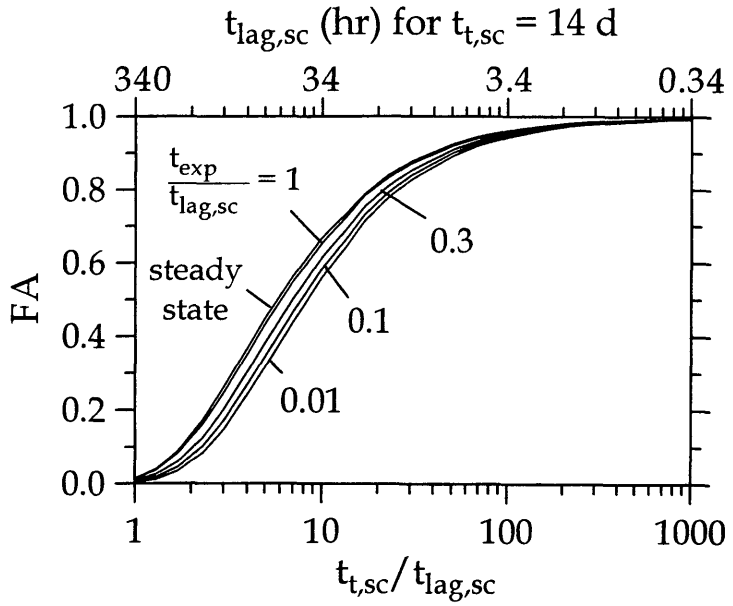

Figure 5.1 – The effect of $t_{t,sc}$ / $t_{lag,sc}$ on FA for varying exposure times calculated assuming the ve adds no significant resistance to dermal absorption.

The effect of t_{exp} / $t_{lag,sc}$ on FA is relatively minor, although more chemical is removed from the skin by desquamation as t_{exp} decreases. This effect is minor because at short exposure times, chemical has penetrated only a short distance into the sc. Consequently, the concentration gradient (i.e., the driving force for mass transfer) is larger than at longer exposure times. As a result, the concentration of the absorbing chemical in the outer layers of the sc is reduced more quickly by diffusion into the sc following a short exposure compared to a longer exposure.

Figure 5.1 was developed assuming that the sc is the only significant resistance to mass transfer across skin. However, the conclusions should be similar even when the ve contributes significantly because at short exposure times relative to the time required to reach steady state the absorbing chemical has not penetrated far enough into the sc to be affected by the resistance from the ve.

Because the duration of the exposure has only a small effect on FA, we examined the effect of the sc–ve permeability ratio (i.e., the B parameter) assuming that the exposure time was long enough to establish steady-state concentration profiles. The concentration profile in the membrane looks the same for short exposures whether or not the ve is contributing a resistance because the chemical has not penetrated far enough into the membrane to be 'aware' of it. Because of this and the results in Figure 5.1, the steady-state results will represent approximately the unsteady-state conditions.

Figure 5.2 shows the effect of epidermal turnover on steady-state flux, J_{ss}, through the epi for B values varying from 0.01 (i.e., the sc entirely controls the rate of dermal penetration) to 10 (i.e., the ve entirely controls the rate of dermal penetration). In Figure 5.2, J_{ss} is normalized by the steady-state flux that would occur if there were no epidermal turnover, derived from eq 5-11 assuming that $u_{sc} = 0$ and defined in eq 5-22:

$$J_{ss}(u_{sc} = 0) = P_{sc,v}C_v^0/(B+1) \tag{5-22}$$

It is clear from Figure 5.2 that epi turnover does reduce steady-state flux. However, the B parameter does not significantly affect the role of epi turnover in reducing J_{ss} compared to J_{ss} for $u_{sc} = 0$, as indicated by the narrow spread between curves for B = 0.01 to 10.

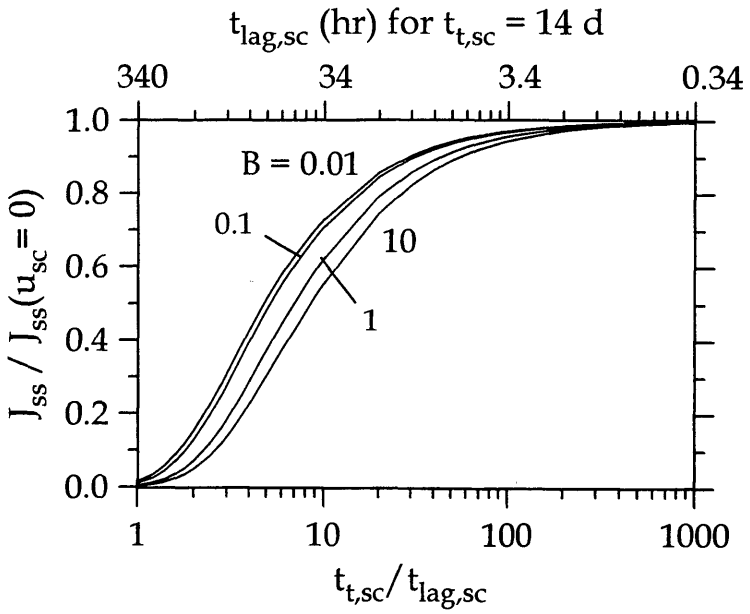

Figure 5.2 – The effect of $t_{t,sc}$ / $t_{lag,sc}$ on steady-state flux through the epi for varying values of B.

Once the exposure ends, the B parameter plays a larger role as illustrated in Figure 5.3, which shows FA plotted as a function of $t_{t,sc}$ / $t_{lag,sc}$ for varying values of B. As B increases, the ve becomes a more significant mass transfer barrier, preventing chemical entrance to systemic circulation from the sc. Thus, the effect of epi turnover on percutaneous penetration is greater when the ve is a significant barrier (i.e., when B is large). For example, if the barrier contributions of the sc and the ve are the same (i.e., B = 1), 70% of the chemical in the skin systemically absorbs when $t_{lag,sc}$ is less than about 5% of $t_{t,sc}$. For the same situation, only about 20% systemically absorbs if the ve permeability coefficient is one-tenth of the sc permeability coefficient (i.e., B = 10). The heavy dashed curve in Figure 5.3 is the steady-state curve from Figure 5.1, which was calculated assuming the sc was the only barrier to dermal absorption (i.e., $C_{ve} \sim 0$). As expected, this curve coincides with curves calculated assuming $B < 0.1$.

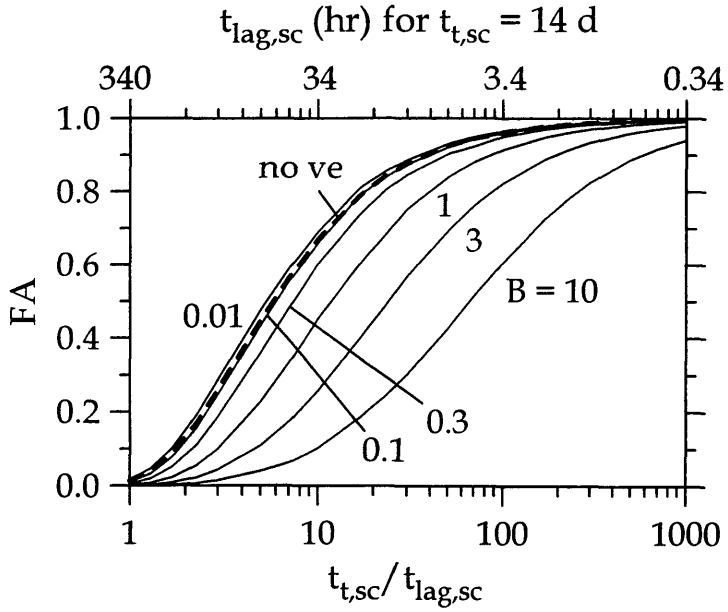

Figure 5.3 – The effect of $t_{t,sc}$ / $t_{lag,sc}$ on FA for varying values of B.

It is evident from both Figures 5.1 and 5.3 that significant amounts of chemical can be removed from the skin by desquamation if $t_{t,sc}$ is short relative to $t_{lag,sc}$. This suggests that chemical removal by desquamation could be more significant in diseased skin involving hyperproliferation (e.g., psoriasis). However, this might not be the case if the barrier function of the sc is reduced as this would simultaneously decrease $t_{lag,sc}$.

Figure 5.4 shows combinations of B and $t_{lag,sc}$ that produce FA = 0.2, 0.5, 0.8, and 0.9, and can be used to identify those situations in which desquamation may be an important mechanism for eliminating chemical from the skin after an exposure ends. However, to apply the results in Figures 5.1 through 5.4 to a specific chemical requires an estimate for B and $t_{lag,sc}$. We consider this issue next.

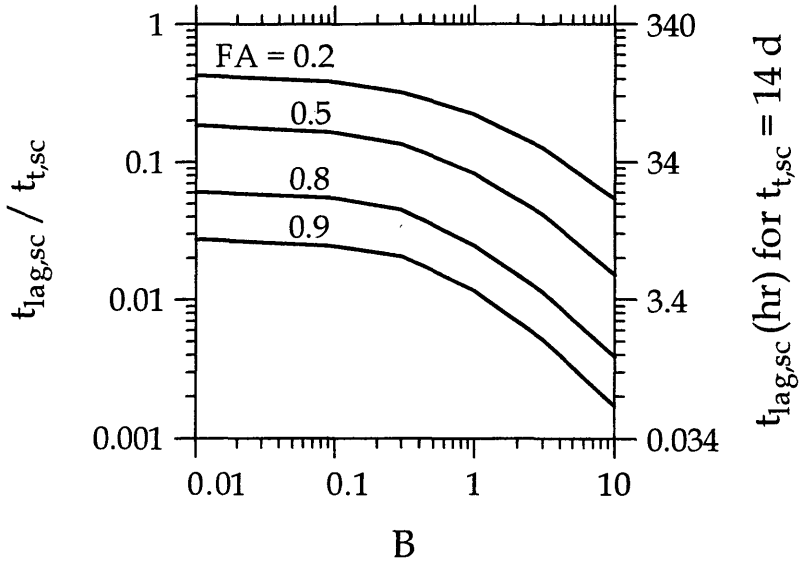

Figure 5.4 – Values of FA corresponding to specific combinations of $t_{lag,sc}$ / $t_{t,sc}$ and B.

Permeability coefficients in both the sc and ve have been measured for only a few chemicals, and there are only a few experimental values for B (Vecchia, 1997). Based on differences in the physical characteristics of the sc and the ve, the sc-ve permeability ratio (i.e., B) should vary with a chemical's lipophilic character, which can be represented approximately by the octanol-water partition coefficient ($K_{o/w}$). In addition, the effect of molecular size is likely to be different in the sc and ve, causing B to depend on molecular size as well. Bunge and Cleek (1995) proposed that B may be estimated as a function of the absorbing chemical's $K_{o/w}$ and MW as follows:

$$B = 0.00061\sqrt{MW}10^{-0.006MW}K_{o/w}^{0.74} \tag{5-23}$$

This equation was developed using the following estimates for permeability coefficients in the sc and the ve from an aqueous vehicle (i.e., $B = P_{sc,w} / P_{ve,w}$, where the subscript w denotes the vehicle water):

$$P_{sc/w}[cm/h] = 0.00158 \times 10^{-0.006MW}K_{o/w}^{0.74} \tag{5-24}$$

$$P_{ve,w}[cm/h] = \frac{K_{ve/w} D_{ve}}{L_{ve}} = 2.6/\sqrt{MW} \qquad (5\text{-}25)$$

Eq 5-24 is the correlation proposed by Potts and Guy, (Potts and Guy, 1992) as presented by Bunge *et al.* (1994). Eq 5-25 was developed assuming that: (1) L_{ve} = 100 μm, (2) D_{ve} = 10^{-6} cm^2/s for a chemical with MW = 50 and decreases as $1/\sqrt{MW}$, and (3) the chemical's solubility in the ve is the same as in water (i.e., $K_{ve/w}$ = 1). Figure 5.5 presents $\log K_{o/w}$ as a function of MW for various values of B as estimated using eq 5-23. Based on these calculations, $\log K_{o/w}$ for absorbing chemicals must be larger than ~ 3.5 (and larger than ~ 4 for chemicals with MW > 200) to produce B values of 1 or larger.

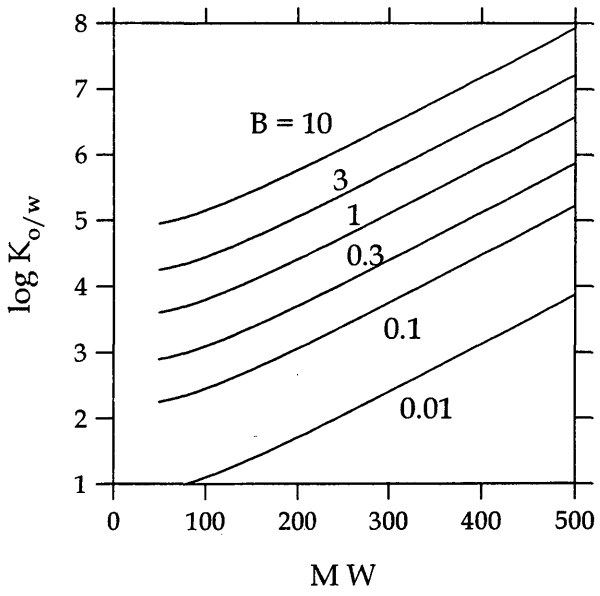

Figure 5.5 – Effect of MW and $\log K_{o/w}$ on B parameter values.

While experimental values for lag times are reported for many chemicals, these must be used cautiously for assessing the effect of epidermal turnover. Most values of lag

time have been derived from *in vitro* diffusion cell measurements. Lag times measured in this way are notoriously variable and occasionally produce impossible results (i.e., negative values). In addition, skin samples used in diffusion cell experiments often include the ve and part or all of the dermis. Consequently, lag time values from these experiments will be larger than $t_{lag,sc}$, the quantity required to use Figures 5.1 through 5.4. The difference between the experimental lag time and $t_{lag,sc}$ could be relatively small if there was no dermis in the experiment, but could be large if the entire dermis was present. Lacking experimental data, the following equation can be used to provide a preliminary estimate for $t_{lag,sc}$.

$$t_{lag,sc}[\text{hours}] = 0.17\left(10^{0.006\,MW}\right) \tag{5-26}$$

Eq 5-26 was developed using the formula (Bunge and Cleek, 1995):

$$\log\left(D_{sc}/L_{sc}, \text{cm/s}\right) = -6.36 - 0.0060\,(MW) \tag{5-27}$$

and assuming L_{sc} is 16 μm, which is consistent with measurements reported by Kalia *et al.* (1996) for the human forearm. Because $t_{lag,sc}$ varies exponentially with MW, it increases dramatically when MW is greater than ~ 350. For example, estimated by eq 5-26, $t_{lag,sc} \approx 0.68$, 21, and 170 hours when MW ≈ 100, 350, and 500.

Conclusions

Except for highly lipophilic or large MW chemicals, nearly all of the chemical in the epi at the end of an exposure will systemically absorb (i.e., FA ~ 1), regardless of the length of time the skin was exposed to the chemical. Only for chemicals with large values of MW or $\log K_{o/w}$ (greater than ~ 4 for most chemicals) will epidermal turnover reduce FA significantly.

Notation

A	surface area of chemical exposure
B	ratio of the permeability coefficients of the absorbing chemical in the sc to the permeability coefficient in the ve from the same vehicle, $P_{sc,v} / P_{ve,v}$
C_j	concentration of the absorbing chemical in membrane layer j
C_v^o	initial concentration of the absorbing chemical in the vehicle
D_j	effective diffusion coefficient of the absorbing chemical in membrane layer j
epi	epidermis
FA	fraction of chemical in the epi at t_{exp} that systemically absorbs, M_{abs}/M_{epi}^o
G	ratio of $t_{lag,sc}$ to $t_{lag,ve}$, $G = D_{ve}L_{sc}^2/\left(D_{sc}L_{ve}^2\right)$
j	variable denoting sc or ve
J	flux (i.e., mass / area / time) of absorbing chemical through a position in the epi
J_{ss}	steady-state flux of the absorbing chemical
$J_{ss}(u_{sc} = 0)$	steady-state flux of the absorbing chemical with no epidermal turnover
$K_{j/v}$	equilibrium partition coefficient between membrane layer j and the vehicle for the absorbing chemical
$K_{j/w}$	equilibrium partition coefficient between membrane layer j and the vehicle water for the absorbing chemical
$K_{o/w}$	octanol – water partition coefficient
L_j	apparent thickness of membrane layer j
M_{abs}	total mass of chemical absorbed systemically after an exposure ends
M_{desq}	cumulative mass of chemical removed from the sc by desquamation
M_{epi}	mass of absorbing chemical in the epi

M^{o}_{epi}	mass of absorbing chemical in the epi at $t = t_{exp}$
MW	molecular weight
N_j	number of nodes in membrane layer j for the finite difference solution
$P_{j,v}$	steady-state permeability coefficient of the absorbing chemical through membrane layer j from the vehicle, $K_{j/v} D_j / L_j$
$P_{j,w}$	steady-state permeability coefficient of the absorbing chemical through membrane layer j from the vehicle water, $K_{j/w} D_j / L_j$
sc	stratum corneum
t	time
t_{exp}	duration of the exposure
$t_{lag,j}$	lag time for chemical penetrating through membrane layer j, $L_j^2 / (6D_j)$
$t_{t,j}$	turnover time of membrane layer j
u_j	velocity at which membrane layer j moves, $L_j / t_{t,j}$
ve	viable epidermis
x	position in the sc
Δx_j	distance between finite difference nodes in membrane layer j

Greek

γ	ratio of the sc and ve turnover times, $t_{t,sc} / t_{t,ve}$
λ_n	eigenvalues
η_{ve}	ratio of the ve and sc thicknesses, L_{ve} / L_{sc}

References

Auton, T. R., D. R. Westhead, B. H. Woolen, R. C. Scott and M. F. Wilks (1994). "A physiologically based mathematical model of dermal absorption in man." Human and Experimental Toxicology **13**:51-60.

Bergstresser, P. R. and J. R. Taylor (1977). "Epidermal 'turnover time' - a new examiniation." British Journal of Dermatology **96**:503-509.

Bunge, A. L. and R. L. Cleek (1995). "A new method for estimating dermal absorption from chemical exposure. 2. Effect of molecular weight and octanol-water partitioning." Pharmaceutical Research **12**:88-95.

Bunge, A. L., G. L. Flynn and R. H. Guy (1994). Predictive model for dermal exposure assessment. Water Contamination and Health: Integration of Exposure Assessment, Toxicology, and Risk Assessment. R. Wang, ed. New York, Marcel Dekker, 347-373.

Cleek, R. L. and A. L. Bunge (1993). "A new method for estimating dermal absorption from chemical exposure. 1. General approach." Pharmaceutical Research **10**:497-506.

EPA, U. S. (1992). Dermal Exposure Assessment: Principles and Applications, EPA/600/8-91/011B. Exposure Assessment Group, Office of Health and Environmental Assessment, Washington.

Finlay, A. Y., R. J. Marshall and R. Marks (1982). "A fluorescence photographic photometric technique to assess stratum corneum turnover rate and barrier function *in vivo*." British Journal of Dermatology **107**:35-42.

Grove, G. L. (1986). "Physiologic changes in older skin." Dermatologic Clinics **4**:425-432.

Halprin, K. M. (1972). "Epidermal "turnover time" - a re-examination." British Journal of Dermatology **86**:14-19.

Iizuka, H. (1994). "Epidermal turnover time." Journal of Dermatological Sciences **8**:215-217.

Kalia, Y. N., F. Pirot and R. H. Guy (1996). "Homogenous transport in a heterogeneous membrane: water diffusion across human stratum corneum *in vivo*." Biophysical Journal **71**:2692-2700.

Kligman, A. M. (1964). The biology of the stratum corneum. The Epidermis. W. Montagna and W. C. Lobitz, eds. New York, Academic Press, 387-433.

Parry, G. E., A. L. Bunge, G. D. Silcox, L. K. Pershing and D. W. Pershing (1990). "Percutaneous absorption across human skin. I. *In vitro* experiments and mathematical modeling." Pharmaceutical Research **7**:230-236.

Pirot, F., Y. N. Kalia, A. L. Stinchcomb, G. Keating, A. L. Bunge and R. H. Guy (1997). "Characterization of the permeability barrier of human skin *in vivo*." Proceedings of the National Academy of Sciences of the United States of America **94**:1562-1567.

Potts, R. O. and R. H. Guy (1992). "Predicting skin permeability." Pharmaceutical Research **9**:663-669.

Reddy, M. B., K. D. McCarley and A. L. Bunge (1998). "Physiologically relevant one-compartment pharmacokinetic models for skin. 2. Comparison of models when combined with a systemic pharmacokinetic model." Journal of Pharmaceutical Sciences **87**:482-490.

Roberts, D. and R. Marks (1980). "The determination of regional and age variations in the rate of desquamation: a comparison of four techniques." Journal of Investigative Dermatology **74**:13-16.

Schaefer, H., A. Zesch and G. Stuttgen (1982). Skin Permeability. Berlin, Springer-Verlag.

Scheuplein, R. J. (1972). "Properties of the skin as a membrane." Advances in Biology of Skin (New York) **12**:125-152.

Scheuplein, R. J. (1976). "Permeability of the skin: a review of major concepts and some new developments." Journal of Investigative Dermatology **67**:672-676.

Scheuplein, R. J. and R. L. Bronaugh (1983). Percutaneous absorption. Biochemistry and Physiology of the Skin, vol. II. L. A. Goldsmith, ed. New York, Oxford University Press, 1255-1295.

Silcox, G. D., G. E. Parry, A. L. Bunge, L. K. Pershing and D. W. Pershing (1990). "Percutaneous absorption of benzoic acid across human skin. II. Prediction of an *in vivo*, skin-flap system using *in vitro* parameters." Pharmaceutical Research **7**:352-358.

Vecchia, B. (1997). Estimating the Dermally Absorbed Dose from Chemical Exposure: Data Analysis, Parameter Estimation, and Sensitivity to Parameter Uncertainties. M.S. thesis, Department of Chemical Engineering and Petrolium Refining, Colorado School of Mines, Golden, CO.

Weinstein, G. D., J. L. McCullough and P. Ross (1984). "Cell proliferation in normal epidermis." Journal of Investigative Dermatology **82**:623-628.

Appendix 5A – Finite Difference Scheme

The sc and ve were split into N_{sc} and N_{ve} nodes, respectively. The spatial derivatives were represented by the following finite difference formulas that are second-order accurate in x:

$$\left.\frac{\partial^2 C_j}{\partial x^2}\right|_i = \frac{C_{j,i-1} - C_{j,i} + C_{j,i+1}}{\left(\Delta x_j\right)^2} \tag{5A-1}$$

$$\left.\frac{\partial C_j}{\partial x}\right|_i = \frac{C_{j,i+1} - C_{j,i-1}}{2\Delta x_j} \tag{5A-2}$$

$$\left.\frac{\partial C_j}{\partial x}\right|_i = \frac{-3C_{j,i} + 4C_{j,i+1} - C_{j,i+2}}{2\Delta x_j} \tag{5A-3}$$

$$\left.\frac{\partial C_j}{\partial x}\right|_i = \frac{C_{j,i-2} - 4C_{j,i-1} + 3C_{j,i}}{2\Delta x_j} \tag{5A-4}$$

$$\Delta x_j = L_j / \left(N_j - 1\right) \tag{5A-5}$$

where i designates a node and j designates either the sc or ve. Eqs 5A-1 and 5A-2 were used with eqs 5-1 and 5-2, eq 5A-3 was used with eq 5-5 and eq 5-7 in the ve, and eq 5A-4 was used with eq 5-7 in the sc. The resulting system of ordinary differential equations were solved using the FORTRAN computer program shown in Appendix 5B which uses the IVPAG routine from the IMSL library to solve initial-value ordinary differential equation problems.

The accuracy of the numerical solution was checked by showing that increasing N_{sc} and N_{ve} did not change results. Also, the sum of the calculated mass of chemical in the epi, removed by desquamation, and absorbed systemically was within 0.3% of the mass of chemical in the epi at $t = t_{exp}$ (i.e., $\left| 1 - (M_{epi} + M_{abs} + M_{desq}) / M^{o}_{epi} \right| < 0.003$).

Appendix 5B – FORTRAN Programs

Table 5B.1 lists the names of variables in the following programs. The programs need to be compiled so that the IVPAG subroutine in the IMSL library can be accessed.

Table 5B.1 – Variable names in the FORTRAN programs.

variable in program	variable in chapter
T	$D_{sc}t/L_{sc}^2$
Y(i), i = 1, N_{sc}	$C_{sc}/\left(K_{sc/v}C_v^o\right)$
Y(i), i = N_{sc}+1,N_{sc}+N_{ve}	$C_{ve}/\left(K_{ve/v}C_v^o\right)$ (not present in two-layer solution)
YPRIME(N)	spatial derivative of Y calculated with finite differencing
N	N_{sc} (1-layer solution) or N_{sc} + N_{ve} (2-layer solution)
MEL	$M_{abs}/\left(A\,L_{sc}K_{sc/v}C_v^o\right)$
MDESQ	$M_{desq}/\left(A\,L_{sc}K_{sc/v}C_v^o\right)$
LEFT	$M_{epi}/\left(A\,L_{sc}K_{sc/v}C_v^o\right)$
MTOT	M_{epi}/M_{epi}^o
MABS	M_{abs}/M_{epi}^o , = FA when $M_{epi} \approx 0$
MRAT	M_{desq}/M_{epi}^o
XL	x / L_{sc}
RAT2	$t_{t,sc} / t_{lag,sc}$
R	$t_{t,sc} / t_{t,ve}$ (2-layer solution)
G	G
B	B
EVE	η_{ve}
MB	$1-(M_{epi}+M_{abs}+M_{desq})/M_{epi}^o$ (remains ~ 1 for adequate solution)

```
PROGRAM DESQUAM
C ********** PROGRAM STUDYING EFFECT OF DESQUAMATION ON DERMAL
C ********** ABSORPTION THROUGH ONE-LAYER MEMBRANE (i.e., for Fig. 5.1)

      INTEGER NPARAM, N
C     ********** N is the number of nodes, Nsc
      PARAMETER (NPARAM = 50, N = 101)
      INTEGER IDO, NOUT, MM
      DOUBLE PRECISION PARAM(NPARAM), LLL, MABS, RAT2, MABS2, LEFT
      DOUBLE PRECISION T, TEND, Y(N), A(1,1), MDESQ, TSIZE, MEL
      DOUBLE PRECISION IEND, MRAT, TOL, XL, TFINAL, MTOT, MB

      COMMON/CARRY/MEL, MDESQ, RAT2

C     ********** SPECIFICATIONS FOR SUBROUTINES
      EXTERNAL DIVPAG, SSET, UMACH
      EXTERNAL FCN, FCNJ
      CALL SSET(NPARAM, 0.0, PARAM, 1)

C Files listed as old contain parameters for program to run.
      OPEN (1, FILE='data.dat', STATUS = 'NEW')
      OPEN (2, FILE='data2.dat', STATUS = 'NEW')
      OPEN (3, FILE='tsize.dat', STATUS = 'OLD')
      OPEN (5, FILE='tfinal.dat', STATUS = 'OLD')
      OPEN (6, FILE='rat2.dat', STATUS = 'OLD')

C     ********** SETTING MAXIMUM NUMBER OF STEPS
      PARAM(4) = 5000000

C ********** SETTINGS FOR THE IVPAG SUBROUTINE
      PARAM(12) = 2
      PARAM(10) = 1.

C ********** Setting parameters
C ********** RAT2 = T_T,SC/T_LAG,SC
      READ(3,*) TSIZE
      READ(6,*) RAT2

C ********** Setting maximum step size in time for short exposures
      IF (RAT2 .LT. 1.1) THEN
         PARAM(3) = 1D-6
      END IF
      IF (RAT2 .LT. 0.2) THEN
         PARAM(3) = 1D-7
      END IF
      RAT2 = 6. / RAT2

C ********** SETTING INITIAL CONDITIONS
      IDO = 1
      T = 0.
      Y(1) = 1.
      Y(N) = 0.
```

```
C ********** INITIAL CONCENTRATION PROFILE FROM FORMULA, THIS IS THE
C STEADY STATE FORMULA BUT IT CAN BE MODIFIED TO THE TRANSIENT FORMULA
      DO 6, I = 2, N-1
      XL = DBLE (I-1) / DBLE (N-1)
   6  Y(I)=(DEXP(-1.*RAT2*XL)-DEXP(-1.*RAT2))/(1.-DEXP(-1.*RAT2))

      MTOT = 0.
      DO 7, I = 1,N-1
   7  MTOT = MTOT + (Y(I)+Y(I+1))/2./DBLE(N-1)
      WRITE(1,99999) MTOT

C ********** SETTING ERROR TOLERANCE
      TOL = 1.0D-6
      CALL UMACH (2, NOUT)

      MM = 0
      READ(5,*) TFINAL
      IEND = 0.0
 10   CONTINUE
      IEND = IEND + TSIZE
      TEND = IEND

      CALL DIVPAG(IDO,N,FCN,FCNJ,A,T,TEND,TOL,PARAM,Y)

      LEFT = 0.
      DO 88,I = 1,N-1
  88  LEFT = LEFT + (Y(I)+Y(I+1))/2./(DBLE(N)-1.)

      MB = (LEFT+MDESQ+MEL)/MTOT
      MRAT = MDESQ/MTOT
      MABS = 1. - MRAT - LEFT/MTOT
      MDESQ2 = MDESQ/MTOT
      LLL = LEFT/MTOT

C When MRAT and MABS do not change anymore in time, MABS = FA
      WRITE(2,99997) T,MB,Y(1),MRAT,MABS
      IF (IEND .LE. TFINAL) THEN
          MRAT = MDESQ/MTOT
C          WRITE (1,99999) T,Y
C          WRITE (1,*)
          IF (IEND .GE. TFINAL) IDO = 3
          GO TO 10
      END IF
99999 FORMAT(F13.7)
99997 FORMAT(6F13.7)
99998 FORMAT(8F9.3)
      END

      SUBROUTINE FCN (N, T, Y, YPRIME)
      INTEGER N,IJ
      DOUBLE PRECISION X, Y(N), YPRIME(N), T
      DOUBLE PRECISION DZ, DZS, MEL, T2, RAT2, MDESQ

      COMMON/CARRY/MEL,MDESQ,RAT2
```

```
      SAVE T2

      DZ = 1. / (DBLE(N) - 1.)
      DZS = DZ * DZ

      DO 111, J = 2,(N-1)
      YPRIME(J) = (Y(J-1)-2.*Y(J)+Y(J+1))/DZS
C  111  YPRIME(J) = YPRIME(J) + RAT2*(Y(J+1)-Y(J))/DZ
  111  YPRIME(J) = YPRIME(J) + RAT2*(Y(J+1)-Y(J-1))/2./DZ
      YPRIME(N) = 0.

      Y(1) = -1./3.*(Y(3)-4.*Y(2))
C      Y(1) = 1./11.*(18.*Y(2)-9.*Y(3)+2.*Y(4))
      YPRIME(1) = 0.

      MEL=MEL-(Y(N-2)-4.*Y(N-1)+3.*Y(N))/2./DZ*(T-T2)
C      MEL=MEL-(-2.*Y(N-3)+9.*Y(N-2)-18.*Y(N-1))/6./DZ*(T-T2)
      MDESQ = MDESQ+RAT2*Y(1)*(T-T2)
      T2 = T

      RETURN
      END

      SUBROUTINE FCNJ(N, X, Y, DYPDY)
      INTEGER N
      DOUBLE PRECISION X, Y(N), DYPDY(N,*)
      RETURN
      END

*************************************************************************

      PROGRAM DESQUAM
C ********** FOR STUDYING EFFECTS OF DESQUAMATION ON DERMAL ABSORPTION
C ********** THROUGH TWO-LAYER MEMBRANE AT STEADY STATE (i.e., fig. 5.3)

      INTEGER NPARAM, N
C     ********** N is the total number of nodes in sc and ve, Nsc + Nve
      PARAMETER (NPARAM = 50, N = 162)
      INTEGER IDO,NOUT,MM,NVE,NSC,III
      DOUBLE PRECISION PARAM(NPARAM), T,TEND,Y(N),A(1,1),R6
      DOUBLE PRECISION TFINAL,MTOT,MDESQ,TSIZE,MB,MEL,MABS
      DOUBLE PRECISION IEND,MRAT,PP,TOL,W,XL,R3,R4,R5,RAT2
      DOUBLE PRECISION B,G,EVE,LEFTSC,LEFTVE,R,R1,R2,MABS2

      COMMON/CARRY/MEL,MDESQ,RAT2,B,G,EVE,NVE,NSC

C     ********** SPECIFICATIONS FOR SUBROUTINES
      EXTERNAL DIVPAG, SSET, UMACH
      EXTERNAL FCN, FCNJ
      CALL SSET(NPARAM, 0.0, PARAM, 1)

C ********** THESE ARE INPUT AND OUTPUT FILES
      OPEN (2, FILE='data2.dat', STATUS = 'NEW')
      OPEN (3, FILE='tsize.dat', STATUS = 'OLD')
```

```
      OPEN (5, FILE='tfinal.dat', STATUS = 'OLD')
      OPEN (6, FILE='rat2.dat', STATUS = 'OLD')
      OPEN (7, FILE='b.dat', STATUS = 'OLD')

C ********** SETTINGS FOR THE IVPAG SUBROUTINE
      PARAM(10) = 1.
      PARAM(4) = 90000000
      PARAM(12) = 2

C ********** Setting parameters
C ********** RAT2 = T_T,SC/T_LAG,SC
      READ(3,*) TSIZE
      READ(6,*) RAT2
      PP = 3.1415927
      READ(7,*) B
      G = 10.
      NSC = 100
      NVE = 60
      EVE = 10.

      RAT2 = 6. / RAT2
C ********* R1 THROUGH R6 ARE USED TO CALCULATE INITIAL CONDITION
      R = 0.5
      R1 = B * G / R
      R2 = RAT2 * R / G / EVE
      R3 = R1 * (1. - DEXP(RAT2 * R / G))
      R4 = DEXP(-1.*R2)
      R5 = DEXP(-1.*RAT2)
      R6 = DEXP(-1.*R2*(1.+EVE))

C ********** Setting maximum step size in time
      IF (RAT2 .LT. 2.0) THEN
         PARAM(3) = 1D-6
      END IF

C ********** SETTING INITIAL CONDITIONS
      IDO = 1
      T = 0.
      Y(1) = 1.
      Y(N) = 0.

C ********** INITIAL CONCENTRATION PROFILE FROM FORMULA
      DO 6, I = 2, NSC+1
        XL = DBLE (I-1) / DBLE (NSC)
        Y(I) = DEXP(-1.*RAT2*XL)*(1.-R3)-R5
   6  Y(I) = Y(I)/(1.-R5-R3)
      DO 66, I = NSC+2, N - 1
        III = I - NSC - 2
        XL = 1. + EVE * DBLE(III) / DBLE(NVE)
      Y(I)= R5 * (DEXP(-1.*R2*XL)-R6)
  66  Y(I)=Y(I)/(R6*(1.-R5)/R1 - R6 + R4)

      MTOT = 0.
      DO 667, I = 1,NSC
```

```
  667   MTOT = MTOT + (Y(I)+Y(I+1))/2. /DBLE(NSC)
        DO 668, I = NSC+2,N - 1
  668   MTOT = MTOT + (Y(I)+Y(I+1))/2./B/G/DBLE(NVE)

C       ********** SETTING ERROR TOLERANCE
        TOL = 1.0D-6
        CALL UMACH (2, NOUT)

        MM = 0
        READ(5,*) TFINAL
        IEND = 0.0
  10    CONTINUE
        IEND = IEND + TSIZE
        TEND = IEND

        CALL DIVPAG(IDO,N,FCN,FCNJ,A,T,TEND,TOL,PARAM,Y)
        LEFTSC = 0.
        DO 88, I = 1,NSC
   88   LEFTSC = LEFTSC + (Y(I)+Y(I+1))/2./DBLE(NSC)

        LEFTVE = 0.
        DO 89, I = NSC+2,N-1
   89   LEFTVE = LEFTVE + (Y(I)+Y(I+1))/2./DBLE(NVE)/B/G

        MB = (LEFTSC+LEFTVE+MDESQ+MEL)/MTOT
        MRAT = MDESQ/MTOT
        MABS = 1. - MRAT
        MABS2 = MEL/MTOT

C When MRAT and MABS do not change anymore in time, MABS = FA
        WRITE(2,99997) T,MB,Y(1),MABS,MABS2
        IF (IEND .LE. TFINAL) THEN
            MRAT = MDESQ/MTOT
            IF (IEND .GE. TFINAL) IDO = 3
            GO TO 10
        END IF

99999   FORMAT(F11.5)
99997   FORMAT(F5.2,5F15.7)
99998   FORMAT(8F9.3)
        END

        SUBROUTINE FCN (N, T, Y, YPRIME)
C       ********** SPECIFICATIONS FOR ARGUMENTS
        INTEGER N,IJ,NSC,NVE
        DOUBLE PRECISION DZSC,DZSCS,MEL,T2,RAT2,MDESQ,YPRIME(N),T,DUMM2
        DOUBLE PRECISION B,G,EVE,DZVE,DZVES,DUMMY,R,X,Y(N)

        COMMON/CARRY/MEL,MDESQ,RAT2,B,G,EVE,NVE,NSC
        SAVE T2

        DZSC = 1. / DBLE(NSC)
        DZSCS = DZSC * DZSC
        DZVE = EVE / DBLE(NVE)
```

```
      DZVES = DZVE*DZVE
      R = 0.5

      DO 111, J = 2,NSC
      YPRIME(J) = (Y(J-1)-2.*Y(J)+Y(J+1))/DZSCS
C  111  YPRIME(J) = YPRIME(J) + RAT2*(Y(J+1)-Y(J))/DZSC
  111 YPRIME(J) = YPRIME(J) + RAT2*(Y(J+1)-Y(J-1))/2./DZSC
      YPRIME(N) = 0.

      DO 112, J = NSC+3, NSC+NVE+1
      YPRIME(J) = G*EVE*EVE*(Y(J-1)-2.*Y(J)+Y(J+1))/DZVES
  112 YPRIME(J) = YPRIME(J) + RAT2*EVE*R*(Y(J+1)-Y(J-1))/2./DZVE

      Y(1) = -1./3.*(Y(3)-4.*Y(2))
C      Y(1) = 1./11.*(18.*Y(2)-9.*Y(3)+2.*Y(4))
      YPRIME(1) = 0.

      Y(NSC+2) = EVE/B*(4.*Y(NSC+3)-Y(NSC+4))/DZVE
      Y(NSC+2) = Y(NSC+2) + (4.*Y(NSC)-Y(NSC-1))/DZSC
      Y(NSC+2) = Y(NSC+2)/3./(1./DZSC+EVE/B/DZVE)
C      Y(NSC+2) = B/EVE*(2.*Y(NSC-2)-9*Y(NSC-1)+18*Y(NSC))/6./DZSC
C      DUMM2 = (18.*Y(NSC+3)-9.*Y(NSC+4)+2.*Y(NSC+5))/6./DZVE
C      Y(NSC+2) = Y(NSC+2) + DUMM2
C      DUMM2 = 11./6.*(1./DZVE+B/EVE/DZSC)+RAT2*(B/EVE-R/G/EVE)
C      Y(NSC+2) = Y(NSC+2)/DUMM2
      Y(NSC+1) = Y(NSC+2)
      YPRIME(NSC+2) = 0.
      YPRIME(NSC+1) = 0.

      DUMMY = (Y(N-2)-4.*Y(N-1)+3.*Y(N))/2.
      MEL = MEL - EVE/B*DUMMY/DZVE*(T-T2)
      MDESQ = MDESQ+RAT2*Y(1)*(T-T2)
      T2 = T
      RETURN
      END

      SUBROUTINE FCNJ(N, X, Y, DYPDY)
      INTEGER N
      DOUBLE PRECISION X, Y(N), DYPDY(N,*)
      RETURN
      END
```

Chapter 6. DERMAL ABSORPTION FROM PESTICIDE RESIDUES: DATA ANALYSIS

Introduction

Pesticides benefit society in many ways, but risk is associated with their use. Besides professional pesticide applicators, farmers and field workers, the general population can be exposed to pesticides in their offices, homes, lawns, or swimming pools. Of the routes of human exposure to pesticides (i.e., inhalation, ingestion, and dermal absorption), dermal exposure is the least understood in part due to the limited quantity of pertinent published data.

Most published dermal absorption studies examine exposures to neat chemicals, to large volumes of aqueous solutions, or to residues deposited from acetone. While interesting, results from these investigations are not directly relevant to a typical pesticide exposure, in which the active pesticide component and other additives (e.g., surfactants or emulsifiers) contact the skin in a small volume of water. In most cases, the water will evaporate leaving a residue of pesticide and formulation additives on the skin surface.

In its regulatory role, the U. S. EPA is the repository for a large collection of dermal absorption data supplied by pesticide registrants in compliance with federal regulations. This database contains almost 300 dermal absorption studies of more than 160 different pesticides (Zendzian, 2000a). Many of these studies followed the Zendzian protocol (Zendzian, 1994), which prescribes procedural details of *in vivo* rat experiments measuring dermal absorption as a function of both the amount of pesticide applied and the exposure time. Recently, Zendzian (2000b) reported data collected using the Zendzian protocol for representative pesticides from each of three classifications

described as volatile, skin damaging, and neither volatile nor skin damaging. In this chapter, we examine dermal absorption data obtained using the Zendzian protocol for 18 pesticides including data published by Zendzian (2000b) and data from study summaries provided to us by Dr. Zendzian. Chemical properties for these pesticides are listed in Table 6.1. Although many of the 18 studies were performed before the Zendzian protocol was formally issued as a guideline, it is our understanding that these 18 studies all followed the protocol.

Background

In addition to the active ingredient, pesticide formulations usually contain inert ingredients that could affect dermal absorption. For example, surfactants are commonly added to improve solution wettability on plant foliage or soil and these might increase dermal absorption by altering the skin barrier or by enlarging the area that the deposited residue covers. It is likely that two pesticide products with the same active ingredient might have completely different penetration rates due to formulation differences. Unfortunately, details about formulation ingredients are not generally available.

Experiments studying specific formulations of the 18 pesticides listed in Table 6.1 were conducted at 3 and sometimes 4 different applied doses, defined as the moles of pesticide applied to skin, M_{app} (nM), per exposed area, A (cm^2). Table 6.2 lists the applied doses in each study as high (H), medium (M), low (L), and lowest (LL) represented as an apparent film thickness, L_{film} (μm), calculated using eq 6-1.

$$L_{film} = M_{app}\, MW / (A\, \rho) \qquad (6\text{-}1)$$

where MW is molecular weight and ρ is the density of the pesticide film estimated as the density of the pure pesticide. As defined in eq 6-1, L_{film} is the theoretical thickness of the pesticide film if the applied dose forms a uniformly thick layer on a flat surface with an

Table 6.1 – Chemical properties of pesticides (Tomlin, 1997).[a]

Pesticide (Abbr.)	Molecular Formula	MW	MP °C	ρ g/cm^3	log$K_{o/w}$	p_{vap} mPa	S_w mg/L	Pesticide Class
2,4-DP-P-2EHE (DP)		347	< 25	U[b]				
acetochlor (AC)	$C_{14}H_{20}ClNO_2$	270	< 0	1.11	3.03	0.0045[d]	223[d]	chloroacetanilide
azinphos-methyl (AZ)	$C_{10}H_{12}N_3O_3PS_2$	317	73	1.52	2.96	0.001[d]	28[c]	organophosphorous
diclofop-methyl (DM)	$C_{16}H_{14}Cl_2O_4$	341	39-41	1.3	4.58	0.25[c]	0.8[c,g]	phenoxy
diniconazole (DN)	$C_{15}H_{17}Cl_2N_3O$	326	~ 145	1.32	4.3	4.9[d]	4[d]	azole
disulfoton (DS)	$C_8H_{19}O_2PS_3$	274	< - 25	1.14	3.95	13[d]	25[c]	organophosphorous
EPTC (EP)	$C_9H_{19}NOS$	189	< 25	0.95	3.2	0.01[d]	375[d]	thiocarbamate
imazalil (IM)	$C_{14}H_{14}Cl_2N_2O$	297	52.7	1.35	3.82	0.158[d]	180[c]	azole
iprodione (IP)	$C_{13}H_{13}Cl_2N_3O_3$	330	134	1.43[h]	3.0	0.0005[d]	13[c]	dicarboximide
isoxaflutole (IS)	$C_{15}H_{12}F_3NO_4S$	359	140	1.59	0.365	0.001[d]	6.2[c]	
lindane (LI)	$C_6H_6Cl_6$	291	113	1.85[f]	3.72[i]	5.6[c]	7.3[d]	organochlorine
metolachlor (MT)	$C_{15}H_{22}ClNO_2$	284	- 62.1	1.12	2.9	4.2[d]	488[d]	chloroacetanilide
mevinphos (MV)	$C_7H_{13}O_6P$	224	< 25	1.2	0.127	17[c]	misc.[j]	organophosphorous
molinate (MO)	$C_9H_{17}NOS$	187	< 25	1.06	2.88	746[d]	88[c]	thiocarbamate
phosmet (PH)	$C_{11}H_{12}NO_4PS_2$	317	72-73	1.03[f]	2.95	0.065[d]	25[d]	organophosphorous

(continued)

Table 6.1 (continued)

Pesticide (Abbr.)	Molecular Formula	MW	MP °C	ρ g/cm^3	log$K_{o/w}$	p_{vap} mPa	S_w mg/L	Pesticide Class
thiobencarb (TH)	$C_{12}H_{16}ClNOS$	258	3.3	1.15	3.42	2.93[e]	30[c]	thiocarbamate
tribufos (TR)	$C_{12}H_{27}OPS_3$	315	< - 25	1.06	3.23	0.71[d]	2.3[c]	
vinclozlin (VI)	$C_{12}H_9Cl_2NO_3$	286	108	1.51	3	0.13[c]	2.6[c]	dicarboximide

[a] Abbr. denotes the abbreviation used in Appendix 6A, MW = molecular weight, MP = melting point, ρ = density, log$K_{o/w}$ = base ten log of the octanol / water partition coefficient, p_{vap} = vapor pressure, S_w = solubility in water. [b] Unknown, estimated as 1.2. [c] At 20°C. [d] At 25 °C. [e] At 23 °C. [f] From SPECTRUM website, http://www.speclab.com. [g] At pH = 5.7. [h] For technical grade. [i] From Hansch *et al.*, 1995. [j] Miscible.

Table 6.2 – Experimental details and selected results.[a]

Pesticide	Exposure Periods, hours	L_{film}, μm				S/L	Did the amount in skin reach a maximum and then decrease?[f]	At 10 h, % on skin for all doses	
		LL	L	M	H			<50%[d]	>50%
2,4-DP-P-2EHE[e]	0.5, 1, 2, 4, 10, 24	0.16	0.65	4.1	24	L	No	X[d]	
acetochlor	0.5, 1, 2, 4, 10, 24	0.03	0.37	2.4	26	L	No		
azinphos-methyl	1, 4, 10	NA	0.006	0.061	0.61	S	No		
diclofop-methyl	1, 2, 4, 10, 24	NA	0.076	0.76	7.7	?[b]	No	X[d]	
diniconazole	1, 2, 4, 10, 24	NA	0.037	0.38	3.8	S	No		X (?)[c]
disulfoton	1, 4, 10	NA	0.0075	0.075	0.75	S	Yes, all doses > 1h	X[d]	
EPTC	1, 4, 10, 24	0.99	2.1	9.5	92	L	Yes, all doses > 1h	X[d]	
imazalil	0.5, 1, 2, 4, 10, 24	0.03	0.3	3	30	S	No		
iprodione	0.5, 1, 2, 4, 10, 24	NA	0.22	2.2	22	S	No		X
isoxaflutole	0.5, 1, 2, 4, 10, 24	NA	0.005	0.05	0.5	S	No		X
lindane	0.5, 1, 2, 4, 10, 24	NA	0.11	1.1	11	S	Yes, dose L & M > 4h		
metolachlor	2, 4, 10, 24	NA	0.089	0.89	8.9	L	Yes, dose L > 4 h		
mevinphos	6, 10, 24	NA	0.004	0.021	0.11	L	No	X[d]	
molinate	4, 10, 24	NA	0.084	0.84	8.4	L	Yes, all doses > 4h	X[d]	
phosmet	1, 2, 4, 10, 24	NA	0.56	5.1	26	S	No		X (?)[c]

(continued)

Table 6.2 (continued)

Pesticide	Exposure Periods, hours	L_{film}, μm				S/L	Did the amount in skin reach a maximum and then decrease?[f]	At 10 h, % on skin for all doses	
		LL	L	M	H			<50%[d]	>50%
thiobencarb	1, 2, 4, 10, 24	NA	0.045	0.44	4.3	L	Yes, doses L & M > 2h		
tribufos	1, 4, 10	NA	0.019	0.095	0.95	L	No		
vinclozlin	0.5, 1, 2, 4, 10	0.013	0.13	1.3	13	S	No		X

[a] NA = not applicable. S / L denotes solid or liquid at skin temperature (~32°C). [b] The melting point of pure diclofop-methyl is slightly higher than skin temperature (i.e., 39 - 41°C), but the formulation is not pure pesticide and could have a lower melting point. [c] The ? indicates that the percent of applied dose on the skin was not reported, but it probably remained > 50% because the percent in skin and absorbed systemically were low and it is not likely these pesticides evaporated. [d] These pesticides were not included in Figures 6.9 and 6.10 because the percent of applied dose on the skin at 10 hours was less than 50% for all applied doses (i.e., the exposed dose changed rapidly). [e] This pesticide was applied in a vehicle of A260 light mineral oil. [f] This column notes the doses and exposure times at which the amount in the skin started to decreased due to a decrease in the exposed dose.

area equal to the exposed area. Usually, dose H was the concentrated formulation, and the other doses were 10-fold dilutions of the next larger dose (e.g., dose M is $1/10^{th}$ of dose H). The large variations in L_{film} for dose H (from 0.11 to 92 μm) reflect considerable differences in concentrations of active ingredient in the pesticide formulations. Values of L_{film} in Table 6.2 vary from a low of 0.004 μm for mevinphos to a high of 92 μm for EPTC.

Topographic features of the skin's surface make it likely that L_{film} would need to be larger than about 1 - 10 μm to completely cover the exposed surface. For pesticide exposures like those simulated by the Zendzian protocol, the amount of pesticide on the skin probably does not cover the exposed skin completely. Indeed, environmental scanning electron studies of 4-cyanophenol, which is a solid at skin temperature, applied to normally hydrated excised human skin at 0.01 mg/cm^2 ($L_{film} \cong 0.1$ μm) using acetone showed chemical-free regions distributed among regions covered by chemical (see Chapter 7, Figure 7.1). Similar types of distributions might be expected from dermal exposure to pesticide formulations in which the liquid components evaporate leaving a residue of solid pesticide on the skin surface. The surface distribution of residues might be different for pesticides that are liquids at skin temperature, or for formulations in which liquid components do not evaporate.

Changes in the applied dose or the distribution of a given dose on the skin surface will change the amount of absorption in some situations, and produce no change in others. For example, if the applied dose is large enough that chemical completely covers the skin surface for the entire exposure time, the exposed surface is saturated and the absorption rate is maximized. In this case, increasing the applied dose further will not increase the amount that dermally absorbs. But if the amount of chemical on the skin surface is small enough that only a small portion of the exposed area is covered by chemical, then increasing the applied dose will probably increase the area in contact with pesticide, thereby increasing the amount of chemical that dermally absorbs. However,

Chapter 7 shows that absorption from residues partially covering the exposed area with many small piles can be the same as for applied doses that completely cover the exposed area. Thus, an important goal of this investigation was to examine the effects of changes in the applied dose on the rate and extent of dermal absorption.

Dermal absorption and evaporation reduce the amount of pesticide remaining on the skin surface. The exposed dose, defined as the amount of pesticide on the skin per exposed area at any time during the exposure, decreases with increased exposure time. If the applied dose is large and dermal absorption and evaporation are slow, the exposed dose will be nearly constant and equal to the applied dose during the entire exposure. However, if dermal absorption or evaporation is rapid, then the exposed dose decreases significantly during the exposure, and the rate of continued dermal absorption will be affected. In this case, the exposed dose may not be large enough to saturate the skin surface even if the applied dose was large enough to completely cover the skin surface.

Increasing the length of the exposure time will increase the amount of dermal absorption, but not always proportionally. After the pesticide formulation is applied to the skin, liquid components of the formulation (e.g., water) will evaporate if their vapor pressure is relatively large. As shown later, dermal absorption does occur during and after liquid components have evaporated. However, the presence of liquid components or the increase in pesticide concentration that occurs as the volume of the remaining liquid components decreases may affect the absorption rate. Furthermore, the rate of dermal absorption usually decreases with exposure time as the skin's capacity for holding chemical is filled. The exposed dose will deviate more from the applied dose with increased exposure time, which also can cause the absorption rate to decrease with exposure time. Clearly, meaningful predictions for dermal absorption of pesticides (and other chemicals with similar types of exposures) will only be possible when the effects of exposure time and applied dose are understood. The goal of this study was to investigate these effects for the 18 pesticides listed in Table 6.1.

The Zendzian Protocol

The Zendzian Protocol (Zendzian, 1994) prescribes the methodology for dermal absorption experiments on young, adult, male laboratory rats (200-250 g). Radiolabeled pesticide is applied to at least 10 cm^2 of the back of a rat that was shaved 24 hrs earlier. The applied volume of a solution does not exceed 10 $\mu L/cm^2$, which is large enough for easy spreading and small enough to minimize the amount that flows to the enclosure. The highest applied dose is typically the concentrated pesticide solution, and lower doses are 10-fold dilutions. The solutions are prepared so that the same amount of radiolabeled chemical is applied to the skin irrespective of dose. Thus, the fraction of active ingredient that is radioactive is smallest in the largest dose solution. After application the exposed area is protected by a cover, usually filter paper or gauze, which allows the flow of air without rubbing the surface. If the pesticide is known to evaporate, the cover is impregnated with activated charcoal to prevent additional exposure by vapor inhalation.

At each applied dose and exposure time (often including 0.5, 1, 2, 4, 10, and 24 hours), four animals are exposed. After the exposure ends, the exposed area is washed with soap and water and rinsed, and the animal is then sacrificed. The urine, fecal material, and cage washes are collected and analyzed. The amount of pesticide found on the enclosure and cover, in the skin wash, in the exposed area of the skin, and absorbed through the skin (i.e., found in the carcass, urine, feces, and cage wash) are reported, along with an overall mass balance.

The studies presented here were performed by a variety of different labs. While all used the Zendzian protocol for the basic procedure, the details not precisely specified by the experimental protocol may vary from lab to lab. For example, some labs might apply the pesticide to a circle inside the 10 cm^2 that does not extend to the enclosure and cover, while others spread the pesticide over the complete area.

Results and Discussion

Experimental results for all pesticides listed in Table 6.1 are presented in Appendix 6A. Except for one pesticide, acetochlor, the data provided to us (either in (Zendzian, 2000b) or directly by Zendzian) was in the form of the average for four animals with no other statistical information. Here we present example results for four pesticides selected from Table 6.1. In most cases, we present the percent of applied dose on the skin surface (i.e., from the skin wash), in the skin at the exposed site, systemically absorbed and recovered as a function of time.

If a pesticide evaporates, the exposed dose on the skin can decrease continuously and significantly during the exposure. Figure 6.1 shows example results for an evaporating pesticide, disulfoton. Because disulfoton was known to evaporate, activated carbon was included in the cover. As shown in Figure 6.1a, the percent of applied dose on the enclosure and cover increased with time, indicating that evaporation continued during the entire 10-hour exposure. The percent on the enclosure and cover was smallest for dose H, suggesting that evaporation was more important for the two smaller doses. As indicated in Figure 6.1e, the percent of applied dose that was recovered was good (i.e., on average it was > 90%) for doses M and H, but was poorer for dose L.

Figure 6.1c shows that the amount of disulfoton in the skin reached a maximum at or before one hour, the earliest time for which data were available. For all exposure times studied, the amount in the skin decreased as the amount on the skin decreased. This type of behavior was common when the exposed dose decreased rapidly. By comparing the results from Figure 6.1b to those in Figure 6.1a, c and d, it is evident that the amount of pesticide on the skin was decreased by dermal absorption in addition to evaporation. Dermal absorption was responsible for more than half of the pesticide that left the skin surface.

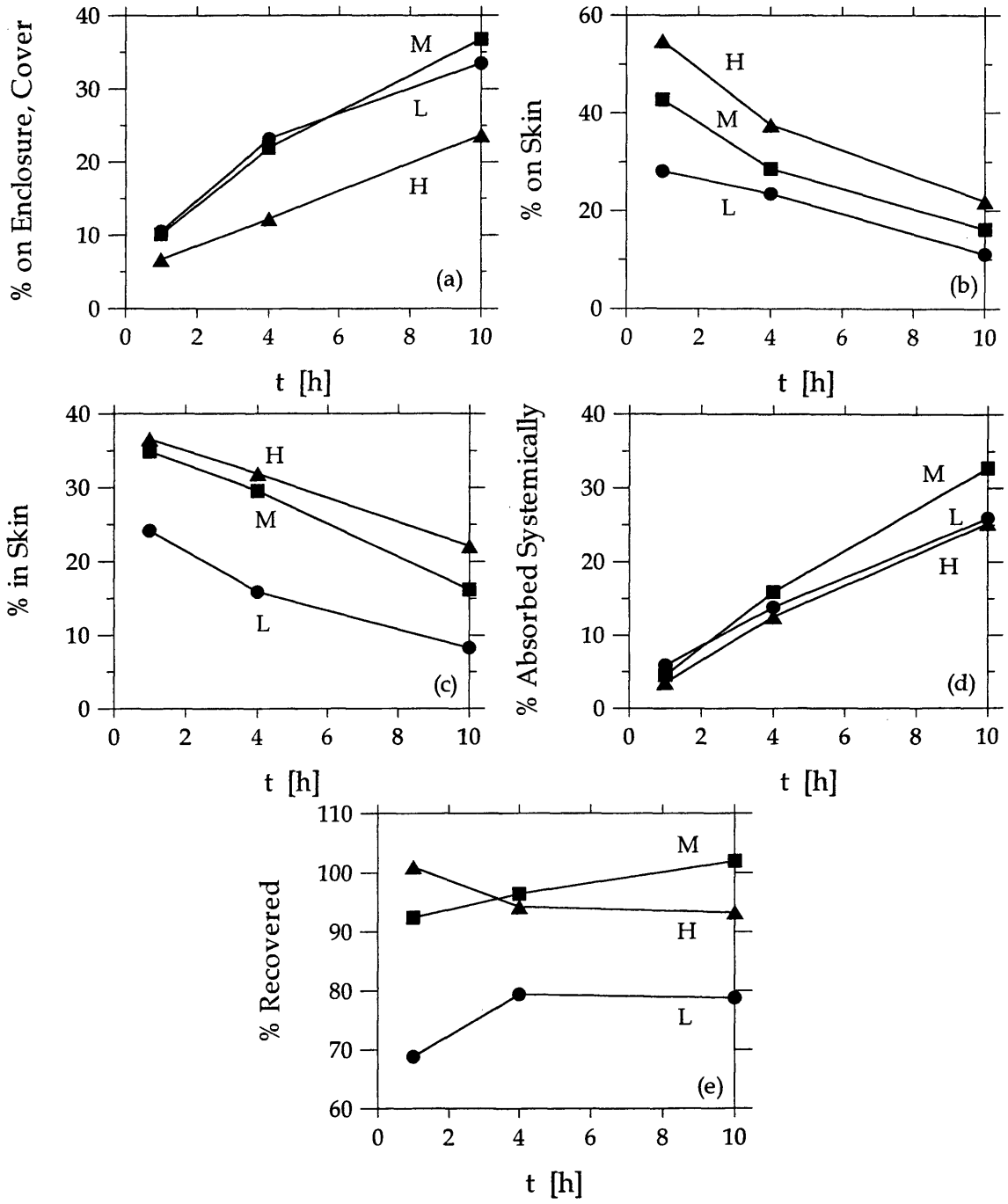

Figure 6.1 – Percent of applied dose of disulfoton (a) on the enclosure and cover, (b) on the skin, (c) in the skin, (d) absorbed systemically and (e) recovered as a function of time for applied doses (●) L, (■) M and (▲) H.

The likelihood of evaporation is indicated by a pesticide's vapor pressure, p_{vap}. For example, the vapor pressure for disulfoton is 13 mPa. For 7 of the 18 pesticides listed in Table 6.1, p_{vap} exceeds 2 mPa. Except for diniconazole and possibly metolachlor, some evaporation was indicated for all pesticides in this group. Activated carbon covers were not used in the studies of all of these seven pesticides. When activated carbon was not used, then evidence for evaporation was found in other measurements. As an example, for lindane (p_{vap} = 5.6 mPa) the percent of applied dose on the enclosure and cover with no activated carbon was always < 3% (data not shown), but the percent lost in the analysis increased (i.e., the % recovery decreased) continuously over 24 hours (see Figure 6.2d). For dose L at 24 hours, the percent recovery was less than 60%. It is likely that poor recoveries, especially those that worsen with time, indicate evaporation for pesticides like lindane with p_{vap} greater than 2 mPa.

Despite the evaporation of lindane, significant amounts absorbed systemically. For dose L at 24 hours, 28% of the applied dose had absorbed systemically. It has been hypothesized that the majority of dermal absorption of pesticides that are solid at skin temperature will only occur while the liquid solution is present. Clearly, systemic absorption occurred during the entire exposure for lindane (MP = 113°C). The amount of lindane in the skin increased between 2 and 4 hours for doses L and M (see Figure 6.2c). The liquid components in the applied solution would have evaporated within about an hour, and so dermal absorption into the skin continued from the lindane residue remaining on the skin surface.

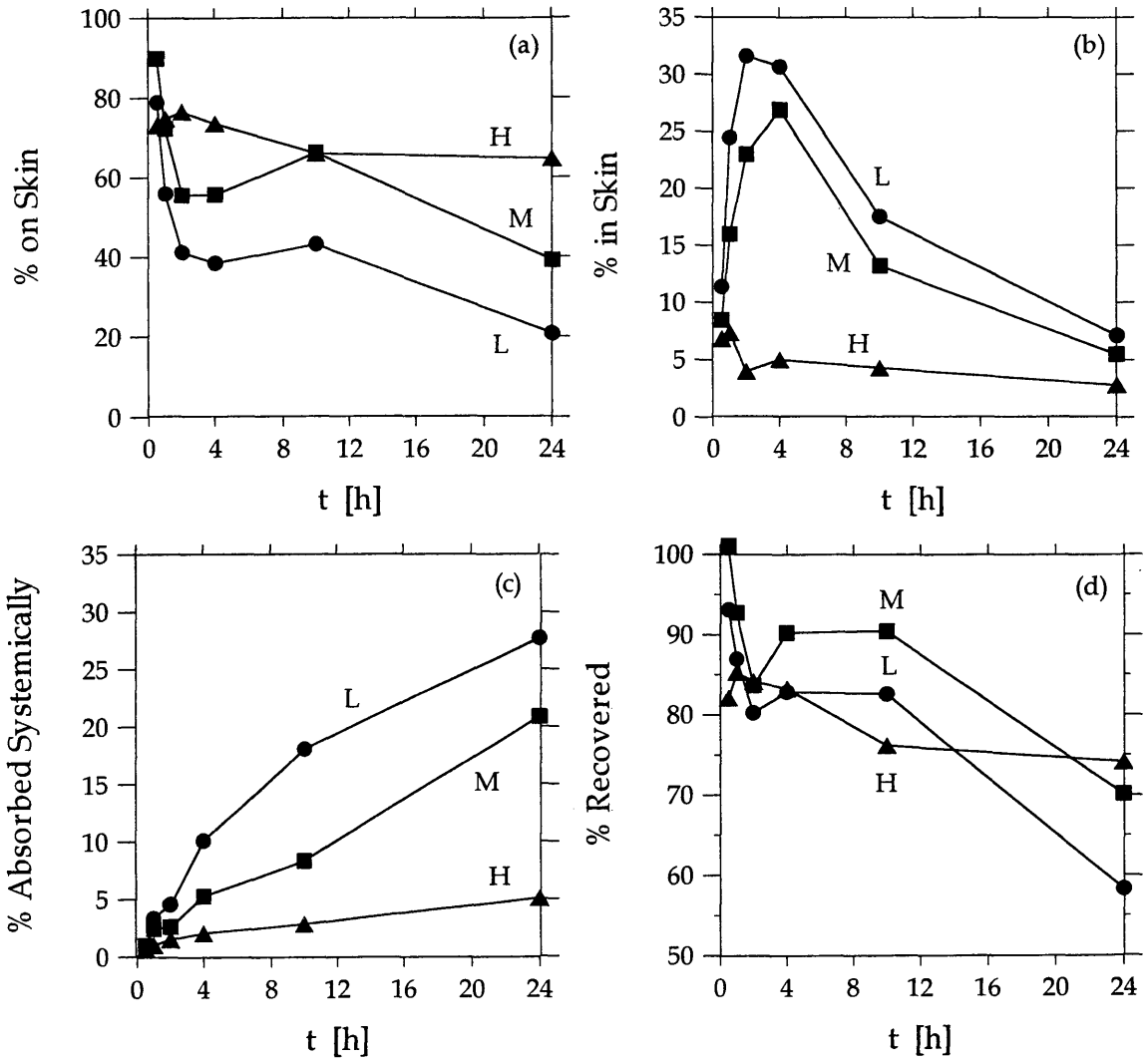

Figure 6.2 – Percent of applied dose of lindane (a) on the skin, (b) in the skin, (c) absorbed systemically and (d) recovered as a function of time for applied doses (●) L, (■) M and (▲) H.

Figure 6.3 shows that the amount of lindane in the skin reached a maximum between 2 and 4 hours, and for doses L and M decreased rapidly after 4 hours as the exposed dose decreased. For the dose H, the amount in skin did not decrease. This is consistent with the exposed dose at 24 hours, which was 21% for dose L and 39% for dose M, compared to 65% for dose H.

Experimental results for acetochlor are shown in Figure 6.4. The error bars in Figure 6.4 represent one standard deviation of a measurement repeated in four rats. To distinguish between applied doses, the error bars increase in width from the lowest to the highest applied dose. Figure 6.4a shows the percent of applied dose on the cover. The data for dose LL do not include pesticide on the activated carbon filter, which is shown in Figure 6.4b. The amount of acetochlor on the activated carbon filter was only measured for dose LL because separate experiments (i.e., loss of chemical from a glass slide) suggested that losses by evaporation would only be significant at the smallest dose. Figure 6.4a shows that up to 20% of the applied dose was found on the cover. The large amount of acetochlor found on the cover probably resulted from a mechanism besides evaporation because it did not increase much with time. For dose LL, the percent on the activated carbon filter increased with exposure time and reached 22% at 24 hours.

There are several reasons that a significant amount of the applied dose may be found on the enclosure and cover. The pesticide might be volatile, the vehicle might migrate to the enclosure over the course of the experiment, or pesticide solution might run to the enclosing ring during application. When a significant amount of chemical is found on the enclosure and cover, the amount of chemical available for dermal absorption is less than the applied dose indicates.

For acetochlor, the percent of applied dose remaining on the skin decreased for all exposure times due to dermal penetration. The percent in the skin was essentially independent of exposure time, but the percent absorbed systemically increased with time

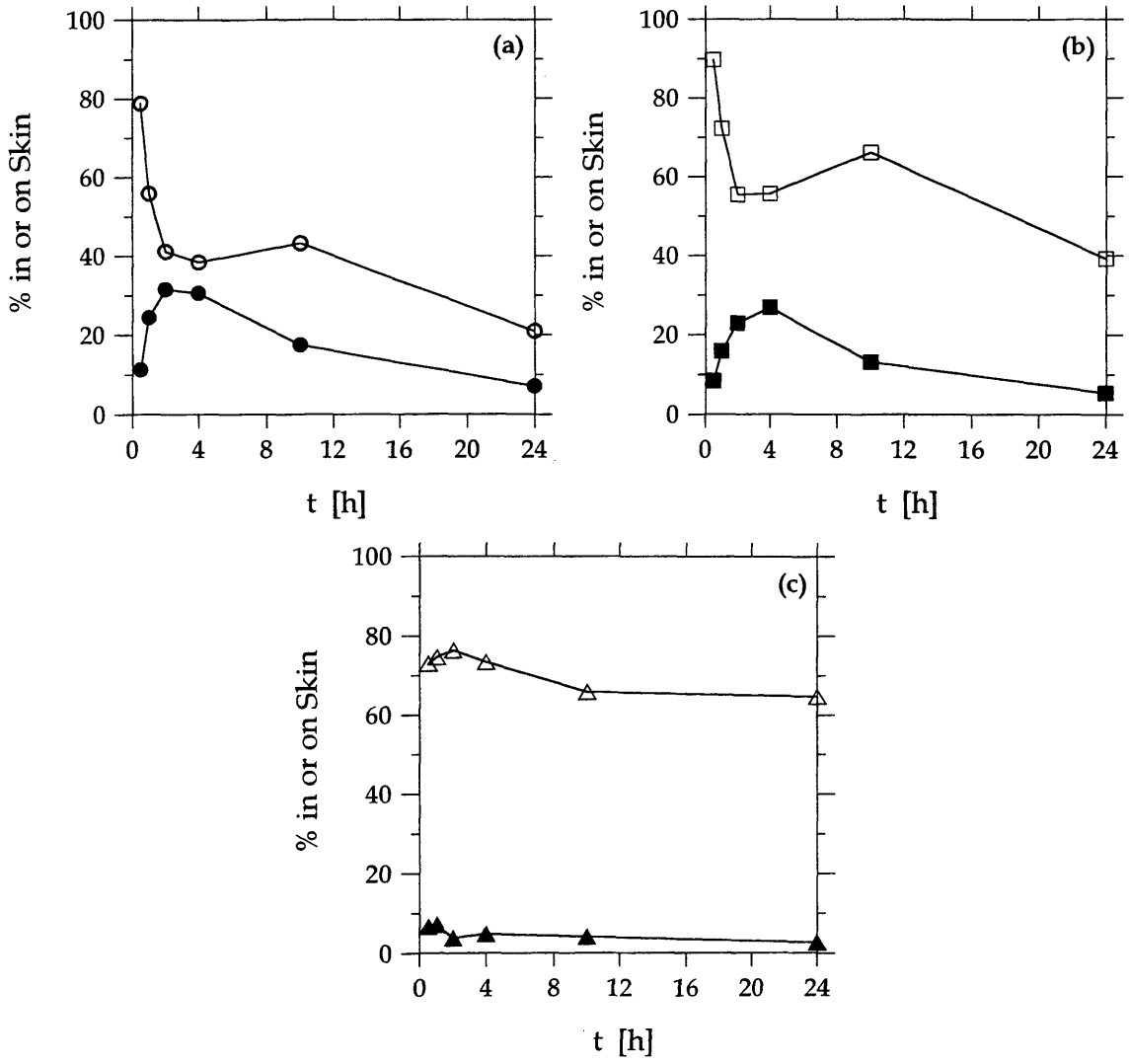

Figure 6.3 – Percent of applied dose of lindane on (open symbols) and in (closed symbols) the skin as a function of time for all doses: (a) L, (b) M and (c) H.

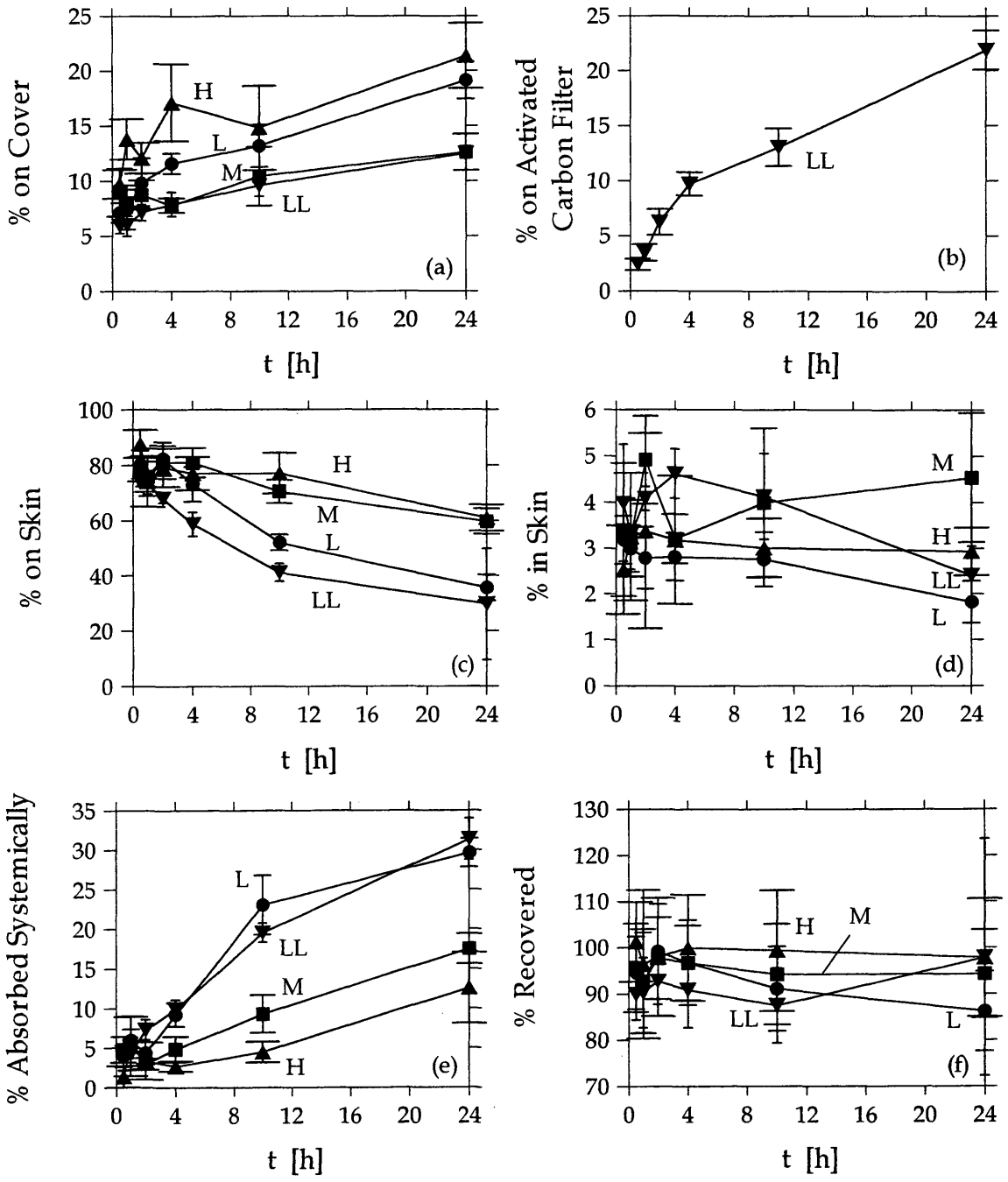

Figure 6.4 – Percent of applied dose of acetochlor (a) on the enclosure and cover, (b) on the activated carbon filter for dose LL, (c) on the skin, (d) in the skin, (e) absorbed systemically and (f) recovered as a function of time for applied doses (▼) LL, (●) L, (■) M and (▲) H.

for all doses. In Figures 6.4a, d and f, there is no significant difference between the doses based on the overlapping error bars. In Figure 6.4e, the percent absorbed systemically seems to be significantly lower for doses M and H than for doses LL and L. Figure 6.4d shows that there is probably no statistical difference between the amount of pesticide in the skin at 0.5 and 24 hours.

The exposed dose of acetochlor decreased with increasing exposure time, as shown in Figure 6.4c. For dose LL at 24 hours, less than 30% of the applied dose remains on the skin. Figure 6.5 shows, however, that the amount of acetochlor in the skin did not decrease significantly in response to the decreasing exposed dose. Figure 6.4d shows that the amount of acetochlor in the skin at 24 hours did drop for doses L and LL, but based on the error bars the drop was not significant. Thus, the decrease in the exposed dose probably had a minimal effect on the amount of acetochlor in the skin. For some of the other pesticides, the exposed dose decreased more rapidly.

The experimental results for vinclozlin shown in Figure 6.6 do not include the percent of applied dose on the enclosure and cover because it was not available, or the percent recoveries because they were always greater than 87%. In Figure 6.6a, the percent of applied dose on the skin was lowest for dose LL, and highest for dose H. The percent in the skin is independent of time (Figure 6.6b), while the percent absorbed systemically increased with time for all doses. For several data points, the symbol "D" (for detection limit) marks the value that systemic absorption was reported as less than. For these data points, at least one animal had undetectable systemic absorption, included in the mean value calculation as the detection limit. Dose H is most likely to have values below the detection limit because as dose increases the percent absorbed often decreases, but the applied dose contains the same amount of radioactivity as the lower applied doses.

The percent on the skin for vinclozlin decreased by almost 40% for dose LL. However, the amount in the skin did not decrease significantly, as shown in Figure 6.6b. Apparently, the exposed dose decreased slowly enough or in a way (e.g., the surface area

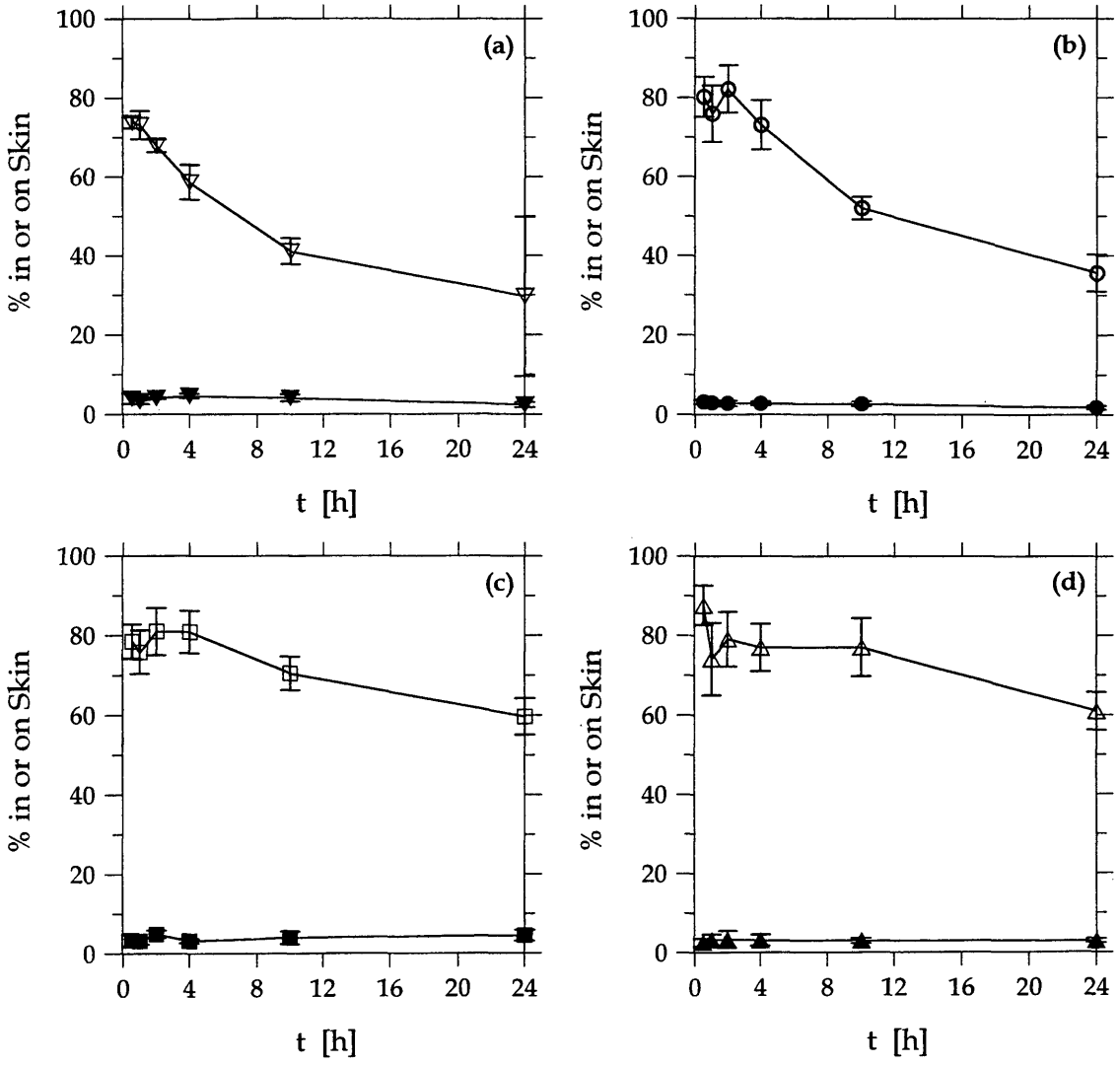

Figure 6.5 – Percent of applied dose of acetochlor on (open symbol) and in (closed symbol) the skin as a function of time for all doses: (a) LL, (b) L, (c) M and (d) H.

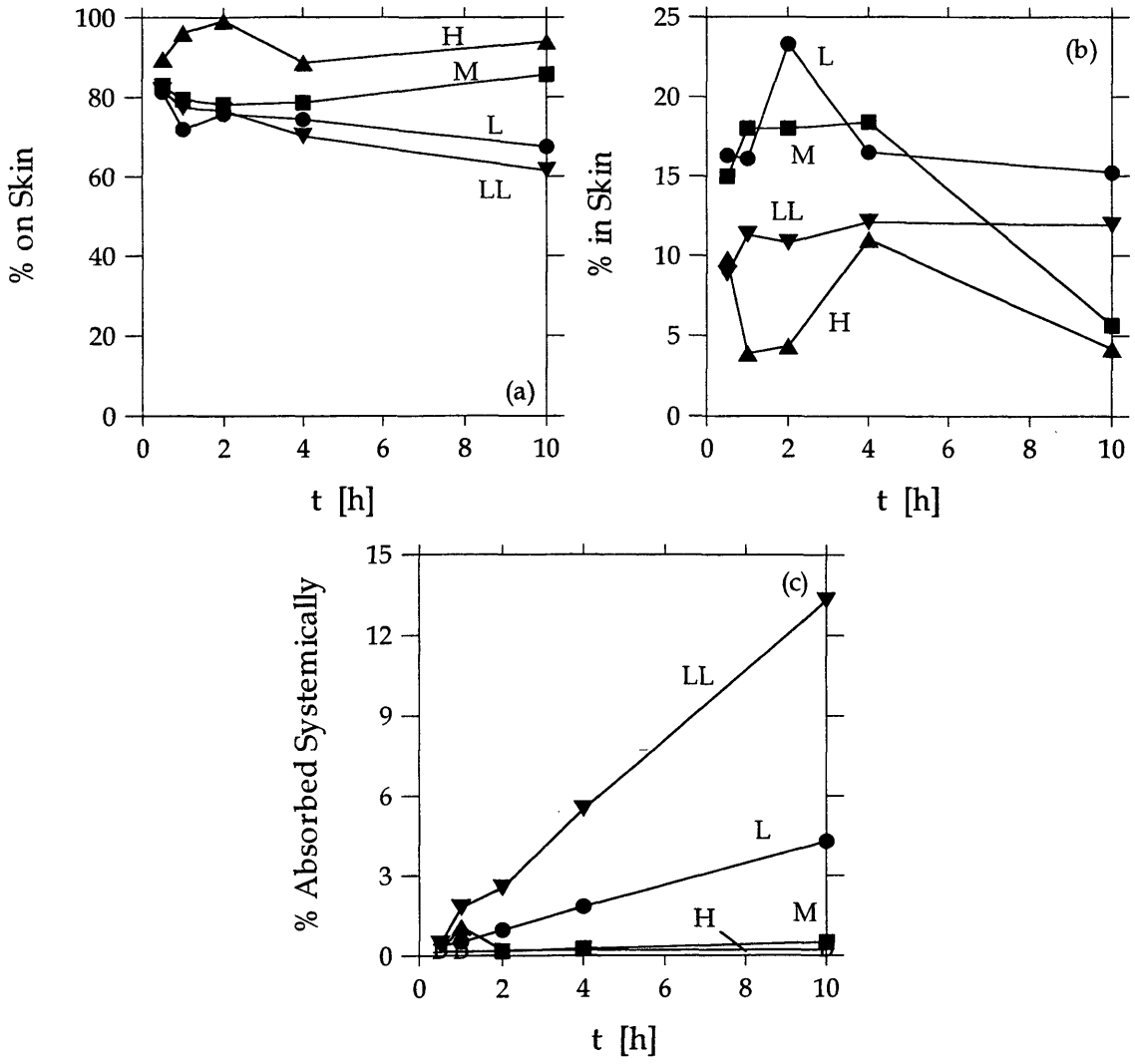

Figure 6.6 – Percent of applied dose of vinclozlin (a) on the skin, (b) in the skin and (c) absorbed systemically as a function of time for applied doses (▼) LL, (●) L, (■) M and (▲) H.

in contact with pesticide did not change) that dermal absorption was not affected. Figure 6.6 shows that vinclozlin, which is a solid at skin temperature, absorbs into and through the skin after the liquid portion of the formulation has evaporated. For dose LL, the percent of applied dose in the skin remained constant at about 12% between 1 and 24 hours. During that time, systemically absorption increased from 0.4 to 13%.

Comparing the percent in the skin and absorbed systemically as a function of time shows the relative rates of absorption into and through the skin. Some chemicals absorb quickly into the skin, but absorb into the bloodstream from the skin slowly. Doses L to H for lindane (L_{film} = 0.11-11 μm) and vinclozlin (L_{film} = 0.13-13 μm) were similar, and lindane (MW = 291, MP = 113°C, $\log K_{o/w}$ = 3.72) and vinclozlin (MW = 286, MP = 108°C, $\log K_{o/w}$ = 3) have similar properties. Comparing Figures 6.2b to 6.6b, the percent in the skin was similar for lindane and vinclozlin. After 10 hours, about 5 times more lindane had absorbed systemically than had vinclozlin, even though the exposed dose of lindane decreased more rapidly than it did for vinclozlin. Lindane probably has a larger diffusion coefficient than vinclozlin because it contains more chlorine atoms, which contribute a smaller molecular volume for their MW compared to carbon and hydrogen.

When decreases in the exposed dose cause the area in contact with pesticide to decrease, steady state might not occur. In this situation, the amount of pesticide absorbed in the skin will increase with time to a maximum value and then may decrease. This was observed for four pesticides (i.e., lindane, metolachlor, molinate and thiobencarb) that reached a maximum amount in the skin within four hours that then decreased significantly for dose L. For dose H of four of these same pesticides, the amount in the skin increased to a constant value indicating that the amount on skin was sufficient to apparently saturate the skin. This may or may not coincide with complete coverage of the exposed area. Theoretical calculations presented in Chapter 7 demonstrated that applied doses partly covering the exposed area with many small piles of pesticide can produce as much dermal absorption as a completely covered exposed surface. Thus, it is

theoretically possible that decreasing the exposed area by depleting the exposed dose through evaporation or absorption may not always cause the amount of pesticide in the skin to decrease.

Sixteen of the pesticides listed in Table 6.2 took less than four hours to reach a maximum amount in the skin. If the exposed dose decreased slowly enough, then the time to reach the maximum amount in skin should have been related to the lag time for penetration. However, when the exposed dose decreased rapidly, then the maximum might occur more quickly than expected based on the lag time. This is probably what happened for EPTC and disulfoton, which reached a maximum amount in skin at or before the shortest exposure time measured. It is perhaps significant that the two pesticides taking more than four hours to reach a maximum amount in skin had the largest MW's (i.e., MW is 359 for isoxaflutole and 347 for 2,4-DP-P-2EHE) and perhaps the smallest diffusion coefficients. However, diclofop-methyl (MW = 341) which appeared to reach a maximum within one hour is an apparent contradiction to this theory.

For diclofop-methyl, the percent in skin reached a constant value before one hour (i.e., for dose L, the percent in skin was 62% at 1 hour and 60% at 10 h) although the exposed dose had decreased in 1 hour to only 25% of the applied dose. The exposed dose decreased rapidly during the first hour of exposure, maybe while the liquid components of the pesticide solution were evaporating. Mevinphos showed a similar pattern. For dose L, the exposed dose decreased to 26% of the applied dose at 6 hours (the shortest exposure time) and 23% at 24 hours, while the percent in skin was 32% of the applied dose at 6 hours and 30% at 24 hours. Perhaps when the exposed dose decreases rapidly enough, the amount in skin does not decrease after reaching a maximum. For both diclofop-methyl and mevinphos, the maximum amount in the skin was probably smaller than would have been achieved if the exposed dose was the same as the applied dose.

The amount in the skin and absorbed systemically as a function of L_{film} are shown in Figures 6.7 and 6.8, respectively, for the four example pesticides to illustrate the effect

of applied dose on dermal absorption. In all cases, both the amount in skin and the amount absorbed systemically increased as the applied dose increased. Figures 6.7a and b show that for the two pesticides with exposed doses that decreased significantly, the amount in the skin was lower for longer exposure times.

Figures 6.7 and 6.8 suggest that it might be possible to represent the data using the following equation:

$$M = I\ L_{film}^{\hat{S}} \tag{6-2}$$

in which M is the moles per exposed area in the skin or absorbed systemically. Values of $\hat{S}$ and I can be calculated by linearly regressing experimental data to eq 6-3:

$$\log M = \hat{S}\ \log L_{film} + \hat{I} \tag{6-3}$$

where $\hat{I} = \log I$. If the slope value $\hat{S}$ is approximately 1, the moles in the skin or absorbed systemically increased proportionally to dose. If $\hat{S}$ is nearly 0, the moles in the skin or absorbed systemically were independent of applied dose, and further increases in the applied dose caused no increase in the amount absorbed. A value of $\hat{S}$ between zero and 1 could indicate that dermal absorption is not proportional to applied dose. It could also indicate that for lower applied doses, M increased proportionally to L_{film}, and for higher applied doses M was independent of L_{film}. This might be expected if the amount absorbed was proportional to the surface area in contact with pesticide for applied doses that were too small to completely cover the skin, and independent of applied dose when the skin is covered enough to saturate. Coefficients for the regression fits to eq 6-3 for exposure times of 2 to 24 hours are summarized for each pesticide in Appendix 6A.

The effect of applied dose is more complicated when the exposed dose changes

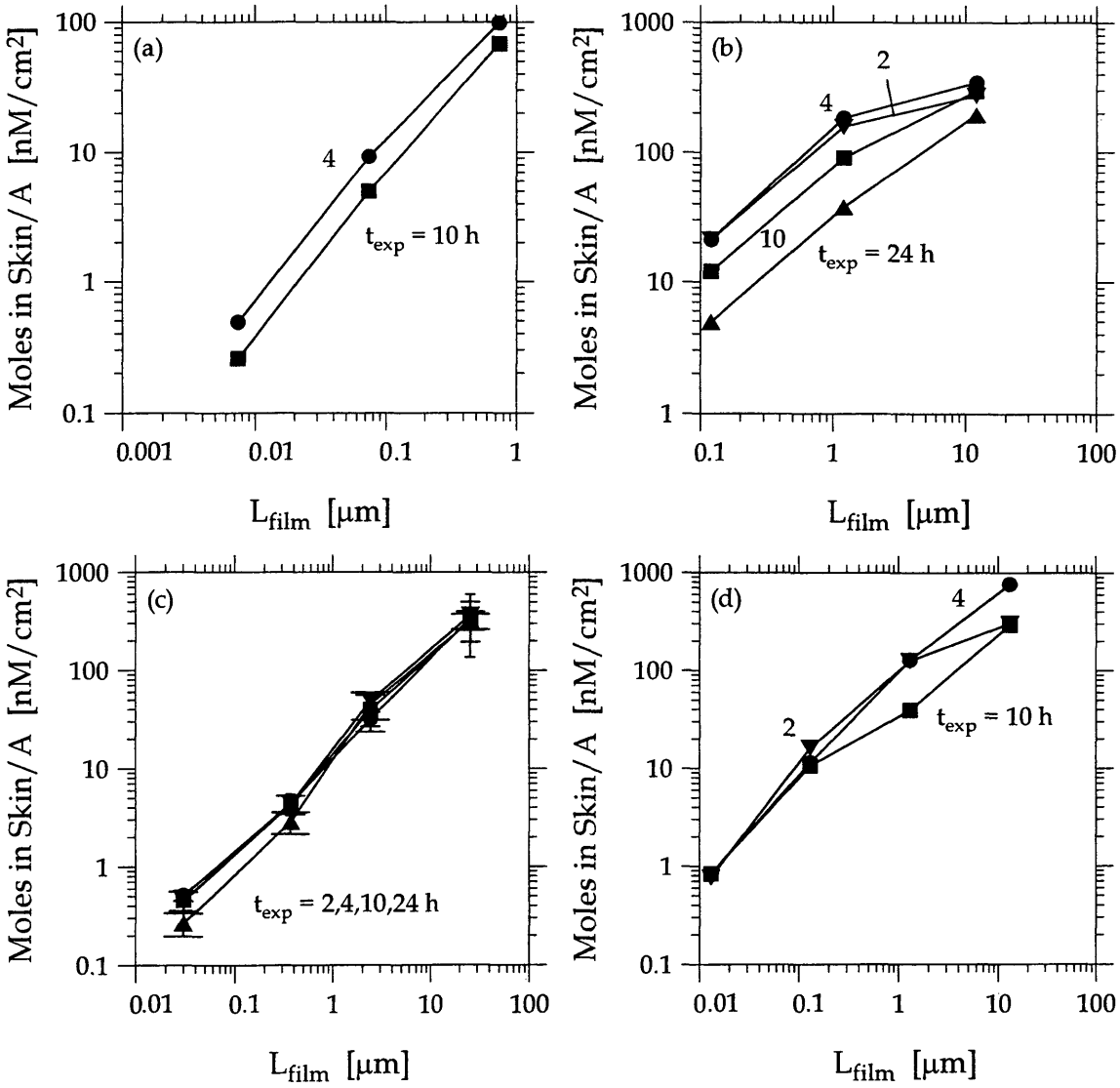

Figure 6.7 – Moles of chemical in the skin as a function of L_{film} for (a) disulfoton, (b) lindane, (c) acetochlor and (d) vinclozlin.

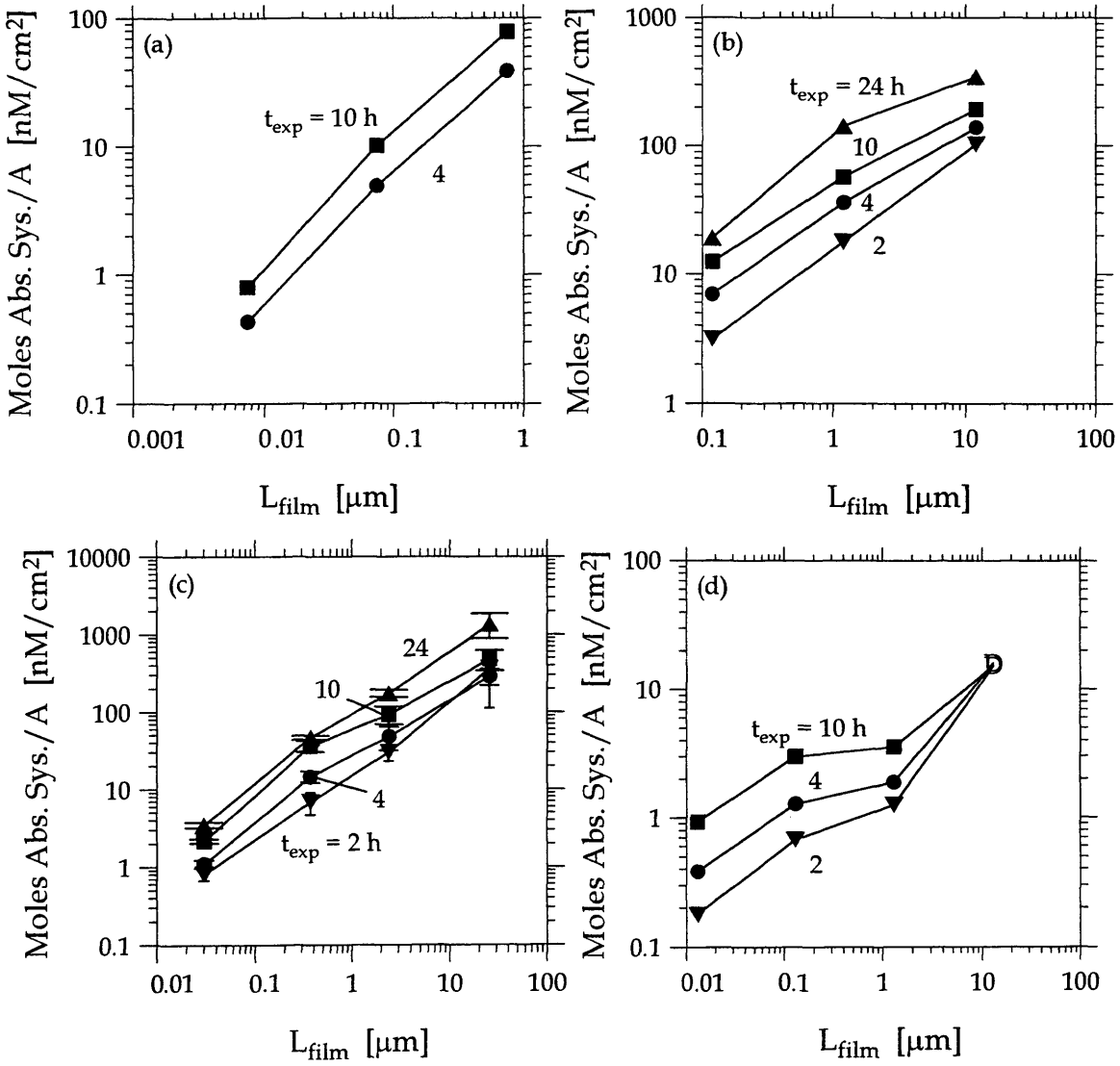

Figure 6.8 – Moles of chemical absorbed systemically as a function of L_{film} for (a) disulfoton, (b) lindane, (c) acetochlor and (d) vinclozlin.

rapidly with time. For this reason, the data analysis shown in Figure 6.9 and 6.10 did not include those pesticides for which the 10-hour exposed dose was less than 50% of the applied dose for all doses (see designation in Table 6.2). Figure 6.9 presents the amount in skin and absorbed systemically at 10 hours as a function of L_{film} for four pesticides that are liquids at skin temperature. Figure 6.10 shows the 10-hour data for eight pesticides that are solid at skin temperature. The 10-hour data were examined because all the studies included a 10-hour exposure, and 10 hours was long enough for the effects of the evaporating vehicle to diminish. In Figures 6.9 and 6.10, numbers represent data points and solid lines represent the best-fit unweighted linear regressions to eq 6-3. The dashed line in each plot has a slope of one for visual comparison with the regression lines. Table 6.3 lists the slope values for the best-fit lines.

Unfortunately, only four liquid pesticides met the 50% criterion because, as shown in Table 6.2, the exposed doses for liquid pesticides tended to be lower than for solid pesticides and the vapor pressures larger. Of the pesticides for which the exposed dose was greater than 50% at 10 hours, all five were solids. Of the pesticides for which all the exposed doses at 10 hours were less than 50%, five out of six were liquid pesticides.

As indicated in Table 6.3, $\hat{S}$ for the amount in skin was typically greater than or equal to $\hat{S}$ for the amount absorbed systemically. Imazalil is the notable exception. For imazalil, values of $\hat{S}$ for the amount in the skin were 0.7 – 0.8 for all exposure times, but for the amount absorbed systemically $\hat{S}$ increased with exposure time from 0.5 at 4 hours to 0.9 at 24 hours. Exposure to imazalil has caused some sensitive test animals to experience contact dermatitis (EXTOXNET, 1996). Also, some formulations of imazalil have been given the EPA toxicity classification II, indicating that it can cause severe skin irritation within 72 hours (Tomlin, 1997). Thus, imazalil may damage skin, which would explain the slope values for systemic absorption increasing with exposure time and slope

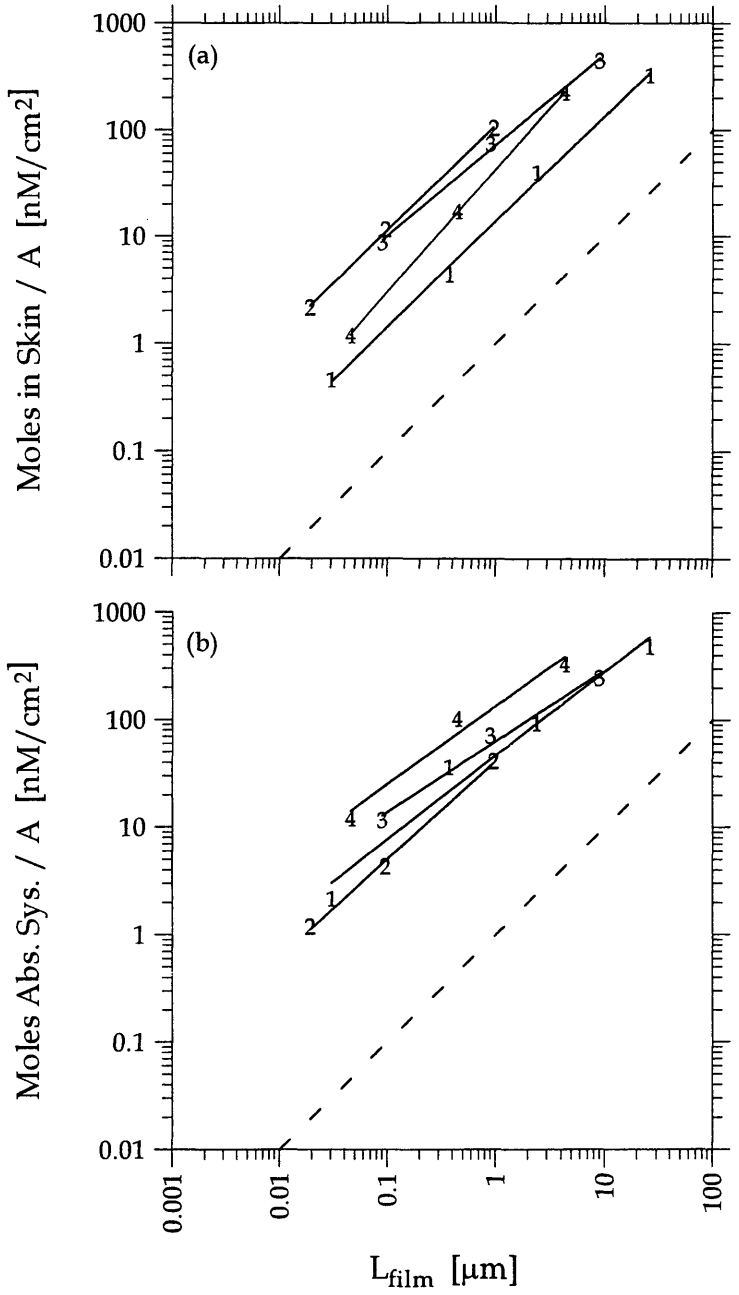

Figure 6.9 – Moles in the skin (a) and moles absorbed systemically (b) as a function of L_{film} for a 10-hour exposure to liquid pesticides: 1 – acetochlor, 2 – tribufos, 3 – metolachlor and 4 – thiobencarb. The dashed line, included as a visual reference, has a slope value of one.

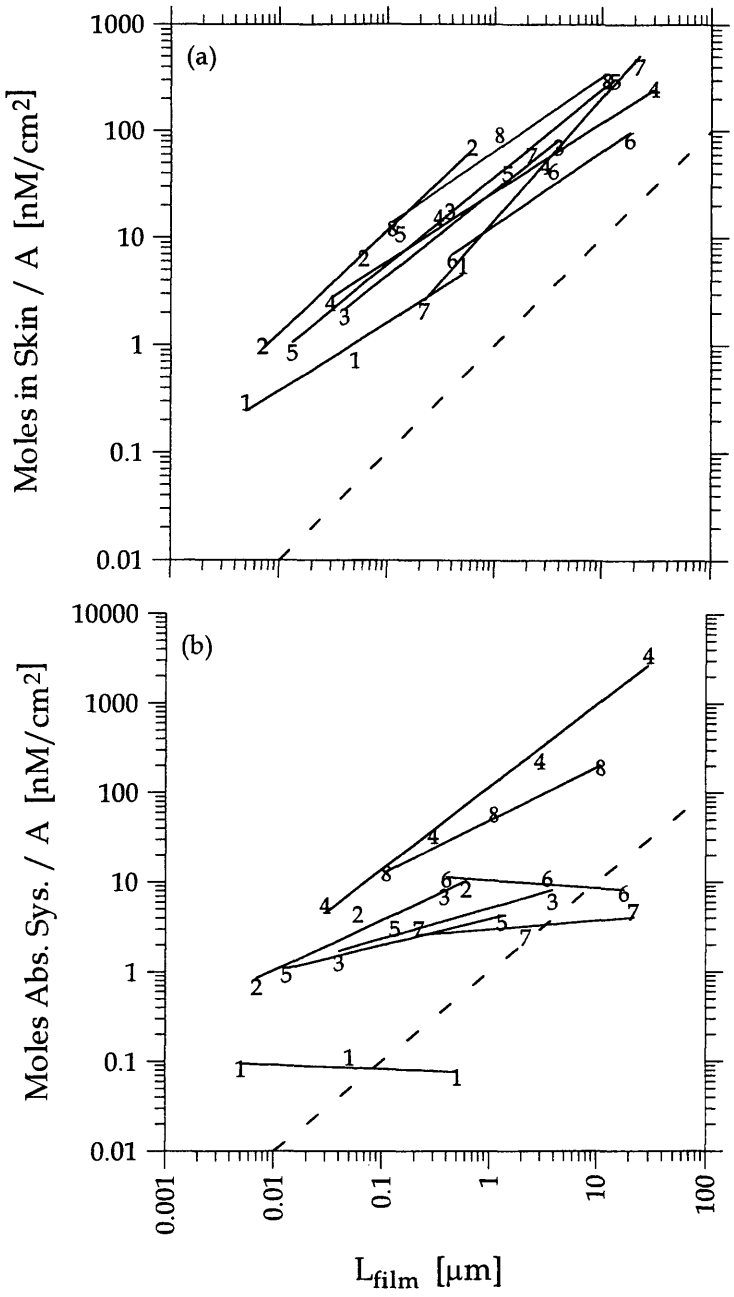

Figure 6.10 – Moles in the skin (a) and moles absorbed systemically (b) as a function of L_{film} for a 10-hour exposure to solid pesticides: 1 – isoxaflutole, 2 – azinphos-methyl, 3 – diniconazole, 4 – imazalil, 5 –vinclozlin, 6 – phosmet, 7 – iprodione and 8 – lindane. The dashed line, included as a visual reference, has a slope value of one.

Table 6.3 – Regression coefficients for moles of chemical in the skin and absorbed systemically as a function of L_{film}.

S / L[a]	Chemical	$\log K_{o/w}$[b]	Range of L_{film}, μm	$\hat{S}$	
				in skin	abs. sys.
L	acetochlor	3.03	0.027-26	1.1	0.87
L	metolachlor	2.9	0.089-8.9	0.86	0.54
L	thiobencarb	3.42	0.045-4.3	1.1	0.72
L	tribufos	3.23	0.019-0.95	0.99	0.91
S	azinphos-methyl	2.96	0.006-0.61	0.93	0.55
S	diniconazole	4.3	0.037-3.8	0.79	0.34
S	imazalil	3.82	0.03-30	0.65	0.92
S	iprodione	3.0	0.22-22	1.1	0.098
S	isoxaflutole	0.365	0.005-0.5	0.64	-0.049
S	lindane	3.72	0.11-11	0.70	0.59
S	phosmet	2.95	0.56-26	0.69	-0.086
S	vinclozlin	3	0.013-13	0.82[c]	
				0.84	0.29

[a] S / L denotes solid or liquid at skin temperature (~ 32°C). [b] See Table 6.1 for references. [c] Calculated using data for doses LL, L, and M because the amount absorbed systemically for dose H was below the detection limit.

values for the 4, 10 and 24-hour systemic absorption being larger than slope values for the amount in the skin.

For both solid and liquid pesticides, the amount in the skin increased with L_{film}. This indicates that for doses lower than dose H, the skin could not have been completely covered with pesticide. To clearly identify the applied dose that saturates the skin, data for at least two larger doses and two smaller doses are needed. Dose H might or might not have been completely covered by pesticide.

Figures 6.9 and 6.10 indicate that there could be a difference in the effect of applied dose on dermal absorption for solid and liquid pesticides. In fact, for three of the solid pesticides (i.e., iprodione, isoxaflutole, and phosmet) the amount absorbed systemically was essentially independent of L_{film} but the amount in the skin was almost proportional to L_{film}. For liquid pesticides, the slope values for the moles absorbed systemically tend to be only slightly smaller than slope values for the moles of pesticide in the skin. One possible explanation for this is examined theoretically in Chapter 7. There we show that the flux through the skin can reach a maximum value at smaller applied doses than the amount in the skin when chemical is distributed spatially on skin in piles with dimensions that are comparable to or smaller than the apparent thickness of the sc. The data shown in Figures 6.9 and 6.10 suggest that the distribution of solid and liquid pesticide residues on the skin surface might be different.

Conclusions

The amount of pesticide absorption increased with exposure time. For all but two of the pesticides (isoxaflutole and 2,4-DP-P-2EHE), the amount of chemical in the skin reached a maximum within 4 hours of exposure. For all 18 pesticides, the cumulative amount absorbed systemically increased for all exposure times up to 24 hours.

Significantly, dermal absorption continued even after the liquid components of the applied solution had evaporated.

When either evaporation or dermal absorption was significant, the exposed dose remaining on the skin surface decreased enough to affect dermal absorption. For six pesticides (disulfoton, EPTC, lindane, metolachlor, molinate, and thiobencarb), the effects of the decreasing exposed dose were apparent in that the amount in the skin increased, reached a maximum, and then decreased with time. For two pesticides (diclofop-methyl and mevinphos), the exposed dose decreased rapidly to less than 35% of the applied dose, and the amount in the skin reached a constant that was probably related to the exposed dose rather than the applied dose.

The effect of applied dose was more complicated when the exposed dose decreased significantly during the exposure from either evaporation or dermal absorption. Consequently, we examined the effect of applied dose on data for 12 of the 18 pesticides, excluding pesticides that had less than 50% of the applied dose remaining on the skin for all doses at 10 hours. This analysis showed a difference between solid and liquid pesticides. For pesticides with melting points below skin temperature (i.e., liquids), both the amount of pesticide in the skin and the amount absorbed systemically increased almost proportionally with applied dose. For pesticides with melting points above skin temperature (i.e., solids), the amount in the skin increased almost proportionally to the applied dose, but the amount absorbed systemically was less than proportional to applied dose for some pesticides and was independent of applied dose for others.

Notation

A	surface area of chemical exposure
I	coefficient of an equation that can be used to describe data for the amount in the skin or the amount absorbed systemically
$\hat{I}$	intercept of the best-fit line for the log-log plot of the amount in the skin or absorbed systemically as a function of L_{film}
$K_{o/w}$	octanol – water partition coefficient
L_{film}	theoretical thickness of the applied dose if it formed a uniformly thick layer on a flat surface with an area equal to the exposed area
M	variable in regression equation representing either the moles per area in skin or absorbed systemically
M_{app}	moles of pesticide applied to the skin
MP	melting point
MW	molecular weight
p_{vap}	vapor pressure
$\hat{S}$	slope of the best-fit line for the log-log plot of the amount in the skin or absorbed systemically as a function of L_{film}
S_w	water solubility

Greek

ρ	density of a pure pesticide

References

EXTOXNET (last updated June, 1996). Pesticide information profile: imazalil. Website, http://ace.orst.edu/info/extoxnet/ (accessed August, 1999).

Hansch, C., A. Leo and D. Hoekman (1995). Exploring QSAR. Hydrophobic, electronic, and steric constants. Washington, DC, American Chemical Society.

Tomlin, C., Ed. (1997). The Pesticide Manual. England, The British Crop Protection Council.

Zendzian, R. P. (1994). Pesticide Assessment Guidelines. Subdivision F, Hazard Evaluation, Human and Domestic Animals: Dermal Absorption of Pesticides. Office of Pesticide Programs, US Environmental Protection Agency, Washington, DC.

Zendzian, R. P. (2000a). Personal communication.

Zendzian, R. P. (2000b). "Dermal absorption of pesticides in the rat." American Industrial Hygiene Association Journal. Scheduled for publication July, 2000.

Appendix 6A

Complete results for the 18 pesticides listed in Table 6.1 are presented here. The most complete studies reported percent recoveries and the percent of applied dose in the skin wash, on the enclosure and cover, in the skin and absorbed systemically. All of these data, if available, were listed in the data tables. The percent recovered as a function of time was plotted if it dropped below about 90%, and the percent of applied dose on the enclosure and cover as a function of time was plotted if it rose above about 10%. The percent on the skin (i.e., in the skin wash), in the skin under the exposed site, and absorbed systemically were shown as a function of time when this information was available. The percent on the skin measures the exposed dose, which is defined as the amount of pesticide on the skin per exposed area at any time during an exposure. The moles in the skin and absorbed systemically as well as the percent of applied dose in the skin and absorbed systemically as a function of L_{film} were shown for exposure times between 2 and 24 hours. Table 6A.1 presents the legend for all the plots. Unweighted linear regressions were performed on the moles in the skin and absorbed systemically as a function of L_{film} using eq 6-3.

Table 6A.1 – Legend for plots in Appendix 6A.

x-axis is time		x-axis is L_{film}	
applied dose	symbol	exposure time, h	symbol
LL	▼	2	▼
L	●	4	●
M	■	10	■
H	▲	24	▲

Except for acetochlor, the data provided to us were mean values from 4 animals. For data points where some animals were below the detection limit and other animals had a specific amount absorbed, the average value can be calculated in several ways, and we do not know how it was done. For example, a mean value could be calculated assuming that the amount absorbed for animals below the detection level is zero. Alternatively, the detection limit could be included for animals below detection, and the mean value could be reported as less than the resulting value. In the case of acetochlor, standard deviations were provided in the summary report and were included in the data analysis. With no information on data variability for any of the other pesticides, it is impossible to draw statistically meaningful conclusions about whether variables (e.g., the amount in the skin or absorbed systemically) are functions of applied dose and time. Also, it is impossible to meaningfully compare results of different pesticides.

2,4-DP-P-2EHE (DP)

The molecular structure and most chemical properties of 2,4-DP-P-2EHE, a liquid at room temperature with MW = 347, are not reported. Table 6DP.1 shows the applied doses used in the 2,4-DP-P-2EHE study. The pesticide was applied in a vehicle of A260 light mineral oil that probably did not evaporate to leave a residue of solid pesticide on the skin. Dermal absorption would take place from the small volume of mineral oil solution on the skin surface. The volume of pesticide solution applied to the skin was 10 $\mu l/cm^2$ for all applied doses. Tabulated results for the 2,4-DP-P-2EHE study are shown in Table 6DP.2.

Table 6DP.1 – Applied doses used in 2-4-DP-P-2EHE study.

dose	moles /A , nM / cm^2	mass / A, μg / cm^2	L_{film}, μm[a]
LL	55	19	0.16
L	225	78	0.65
M	1410	489	4.1
H	8394	2913	24

[a] Calculated assuming $\rho = 1.2$.

Table 6DP.2 – Results of 2,4-DP-P-2EHE dermal absorption study.[a]

Dose	Expo-sure	Dressings[b]	Skin Wash	Skin		Absorbed[c]		Total Recov-ery
	hours	%	%	%	nM/cm^{2} [d]	%	nM/cm^{2} [d]	%
LL	0.5	22.86	61.92	2.80	1.53	0.42	0.23	88.00
	1	21.37	67.22	8.50	4.65	0.01[f]	----[f]	97.10
	2	33.51	47.57	8.20	4.48	0.43	0.235	89.70
	4	24.95	45.93	12.0	6.54	2.63	1.44	84.11
	10	29.50	34.08	14.8	8.11	9.84	5.38	88.36
	24	29.31	20.05	16.8	9.19	16.5	9.01	82.66
L	0.5	30.81	57.68	3.35	7.52	0.13	0.29	91.98
	1	33.67	38.80	8.51	19.1	0.54	1.2	81.53
	2	35.20	49.77	5.64	12.7	0.43	0.968	91.04
	4	39.02	38.26	8.08	18.2	1.69	3.80	87.04
	10	50.04	19.98	9.19	20.7	9.34	21.0	88.61
	24	35.58	27.36	10.1	22.8	16.3	36.7	89.39
M	0.5	21.79	66.35	4.80	67.6	0.22	3.11	93.16
	1	30.17	57.32	3.96	55.8	0.01	0.14	91.48
	2	34.12	46.99	6.62	93.2	0.04	0.563	87.79
	4	38.71	42.14	7.82	110.	0.88	12.4	89.58
	10	45.81	31.19	13.6	192	3.90	54.9	94.56
	24	48.09	21.61	12.3	173	11.1	156	93.08
H	0.5	18.47	77.56	2.84	238	ND[e]	----	98.88
	1	23.45	59.42	6.45	541	0.72	60.4	90.04
	2	18.04	63.63	5.27	442	0.14	11.7	87.10
	4	34.34	55.14	3.20	268	0.40	33.6	93.08
	10	41.07	46.59	4.75	398	1.35	113.	93.77
	24	56.37	13.67	7.69	645	4.69	393.	82.44

[a] Data are from study of 2,4-DP-P-2EHE applied in A260 light mineral oil with MRID 442293-01 dated 1/23/97. [b] Data include pesticide on the silicone rings, dressings and bandage. [c] Data include pesticide in the urine, feces, cage wash, skin wash, liver, kidney and carcass. [d] Calculated from values of percent of applied dose in the skin and absorbed. [e] ND = none detected. [f] This inconsistency matches the study summary.

Percent recoveries, shown in Figure 6DP.1 as a function of time, range from 81 – 99%. There were no significant differences between doses or exposure times. Figure 6DP.2 illustrates that 18 – 56% of the applied dose was recovered from the enclosure and cover. Except for applied dose LL, the percent of the applied dose on the enclosure and cover increased with time. As a result, the exposed dose was significantly less than the applied dose.

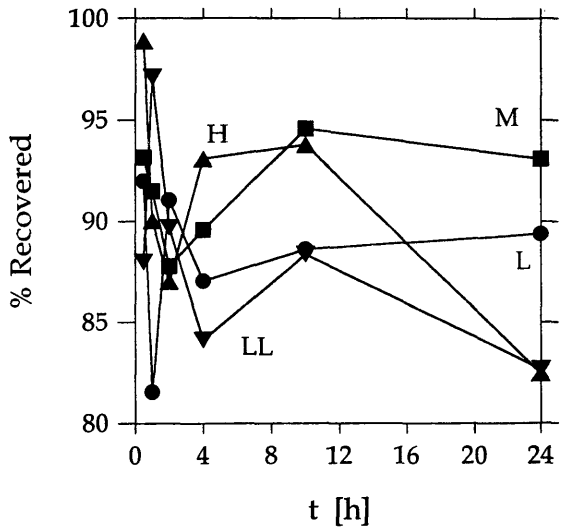

Figure 6DP.1 – Percent of applied dose recovered as a function of time.

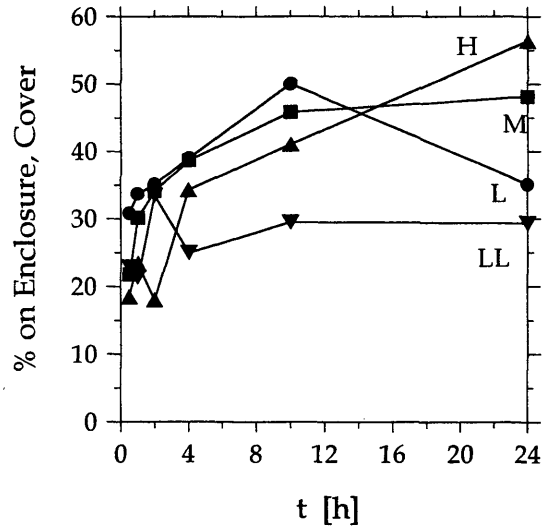

Figure 6DP.2 – Percent of applied dose on the enclosure and cover as a function of time.

Figure 6DP.3 shows the percent of applied dose on and in the skin as a function of time. The percent on the skin decreased significantly during the experiment. For all doses, after 24 hours of exposure only 14-27% of the applied dose remained on the skin surface. The decrease in chemical on the skin surface was due to both chemical accumulation on the enclosure and cover and to dermal absorption. However, the percent in the skin did not decrease with decreases in the amount on the skin.

The percent of applied dose in the skin and absorbed systemically are shown in Figure 6DP.4 as a function of time. Except for dose H, the amount in the skin increased for about ten hours, after which the rate of increase slowed. Ten hours is longer than for the other pesticides examined here but might be expected as 2,4-DP-P-2EHE has a molecular weight of 347, which is the second highest of the pesticides studied here. As a result, 2,4-DP-P-2EHE probably has a smaller diffusion coefficient and a longer lag time than the other pesticides of this study. The percent of applied dose absorbed systemically increased with dose, and is largest for the low doses.

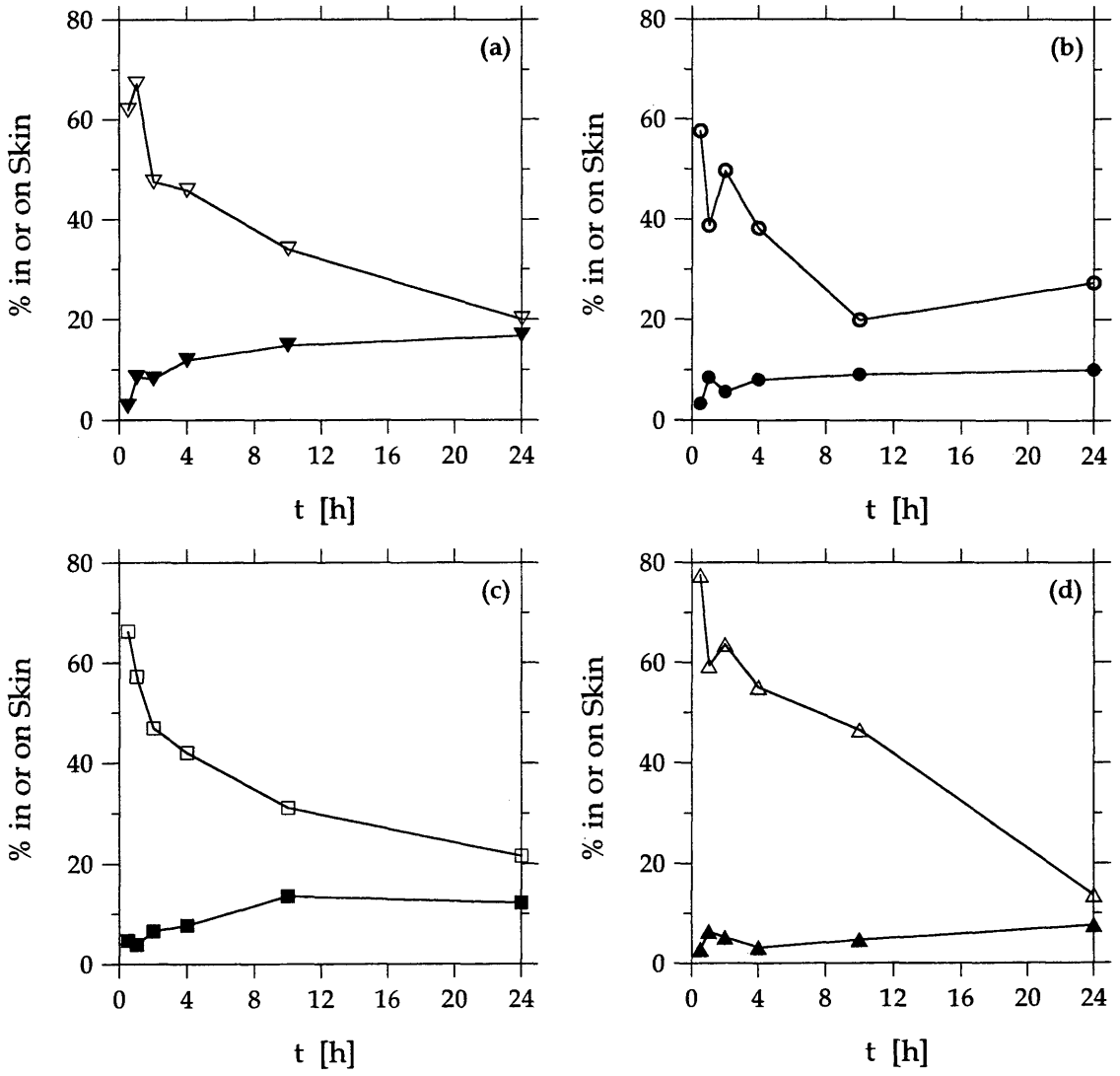

Figure 6DP.3 – Percent of applied dose on (open symbols) and in (closed symbols) the skin as a function of time for all doses: (a) LL, (b) L, (c) M, and (d) H.

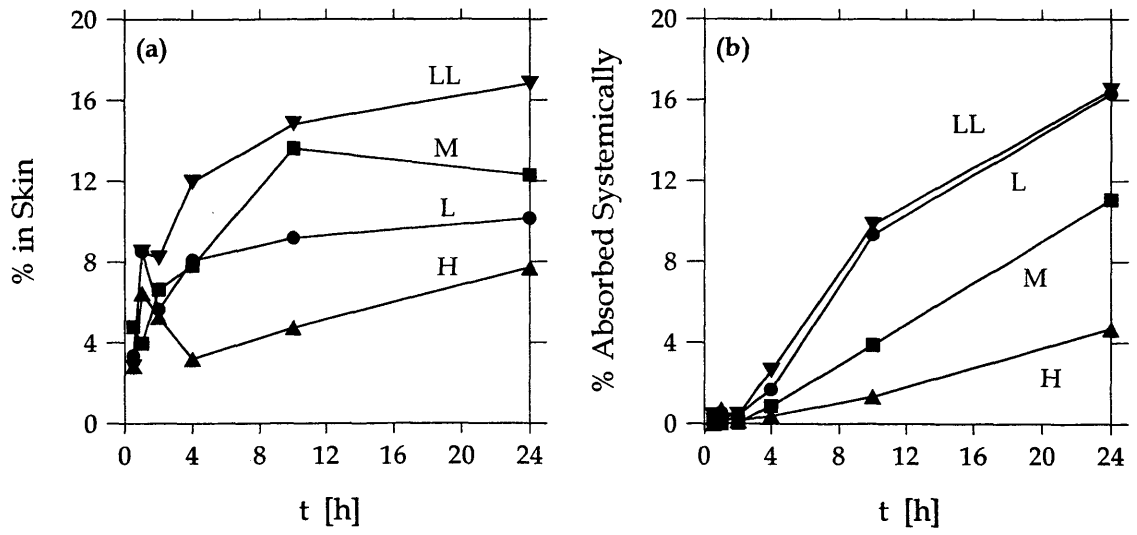

Figure 6DP.4 – Percent of applied dose (a) in the skin and (b) absorbed systemically as a function of time.

Moles in the skin and absorbed systemically are shown in Figure 6DP.5 as a function of L_{film}. The coefficients for best-fit lines through these data are listed in Table 6DP.3. For the amount in the skin, the slope values, at 0.8 – 0.9, were probably not significantly different from 1. We would expect a slope of 1 if 2,4-DP-P-2EHE were diffusing from a constant-concentration well-stirred solution. Slope values for the amount absorbed systemically were 0.6-0.8, which were slightly lower than for the amount in skin. Figure 6DP.6 shows that the percent of applied dose in the skin was essentially independent of applied dose. However, the percent absorbed systemically decreased with increasing applied dose. This effect was more evident for long exposure times.

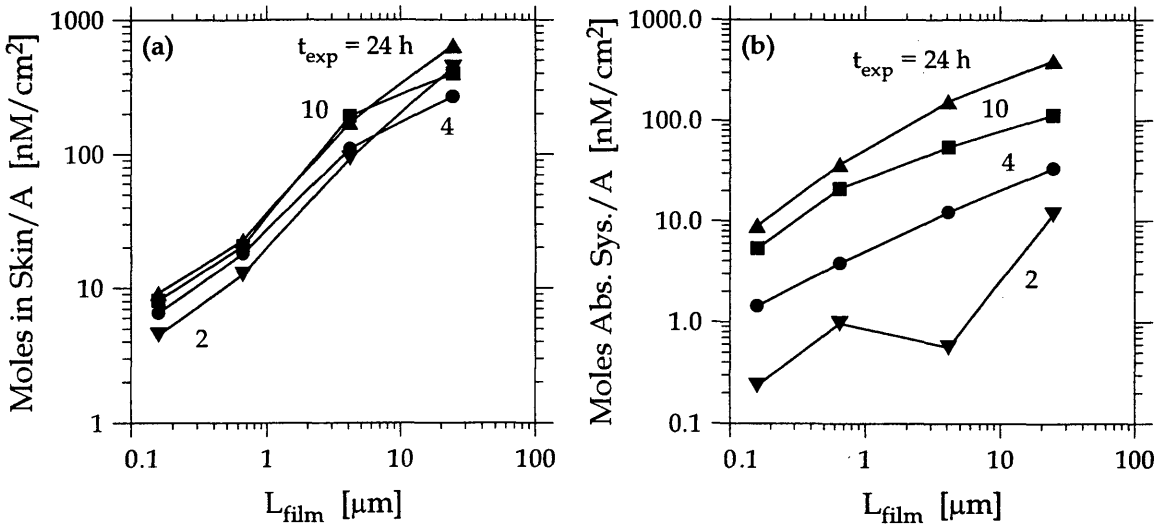

Figure 6DP.5 – Moles of chemical (a) in the skin and (b) absorbed systemically as a function of L_{film}.

Table 6DP.3 – Coefficients for best-fit lines through log-log plots of moles of chemical in the skin and absorbed systemically as a function of dose.

time, h	moles in skin		moles absorbed systemically	
	$\hat{S}$	$\hat{I}$	$\hat{S}$	$\hat{I}$
2	0.94	3.3	0.66	-0.14
4	0.77	3.5	0.63	1.7
10	0.83	3.8	0.59	3.2
24	0.88	3.9	0.76	3.9

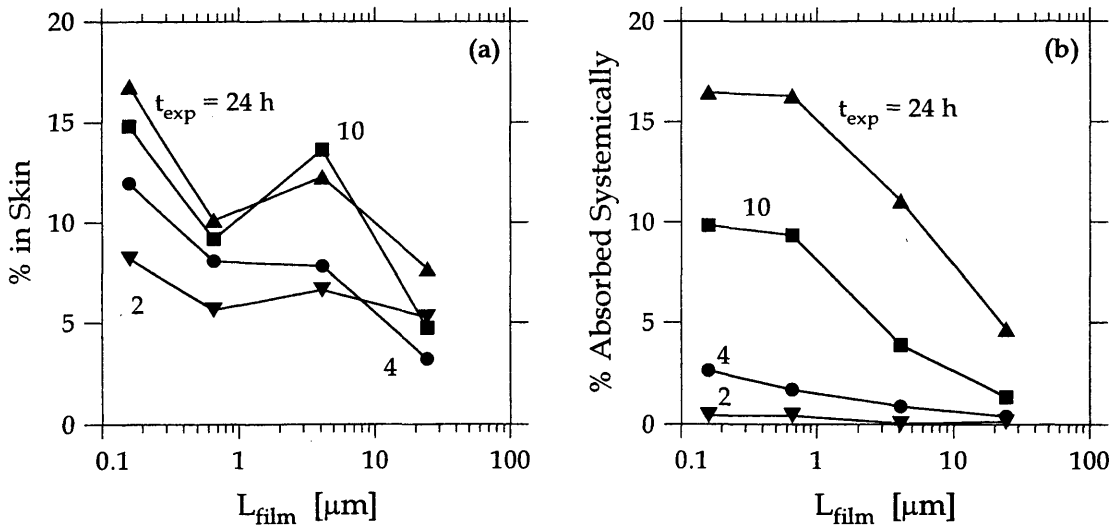

Figure 6DP.6 – Percent of applied dose (a) in the skin and (b) absorbed systemically as a function of L_{film}.

Acetochlor (AC)

Figure 6AC.1 shows the molecular structure of acetochlor, an herbicide used for control of annual grasses, some broad-leaved weeds and yellow nutsedge in maize, peanuts, soya beans, cotton, potatoes, and sugar cane. It is a liquid, lipophilic pesticide ($\log K_{o/w} = 3.03$) available as an emulsifiable concentrate with tradenames including Harness, Acenit and Surpass (Tomlin, 1997). The applied doses in the acetochlor dermal absorption study are given in Table 6AC.1. Tabulated results of the acetochlor study, shown in Table 6AC.2, include standard deviations. In the following plots, error bars designating ± one standard deviation are longer for higher doses and longer exposure times. Table 6AC.3 lists reported blood concentrations.

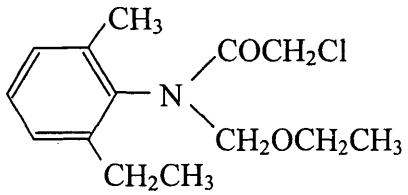

Figure 6AC.1 – Molecular structure of acetochlor.

Table 6AC.1 – Applied doses used in acetochlor study.

dose	moles /A , nM / cm^2	mass / A, μg / cm^2	L_{film}, μm
LL	11	3.0	0.027
L	157	42.5	0.38
M	1000	270.	2.4
H	10870	2934	26

Table 6AC.2 – Results of acetochlor dermal absorption study.[a]

Dose	Exposure	Cover	Skin Wash	Skin		Absorbed[b]		Total Recovery
	hours	%	%	%	nM/cm^2	%	nM/cm^2	%
LL[c]	0.5	5.94 ±0.68[c]	73.82 ±1.38	3.98 ±1.27	0.443 ±0.141	3.79 ±1.69	0.421 ±0.188	89.96 ±5.53
	1	6.01 ±1.00[c]	73.22 ±3.55	3.31 ±0.78	0.368 ±0.086	4.28 ±1.47	0.476 ±0.164	90.31 ±7.56
	2	7.15 ±0.72[c]	67.99 ±1.56	4.08 ±0.26	0.454 ±0.029	7.33 ±1.28	0.814 ±0.143	92.80 ±5.01
	4	7.92 ±1.10[c]	58.74 ±4.37	4.62 ±0.53	0.513 ±0.059	9.93 ±1.16	1.10 ±0.129	90.94 ±8.23
	10	9.62 ±0.97[c]	41.16 ±3.29	4.13 ±0.93	0.459 ±0.103	19.55 ±1.20	2.17 ±0.133	87.53 ±8.10
	24	12.53 ±0.49[c]	29.74 ±20.15	2.41 ±0.63	0.268 ±0.070	31.37 ±2.61	3.49 ±0.290	97.94 ±25.66
L	0.5	7.15 ±0.88	80.32 ±5.10	3.18 ±0.53	5.01 ±0.830	3.96 ±1.36	6.24 ±2.14	94.61 ±7.87
	1	7.43 ±1.81	76.01 ±7.12	2.99 ±0.51	4.71 ±0.804	5.98 ±1.41	9.42 ±2.22	92.41 ±10.85
	2	9.81 ±2.25	82.24 ±5.98	2.79 ±0.68	4.39 ±1.07	4.38 ±1.38	6.89 ±2.17	99.21 ±10.29
	4	11.61 ±0.92	73.18 ±6.25	2.81 ±0.52	4.43 ±0.815	9.24 ±1.48	14.5 ±2.33	96.84 ±9.17
	10	13.21 ±1.90	52.11 ±2.85	2.76 ±0.60	4.34 ±0.941	23.06 ±3.75	36.3 ±5.9	91.14 ±9.10
	24	19.15 ±1.69	35.65 ±4.69	1.83 ±0.46	2.88 ±0.722	29.64 ±1.80	46.7 ±2.83	86.27 ±8.64

(continued)

Table 6AC.2 (continued)

Dose	Exposure	Cover	Skin Wash	Skin		Absorbed[b]		Total Recovery
	hours	%	%	%	nM/cm^2	%	nM/cm^2	%
M	0.5	8.97 ±2.17	78.53 ±4.29	3.40 ±1.44	34.0 ±14.4	4.79 ±1.64	47.9 ±16.4	95.7 ±9.54
	1	8.04 ±1.58	75.87 ±5.42	3.21 ±0.83	32.1 ±8.33	5.63 ±3.41	56.3 ±34.1	92.76 ±11.24
	2	8.76 ±1.32	81.06 ±5.88	4.91 ±0.95	49.1 ±9.48	3.03 ±0.71	30.3 ±7.11	97.77 ±8.86
	4	7.81 ±0.66	80.92 ±5.30	3.21 ±0.53	32.1 ±5.33	4.83 ±1.62	48.3 ±16.2	96.77 ±8.11
	10	10.45 ±2.68	70.52 ±4.20	3.99 ±1.61	39.9 ±16.1	9.32 ±2.38	93.2 ±23.8	94.28 ±10.87
	24	12.64 ±1.63	59.70 ±4.59	4.53 ±1.4	45.3 ±14.0	17.52 ±1.89	175 ±18.9	94.39 ±9.51
H	0.5	9.74 ±1.30	87.66 ±4.99	2.53 ±0.97	275 ±105	1.39 ±1.37	151 ±148	101.32 ±8.62
	1	13.82 ±1.83	74.15 ±9.09	3.24 ±1.39	353 ±151	5.22 ±3.76	567 ±409	96.43 ±16.07
	2	12.11 ±1.40	79.16 ±6.88	3.37 ±2.12	366 ±231	3.39 ±2.36	369 ±256	98.04 ±12.76
	4	17.13 ±3.50	77.03 ±5.93	3.18 ±1.40	345 ±152	2.67 ±0.63	290 ±68.7	100.01 ±11.46
	10	14.84 ±3.81	77.07 ±7.31	3.01 ±0.64	327 ±69.8	4.47 ±1.31	486 ±142	99.40 ±13.07
	24	21.38 ±2.97	60.97 ±4.77	2.93 ±0.52	319 ±56.6	12.61 ±4.48	1370 ±486	97.89 ±12.74

[a] Calculated using reported values of mean masses from 4 animals ± standard deviations from the study with MRID 417783-01 dated 10/12/1990. [b] Data include pesticide found in the urine, feces, cage wash, and carcass. [c] The percent of applied dose from the activated carbon filter used in the cover for dose LL (i.e., 0.5 hours, 2.42 ± 0.51; 1 hour, 3.49 ± 0.75; 2 hours, 6.25 ± 1.18; 4 hours, 9.73 ± 1.07; 10 hours, 13.1 ± 1.7; 24 hours, 21.9 ± 1.8) were not included in cover data but were included in the total recovery.

Table 6AC.3 – Blood concentrations (μg/g) from acetochlor dermal absorption study.[a]

Sample	Dose	0.5 hours	1 hour	2 hour	4 hours	10 hours	24 hours
Whole blood	LL	0.004 ±0.003	0.004 ±0.001	0.008 ±0.003	0.014 ±0.001	0.026 ±0.002	0.045 0.005±
	L	0.026 ±0.005	0.043 ±0.019	0.071 ±0.018	0.156 ±0.037	0.459 ±0.135	0.511 ±0.176
	M	0.113 ±0.037	0.153 ±0.029	0.253 ±0.034	0.468 ±0.078	1.101 ±0.207	3.050 ±0.629
	H	0.792 ±0.272	1.006 ±0.201	1.756 ±0.298	3.264 ±0.765	6.383 ±0.620	19.534 ±5.245
Plasma	LL	0.001 ±0.001	0.001 ±<0.001	0.002 ±0.001	0.002 ±<0.001	0.003 ±<0.001	0.002 ±<0.001
	L	0.008 ±0.003	0.008 ±0.002	0.014 ±0.003	0.022 ±0.004	0.046 ±0.014	0.038 ±0.005
	M	<0.026	0.029 ±0.005	0.039 ±0.005	0.063 ±0.010	0.145 ±0.060	0.169 ±0.041
	H	<0.259	0.322 ±0.072	0.331 ±0.038	0.483 ±0.117	0.749 ±0.134	1.361 ±0.167

[a] Data are from the study with MRID 417783-01 dated 10/12/1990. Data represent the mean of four animals ± the standard deviation.

Figure 6AC.2 shows that percent recoveries were lowest for doses LL and L, but were not time dependent. Percent recoveries ranged from 86 to 101% and were not significantly different from 100% based on the error bars.

Significant volatilization of acetochlor, which has a vapor pressure of 0.0045 mPa at 25°C (Tomlin, 1997), occurred only for dose LL. An activated carbon filter was only used with the cover for dose LL. Figure 6AC.3a shows the percent of applied dose on the cover for all doses, except that dose LL data does not include the percent of dose on the activated carbon filter which is shown separately in Figure 6AC.3b. Percent recoveries for doses L, M and H were good, which is consistent with volatilization not occurring significantly.

Figure 6AC.4 shows the percent of applied dose on and in the skin as a function of time. For doses L and LL, the amount on the skin dropped more than 60% because of dermal absorption, evaporation, and sorption to the cover. However, the amount in the skin did not decrease in response. Figure 6AC.5 shows the percent of applied dose in the skin and absorbed systemically as a function of time. The amount in the skin was essentially independent of time while the amount absorbed systemically increased with time. Statistically, there is no difference between the percent absorbed systemically for doses LL and L, but doses M and H are statistically different from doses L and LL and from one another.

Moles of chemical in the skin and absorbed systemically are shown in Figure 6AC.6 as a function of L_{film}. Coefficients for the best-fit lines through these data are listed in Table 6AC.4. Slope values for the amount in the skin were approximately 1 – 1.1 indicating that the amount in the skin increased proportionally with applied dose. For the amount absorbed systemically, the slope values were slightly lower at 0.8 - 0.9. Figure 6AC.7 shows that the percent of applied dose in the skin was essentially independent of L_{film}, while the percent absorbed systemically decreased with increasing L_{film}, an effect that is magnified at longer exposure times.

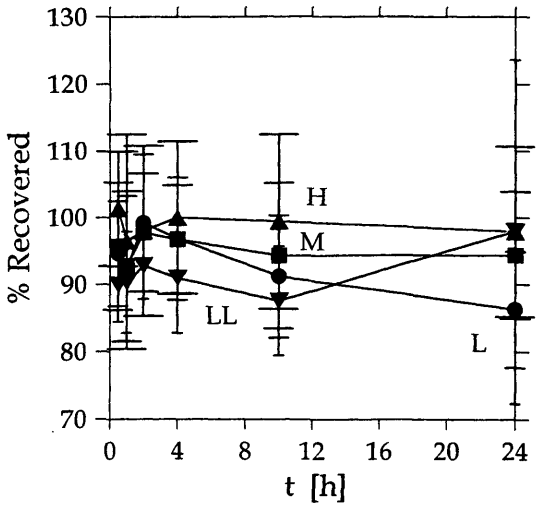

Figure 6AC.2 – Percent of applied dose recovered as a function of time.

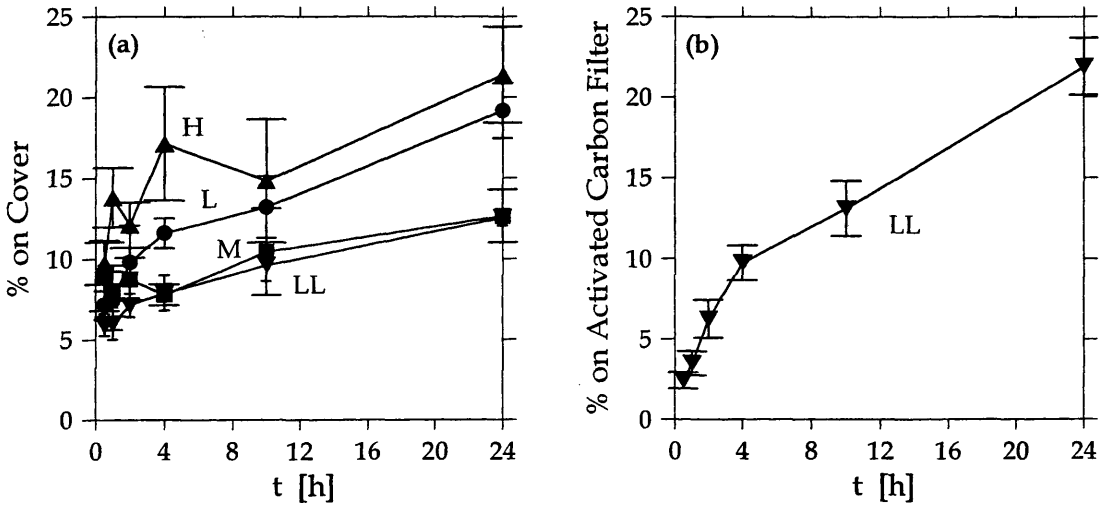

Figure 6AC.3 – Percent of applied dose (a) on the cover for all doses, not including the percent of applied dose on the activated carbon filter for dose LL, and (b) on the activated carbon filter for dose LL as a function of time.

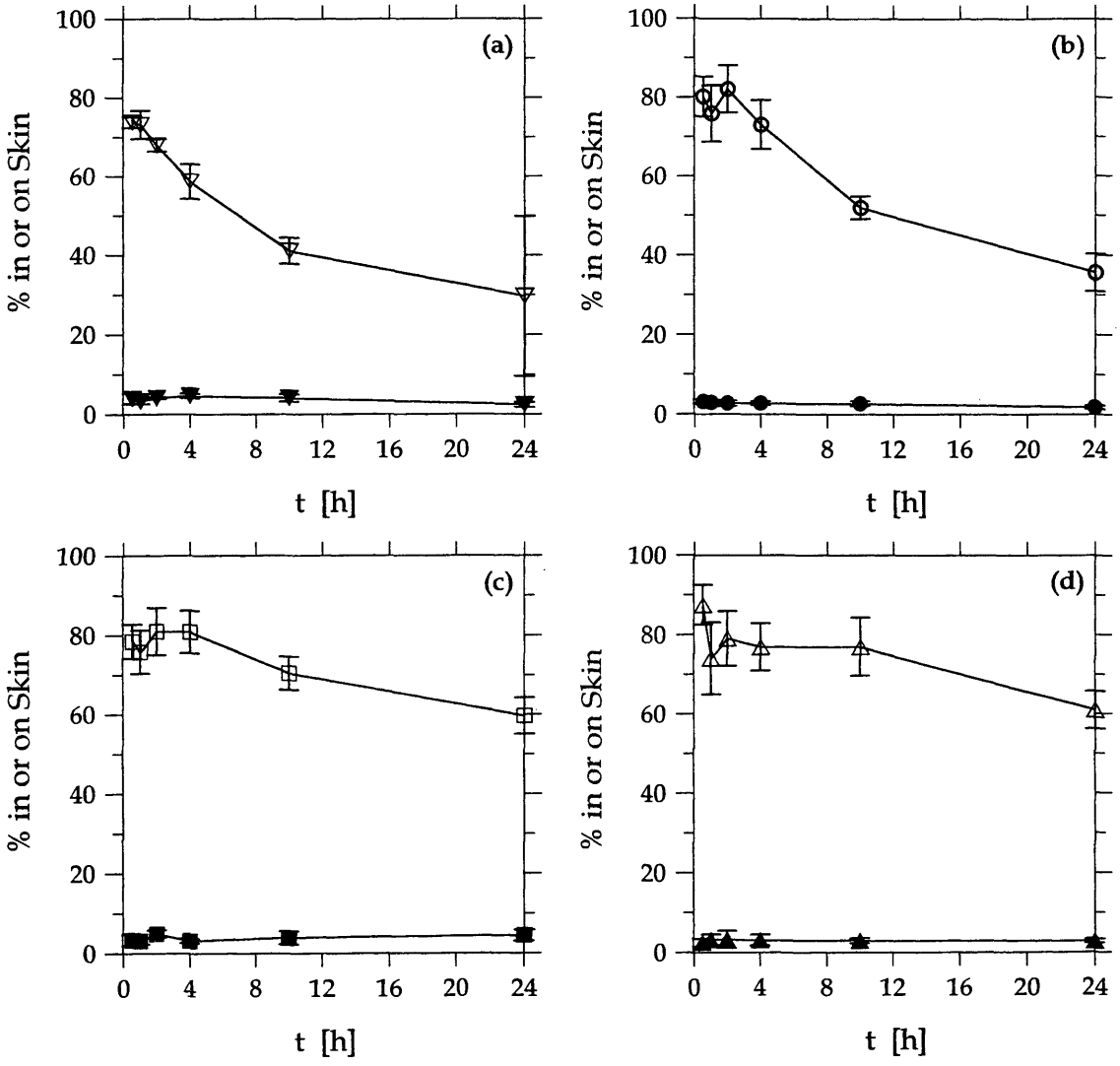

Figure 6AC.4 – Percent of applied dose on (open symbol) and in (closed symbol) the skin as a function of time for all doses: (a) LL, (b) L, (c) M and (d) H.

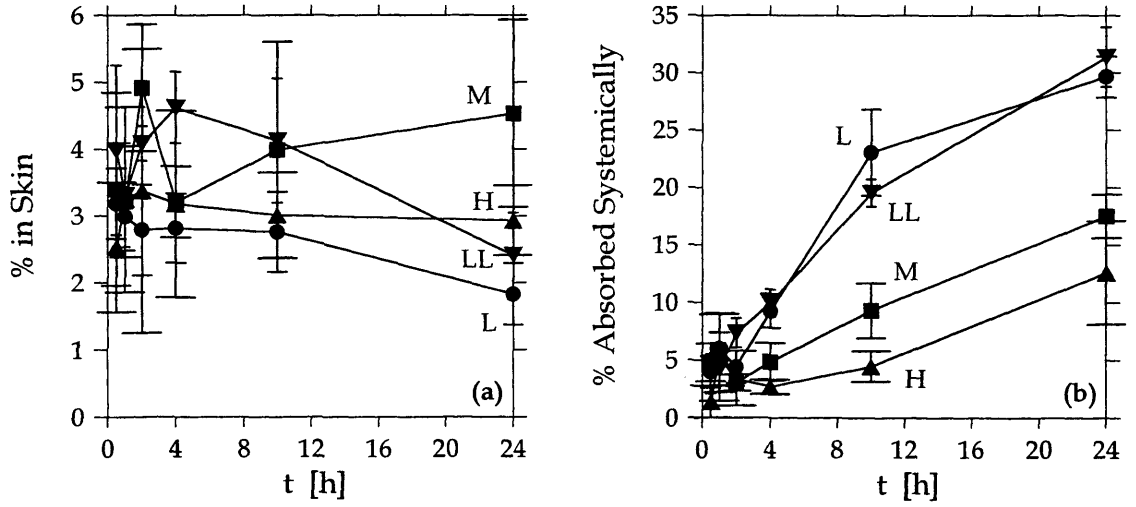

Figure 6AC.5 – Percent of applied dose (a) in the skin and (b) absorbed systemically as a function of time.

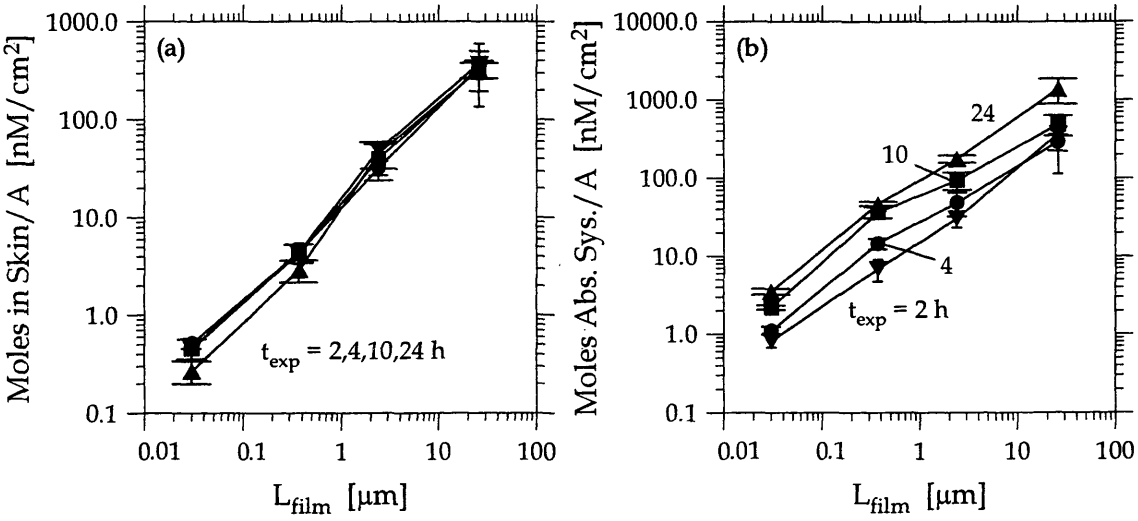

Figure 6AC.6 – Moles of chemical (a) in the skin and (b) absorbed systemically as a function of L_{film}.

Table 6AC.4 – Coefficients for best-fit lines through log-log plots of moles of chemical in the skin and absorbed systemically as a function of dose.

time, h	moles in skin		moles absorbed systemically	
	$\hat{S}$	$\hat{I}$	$\hat{S}$	$\hat{I}$
2	0.99	7.2	0.78	8.4
4	0.97	7.2	0.81	7.8
10	1.1	7.0	0.87	9.1
24	1.0	7.3	0.90	7.4

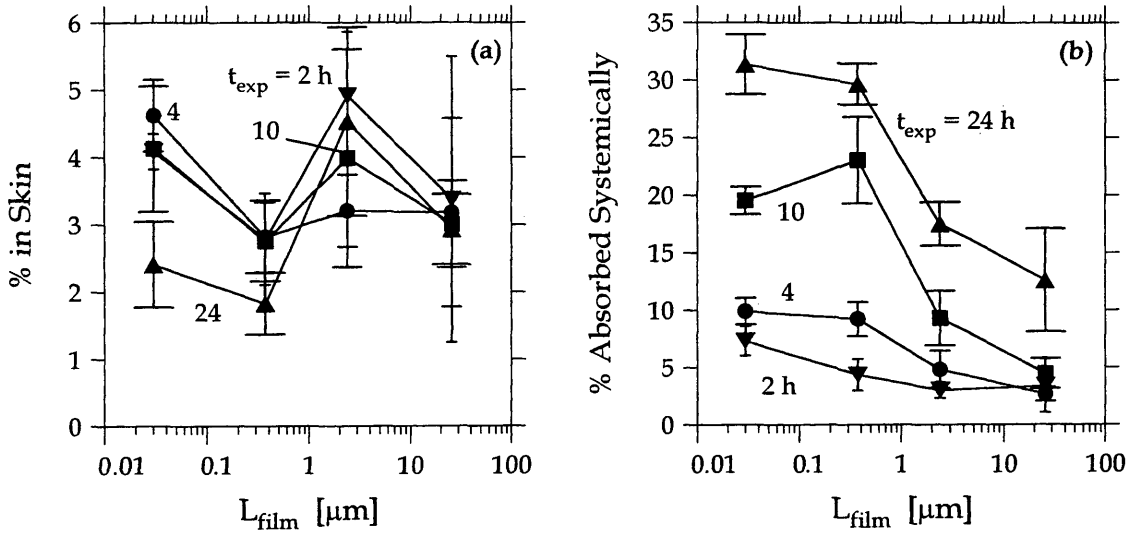

Figure 6AC.7 – Percent of applied dose (a) in the skin and (b) absorbed systemically as a function of L_{film}.

Concentrations in the whole blood and in the blood plasma are shown in Figure 6AC.8 as a function of exposure time. Some blood plasma concentrations were below the detection limit, and are marked at the detection limit value with the symbol "D". The concentration in the bloodstream increased. The concentrations of acetochlor in the blood plasma (i.e., the liquid part of the blood) were much lower than in the whole blood. Apparently, acetochlor was concentrated in the lipophilic, solid components of the whole blood (e.g., red blood cells with lipid cell membranes).

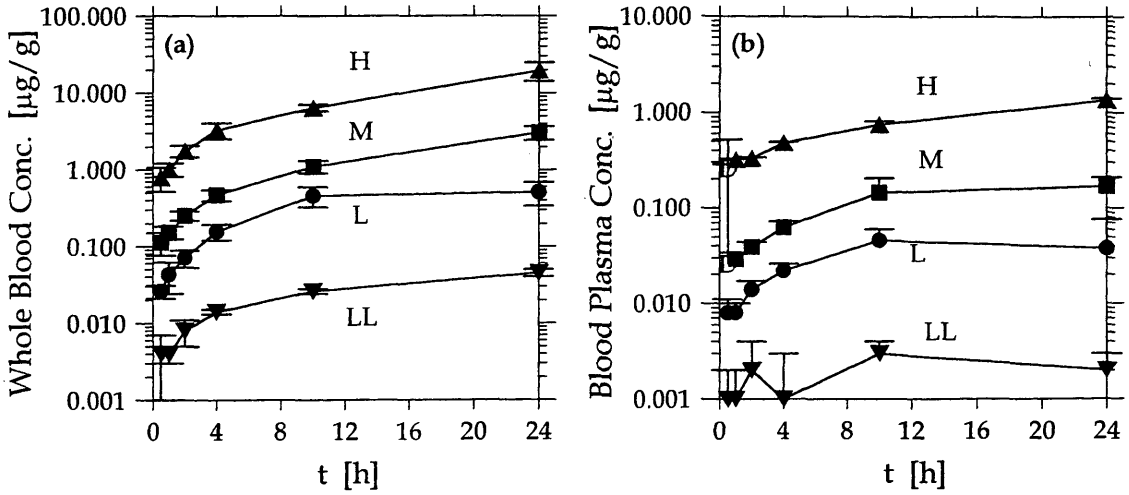

Figure 6AC.8 – Concentration of acetochlor (a) in whole blood and (b) in blood plasma as a function of time.

Azinphos-methyl (AZ)

Figure 6AZ.1 shows the chemical structure of azinphos-methyl, an insecticide used for control of chewing and sucking insects on fruit trees, vines, strawberries and more. Its tradenames include Gusathion M, Acifon and Azinugec. It is a solid, moderately lipophilic pesticide ($\log K_{o/w} = 2.96$) available as suspension and emulsifiable concentrates and as wettable and dispersible powders (Tomlin, 1997). Table 6AZ.1 shows the applied doses in the azinphos-methyl study with the tabulated results listed in Table 6AZ.2.

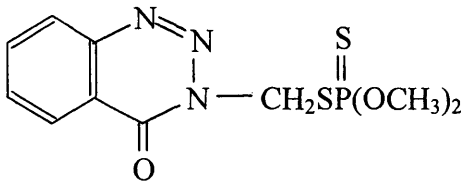

Figure 6AZ.1 – Molecular structure of azinphos-methyl.

Table 6AZ.1 – Applied doses used in azinphos-methyl study.

Dose	moles /A , nM / cm^2	mass / A, μg / cm^2	L_{film}, μm
L	3	1	0.006
M	29	9.2	0.061
H	293	92.9	0.61

Table 6AZ.2 – Results of azinphos-methyl dermal absorption study (Zendzian, 2000b).[a]

Dose	Exposure	Enclosure and Cover	Skin Wash	Skin		Absorbed[b]		Total Recovery
	hours	%	%	%	nM/cm^2	%	nM/cm^2	%
L	1	3.18	52.35	36.44	1.09	9.41	0.29	101.38
	4	8.22	44.50	25.78	0.77	23.12	0.69	101.62
	10	4.41	43.85	32.24	0.97	22.71	0.68	103.21
M	1	8.42	49.99	19.16	5.56	3.67	1.06	81.24
	4	10.37	49.76	21.57	6.26	4.89	1.41	86.60
	10	1.26	45.05	22.08	6.40	15.16	4.40	83.55
H	1	2.77	74.10	19.74	57.84	0.48	1.41	92.28
	4	6.29	72.43	14.61	42.80	1.27	3.72	94.60
	10	5.88	63.03	23.71	69.47	2.86	8.38	95.48

[a] Data are from the study of the guthion 35% wettable powder formulation with MRID 424527-01 dated 3/27/92. [b] Data include pesticide from the blood, urine, feces, carcass, and cage wash.

The percent recoveries are shown in Figure 6AZ.2 as a function of time. Dose M has the poorest recoveries. Less than 10.4% of the applied dose was found on the enclosure and cover for all doses and exposure times. There is no reason to suspect that azinphos-methyl, which has a vapor pressure of only 0.001 mPa at 20°C (Tomlin, 1997), evaporated significantly.

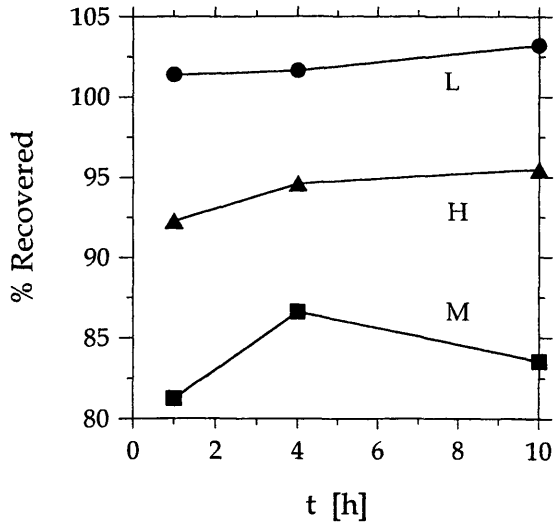

Figure 6AZ.2 – Percent of applied dose recovered as a function of time.

The percent of applied dose on and in the skin are shown in Figure 6AZ.3 as a function of time. The amount on the skin was independent of time for all three doses. As shown in Figure 6AZ.4a, the percent in the skin also was essentially independent of time. Except for dose H between four and ten hours, the percent of applied dose absorbed systemically increased with time, as shown in Figure 6AZ.4b.

Moles of chemical in the skin and absorbed systemically are shown in Figure 6AZ.5 as a function of L_{film}. A relatively linear relationship existed between both moles in the skin and absorbed systemically and applied dose. Coefficients for the best-fit line through the log-log plots of amount in the skin and absorbed systemically are listed in Table 6AZ.3. Slopes values for moles in the skin were ~ 0.9. In contrast, the slope values for moles absorbed systemically were smaller, at 0.4 – 0.6. The percent of the applied dose in the skin and absorbed systemically as a function of L_{film} are shown in Figure 6AZ.6. The percent in the skin was at most a weak function of applied dose, but the percent absorbed systemically decreased significantly with increasing applied dose.

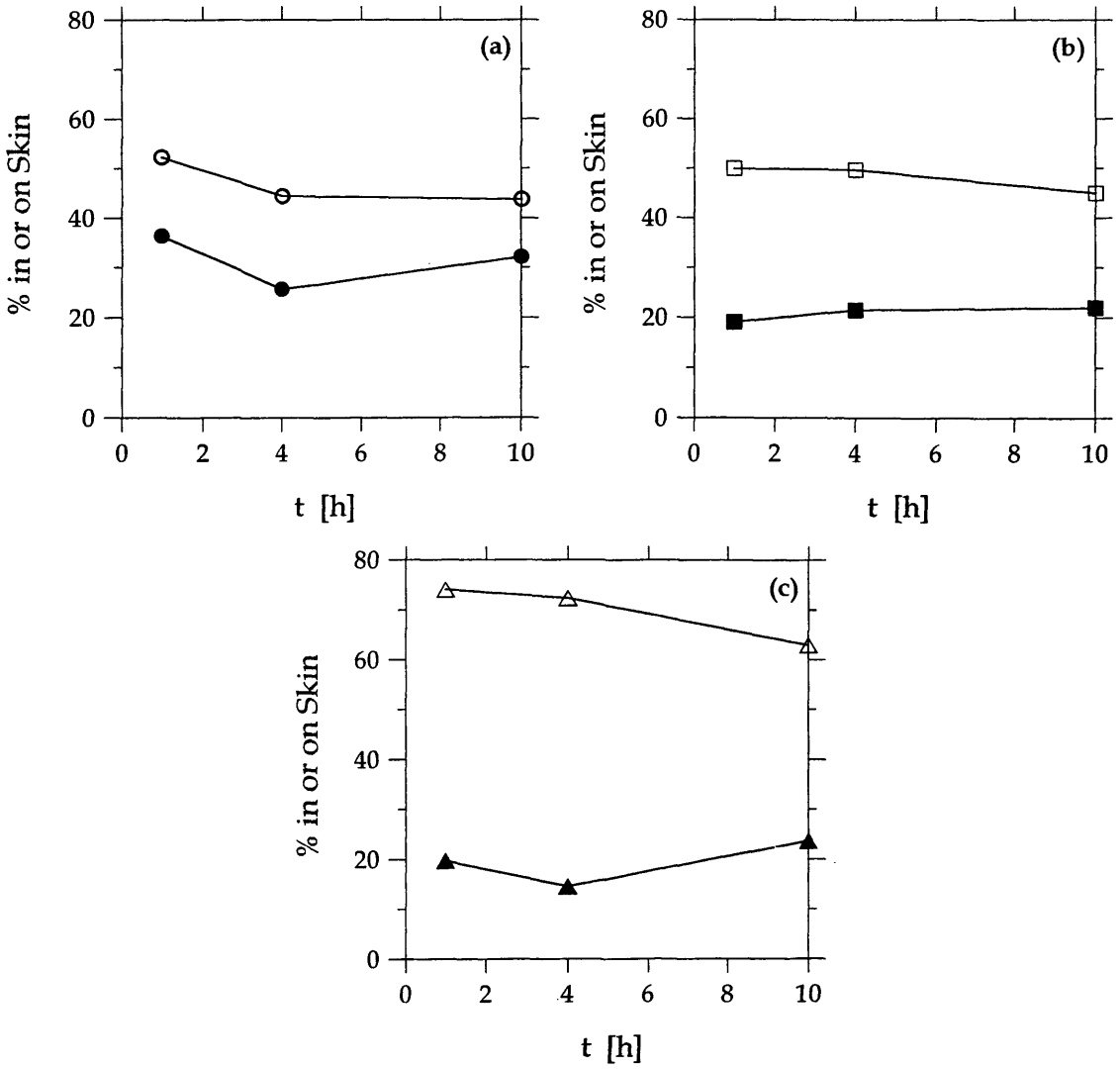

Figure 6AZ.3 – Percent of applied dose on (open symbols) and in (closed symbols) the skin as a function of time for all doses: (a) L, (b) M, and (c) H.

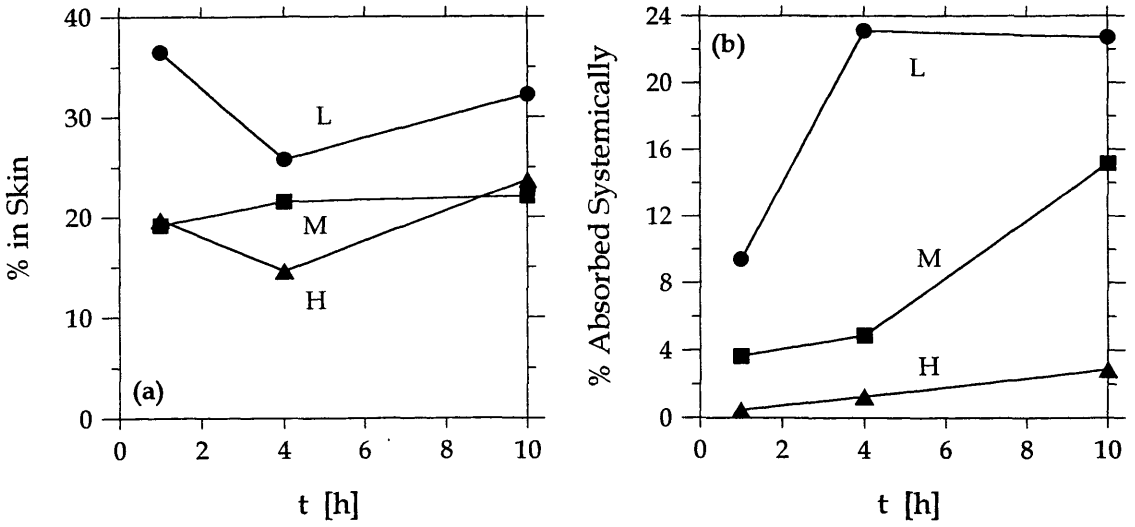

Figure 6AZ.4 – Percent of applied dose (a) in the skin and (b) absorbed systemically as a function of time.

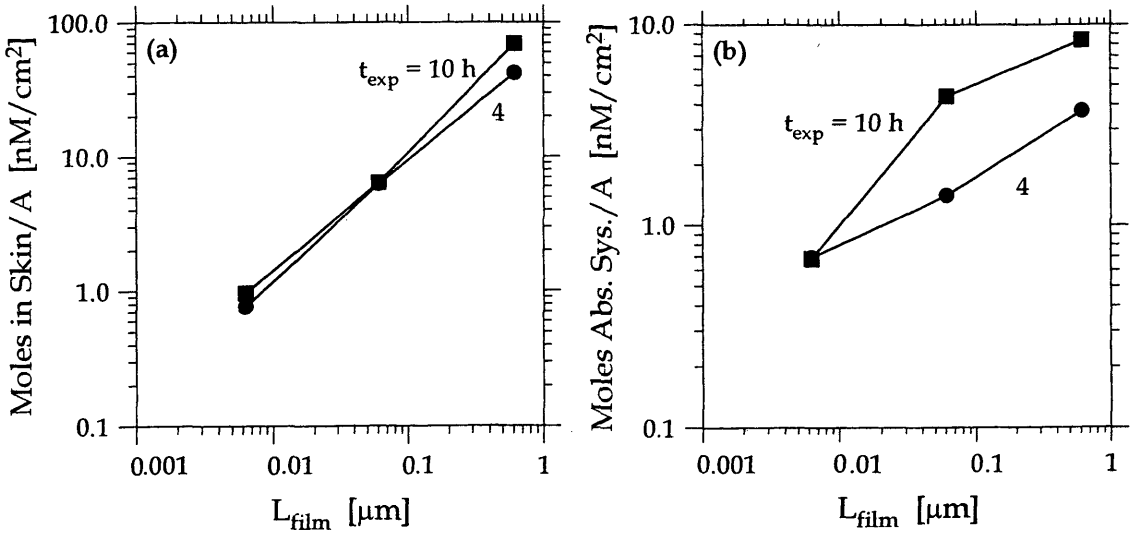

Figure 6AZ.5 – Moles of chemical (a) in the skin and (b) absorbed systemically as a function of L_{film}.

Table 6AZ.3 – Coefficients for best-fit lines through log-log plots of moles of chemical in the skin and absorbed systemically as a function of dose.

time, h	moles in skin		moles absorbed systemically	
	$\hat{S}$	$\hat{I}$	$\hat{S}$	$\hat{I}$
4	0.87	4.2	0.37	1.5
10	0.93	4.6	0.55	2.6

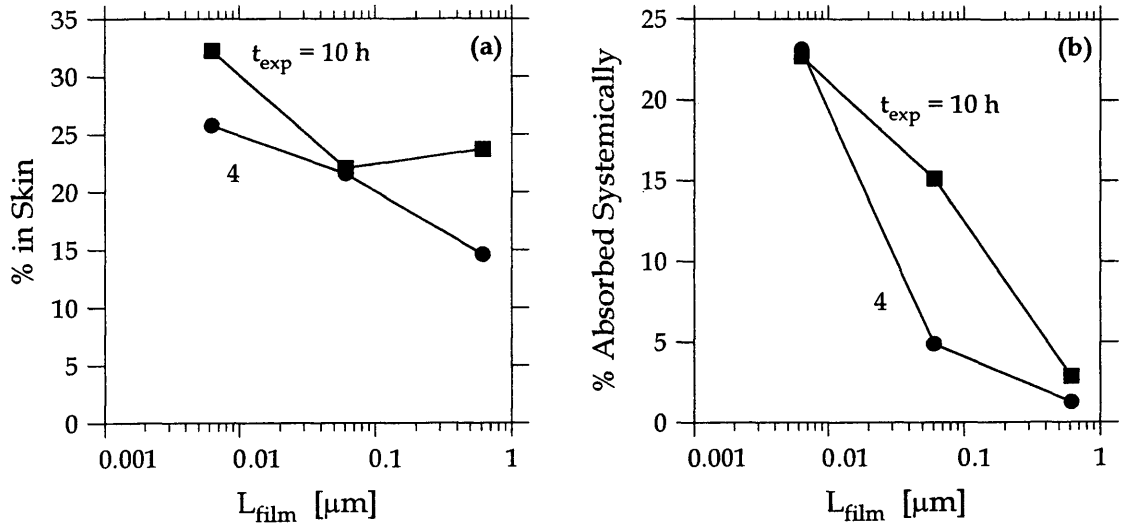

Figure 6AZ.6 – Percent of applied dose (a) in the skin and (b) absorbed systemically as a function of L_{film}.

Diclofop-methyl (DM)

The molecular structure of diclofop-methyl is shown in Figure 6DM.1. It is an herbicide used for post-emergence control of wild oats, wild millets, and other annual grass weeds in wheat, barley, rye, red fescue, and broad-leaved crops such as soya beans, carrots, celery, and more. Diclofop-methyl, a lipophilic solid at room temperature (melting point = 39-41°C, $\log K_{o/w} = 4.58$), is available as an emulsifiable concentrate with tradenames such as Hoegrass, Hoelon, and Illoxan (Tomlin, 1997). Table 6DM.1 shows the applied doses in the diclofop-methyl study with the results listed in Table 6DM.2.

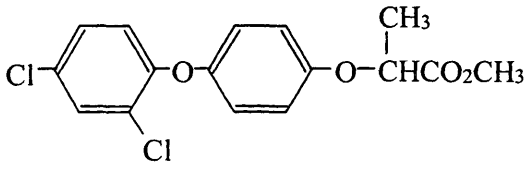

Figure 6DM.1 – Molecular structure of diclofop-methyl.

Table 6DM.1 – Applied doses used in diclofop-methyl study.

dose	moles /A , nM / cm^2	mass / A, µg / cm^2	L_{film}, µm
L	29	9.9	0.076
M	293	99.9	0.76
H	2933	1000.	7.7

Table 6DM.2 – Results of diclofop-methyl dermal absorption study.[a]

Dose	Exposure	Enclosure and Cover	Skin Wash	Skin		Absorbed[b]		Total Recovery
	hours	%	%	%	nM/cm^2	%	nM/cm^2	%
L	1	3.4	24.9	61.8	17.9	2.5	0.7	92.6
	2	3.2	27.4	59.7	17.3	3.2	0.9	93.5
	4	4.8	21.4	51.9	15.1	10.3	3.0	88.1
	10	2.9	24.1	59.5	17.3	9.1	2.6	95.6
	24	4.8	17.6	47.0	13.6	22.1	6.4	91.5
M	1	10.2	20.0	58.3	170.8	3.0	8.8	91.5
	2	4.4	26.7	43.7	128.0	6.2	18.2	80.9
	4	8.9	18.1	51.8	151.8	6.8	19.9	85.6
	10	8.8	22.5	44.0	128.9	14.8	43.4	90.0
	24	12.9	10.7	42.7	125.1	18.4	53.9	84.6
H	1	9.4	28.5	37.1	1088.1	5.7	167.2	80.7
	2	4.4	42.9	41.6	1220.2	2.8	82.1	91.7
	4	5.2	34.5	39.1	1146.8	4.8	140.8	83.6
	10	6.5	35.2	38.2	1120.4	7.8	228.8	87.7
	24	4.2	38.7	37.4	1096.9	11.0	322.6	91.3

[a] Data are from the study of Hoelon 3 EW (an emulsion of oil in water) formulation with MRID 423646-01 dated 5/28/92. [b] Data include pesticide in urine, feces, carcass, and cage wash.

Figure 6DM.2, a plot of percent recoveries as a function of time, indicates that recoveries did not change with exposure time. The percent of applied dose found on the enclosure and cover was always < 13%. Thus, diclofop-methyl, with a vapor pressure of 0.25 mPa at 20°C (Tomlin, 1997), did not evaporate significantly during the experiment.

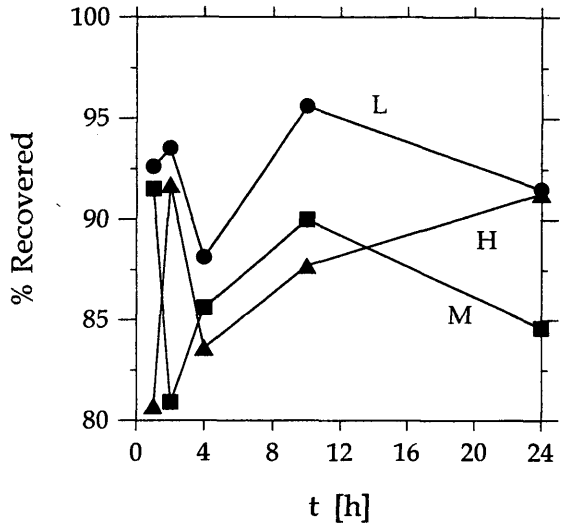

Figure 6DM.2 – Percent of dose recovered as a function of time.

Figure 6DM.3 shows the percent of applied dose on and in the skin as a function of time. For doses L and M, more diclofop-methyl was in the skin than on the skin while for dose H the amount in and on the skin were almost the same. The rapid absorption of pesticide into the skin during the first hour significantly reduced the percent on the skin, and so the reduction of chemical on the skin resulting from systemic absorption looked minor in comparison. On average, the amount in and on skin decreased slowly with increased exposure time as systemic absorption removed chemical from the skin.

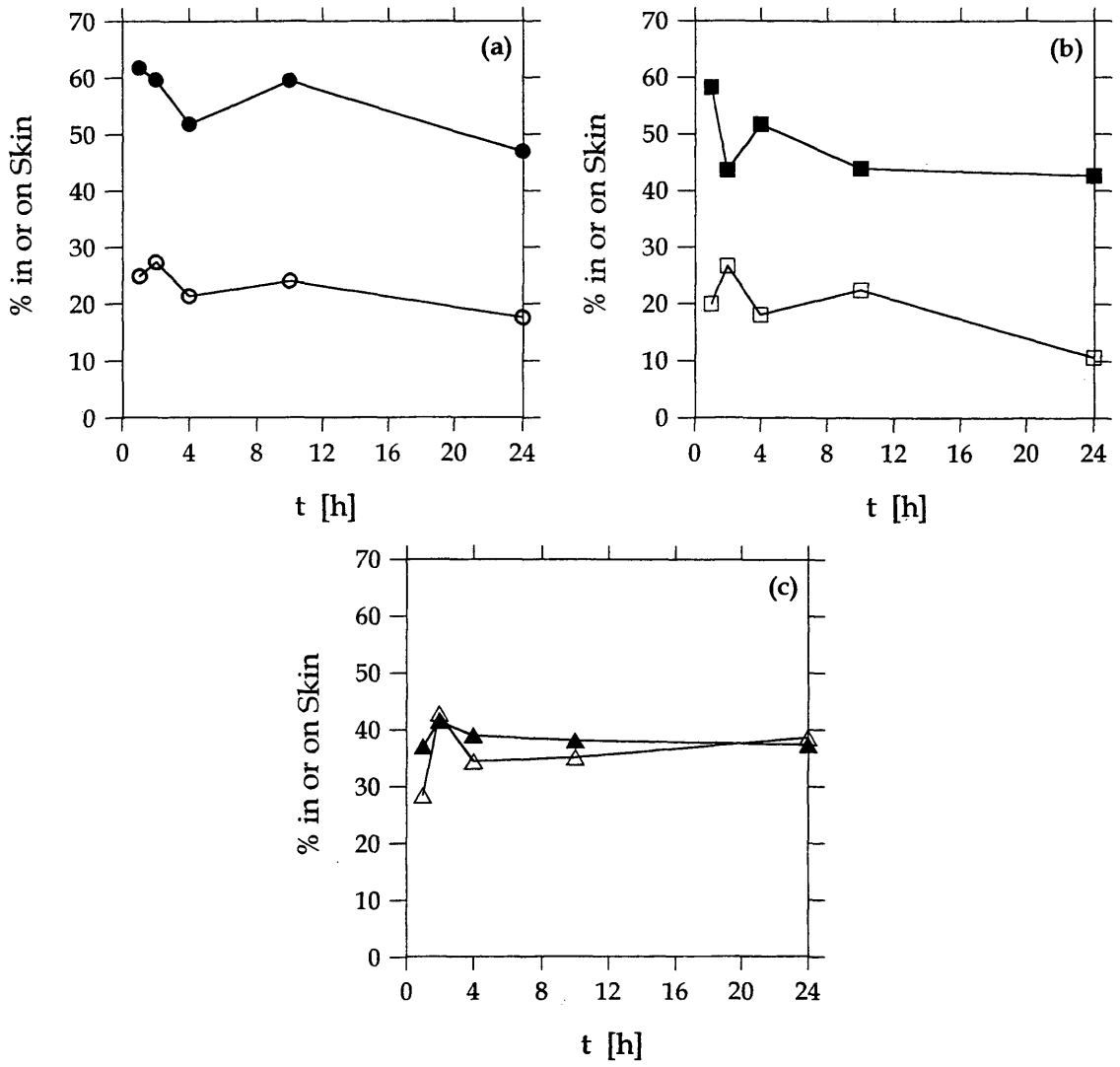

Figure 6DM.3 – Percent of applied dose on (open symbols) and in (closed symbols) the skin as a function of time for all doses: (a) L, (b) M, and (c) H.

Figure 6DM.4 shows the percent of applied dose in the skin and absorbed systemically as a function of time. The percent in the skin decreased slowly for exposure times larger than about one hour, coincident with increases in the percent systemically absorbed. The data for the different doses in Figures 6DM.4a and b might not be statistically different, but dose H did have the smallest percent in the skin and absorbed systemically. The amount of diclofop-methyl in the skin reached a maximum prior to one hour. Pesticides with molecular weights comparable to diclofop-methyl (MW = 341) took longer to reach maximum amounts in skin (e.g., diniconazole (MW = 326) and phosmet (MW = 317) both took between 2 and 4 hours).

Compared to the rate of absorption into the skin, systemic absorption was slow. Diclofop-methyl is highly lipophilic with a $\log K_{o/w} = 4.6$. An estimate of B is 0.25, and so the ve may have contributed a significant resistance to mass transport. This would slow systemic absorption and explain the large amounts of diclofop-methyl in the skin.

Moles of chemical in the skin and absorbed systemically are shown in Figure 6DM.5 as a function of L_{film}. The data for the amount in the skin at 2, 4, 10, and 24 hours were similar indicating that by two hours the exposure time had only a small effect on the amount in the skin. The amount absorbed systemically increased with dose and exposure time. The coefficients for the best-fit line through the data in Figure 6DM.5 are shown in Table 6DM.3. The slope values were 0.9-1 for moles in the skin and 0.8-1 for moles absorbed systemically. Figure 6DM.6 shows that the percent of the applied dose in the skin and absorbed systemically decreased minimally with L_{film}.

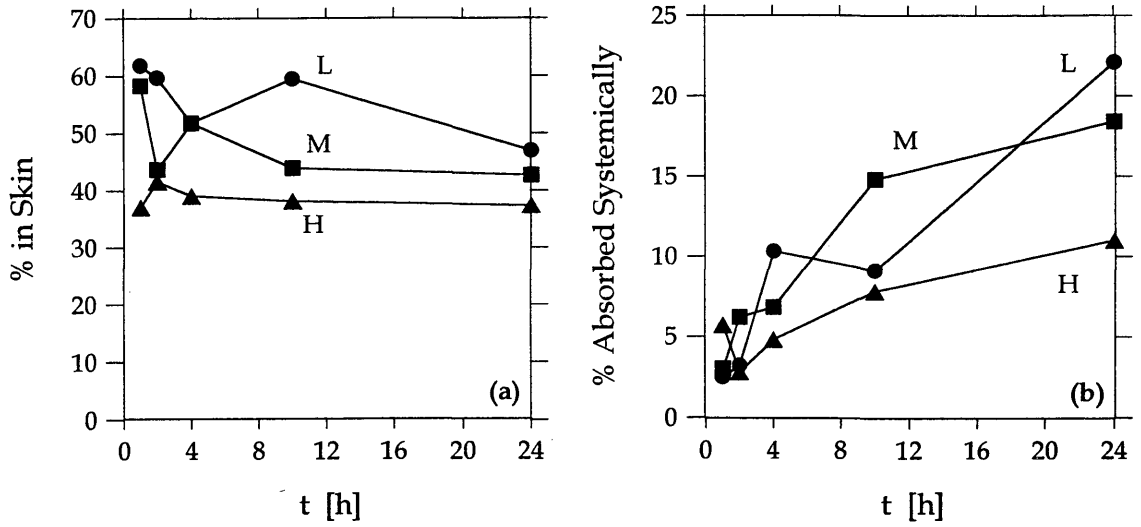

Figure 6DM.4 – Percent of applied dose (a) in the skin and (b) absorbed systemically as a function of time.

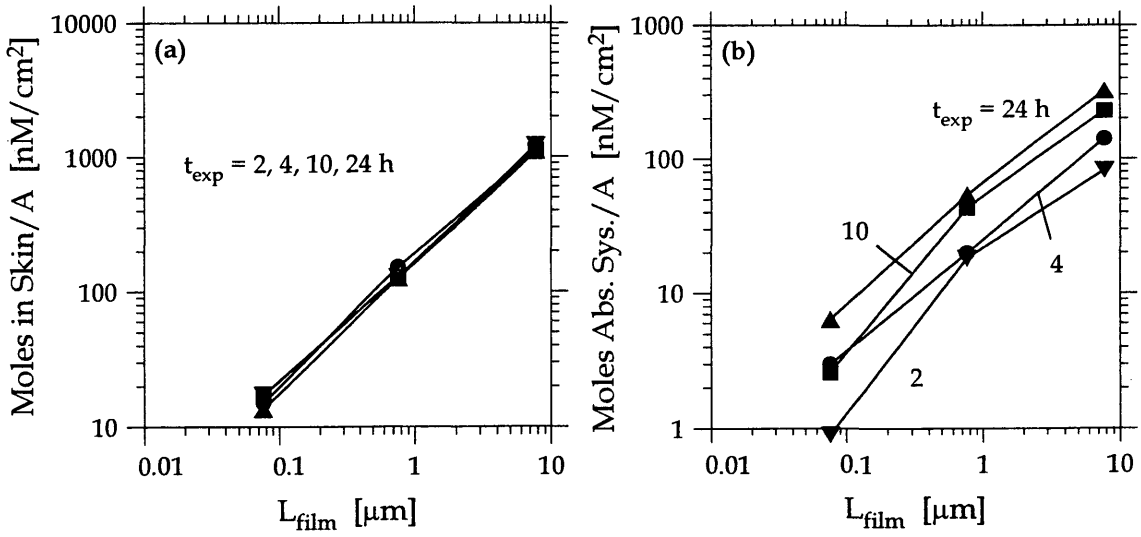

Figure 6DM.5 – Moles of chemical (a) in the skin and (b) absorbed systemically as a function of dose.

Table 6DM.3 – Coefficients for best-fit lines through log-log plots of moles of chemical in the skin and absorbed systemically as a function of dose.

time, h	moles in skin		moles absorbed systemically	
	$\hat{S}$	$\hat{I}$	$\hat{S}$	$\hat{I}$
2	0.92	5.2	0.98	2.7
4	0.94	5.2	0.83	3.2
10	0.90	5.2	0.97	3.6
24	0.95	5.1	0.85	4.1

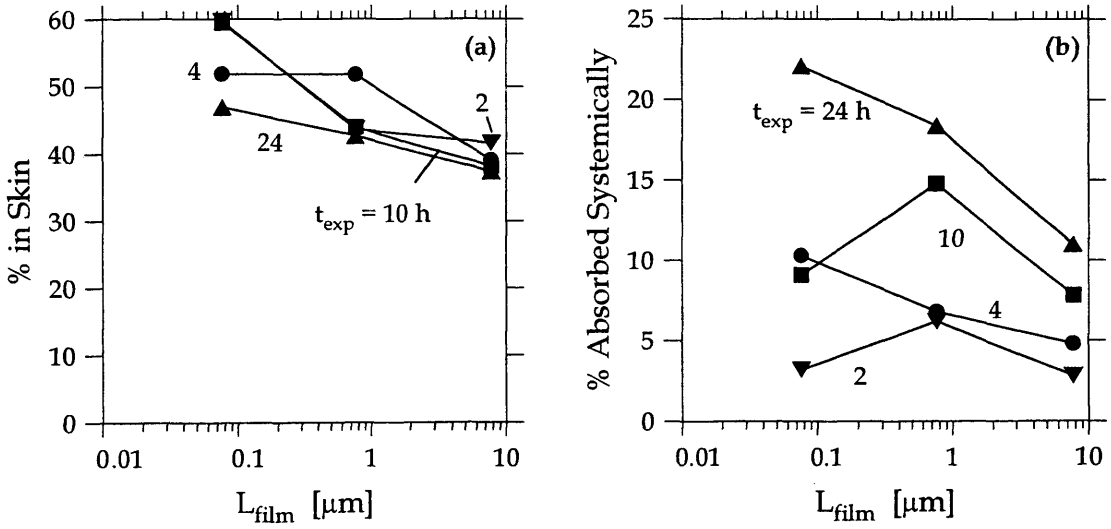

Figure 6DM.6 – Percent of applied dose (a) in the skin and (b) absorbed systemically as a function of dose.

Diniconazole (DN)

The molecular structure of diniconazole is shown in Figure 6DN.1. Diniconazole is a fungicide used for powdery mildew in vines; powdery mildew, rust, and black spot in roses; leaf spot in peanuts; and more. It is also used on fruit, vegetables, cereals, and other ornamentals. Its tradenames include Spotless and Sumi-8. Diniconazole, a solid, lipophilic pesticide ($\log K_{o/w} = 4.3$), is available as suspension and emulsifiable concentrates, a wettable powder, and as water dispersible granules (Tomlin, 1997). Table 6DN.1 shows the applied doses in the diniconazole study with the results listed in Table 6DN.2. The percent of the applied dose recovered, on the enclosure and cover, and in the skin wash were not reported.

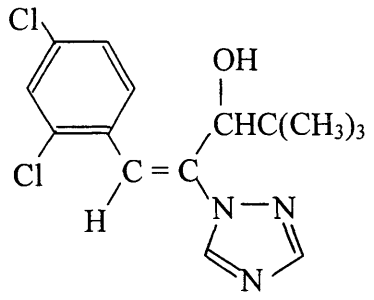

Figure 6DN.1 – Molecular structure of diniconazole.

Table 6DN.1 – Applied doses used in diniconazole study.

dose	moles /A , nM / cm^2	mass / A, µg / cm^2	L_{film}, µm
L	15	4.9	0.037
M	152	49.6	0.38
H	1520	496	3.8

Table 6DN.2 – Results of diniconazole dermal absorption study (Zendzian, 2000b).[a]

Dose	Exposure	Skin		Absorbed[b]	
	hours	%	nM/cm^2	%	nM/cm^2
L	1	6.8	1.02	0.2	0.03
	2	8.0	1.20	1.6	0.24
	4	11.9	1.79	3.2	0.48
	10	12.1	1.82	8.4	1.26
	24	23.6	3.54	8.0	1.20
M	1	9.4	14.28	0.2	0.3
	2	3.0	4.56	0.5	0.75
	4	6.3	9.57	2.1	3.19
	10	11.5	17.48	4.5	6.84
	24	8.6	13.07	10.1	15.35
H	1	2.8	42.56	0.1	1.52
	2	2.7	41.04	0.00	0.00
	4	3.9	59.28	0.2	3.04
	10	4.6	69.92	0.4	6.08
	24	4.1	62.32	0.6	9.12

[a] Data are from the study with MRID 419329-34 dated 6/18/91. [b] Data include pesticide in blood, urine, feces, and carcass.

The percent of applied dose in the skin and absorbed systemically are shown in Figure 6DN.2 as a function of time. For doses M and H, the percent in the skin was essentially independent of time after about 4 hours, but for dose L the percent in skin increased over the entire exposure time. For dose L, the percent in the skin was the same at both 4 and 10 hours, but then increased at 24 hours. It is impossible to know if this effect is real or if the skin wash for this data point had a poor efficiency. In Figure 6DN.2b, the percent absorbed systemically increased with exposure time.

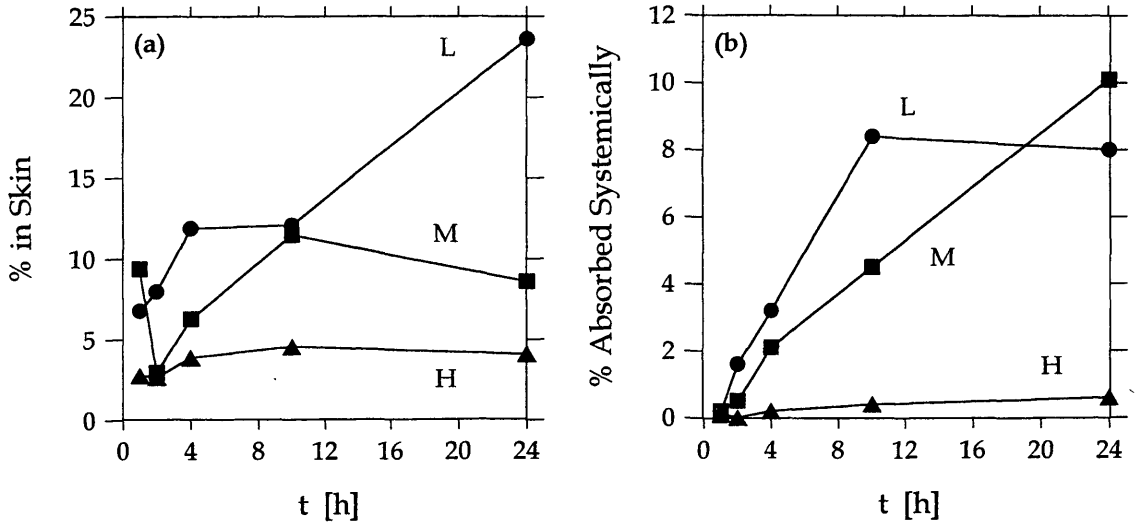

Figure 6DN.2 – Percent of applied dose (a) in the skin and (b) absorbed systemically as a function of time.

Diniconazole has the relatively high vapor pressure of 4.9 mPa at 25°C (Tomlin, 1997). There was evidence that lindane, with a comparable vapor pressure of 5.6 mPa at 20°C (Tomlin, 1997), evaporated. Without the data for the percent of applied dose on the enclosure and cover and the total recoveries, it is impossible to know if diniconazole evaporates. But because the amount in the skin was constant or increased with time, if

evaporation did occur it was unlikely that the rate of dermal absorption was significantly affected.

Figure 6DN.3 shows moles in the skin and absorbed systemically as a function of L_{film}. The amount in skin increased almost proportionally with dose. The amount absorbed systemically was not as strong a function of applied dose. Systemic absorption for dose H at 2 hours was below the detection limit. The coefficients for the best-fit lines through the data in Figure 6DN.3 are listed in Table 6DN.3. Slope values for amount in the skin were ~ 0.8 except for the 24-hour exposure, which had a slope value of about 0.6. That value could be low due to inefficient washing of the dose L data point. The slope values for the amount absorbed systemically are much lower than for the amount in the skin at ≤ 0.4. Figure 6DN.4 shows that both the percent of applied dose in the skin and absorbed systemically decreased with dose.

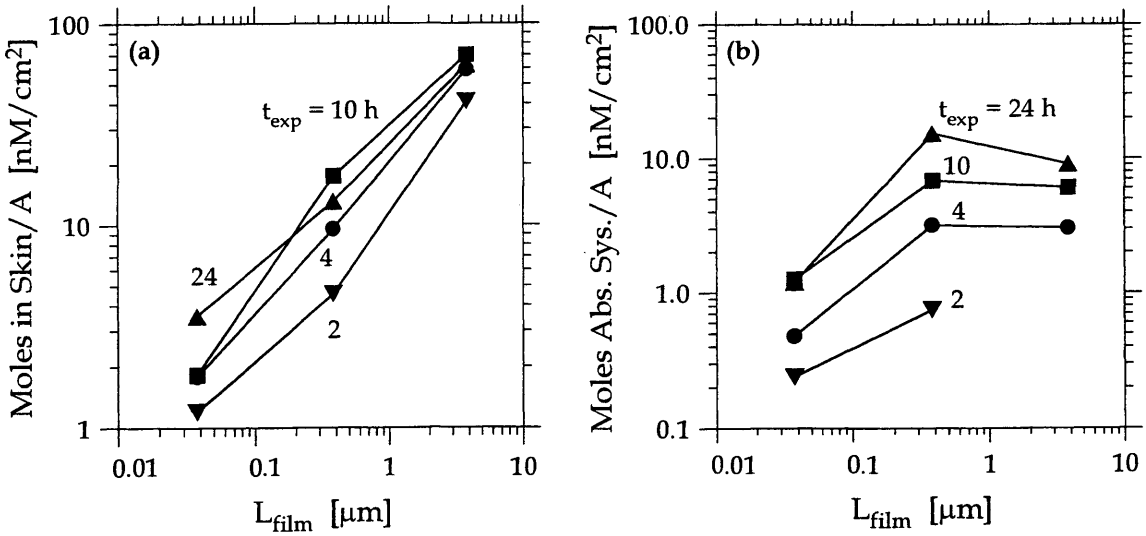

Figure 6DN.3 – Moles of chemical (a) in the skin and (b) absorbed systemically as a function of L_{film}.

Table 6DN.3 – Coefficients for best-fit lines through log-log plots of moles of chemical in the skin and absorbed systemically as a function of dose.

time, h	moles in skin		moles absorbed systemically	
	$\hat{S}$	$\hat{I}$	$\hat{S}$	$\hat{I}$
2	0.76	2.5	ND[a]	ND[a]
4	0.76	3.0	0.40	0.90
10	0.79	3.3	0.34	1.7
24	0.62	3.3	0.44	2.1

[a] Calculation was not done because the two-hour data was below the detection limit.

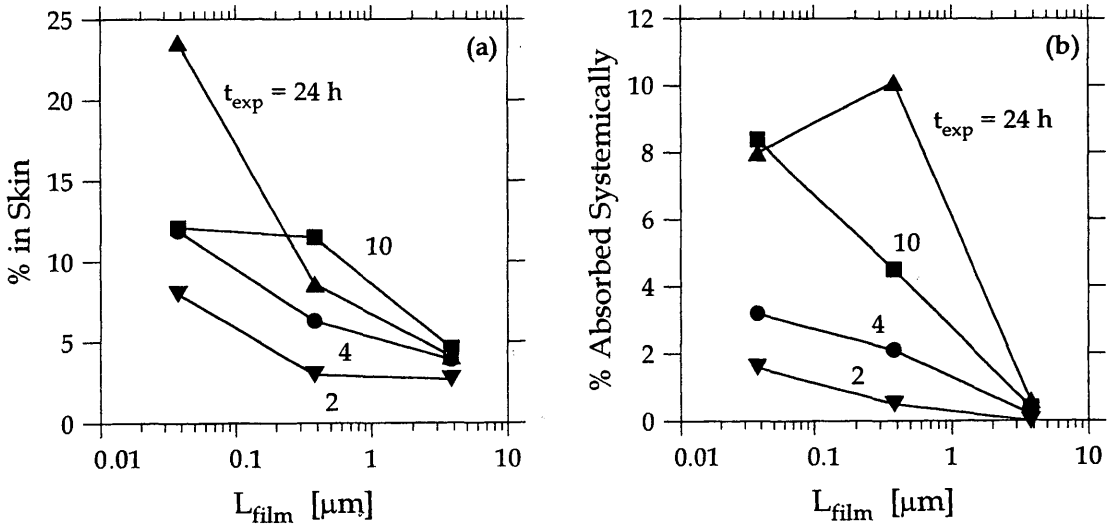

Figure 6DN.4 – Percent of applied dose (a) in the skin and (b) absorbed systemically as a function of L_{film}.

Disulfoton (DS)

The molecular structure of disulfoton is shown in Figure 6DS.1. Disulfoton is an insecticide and acaricide used for control of aphids, thrips, mealybugs, and other sucking insects; it also controls spider mites in potatoes, vegetables, rice, and other crops. It prevents cucumber mosaic and potato leaf roll viruses by controlling the virus vectors. Its tradenames include Disyston, Frumin AL, and Solvirex. Disulfoton, a liquid, lipophilic pesticide ($\log K_{o/w} = 3.95$), is available as a granule, a powder for dry seed treatment, and an emulsifiable concentrate (Tomlin, 1997). Table 6DS.1 shows the applied doses in the disulfoton study with the results listed in Table 6DS.2.

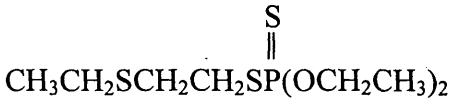

Figure 6DS.1 – Molecular structure of disulfoton.

Table 6DS.1 – Applied doses used in disulfoton study.

dose	moles /A , nM / cm^2	mass / A, μg / cm^2	L_{film}, μm
L	3.1	0.85	0.0075
M	31	8.5	0.075
H	310	85	0.75

Table 6DS.2 – Results of disulfoton dermal absorption study (Zendzian, 2000b).[a]

Dose	Expo-sure	Enclosure and Cover[b]	Skin Wash	Skin		Absorbed[c]		Total Recovery
	hours	%	%	%	nM/cm^2	%	nM/cm^2	%
L	1	10.51	28.1	24.2	0.75	5.93	0.18	68.8
	4	23.19	23.5	15.9	0.49	13.86	0.43	79.4
	10	33.48	11.1	8.3	0.26	25.95	0.80	78.8
M	1	10.14	42.8	34.9	10.82	4.58	1.42	92.4
	4	21.96	28.6	29.6	9.28	15.92	4.94	96.4
	10	36.80	16.2	16.2	5.02	32.73	10.15	102.0
H	1	6.66	54.8	36.6	113.5	3.55	11.0	101.5
	4	12.23	37.6	31.9	98.9	12.54	38.9	94.2
	10	23.69	21.9	22.1	68.5	25.26	78.3	93.3

[a] Data are from the study of the Disyston 8 formulation with MRID 433602-01 dated 8/30/94. [b] Activated charcoal filter was used. [c] Data include pesticide from the blood, urine, feces, carcass, and cage wash.

Figure 6DS.2 shows the percent of applied dose recovered as a function of time. Percent recoveries were > 92% for doses M and H, but were < 80% for dose L. As shown in Figure 6DS.3, the percent of applied dose on the enclosure and cover was significant and increased with exposure time. Disulfoton, with a vapor pressure of 13 mPa at 20°C (Tomlin, 1997), is known to evaporate (Zendzian, 2000), which is consistent with these results.

The percent of applied dose on and in the skin are shown in Figure 6DS.4 as a function of time. These plots show that as the mass of chemical on the skin decreased due to dermal absorption and evaporation, the mass of chemical in the skin also decreased. For all doses, the amount of chemical in the skin was within 3% of the amount of chemical on the skin at 10 hours.

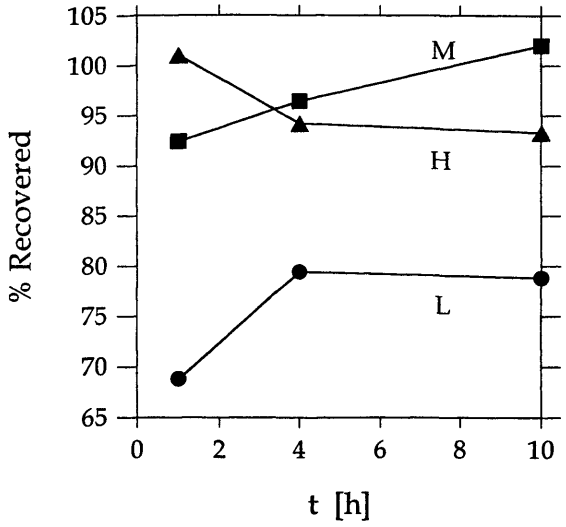

Figure 6DS.2 – Percent of applied dose recovered as a function of time.

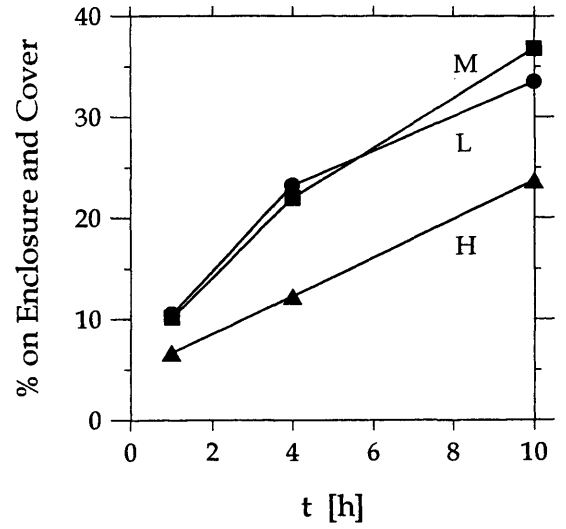

Figure 6DS.3 – Percent of applied dose on the enclosure and cover as a function of time.

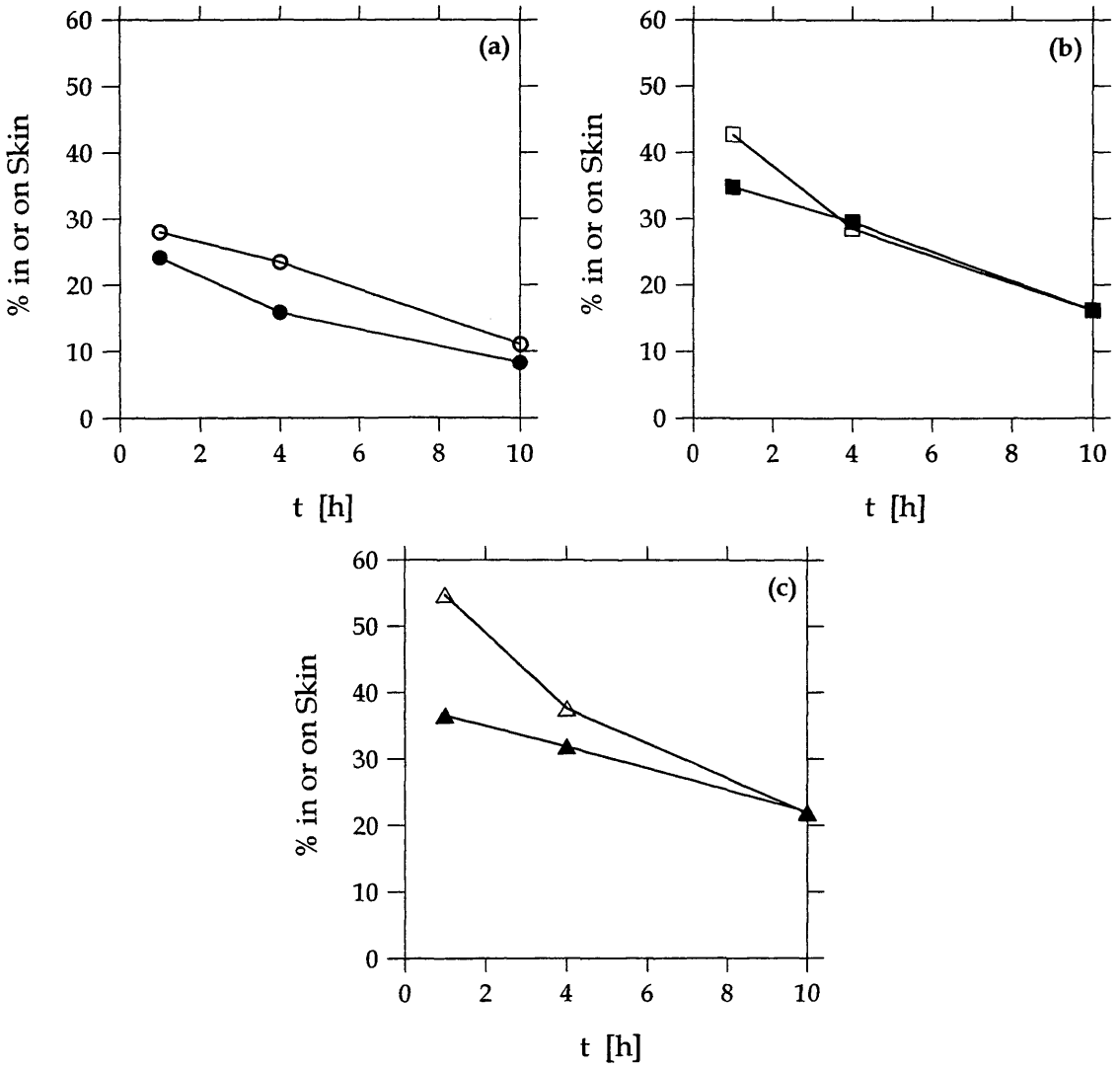

Figure 6DS.4 – Percent of applied dose on (open symbols) and in (closed symbols) the skin as a function of time for all doses: (a) L, (b) M, and (c) H.

The percent of applied dose in the skin and absorbed systemically are shown in Figure 6DS.5 as a function of time. The percent in the skin decreased with exposure time. For many other pesticides (e.g., lindane and isoxaflutole), dose L had the highest percent of applied dose in the skin, but disulfoton differed in that dose H had the highest percent in the skin. This is consistent with evaporation affecting small doses more than large doses (e.g., for acetochlor only dose LL evaporated significantly). The percent absorbed systemically increased with time for all three doses. Interestingly, there was no significant difference between doses. Despite evaporation, significant amounts of disulfoton were absorbed systemically.

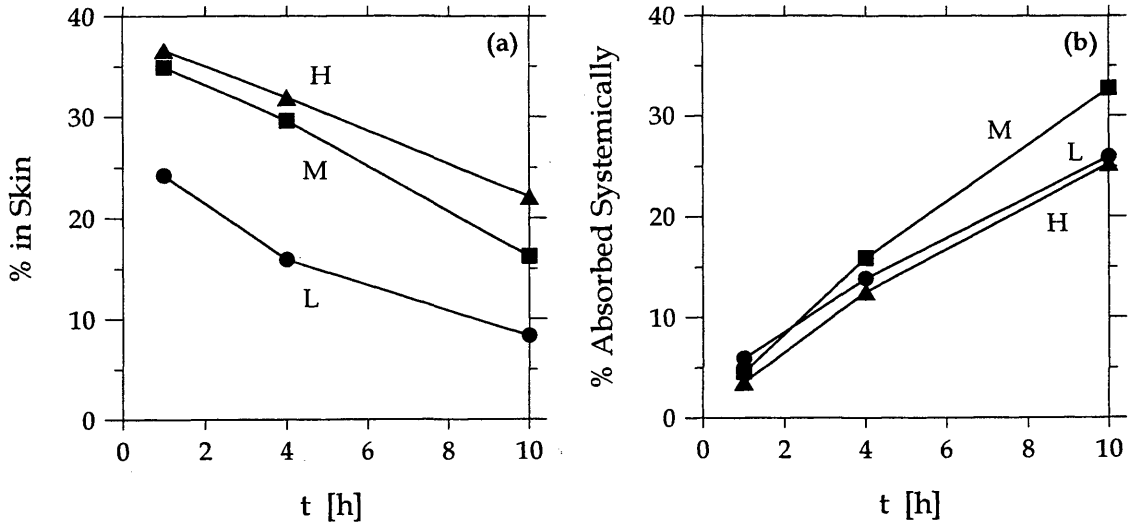

Figure 6DS.5 – Percent of applied dose (a) in the skin and (b) absorbed systemically as a function of time.

Figure 6DS.6 shows that the amount in the skin and absorbed systemically increased with L_{film}. The coefficients for the best-fit lines through these data are listed in Table 6DS.3. Slope values for the amount in the skin were 1.2. Slope values higher than one are unusual, suggesting that evaporation may have affected the low doses more than the high doses. Slope values for the amount absorbed systemically were approximately one, and were lower than the slope values for the amount in the skin.

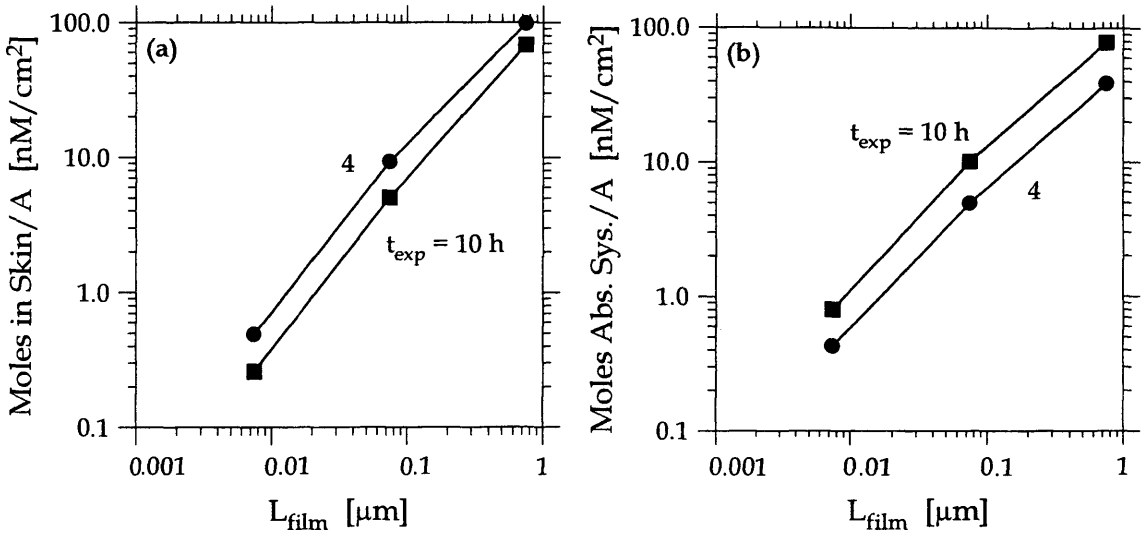

Figure 6DS.6 – Moles of chemical (a) in the skin and (b) absorbed systemically as a function of L_{film}.

Table 6DS.3 – Coefficients for best-fit lines through log-log plots of moles of chemical in the skin and absorbed systemically as a function of dose.

time, h	moles in skin		moles absorbed systemically	
	$\hat{S}$	$\hat{I}$	$\hat{S}$	$\hat{I}$
4	1.2	5.0	0.98	4.0
10	1.2	4.6	1.0	4.7

The percent of applied dose in the skin and absorbed systemically are shown in Figure 6DS.7 as a function of L_{film}. The percent in skin increased with applied dose and the percent absorbed systemically was essentially independent of applied dose. Both of these observations are different than for most of the other pesticides examined here (e.g., for both azinphos-methyl and diniconazole the percent in the skin and absorbed systemically decreased with increasing L_{film}), and could be consistent with a pesticide that evaporates.

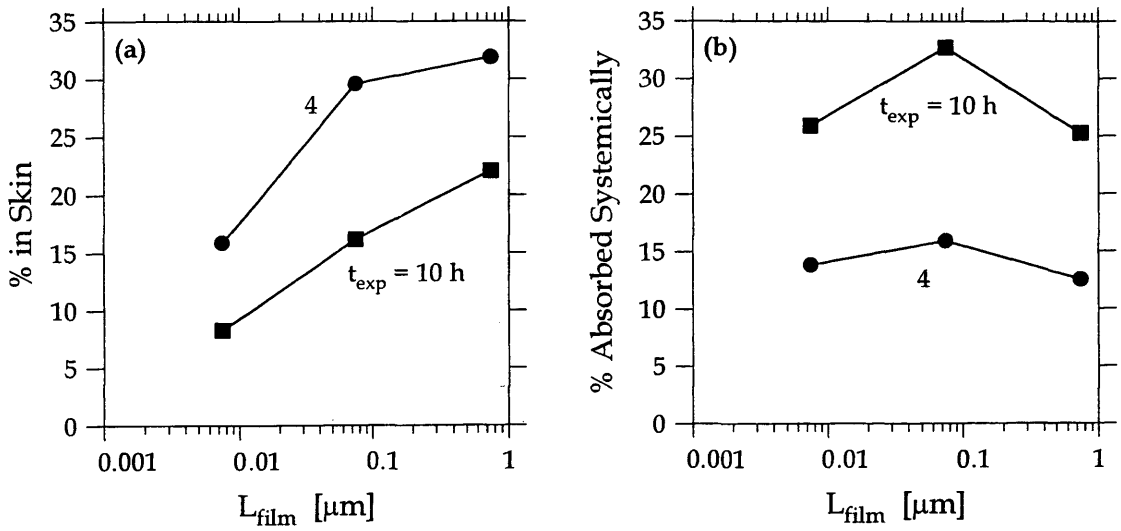

Figure 6DS.7 – Percent of applied dose (a) in the skin and (b) absorbed systemically as a function of L_{film}.

EPTC (EP)

The molecular structure of EPTC is shown in Figure 6EP.1. EPTC is an herbicide used for control of annual and perennial grasses and some broad-leaved weeds in potatoes, beans, peas, beetroot, pineapples, and more. Its tradenames include Eptam, and it is available as a granule and an emulsifiable concentrate (Tomlin, 1997). Table 6EP.1 shows the applied doses in the EPTC study with the results listed in Table 6EP.2.

$[CH_3(CH_2)_2]_2NC(O)SCH_2CH_3$

Figure 6EP.1 – Molecular structure of EPTC.

Table 6EP.1 – Applied doses used in EPTC study.

dose	moles /A , nM / cm^2	mass / A, μg / cm^2	L_{film}, μm
LL	497	93.9	0.99
L	1037	196.0	2.1
M	4772	901.9	9.5
H	46333	8756.9	92

Table 6EP.2 – Results of EPTC dermal absorption study (Zendzian, 2000b).[a]

Dose	Exposure	Enclo-sure and Cover[b]	Skin Wash	Skin		Absorbed[c]		Total Recovery
	hours	%	%	%	nM/cm^2	%	nM/cm^2	%
LL	1	75.6	4.72	2.70	12.42	2.13	16.56	85
	4	79.8	1.72	1.62	8.05	3.85	19.13	87
	10	83.7	1.53	1.52	7.55	4.58	22.76	91
	24	79.4	1.11	1.02	5.07	5.59	27.78	87
L	1	77.1	6.80	3.85	39.93	2.41	24.99	90
	4	82.1	2.06	1.41	14.62	4.02	41.69	90
	10	85.6	1.59	1.15	11.93	3.36	34.84	92
	24	86.1	0.84	0.62	6.43	3.06	31.73	91
M	1	59.9	22.9	8.50	405.6	2.22	105.9	94
	4	82.6	2.27	3.47	165.6	4.29	204.7	93
	10	85.3	1.13	2.40	114.5	4.41	216.4	93
	24	85.3	0.66	1.35	64.4	5.75	274.4	93
H	1	86.8	10.0	2.04	945.2	1.12	518.9	100
	4	86.9	6.66	1.85	857.2	4.73	2191.6	100
	10	88.4	0.97	1.15	532.8	4.94	2288.9	96
	24	81.9	0.35	0.68	315.1	8.59	3980.0	92

[a] Data are from the study of the Eptam formulation with MRID 416862-01 dated 5/9/88.
[b] The an activated charcoal filter was used. [c] Data include pesticide from the urine, feces, and carcass.

Figure 6EP.2 shows that percent recoveries were > 85% and were the lowest for dose LL. The percent of the applied dose on the enclosure and cover is shown in Figure 6EP.3 as a function of time. Notably, by the end of one hour almost 80% of the applied dose was on the enclosure and cover and this increased only slightly with increased exposure time. Since the amount of EPTC on the enclosure and cover were combined, we do not know if EPTC mainly reached the enclosure and cover by rapid evaporation or by spreading to the enclosure during pesticide application. Given the low vapor pressure of EPTC (0.01 mPa at 25°C (Tomlin, 1997)), rapid evaporation is not expected.

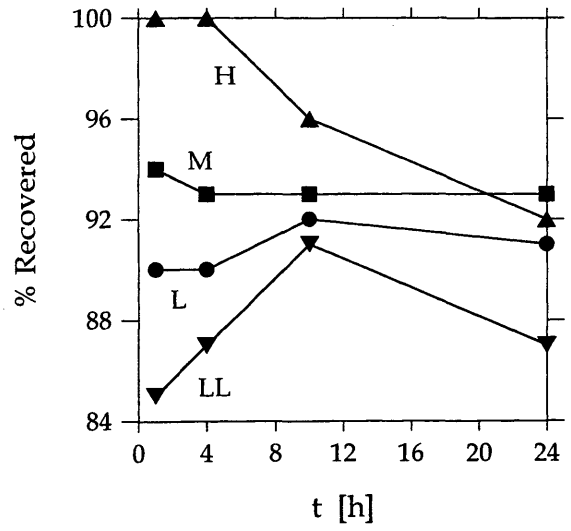

Figure 6EP.2 – Percent of applied dose recovered as a function of time.

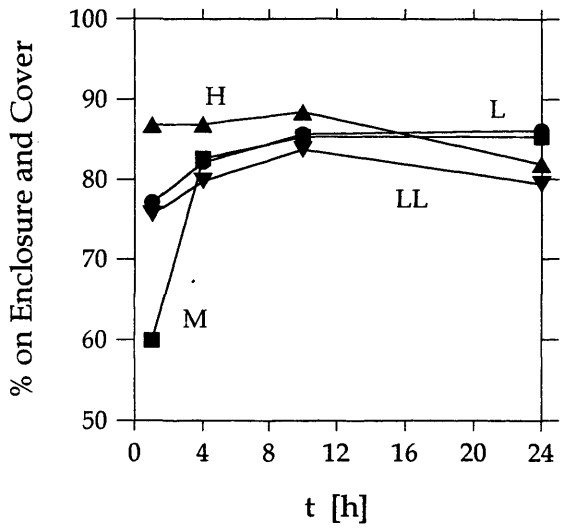

Figure 6EP.3 – Percent of applied dose on the enclosure and cover as a function of time.

Figure 6EP.4 shows the percent of applied dose on and in the skin as a function of time. For the majority of the data, the amount on the skin was approximately the same as the amount in the skin. Figure 6EP.5 shows the percent of applied dose in the skin and absorbed systemically as a function of time. The amount in the skin was a maximum at one hour and decreased with time for all doses. The percent in the skin was largest for dose M while the percent absorbed systemically was largest for dose H. Even though the amount of EPTC available for absorption was lower than might be expected due to the high amount of EPTC on the enclosure and cover, significant amounts of EPTC did absorb systemically. Thus, although the majority of the EPTC was on the enclosure and cover after the first hour of exposure, for exposures longer than one hour the amount of EPTC in the skin apparently dropped mainly due to systemic absorption.

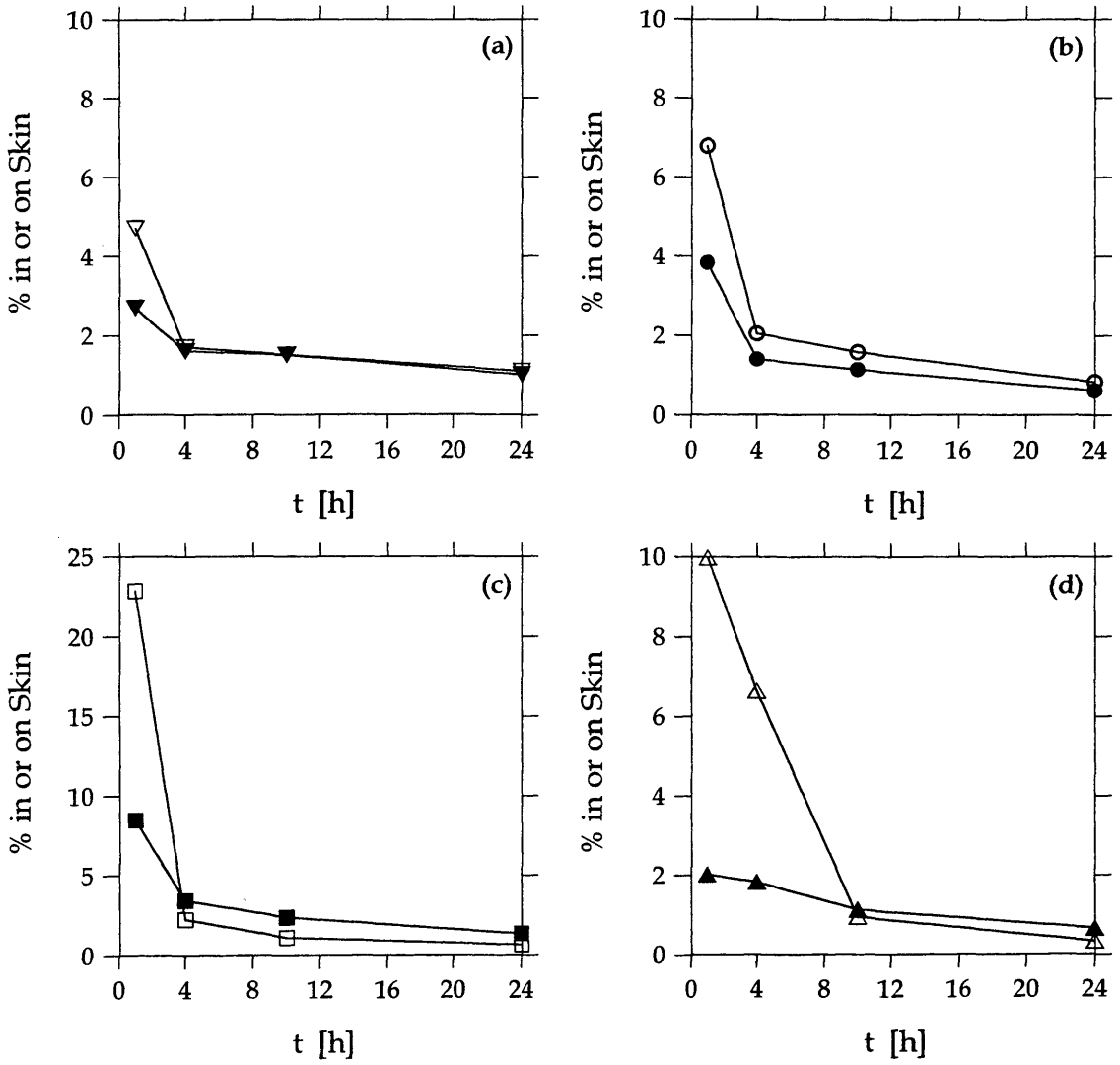

Figure 6EP.4 – Percent of applied dose on (open symbols) and in (closed symbols) the skin as a function of time for all doses: (a) LL, (b) L, (c) M, and (d) H.

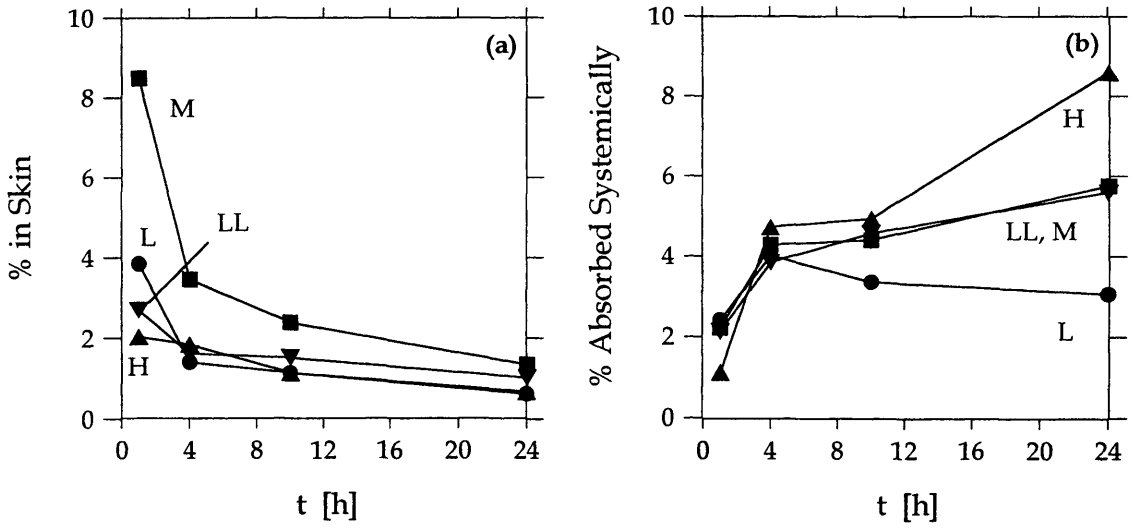

Figure 6EP.5 – Percent of applied dose (a) in the skin and (b) absorbed systemically as a function of time.

Moles in the skin and absorbed systemically, shown in Figure 6EP.6 as a function of L_{film}, both increased proportionally to applied dose. The coefficients of the best-fit line for these data are listed in Table 6EP.3. Slope values for amount in the skin and absorbed systemically were all approximately one. Figure 6EP.7 shows that both the percent of applied dose in the skin and absorbed systemically were essentially independent of L_{film}.

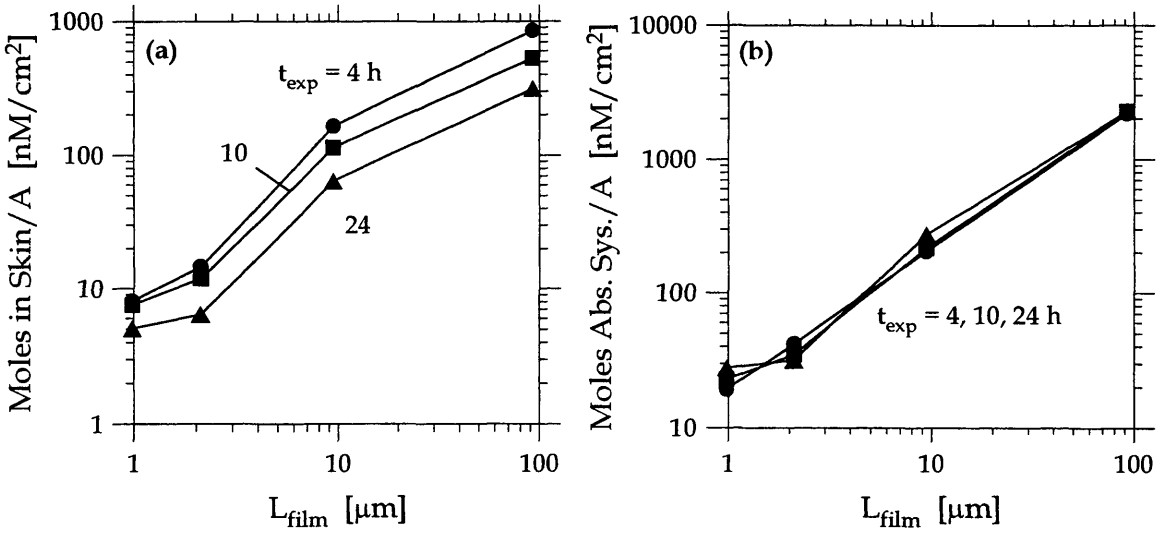

Figure 6EP.6 – Moles of chemical (a) in the skin and (b) absorbed systemically as a function of L_{film}.

Table 6EP.3 – Coefficients for best-fit lines through log-log plots of moles of chemical in the skin and absorbed systemically as a function of dose.

time, h	moles in skin		moles absorbed systemically	
	$\hat{S}$	$\hat{I}$	$\hat{S}$	$\hat{I}$
4	1.1	2.2	1.0	3.0
10	0.98	2.0	1.0	3.0
24	0.97	1.5	1.0	3.1

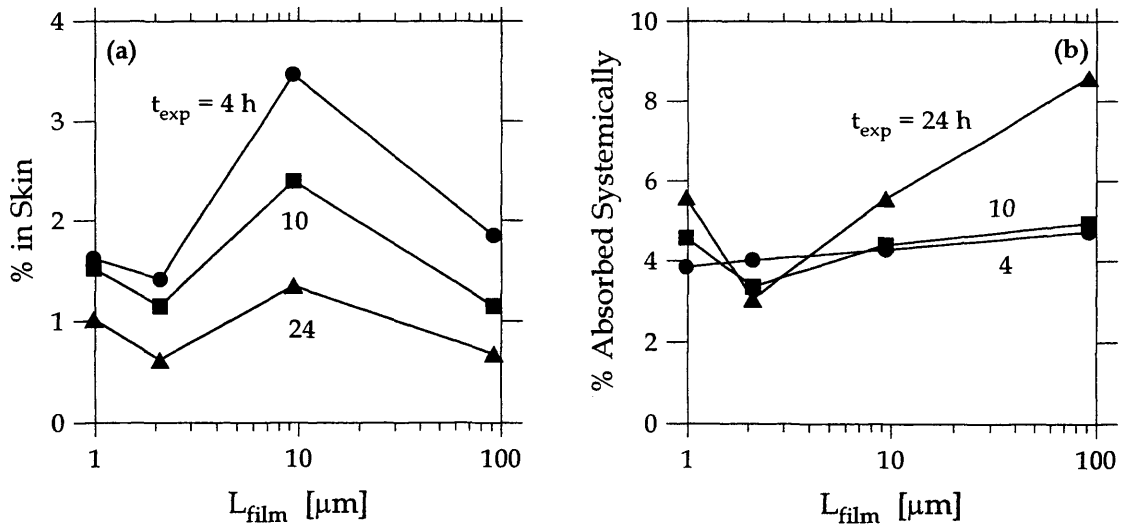

Figure 6EP.7 – Percent of applied dose (a) in the skin and (b) absorbed systemically as a function of L_{film}.

Imazalil (IM)

The molecular structure of imazalil is shown in Figure 6IM.1. Imazalil is a fungicide used for control of a wide range of fungal diseases on fruit, vegetables, and ornamentals; for control of storage diseases of citrus fruit, bananas, and other plants; for seed dressing to control diseases of cereals; and more. Its tradenames include Deccozil, Flo-Pro and Florasan. Imazalil, a solid, lipophilic pesticide ($\log K_{o/w} = 3.82$), is available as a water soluble powder, a soluble liquid, and as an emulsifiable concentrate (Tomlin, 1997). Table 6IM.1 shows the applied doses in the imazalil study with the results listed in Table 6IM.2.

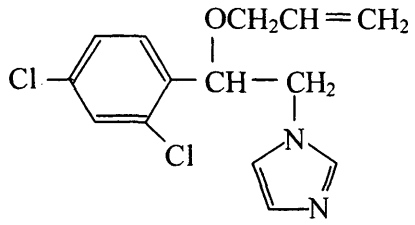

Figure 6IM.1 – Molecular structure of imazalil.

Table 6IM.1 – Applied doses used in the imazalil study.

dose	moles /A , nM / cm^2	mass / A, μg / cm^2	L_{film}, μm
LL	13.5	4	0.03
L	135	40	0.3
M	1350	400	3
H	13500	4000	30

Table 6IM.2 – Results of imazalil dermal absorption study.[a]

Dose	Exposure	Skin Wash	Skin		Absorbed[b]		Sum[c]
	hours	%	%	nM/cm^2	%	nM/cm^2	%
LL	0.5	52.2	17.3	2.33	14.34	1.93	84
	1	38.2	16.4	2.21	29.93	4.03	85
	2	34.7	12.3	1.66	34.72	4.67	82
	4	36.2	14.2	1.91	25.83	3.48	76
	10	27.4	18.2	2.45	41.23	5.55	87
	24	22.6	18.3	2.46	47.93	6.45	89
L	0.5	63.7	11.1	14.9	12.35	16.6	87
	1	52.8	11.7	15.8	21.00	28.3	86
	2	52.0	14.1	19.0	21.38	28.8	87
	4	42.8	9.89	13.3	26.68	35.9	79
	10	43.7	11.4	15.3	24.61	33.1	80
	24	37.6	10.4	14.0	39.39	53.0	87
M	0.5	72.1	2.60	35.0	8.50	114.	83
	1	69.8	5.06	68.1	8.58	115.	83
	2	70.0	5.24	70.5	9.59	129.	85
	4	67.3	3.72	50.1	12.66	170.	84
	10	60.1	3.46	46.6	16.92	228.	80
	24	48.2	5.14	69.2	30.92	416.	84
H	0.5	91.4	2.59	349.	1.19	160.	95
	1	91.4	2.76	371.	0.96	129.	95
	2	92.6	2.16	291.	1.13	152.	96
	4	83.9	2.87	386.	6.22	837.	93
	10	51.2	1.85	249.	25.93	3490	79
	24	52.9	4.51	607.	29.32	3930	87

[a] Data are from the study of the Fungaflor emulsifiable concentrate formulation with MRID 429134-01 dated 2/1/93. [b] Data include pesticide from urine, blood, feces, cage wash, and carcass. [c] Calculated by totaling the other percents reported.

As shown in Table 6IM.1, percent recoveries and percent of applied dose on the enclosure and cover were not reported. Sums of the percent of applied dose in the skin wash, the skin, and absorbed systemically ranged from 76 to 96% and did not vary with exposure time. Based on this and low vapor pressure (0.158 mPa at 25°C (Tomlin, 1997)), imazalil probably did not evaporate significantly during the study.

Figure 6IM.2 shows the percent of applied dose on and in the skin as a function of time. For all doses, the amount of imazalil on the skin decreased substantially, but the amount in skin remained almost constant. The percent of applied dose in the skin and absorbed systemically are shown in Figure 6IM.3 as a function of time. The percent absorbed systemically increased with exposure time. Both the percent on the skin and absorbed systemically were highest for dose LL at 10 and 24 hours.

Moles of chemical in the skin and absorbed systemically are shown in Figure 6IM.4 as a function of L_{film}. Coefficients for the best-fit lines of these data are listed in Table 6IM.3. Slope values for the amount in the skin were 0.7 – 0.8. For the amount absorbed systemically, slope values ranged from 0.5 to 0.9, increasing with exposure time. Exposure to imazalil has caused some sensitive test animals to experience contact dermatitis (EXTOXNET, 1996). Also, some formulations of imazalil have been given the EPA toxicity classification II, indicating that it can cause severe skin irritation within 72 hours (Tomlin, 1997). Thus, imazalil may damage skin. That may explain why the slope values for systemic absorption increased with exposure time and why slope values for the 4, 10 and 24-hour systemic absorption were larger than for the amount in the skin. As shown in Figure 6IM.5, the percent of applied dose in the skin and absorbed systemically both decreased with increases in applied dose.

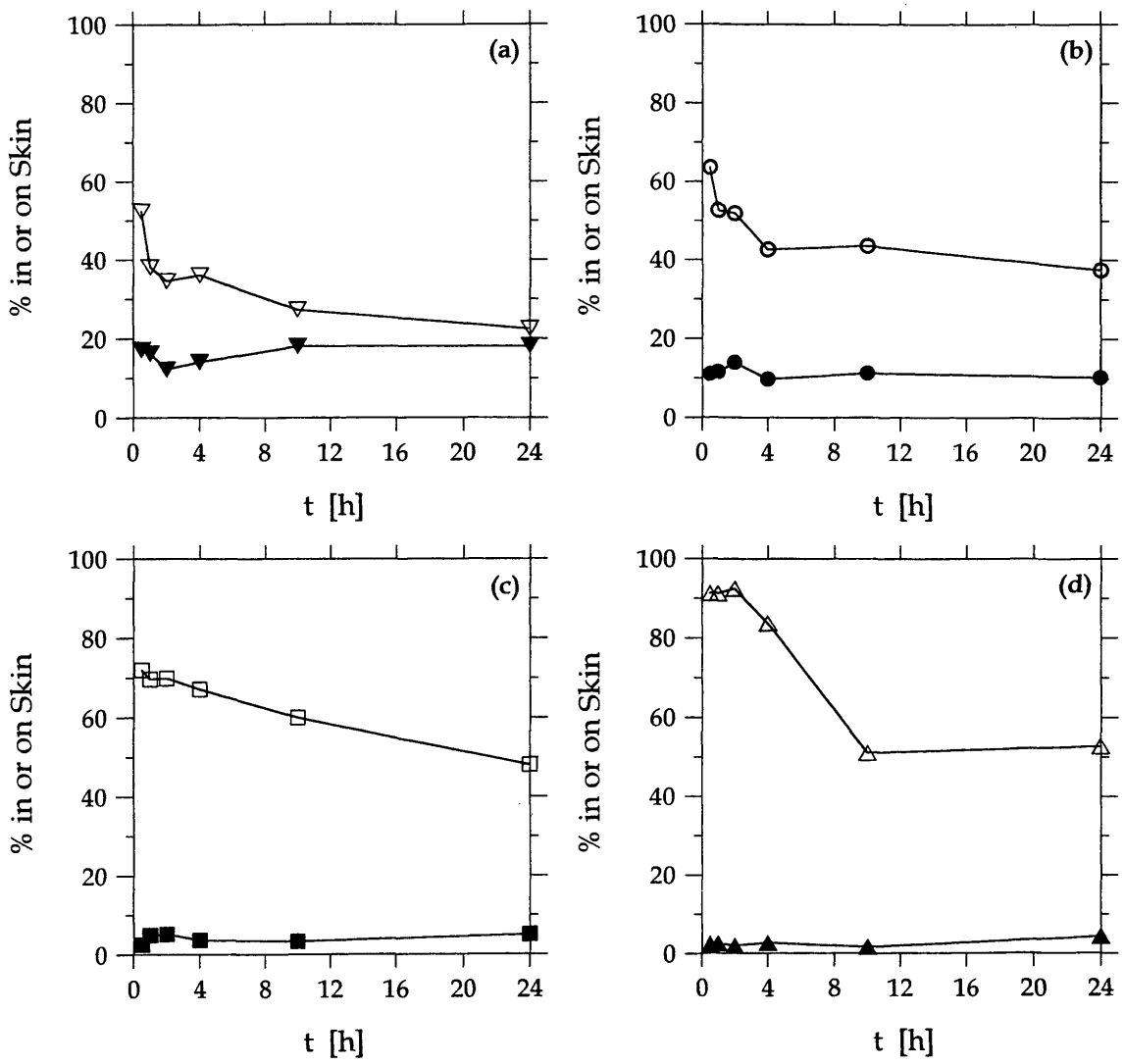

Figure 6IM.2 – Percent of dose on (open symbols) and in (closed symbols) the skin as a function of time for all doses: (a) LL, (b) L, (c) M, and (d) H.

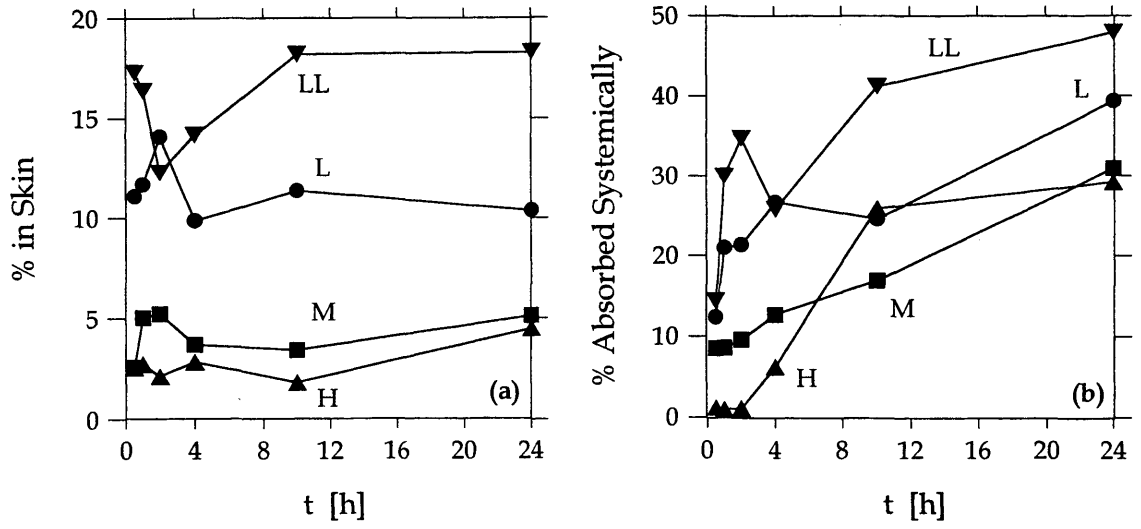

Figure 6IM.3 – Percent of applied dose (a) in the skin and (b) absorbed systemically as a function of time.

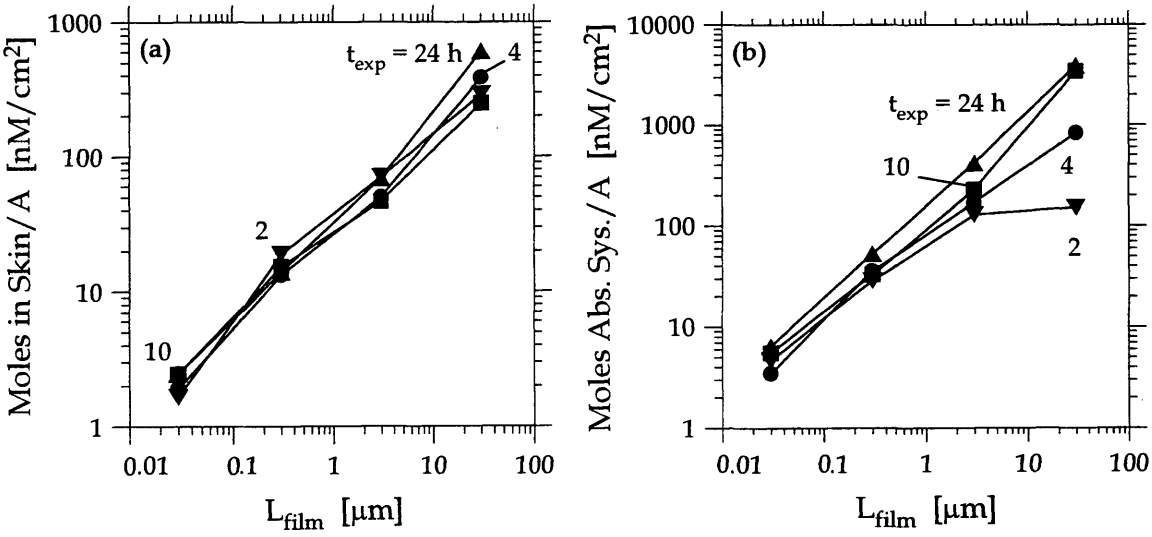

Figure 6IM.4 – Moles of chemical (a) in the skin and (b) absorbed systemically as a function of L_{film}.

Table 6IM.3 – Coefficients for best-fit lines through log-log plots of moles of chemical in the skin and absorbed systemically as a function of dose.

time, h	moles in skin		moles absorbed systemically	
	$\hat{S}$	$\hat{I}$	$\hat{S}$	$\hat{I}$
2	0.73	1.1	0.52	1.4
4	0.75	1.0	0.78	1.9
10	0.65	0.99	0.92	2.5
24	0.79	1.3	0.92	2.8

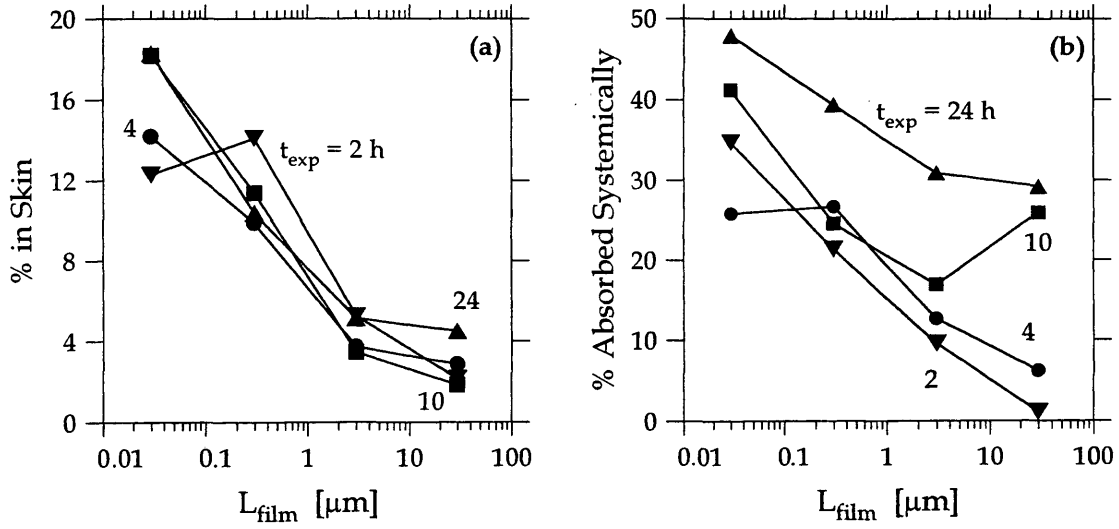

Figure 6IM.5 – Percent of applied dose (a) in the skin and (b) absorbed systemically as a function of L_{film}.

Iprodione (IP)

The molecular structure of iprodione is shown in Figure 6IP.1. Iprodione is a fungicide used for control of Botrytis, Monilia and other fungi on sunflowers, cereals, fruit trees and more. Its tradenames include Kidan, Rovral and Verisan. Iprodione, a lipophilic ($\log K_{o/w} = 3.0$), solid pesticide is available as suspension and emulsifiable concentrates, wettable and dispersible powders, water dispersible granules, flowable concentrate for seed treatment, and ultra-low volume suspensions (Tomlin, 1997). Table 6IP.1 shows the applied doses in the iprodione study with the results listed in Table 6IP.2. Percent recoveries were greater than 96% and the percent of applied dose on the enclosure and cover were less than 1.1%. There is no evidence that iprodione, with a vapor pressure of 0.0005 mPa at 25°C (Tomlin, 1997), evaporated significantly.

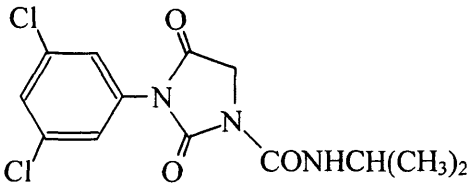

Figure 6IP.1 – Molecular structure of iprodione.

Table 6IP.1 – Applied doses used in iprodione study.

dose	moles /A , nM / cm^2	mass / A, µg / cm^2	L_{film}, µm
L	94	31	0.22
M	936	309	2.2
H	9357	3087	22

Table 6IP.2 – Results of iprodione dermal absorption study (Zendzian, 2000b).[a]

Dose	Exposure	Enclosure and Cover	Skin Wash	Skin		Absorbed[b]		Total Recovery
	hours	%	%	%	nM/cm^2	%	nM/cm^2	%
L	0.5	0.40	94.3	2.85	2.66	0.12	0.12	97.7
	1	0.67	93.3	2.28	2.13	0.43	0.41	96.7
	2	0.78	88.6	5.71	5.35	0.87	0.82	96.0
	4	0.93	92.6	2.79	2.60	1.06	0.99	97.4
	10	0.62	90.9	2.20	2.04	3.21	2.98	96.9
	24	0.91	79.8	8.34	7.81	7.41	6.93	96.5
M	0.5	0.32	96.6	3.94	36.8	1.09[d]	10.20	101
	1	0.96	94.6	6.81	63.7	0.18	1.70	102
	2	0.31	93.1	7.86	73.7	0.36	3.36	101
	4	0.43	86.5	16.10[c]	150.7	0.46	4.30	103
	10	0.73	94.7	6.25	58.5	0.26	2.43	102
	24	1.11	88.4	9.12	85.4	3.16	29.56	101
H	0.5	0.24	96.4	0.75	70.2	<0.005[e]	<0.47[e]	97.4
	1	0.43	97.9	1.03	96.5	0.11	10.29	99.5
	2	0.30	96.9	1.81	169.3	<0.005[e]	<0.47[e]	99.1
	4	0.72	93.6	3.80	354.4	0.01	0.94	98.2
	10	0.67	94.5	4.29	401.5	0.05	4.68	99.5
	24	0.79	92.5	4.81	450.0	0.19	18.22	98.3

[a] Data are from the study with MRID 435350-03 dated 10/25/94. [b] Data include pesticide in the blood, carcass, cage wash and wipe, urine, and feces. [c] Individual animal values were 14.4, 14.4, 16.1, and 17.6%. [d] Individual animal values were 0.29, 4.06, 0.00, and 0.00%, and all pesticide was found in the carcasses. [e] Limit of detection.

The percent of applied dose on and in the skin are shown in Figure 6IP.2 as a function of time. The percent on the skin was always greater than 80%. The four-hour value for percent in the skin from dose M (16%) was inconsistently high relative to other data at this dose, which ranged from 6 to 10%. The values for all four animals were reported, and indicate that the larger than expected value for amount in skin was not from an anomalously high measurement in one animal. The most likely explanation is that the skin wash of these four animals was less effective than the other measurements. This conclusion is supported by the correspondingly low value for the skin wash (86.5%) compared to the 2 and 10-hour data (i.e., 93.1 and 94.7%, respectively).

Figure 6IP.3 shows the percent of applied dose in the skin and systemically absorbed as a function of time. The percent in the skin was relatively independent of time after about four hours, but the percent systemically absorbed increased with time. Dose H had the smallest percent in the skin and absorbed systemically. For two data points at dose H, the symbol "D" (for detection limit) marks the value that systemic absorption was reported as being less than. For these data points, at least one animal had an undetectable amount of systemic absorption.

Moles in the skin and absorbed systemically are shown in Figure 6IP.4 as a function of L_{film}. For all doses, the amount in the skin increased with dose while the amount systemically absorbed was nearly independent of dose. Table 6IP.3 lists values of coefficients for the best-fit lines through the data in Figure 6IP.4. For amount in skin, the slope values at all exposure times were ~ 1. In contrast, slope values for amount absorbed systemically were much smaller (i.e., ≤ 0.21). As indicated in Figure 6IP.5, the percent of applied dose in the skin was essentially independent of dose while the percent of applied dose systemically absorbed decreased with increasing dose.

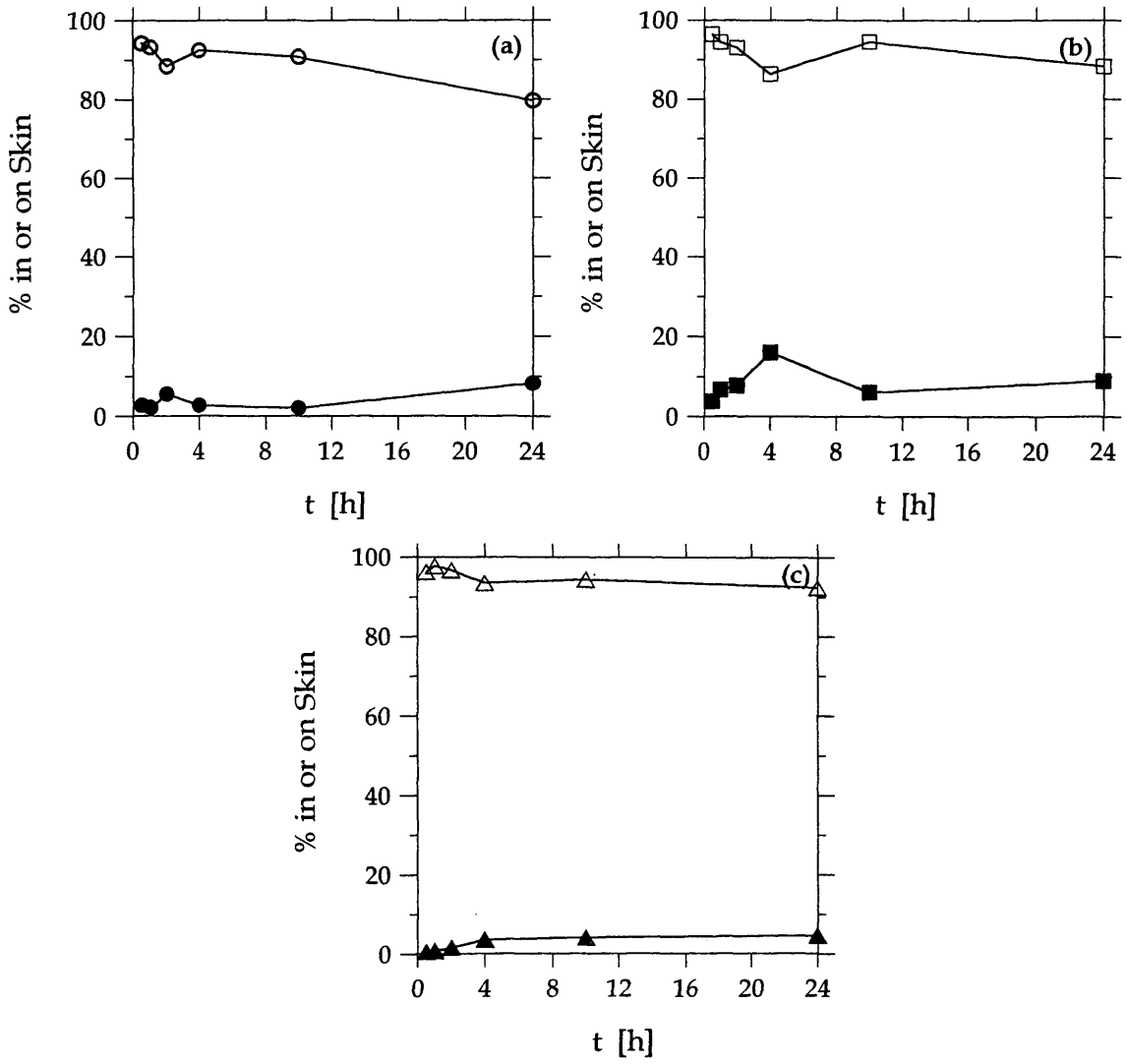

Figure 6IP.2 – Percent of applied dose on (open symbols) and in (closed symbols) the skin as a function of time for all doses: (a) L, (b) M, and (c) H.

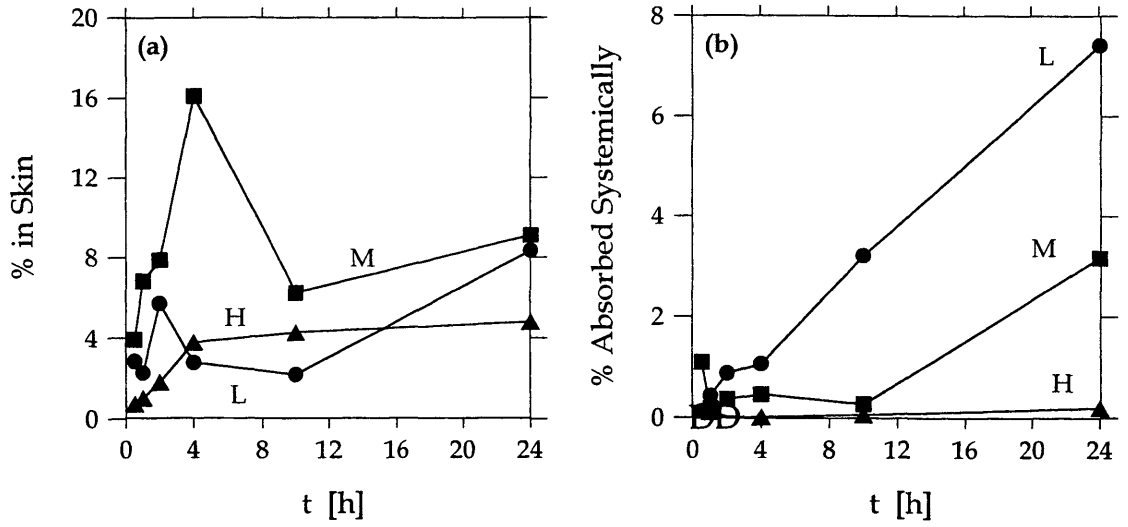

Figure 6IP.3 – Percent of applied dose (a) in the skin and (b) absorbed systemically as a function of time.

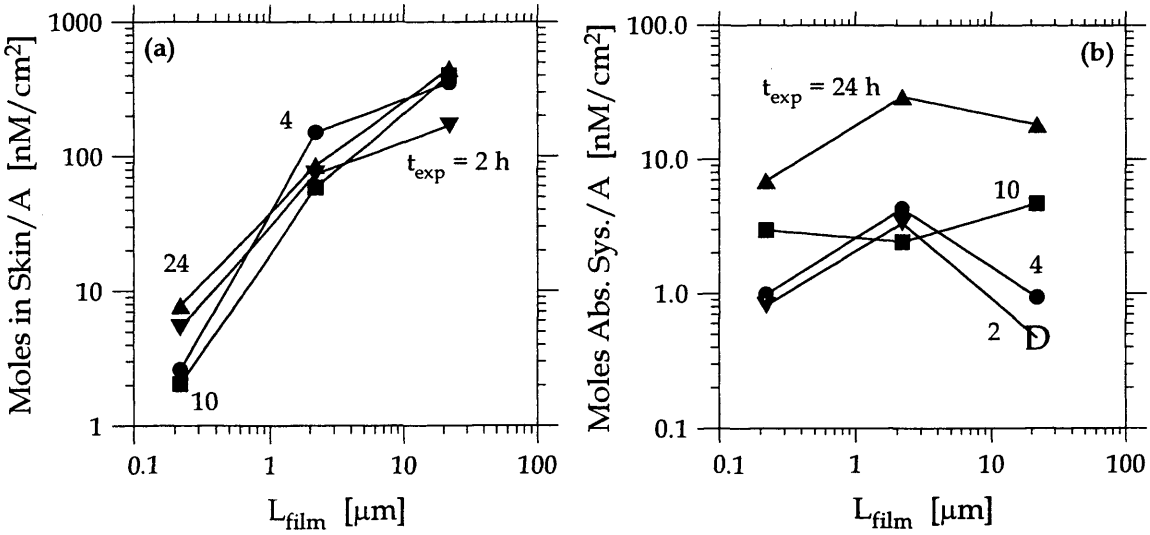

Figure 6IP.4 – Moles of chemical (a) in the skin and (b) absorbed systemically as a function of L_{film}.

Table 6IP.3 – Coefficients for best-fit lines through log-log plots of moles of chemical in the skin and absorbed systemically as a function of dose.

time, h	moles in skin		moles absorbed systemically	
	$\hat{S}$	$\hat{I}$	$\hat{S}$	$\hat{I}$
2	0.75	3.1	ND[a]	ND[a]
4	1.1	3.1	-0.11	0.47
10	1.1	2.7	0.098	1.1
24	0.88	3.5	0.21	2.6

[a] Calculation was not done because the two-hour data were below the detection limit.

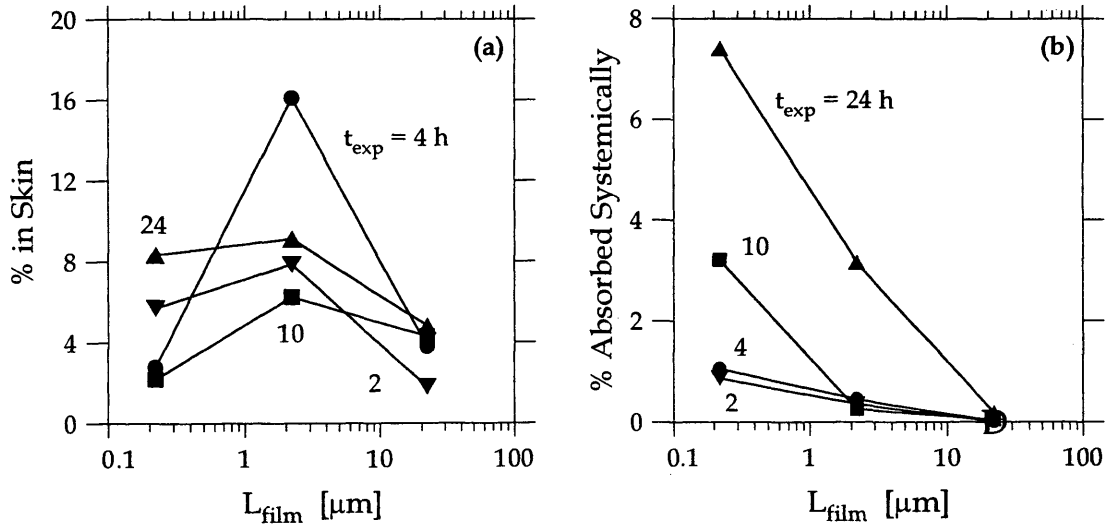

Figure 6IP.5 – Percent of applied dose (a) in the skin and (b) absorbed systemically as a function of L_{film}.

Isoxaflutole (IS)

Figure 6IS.1 shows the molecular structure of isoxaflutole, an herbicide used for broad-spectrum grass and broad-leaved weed control in maize. Its tradenames include Balance and Merlin. Isoxaflutole, a solid, hydrophilic pesticide ($\log K_{o/w} = 0.365$), is available as a suspension concentrate, a wettable powder, and as water dispersible granules (Tomlin, 1997). Table 6IS.1 shows the applied doses in the isoxaflutole study with the results listed in Table 6IS.2. Percent recoveries were greater than 90%, and the percent of applied dose on the enclosure and cover was always 1%. There is no evidence that isoxaflutole, with a vapor pressure of 0.001 mPa at 25°C (Tomlin, 1997), evaporated significantly.

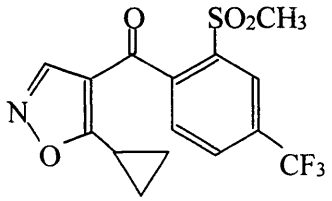

Figure 6IS.1 – Molecular structure of isoxaflutole.

Table 6IS.1 – Applied doses used in isoxaflutole study.

dose	moles /A , nM / cm^2	mass / A, µg / cm^2	L_{film}, µm
L	2.41	0.865	0.005
M	20.4	7.32	0.05
H	220.	79.0	0.50

Table 6IS.2 – Results of isoxaflutole dermal absorption study.[a]

Dose	Expo-sure	Enclosure and Cover	Skin Wash	Skin		Absorbed[b]		Total Recov-ery
	hours	%	%	%	nM/cm^2 [e]	%	nM/cm^2 [e]	%
L	0.5	0.27	92.2	2.81	0.067	ND[c]	ND[c]	95.6
	1	0.17	86.7	4.09	0.097	0.03	0.003	91.3
	2	0.30	92.9	7.53	0.181	0.03	0.0028	102
	4	0.38	86.2	8.87	0.209	1.81	0.0445	97.2
	10	0.42	82.6	12.0	0.289	3.46	0.0835	98.5
	24	0.83	84.1	11.9	0.287	4.42	0.106	101
M	0.5	0.06	100	2.01	0.409	ND[c]	ND[c]	102
	1	0.32	92.1	1.86	0.379	<0.005[d]	<0.003[d]	94.4
	2	0.41	86.5	1.11	0.225	0.14	0.0278	88.1
	4	0.33	96.0	2.89	0.582	0.28	0.0557	99.5
	10	0.15	92.0	3.54	0.721	0.54	0.111	96.2
	24	0.91	82.8	6.3	1.28	0.88	0.178	91.0
H	0.5	0.20	106	1.13	2.49	ND[c]	ND[c]	109
	1	0.40	95.0	1.38	3.03	ND[c]	ND[c]	96.8
	2	0.23	98.2	0.92	2.02	<0.005[d]	<0.011[d]	99.3
	4	0.34	103	1.35	2.97	0.08	0.175	105
	10	0.29	95.9	2.47	5.43	0.03	0.0668	98.7
	24	0.30	92.2	2.11	4.64	0.20	0.417	94.8

[a] Data are from the study with MRID 440447-02 dated 4/25/96. [b] Data include pesticide in blood, urine, feces, carcass, and cage wash/wipe. [c] None detected. [d] Detection limit. [e] Calculated from reported information (i.e., the percent in skin and absorbed systemically).

The percent of applied dose on and in the skin are shown in Figure 6IS.2 as a function of time. The percent on the skin did not decrease significantly over the course of the experiment because less than 16.3% absorbed into and through the skin.

Figure 6IS.3 shows the percent of applied dose in the skin and absorbed systemically as a function of time. By ten hours, the amount in skin was almost constant for doses L and H. The amount of chemical in the skin for dose M at 24 hours was larger than at 10 hours, which could be due to an ineffective skin wash resulting in a high amount of chemical in the skin. In Figure 6IS.3b the symbol "D" (for detection limit) marks either zero (i.e., when no chemical was detected) or the value that systemic absorption was reported as being less than (i.e., when at least one animal had an undetectable amount of systemic absorption, estimated as the detection limit). For all doses, the percent absorbed systemically increased with exposure time. The percent absorbed systemically was relatively small compared to the amount in the skin perhaps because isoxaflutole is relatively large (MW = 359) and would have a lower diffusion coefficient compared to other pesticides examined here. The percent in the skin and absorbed systemically were both largest for dose L.

Moles of isoxaflutole in the skin and absorbed systemically are shown in Figure 6IS.4 as a function of L_{film}. Coefficients of the best-fit lines for these data are listed in Table 6IS.3. The slope values ranged from 0.5-0.6 for the amount in the skin while for the amount systemically absorbed slope values were less than 0.3. Figure 6IS.5 shows that both the percent of applied dose in the skin and absorbed systemically decreased with increasing L_{film}. For systemic absorption, the effect of dose increased with time.

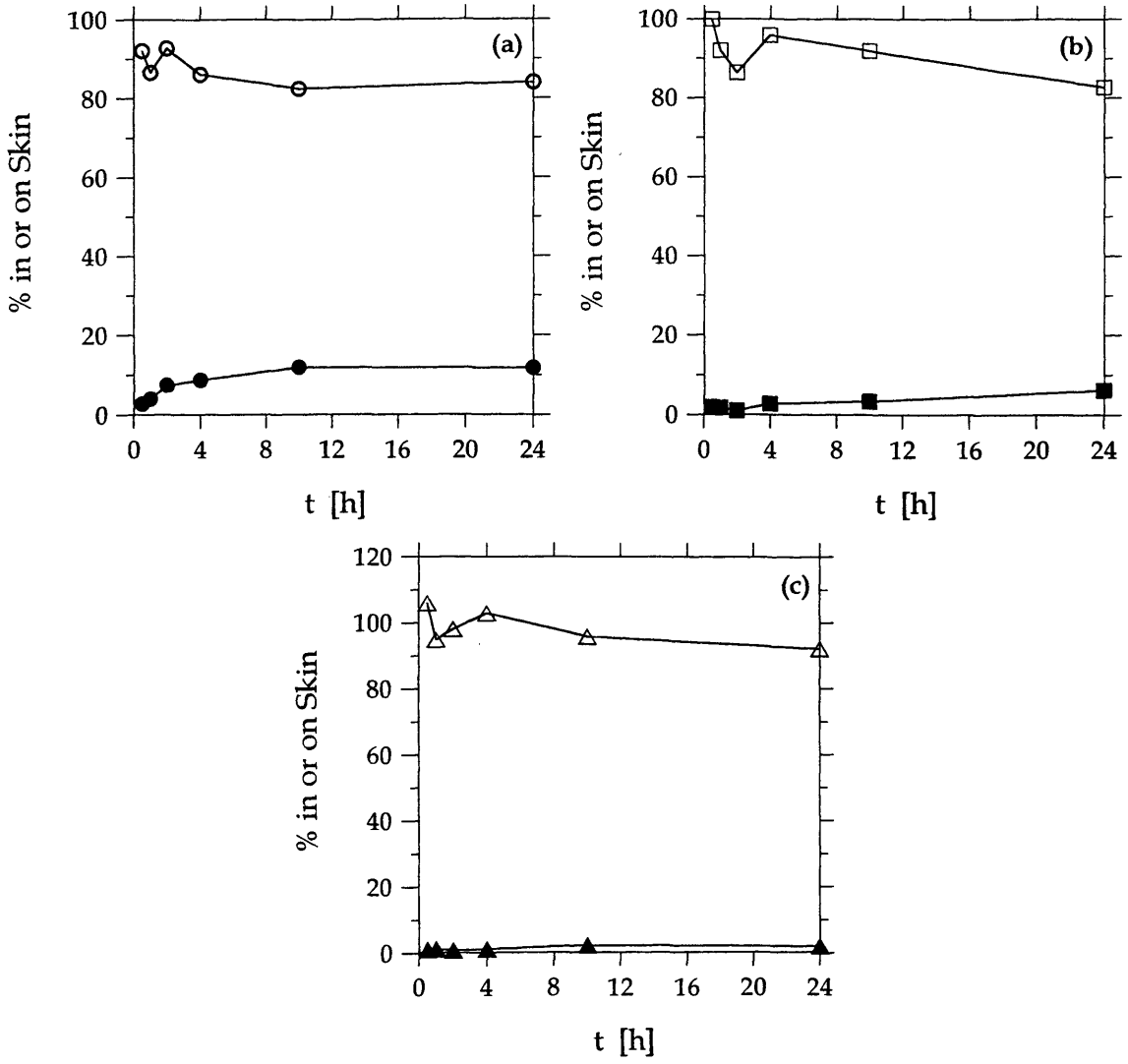

Figure 6IS-2 – Percent of applied dose on (open symbols) and in (closed symbols) the skin as a function of time for all doses: (a) L, (b) M, and (c) H.

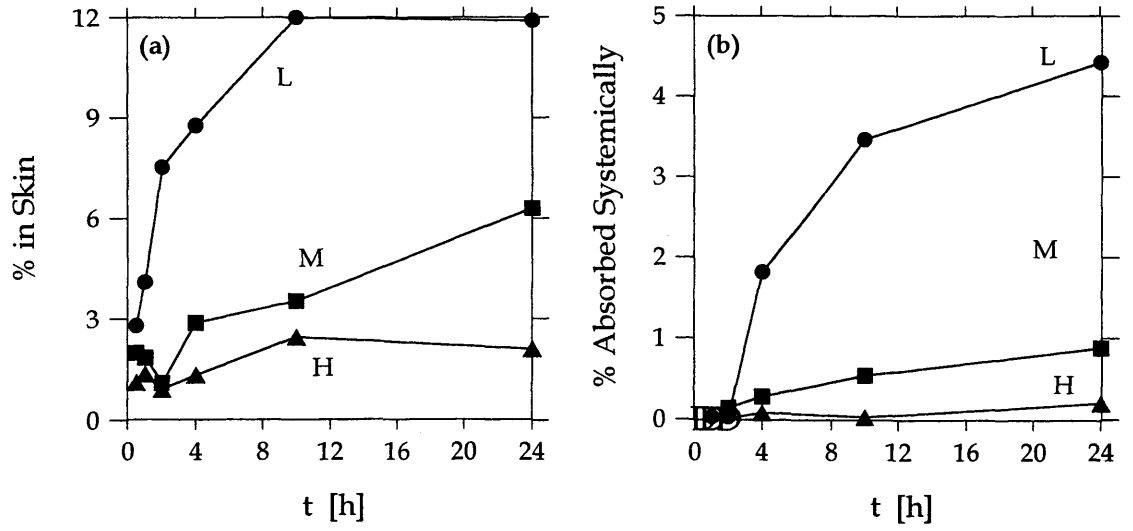

Figure 6IS.3 – Percent of applied dose (a) in the skin and (b) absorbed systemically as a function of time.

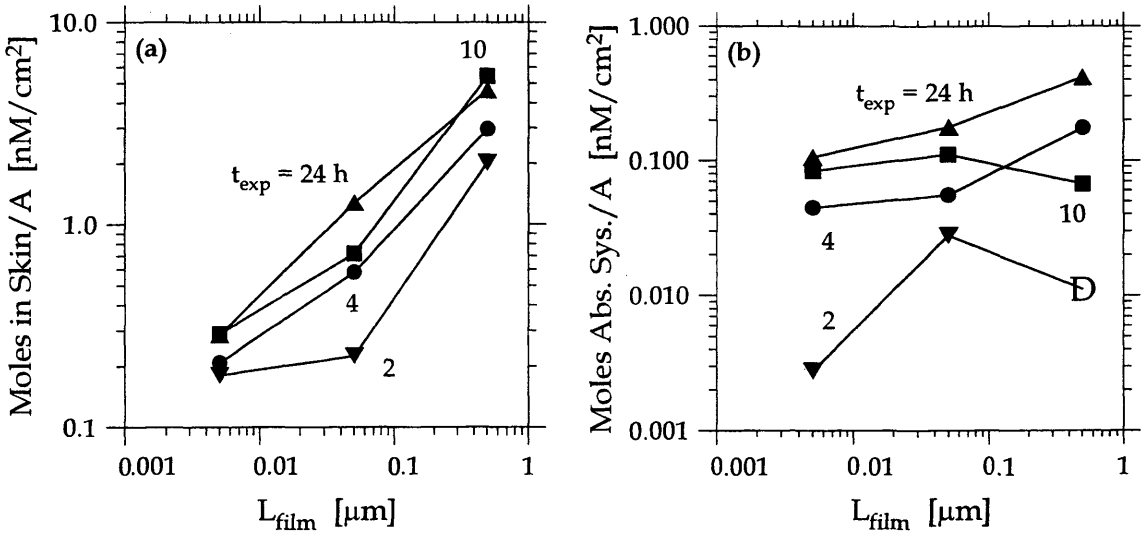

Figure 6IS.4 – Moles of chemical (a) in the skin and (b) absorbed systemically as a function of L_{film}.

Table 6IS.3 – Coefficients for best-fit lines through log-log plots of moles of chemical in the skin and absorbed systemically as a function of dose.

time, h	moles in skin		moles absorbed systemically[a]	
	$\hat{S}$	$\hat{I}$	$\hat{S}$	$\hat{I}$
2	0.52	0.74	ND[a]	ND[a]
4	0.58	1.4	0.30	-1.7
10	0.64	1.9	-0.049	-2.6
24	0.60	2.0	0.30	-0.72

[a] Calculation was not done because two-hour dose H data were below the detection limit.

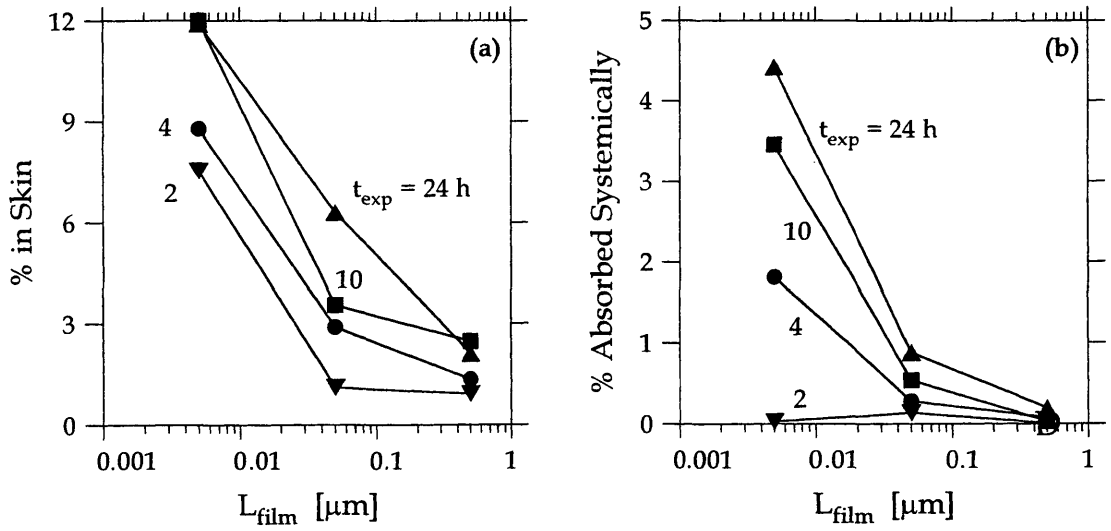

Figure 6IS.5 – Percent of applied dose (a) in the skin and (b) absorbed systemically as a function of L_{film}.

Lindane (LI)

The molecular structure of lindane, also known as gamma-HCH, is shown in Figure 6LI.1. Lindane is an insecticide used for control of a broad spectrum of phytophagous and soil-inhabiting insects, public health pests, and animal ectoparasites. It is used on a wide range of crops, in stored product warehouses and storerooms, in public health applications, and in seed treatments. Its tradenames include Gamma-Col, Lindamul, and Lintox. Lindane, a solid, highly lipophilic pesticide (log $K_{o/w}$ = 3.7), is available as granules, suspension and emulsifiable concentrates, wettable and dispersible powders, solutions for seed treatment, smoke generators, and ultra-low volume liquids (Tomlin, 1997). Table 6LI.1 shows the applied doses in the lindane study with the results listed in Table 6LI.2.

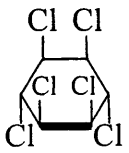

Figure 6LI.1 – Molecular structure of lindane.

Table 6LI.1 – Applied doses used in lindane study.

dose	moles /A , nM / cm^2	mass / A, µg / cm^2	L_{film}, µm
L	69	20.	0.11
M	687	200.	1.1
H	6872	2000.	11

Table 6LI.2 – Results of lindane dermal absorption study (Zendzian, 2000b).[a]

Dose	Exposure	Enclosure and Cover	Skin Wash	Skin		Absorbed[b]		Total Recovery
	hours	%	%	%	nM/cm^2	%	nM/cm^2	%
L	0.5	1.50	78.92	11.39	7.86	0.60	0.41	93.11
	1	2.10	55.98	24.46	16.63	3.34	2.30	86.94
	2	1.96	41.24	31.61	21.81	4.55	3.14	80.27
	4	2.61	38.53	30.68	21.17	10.09	6.96	82.84
	10	2.55	43.34	17.55	12.01	18.07	12.47	82.59
	24	1.81	21.00	7.15	4.93	27.72	19.13	58.35
M	0.5	0.42	89.84	8.48	58.26	0.96	6.59	101.08
	1	0.54	72.36	15.99	109.85	2.42	16.63	92.73
	2	0.65	55.56	22.99	157.94	2.61	17.93	83.66
	4	0.91	55.78	26.91	184.87	5.27	36.20	90.24
	10	0.96	66.32	13.25	91.03	8.31	57.09	90.40
	24	2.05	39.35	5.50	37.79	20.86	143.31	70.19
H	0.5	0.05	73.16	6.85	470.7	0.66	45.36	82.13
	1	0.08	74.79	7.37	506.47	1.00	68.72	85.29
	2	0.71	76.57	4.01	275.57	1.50	103.08	84.15
	4	0.30	73.58	5.04	346.35	2.03	139.56	83.26
	10	1.73	66.04	4.33	297.56	2.81	193.10	76.20
	24	0.14	64.80	2.85	195.85	5.05	347.04	74.19

[a] Data are from the study with MRID 400561-07 dated 1/13/87. [b] Data include pesticide in urine, feces, carcass, and cage wash/wipe.

As shown in Figure 6LI.2, percent recoveries were as low as 58%, worsened with increasing exposure time, and were poorest for dose L. The percent of applied dose on the enclosure and cover was always < 3%. The summary report for lindane did not specify that the cover included an activated carbon filter. If a carbon trap was not used, it is quite possible that evaporation is responsible for the poor recoveries. The vapor pressure of lindane (5.6 mPa at 20°C (Tomlin, 1997)) is similar in magnitude to vapor pressures of other evaporating pesticides. For example, disulfoton with a vapor pressure of 13 mPa at 25°C (Tomlin, 1997) is known to evaporate (Zendzian, 2000), and we suspect that thiobencarb with a vapor pressure of 2.93 mPa at 23°C (Tomlin, 1997) evaporates for reasons similar to those specified here for lindane.

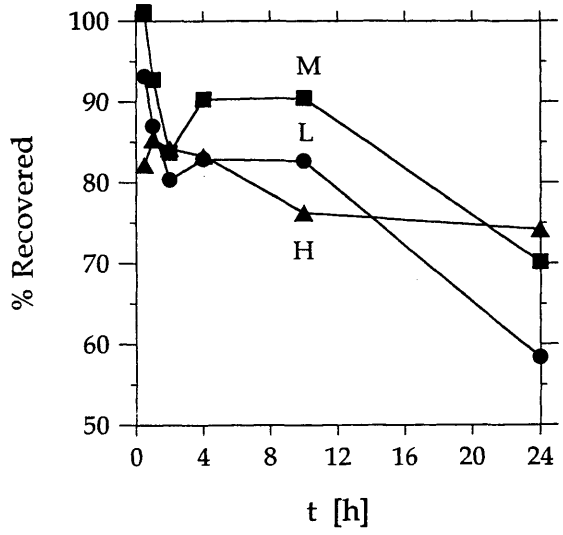

Figure 6LI.2 – Percent of applied dose recovered as a function of time.

The percent of applied dose on and in the skin are shown in Figure 6LI.3 as a function of time. By 24 hours, the percent on the skin had decreased significantly to 21% for dose L and to 65% for dose H because of dermal absorption and perhaps evaporation. For doses L and M, the amount in the skin was affected by the decreasing amount on the skin at 10 and 24 hours and possibly at 4 hours. Figure 6LI.4 shows the percent of the applied dose in the skin and absorbed systemically as a function of time. The percent in the skin for dose L is similar to that of dose M while dose H was always smaller. Even though the percent in skin decreased significantly after 4 hours for doses L and M, the percent absorbed systemically increased with time for all doses.

Moles in the skin and absorbed systemically are shown in Figure 6LI.5 as a function of L_{film}. The 10 and 24-hour data were more linear than the 2 and 4-hour data. This could be because the amount in skin for doses L and M was lower than might be expected due to the significant drop in the amount of lindane on the skin for exposure times longer than 4 hours. Moles absorbed systemically increased with dose and time. Coefficients for best-fit lines through these data are listed in Table 6LI.3. Slope values for amount in the skin increased with exposure time perhaps because the amount of lindane on skin decreased with increasing time. In contrast, slope values for the amount absorbed systemically were essentially independent of exposure time. Notably, for the 2 and 4-hour exposures the slopes for the amount absorbed systemically were larger than the slopes for the amount in the skin, which is unusual.

Percent of the applied dose in the skin and absorbed systemically are shown in Figure 6LI.6 as a function of L_{film}. For the 2 and 4-hour exposures, the percent in skin decreased with dose more dramatically than did the 10 and 24-hour exposure data. This is consistent with the decreased amount of lindane on the skin. The percent absorbed systemically also decreased with dose and more dramatically as exposure time increased.

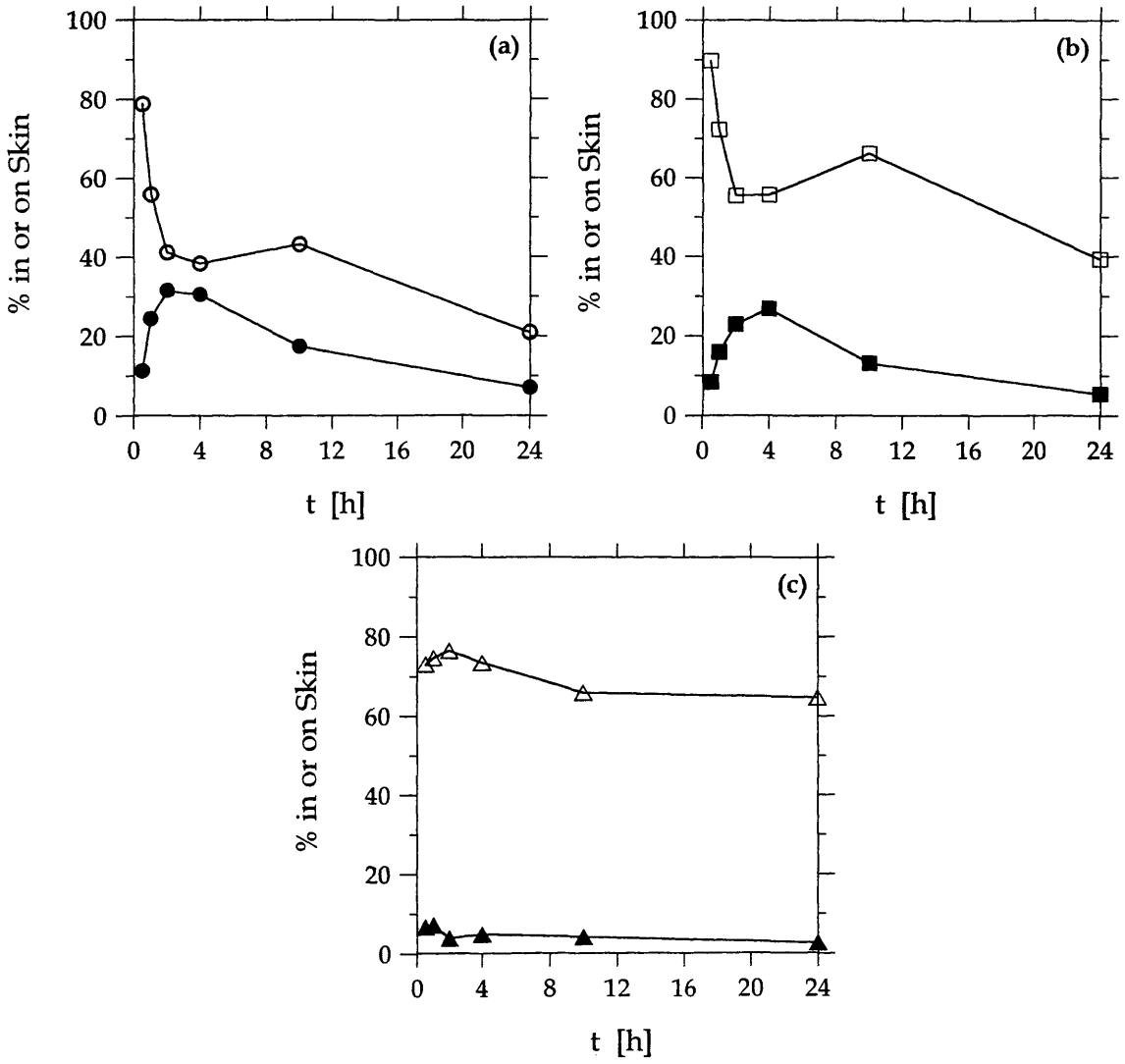

Figure 6LI.3 – Percent of applied dose on (open symbols) and in (closed symbols) the skin as a function of time for all doses: (a) L, (b) M, and (c) H.

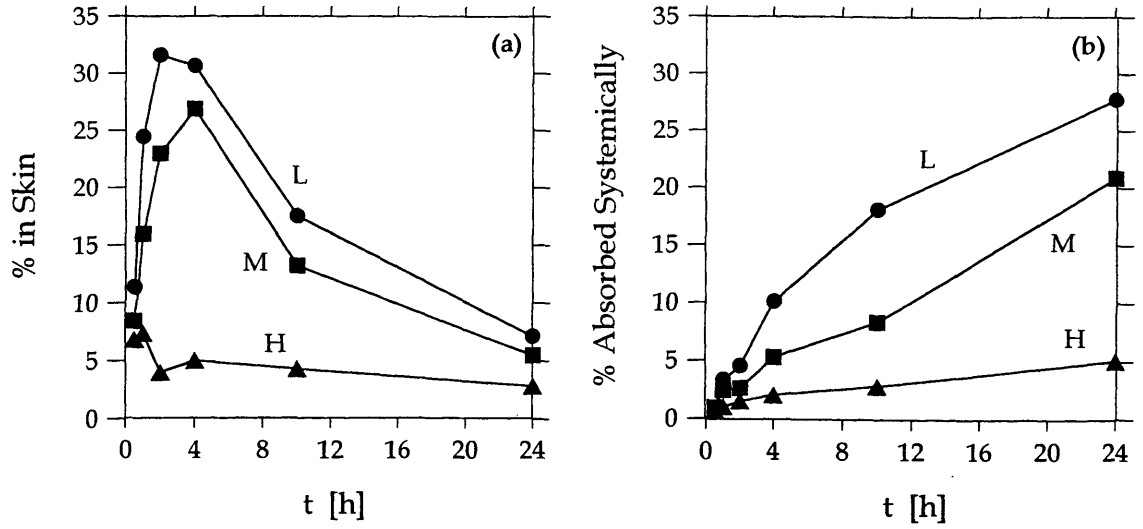

Figure 6LI.4 – Percent of applied dose (a) in the skin and (b) absorbed systemically as a function of time.

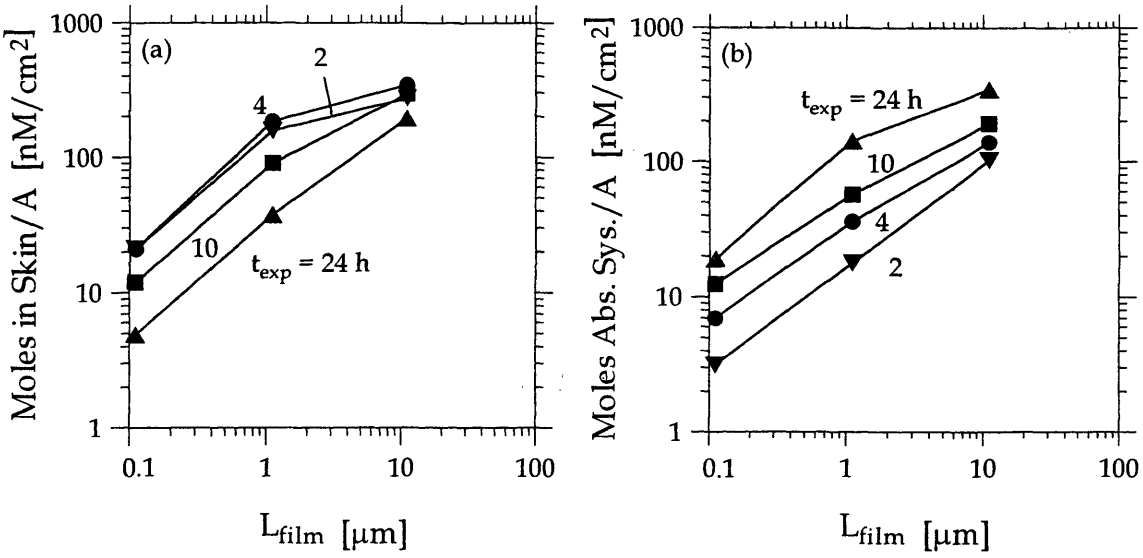

Figure 6LI.5 – Moles of chemical (a) in the skin and (b) absorbed systemically as a function of L_{film}.

Table 6LI.3 – Coefficients for best-fit lines through log-log plots of moles of chemical in the skin and absorbed systemically as a function of dose.

time, h	moles in skin		moles absorbed systemically	
	$\hat{S}$	$\hat{I}$	$\hat{S}$	$\hat{I}$
2	0.56	4.5	0.76	2.8
4	0.61	4.6	0.65	3.4
10	0.70	4.2	0.59	3.9
24	0.80	3.4	0.63	4.5

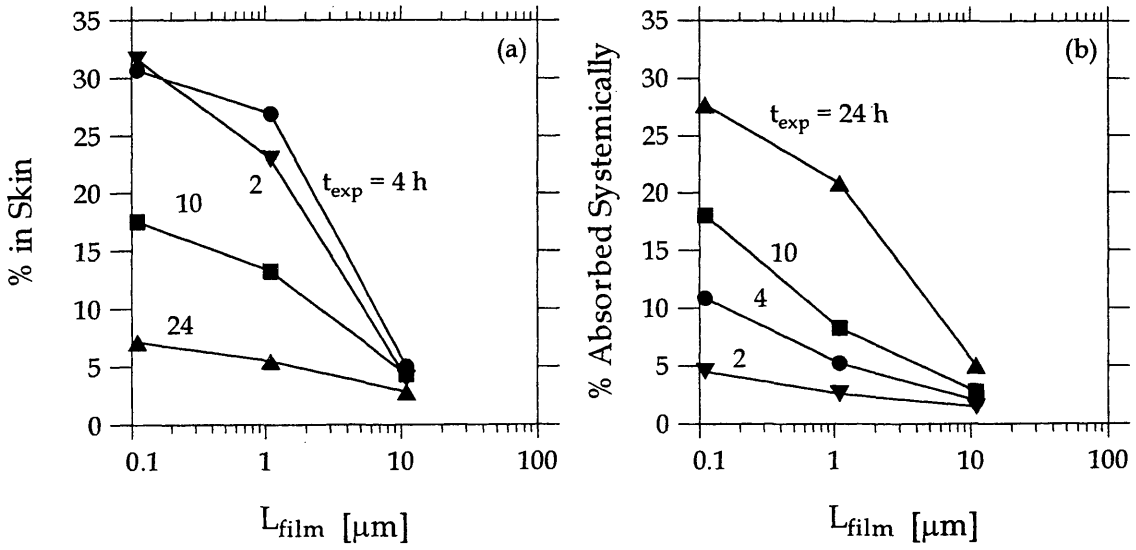

Figure 6LI.6 – Percent of applied dose (a) in the skin and (b) absorbed systemically as a function of L_{film}.

Metolachlor (MT)

Figure 6MT.1 shows the molecular structure of metolachlor, which is an herbicide used for control of annual grasses and some broad-leaved weeds in maize, sorghum, fruit and nut trees, potatoes, and many others plants. Its tradenames include Dual. Metolachlor, a lipophilic ($\log K_{o/w} = 2.9$), liquid pesticide, is available as wettable and dispersible powders, as a microgranule, and as an emulsifiable concentrate (Tomlin, 1997). Table 6MT.1 shows the applied doses in the metolachlor study with results listed in Table 6MT.2.

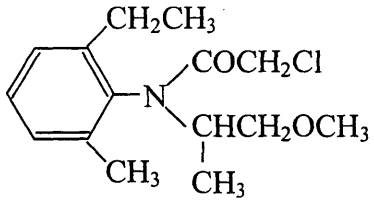

Figure 6MT.1 – Molecular structure of metolachlor.

Table 6MT.1 – Applied doses used in metolachlor study.

dose	moles /A , nM / cm^2	mass / A, μg / cm^2	L_{film}, μm
L	35.2	10	0.089
M	352	100	0.89
H	3520	1000	8.9

Table 6MT.2 – Results of metolachlor dermal absorption study.[a]

Dose	Exposure	Unabsorbed Removable[b]	Skin		Absorbed[c]		Total Recovery
	hours	%	%	nM/cm^2	%	nM/cm^2	%
L	2	59.51	30.79	10.84	14.05	4.95	104.35
	4	48.46	30.86	10.86	23.29	8.20	102.62
	10	37.60	24.66	8.68	32.93	11.59	95.19
	24	23.05	11.09	3.90	62.84	22.12	96.98
M	2	68.14	24.12	84.90	5.15	18.13	97.41
	4	65.08	23.61	83.12	7.95	27.98	96.64
	10	54.83	20.89	73.56	20.26	71.32	95.98
	24	48.70	19.14	67.37	26.85	94.51	94.72
H	2	86.76	15.94	561.1	1.68	59.14	104.38
	4	84.38	11.98	421.7	3.84	135.2	100.20
	10	78.06	12.69	446.8	6.98	245.7	97.73
	24	63.93	15.949	545.2	16.15	568.5	95.58

[a] Data are from the study with MRID 418331-02 dated 8/25/87. [b] Data include the pesticide found in the bandage, bridge wash, paper rinse, paper, soap rinse, water rinse, gauze A, and gauze B. [c] Data include pesticide found in the blood, urine, feces, carcass, and cage wash.

The metolachlor study summary did not report the amount of pesticide on the enclosure and cover separately from the amount washed from the skin. The vapor pressure of metolachlor (4.2 mPa at 25°C (Tomlin, 1997)) is similar to those of pesticides that evaporated (e.g., lindane with a vapor pressure of 5.6 mPa at 20°C (Tomlin, 1997)). Since the percent recoveries were nearly 100% and did not change with time, if metolachlor did evaporate it was trapped in the covering material. Consequently, based on the data reported it is impossible to know whether or not metolachlor evaporated.

As shown in Table 6MT.2, the metolachlor study reported the "unabsorbed removable," which combines pesticide from the enclosure and cover with pesticide washed from the skin. Figure 6MT.2 shows the percent of applied dose in the skin and unabsorbed removable as a function of time for all doses. For dose L only 23% of the applied dose was unabsorbed removable at 24 hours. Thus, for dose L and possibly dose M the amount in the skin decreased as the amount in the unabsorbed removable decreased. Figure 6MT.3 shows the percent of applied dose in the skin and absorbed systemically as a function of time. For doses M and H, the percent in skin was basically independent of time, while the percent in skin decreased from about 31% at 4hours to about 11% at 24 hours. For all three doses, the percent absorbed systemically increased with time.

Figure 6MT.4 shows the moles in the skin and absorbed systemically as a function of L_{film}. Coefficients of the best-fit lines for these data are listed in Table 6MT.3. Slope values for the amount in the skin were about 0.8, except at 24 hours, which was 1.1. The slope for the 24-hour data reflected the reduced amount in the skin for dose L. Slope values for the amount absorbed systemically all have smaller values (0.5 - 0.7) than those of the amount in the skin, but demonstrated the same trends. As shown in Figure 6MT.5, both the percent of applied dose in the skin and absorbed systemically decreased with increasing L_{film}. For the percent in the skin, the 24-hour data looked linear because the decreased mass of chemical on the skin was sufficient to affect the amount in the skin.

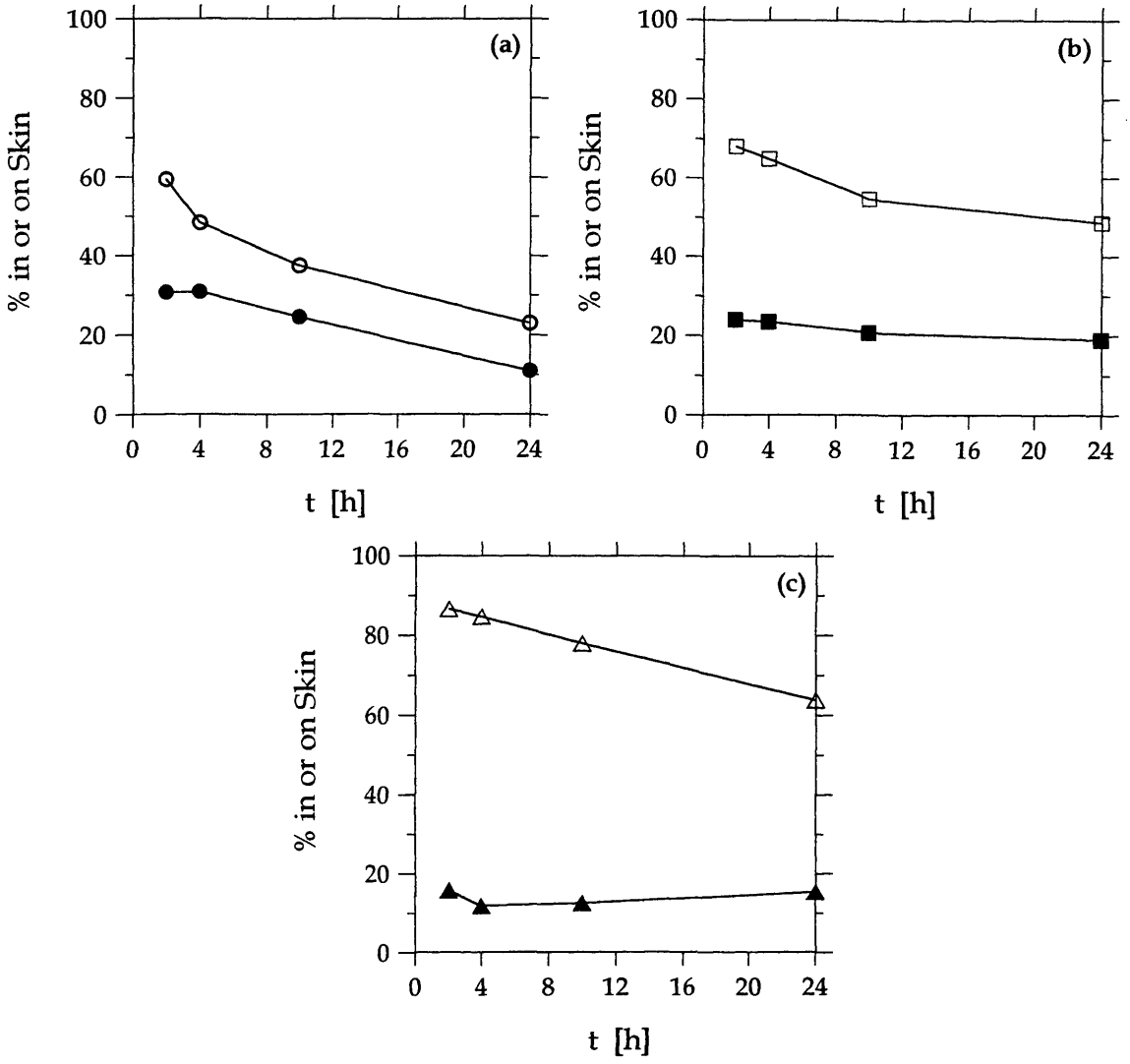

Figure 6MT.2 – Percent of applied dose found to be unabsorbed removable (open symbols) and percent of applied dose in the skin (closed symbols) as a function of time for all doses: (a) L, (b) M, and (c) H.

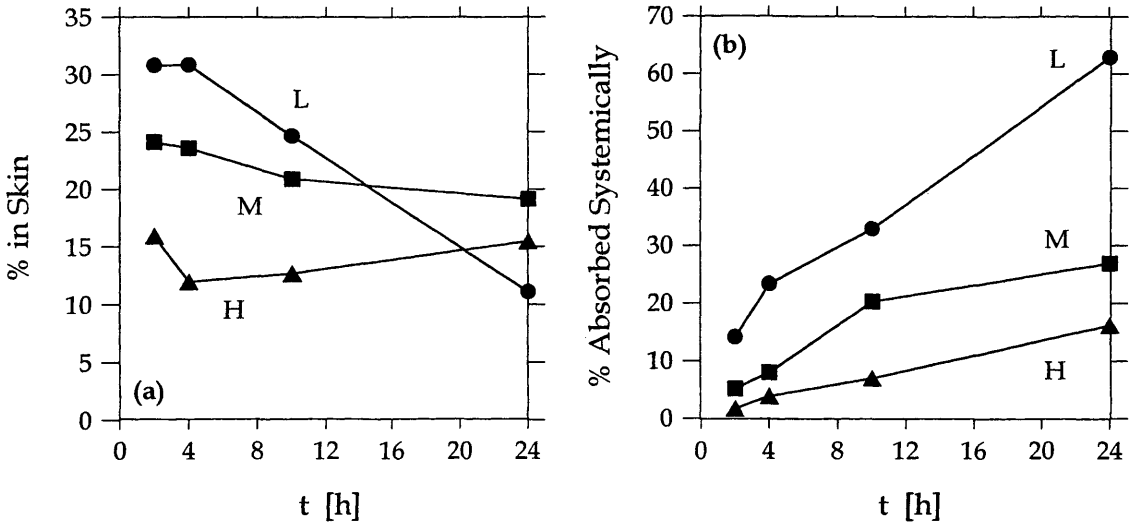

Figure 6MT.3 – Percent of applied dose (a) in the skin and (b) absorbed systemically as a function of time.

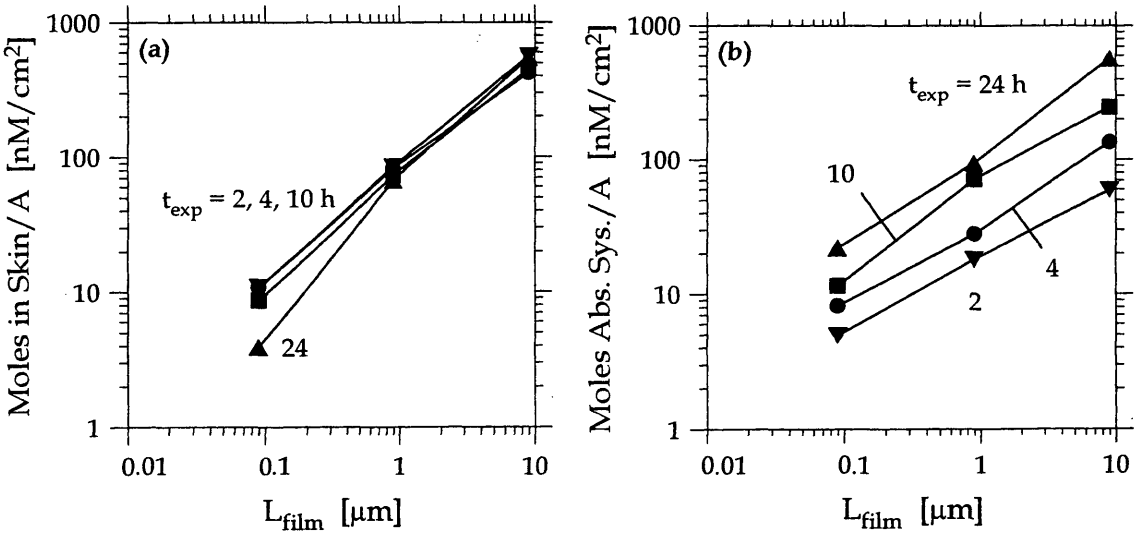

Figure 6MT.4 – Moles of chemical (a) in the skin and (b) absorbed systemically as a function of L_{film}.

Table 6MT.3 – Coefficients for best-fit lines through log-log plots of moles of chemical in the skin and absorbed systemically as a function of dose.

time, h	moles in skin		moles absorbed systemically	
	$\hat{S}$	$\hat{I}$	$\hat{S}$	$\hat{I}$
2	0.86	4.5	0.66	4.1
4	0.79	4.4	0.61	3.5
10	0.86	4.3	0.54	2.9
24	1.1	4.1	0.70	4.7

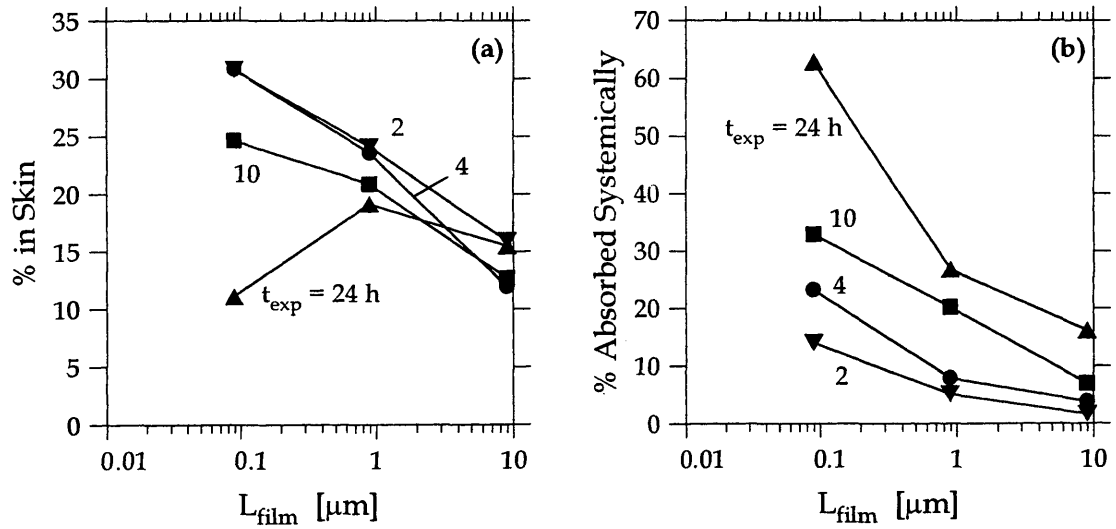

Figure 6MT.5 – Percent of applied dose (a) in the skin and (b) absorbed systemically as a function of L_{film}.

Mevinphos (MV)

The molecular structure of mevinphos is shown in Figure 6MV.1. Mevinphos is an insecticide and acaricide used for control of chewing and sucking insects and spider mites on a wide variety of crops including berry fruit, melons, hops, eggplants and strawberries. Its tradenames include Phosdrin, Duraphos, and Mevindrin. Mevinphos, a liquid, slightly lipophilic pesticide, ($\log K_{o/w} = 0.127$) is available as soluble and emulsifiable concentrates (Tomlin, 1997). Table 6MV.1 shows the applied doses used in the mevinphos study with the results listed in Table 6MV.2.

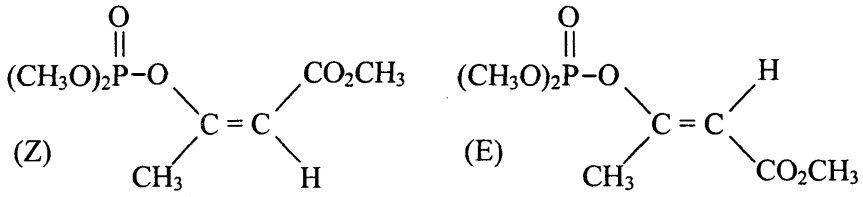

Figure 6MV.1 – Molecular structure of mevinphos. The technical grade of mevinphos contains > 60% m/m of the (E) isomer and about 20% m/m of the (Z) isomer.

Table 6MV.1 – Applied doses used in mevinphos study.

dose	moles /A , nM / cm^2	mass / A, µg / cm^2	L_{film}, µm
L	2	0.5	0.004
M	11	2.5	0.021
H	56	13	0.11

Table 6MV.2 – Results of mevinphos dermal absorption study (Zendzian, 2000b).[a]

Dose	Exposure	Enclosure and Cover[b]	Skin Wash	Skin		Absorbed[c]		Total Recovery
	hours	%	%	%	nM/cm^2	%	nM/cm^2	%
L	6	25.86	23.79	32.08	0.64	12.33	0.25	94.12
	10	26.25	19.61	35.87	0.72	11.75	0.24	93.49
	24	23.35	21.20	30.15	0.60	13.97	0.28	91.80
M	6	21.21	24.87	35.26	3.88	11.75	1.29	93.09
	10	16.56	19.93	34.34	3.77	13.15	1.45	93.97
	24	20.33	19.34	31.82	3.50	13.85	1.52	89.30
H	6	27.18	16.12	32.17	18.02	16.77	9.39	92.24
	10	24.52	15.99	36.02	20.17	15.47	8.68	92.08
	24	27.23	16.62	24.85	13.92	20.21	11.32	89.83

[a] Data are from the study with MRID 429338-01 dated 8/31/93. [b] An activated charcoal filter was used in the cover. [c] Data include pesticide in blood, urine, feces, carcass, cage wash, and expired CO_2.

Percent recoveries were always greater than 89%. The percent of applied dose found on the enclosure and cover, shown in Figure 6MV.2, was high (> 16.6%), but constant after 6 hours, the earliest time reported. In addition, the percent on the enclosure and cover was probably constant with dose. Mevinphos has a relatively high vapor pressure (17 mPa at 20°C (Tomlin, 1997)), and it is likely that most of the pesticide on the enclosure and cover was from evaporation.

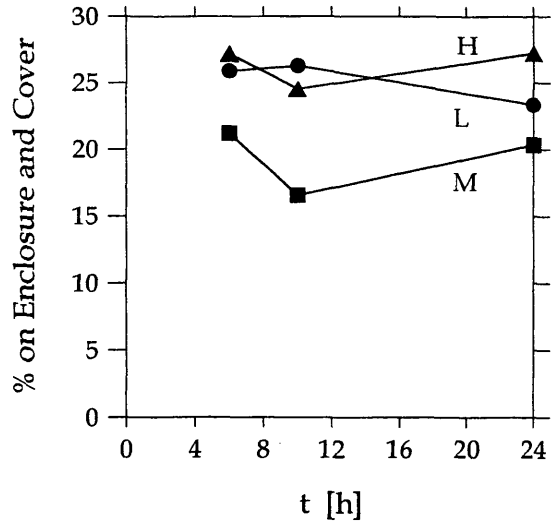

Figure 6MV.2 – Percent of dose on the enclosure and cover as a function of time.

The percent of applied dose on and in the skin are shown in Figure 6MV.3 as a function of time. The amount on the skin was always less than the amount in the skin. Figure 6MV.4 shows the percent of applied dose in the skin and absorbed systemically as a function of time. Both the percent in the skin and absorbed systemically were nearly independent of time. There was probably no significant difference between doses for the percent in the skin or absorbed systemically. Oddly, the percent in the skin and absorbed systemically had increased significantly by 6 hours, but changed only slightly in the next 18 hours. Even if the decrease in the amount on the skin caused the rate of dermal absorption into the skin to decrease, the chemical in the skin should still have transferred into systemic absorption unless mevinphos binds in the sc.

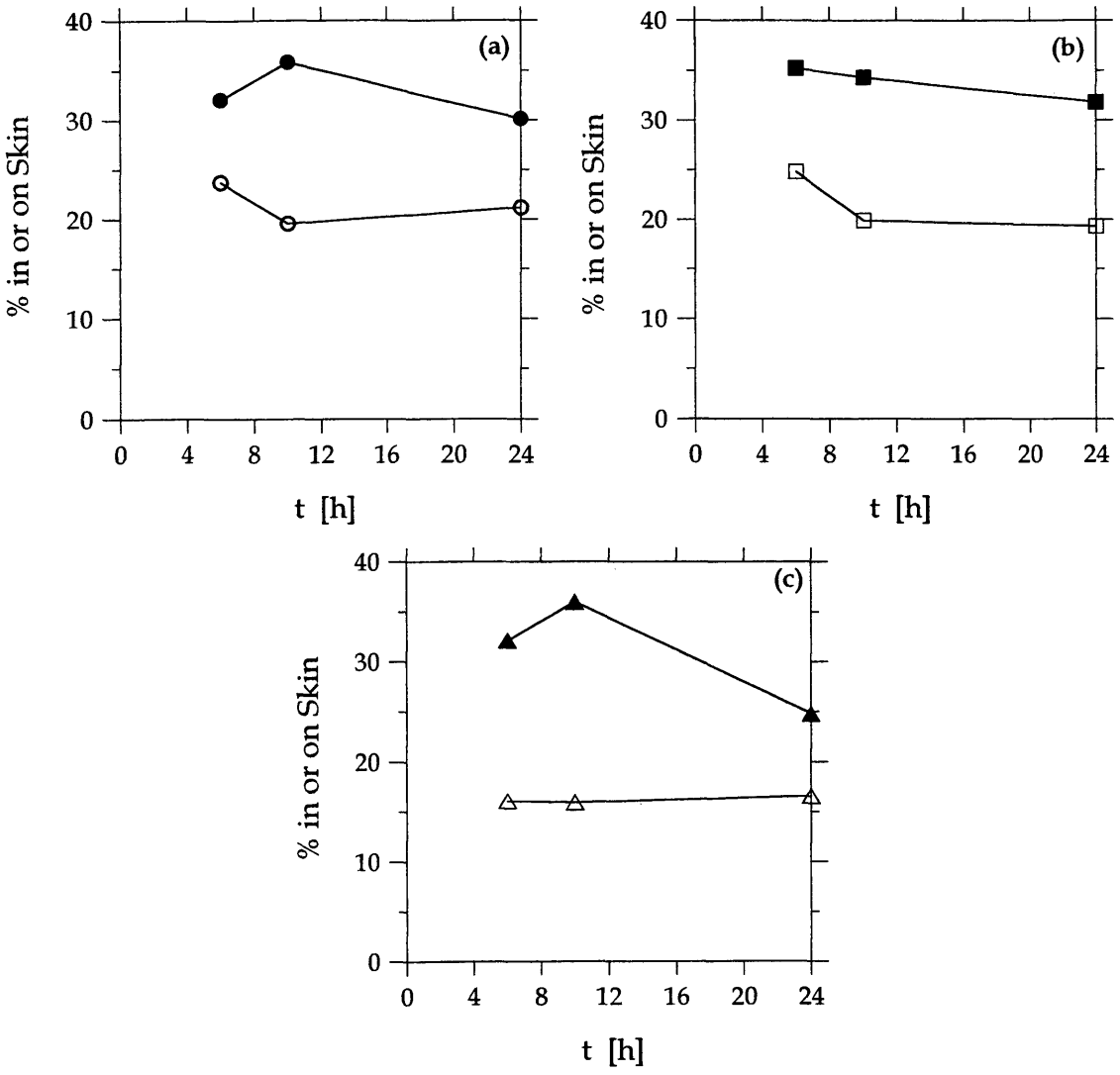

Figure 6MV.3 – Percent of dose on (open symbols) and in (closed symbols) the skin as a function of time for all doses: (a) L, (b) M, and (c) H.

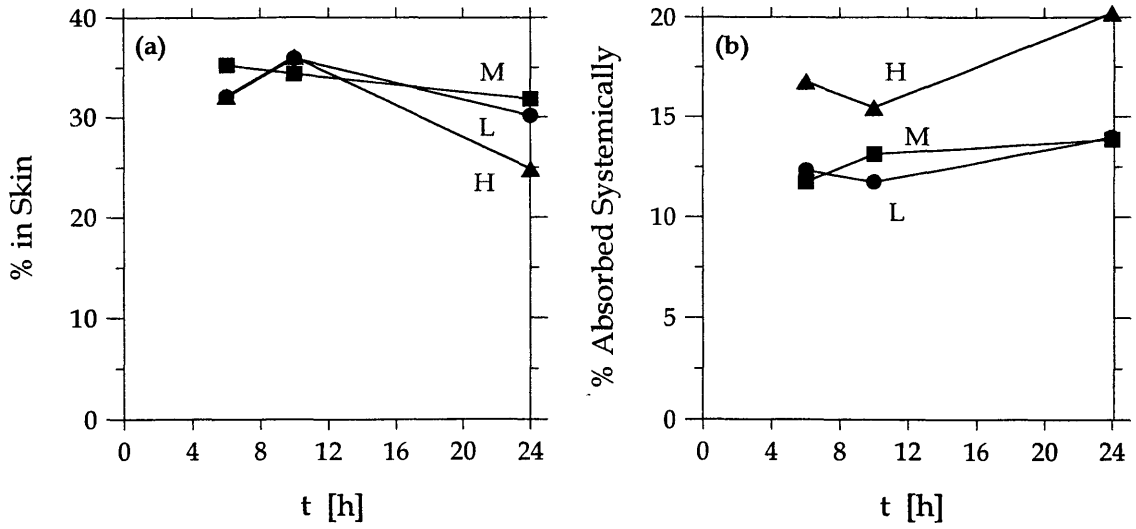

Figure 6MV.4 – Percent of applied dose (a) in the skin and (b) absorbed systemically as a function of time.

Moles in the skin and absorbed systemically are shown in Figure 6MV.5 as a function of L_{film}. Coefficients of the best-fit lines for these data are listed in Table 6MV.3. For moles in the skin, the slope values were all about 1. For moles absorbed systemically, the slope values were about 1.1. It is unusual for the slope of the amount absorbed systemically to be larger than the slope for the amount in the skin, but perhaps the difference between the slope values were not statistically significant. Figure 6MV.6 shows that the percent of applied dose in the skin and absorbed systemically were both relatively independent of L_{film}.

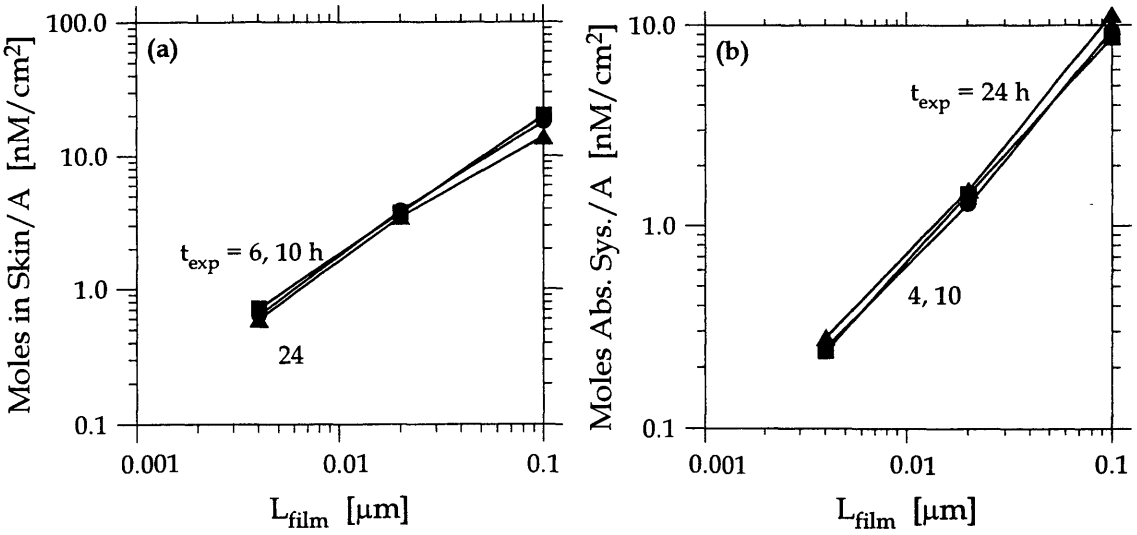

Figure 6MV.5 – Moles of chemical (a) in the skin and (b) absorbed systemically as a function of L_{film}.

Table 6MV.3 – Coefficients for best-fit lines through log-log plots of moles of chemical in the skin and absorbed systemically as a function of dose.

time, h	moles in skin		moles absorbed systemically	
	$\hat{S}$	$\hat{I}$	$\hat{S}$	$\hat{I}$
6	1.0	5.3	1.1	4.8
10	1.0	5.4	1.1	4.7
24	0.98	4.9	1.1	5.0

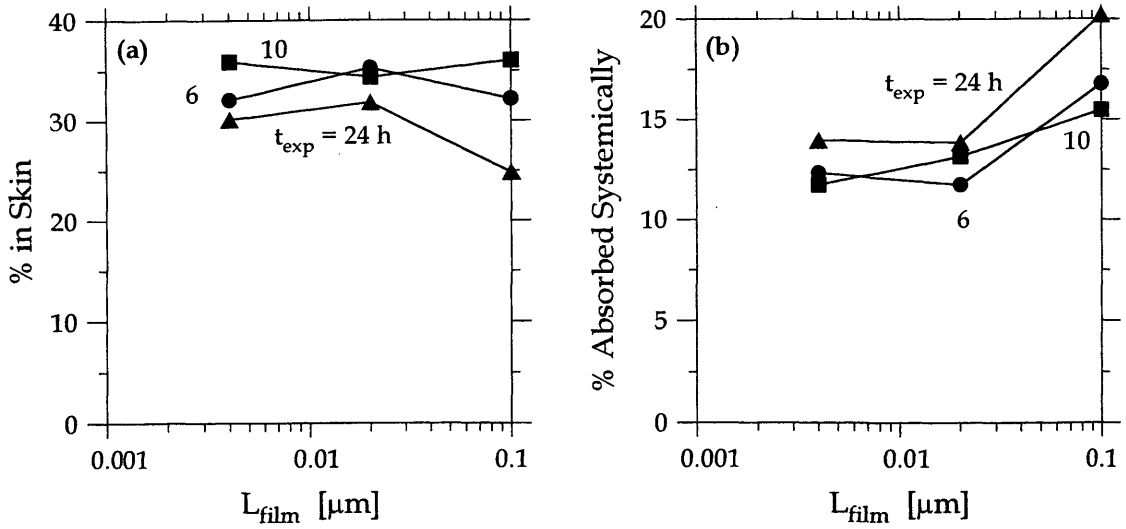

Figure 6MV.6 – Percent of applied dose (a) in the skin and (b) absorbed systemically as a function of L_{film}.

Molinate (MO)

The molecular structure of molinate is shown in Figure 6MO.1. Molinate is an herbicide used for control of germinating broad-leaved and grass weeds in rice. Its tradenames include Ordram and Sakkimol. Molinate, a liquid, moderately lipophilic pesticide ($\log K_{o/w} = 2.88$), is available as granules and as an emulsifiable concentrate (Tomlin, 1997). Table 6MO.1 shows applied doses used in the molinate study with the results listed in Table 6MO.2.

Figure 6MO.1 – Molecular structure of molinate.

Table 6MO.1 – Applied doses used in molinate study.

dose	moles /A , nM / cm^2	mass / A, μg / cm^2	L_{film}, μm
L	48	8.9	0.084
M	478	89.3	0.84
H	4775	892.9	8.4

Table 6MO.2 – Results of molinate dermal absorption study.[a]

Dose	Exposure	Volatile[b]	Skin Wash	Skin		Absorbed[c]		Total Recovery
	hours	%	%	%	nM/cm^2 [d]	%	nM/cm^2 [d]	%
L	4	28.9	12.20	8.84	4.225	24.42	11.60	74.36
	10	37.2	11.98	3.84	1.818	23.42	11.12	76.44
	24	21.4	7.34	3.24	1.551	46.55	22.14	78.53
M	4	26.9	30.5	6.75	32.25	24.82	118.2	66.97
	10	35.5	8.0	6.22	29.68	37.75	180.2	77.47
	24	48.5	2.8	2.94	14.06	31.85	151.9	85.29
H	4	10.5	52.4	4.26	203.4	17.33	827.3	84.49
	10	24.7	17.9	4.82	230.2	34.86	1664.	82.28
	24	42.0	2.8	2.53	120.8	38.86	1856.	86.19

[a] Data are from the study with MRID 43284101 dated 1/10/91. [b] Data include pesticide in charcoal extract, charcoal residue, and sinter washings. [c] Data include pesticide from urine, fecal extract, fecal residue, cage wash, final cage wash, cage debris, and carcass. [d] Calculated from percent of applied dose in skin and absorbed.

Percent recoveries, shown in Figure 6MO.2, were low (i.e., many were less than 80%), especially for low doses. Figure 6MO.3 shows the percent of applied dose found in the charcoal extract, charcoal residue, and sinter washings as a function of time. Molinate evaporation increased with exposure time for doses M and H and through 10 hours for dose L. Significant amounts of molinate, which has a vapor pressure of 746 mPa at 25°C (Tomlin, 1997), evaporated (e.g., as much as 50% at 24 hours for dose M).

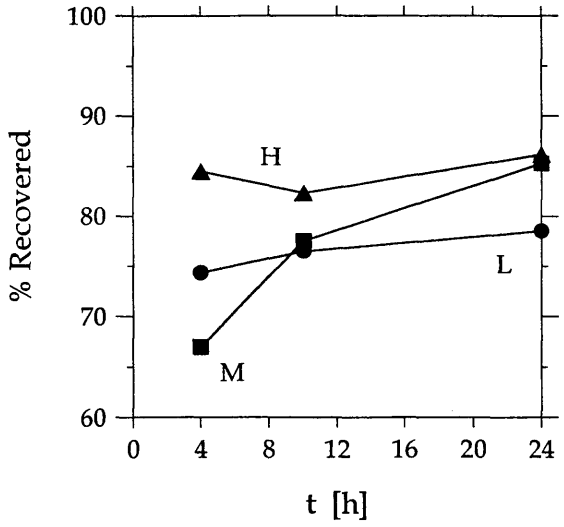

Figure 6MO.2 – Percent of applied dose recovered as a function of time.

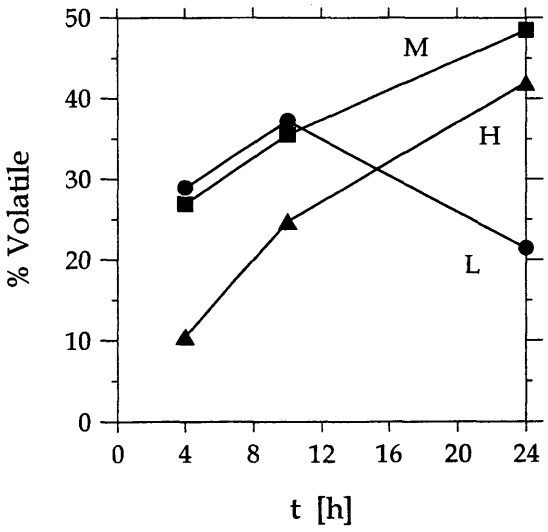

Figure 6MO.3 – Percent of applied dose on the charcoal extract, charcoal residue, and sinter washings as a function of time.

Percent of applied dose on and in the skin are shown in Figure 6MO.4 as a function of time. By four hours, only 12% of dose L remained on the skin, and by 24 hours, only 5 - 10% were left for all three doses. As a result, the percent in skin decreased with increasing exposure time for all three doses.

Figure 6MO.5 shows the percent of applied dose in the skin and absorbed systemically as a function of time. Even though the amount on and in the skin decreased with exposure increasing time, the amount absorbed systemically increased with time. Moles in the skin and absorbed systemically are shown in Figure 6MO.6 as a function of L_{film}. Coefficients of the best-fit lines for these data are listed in Table 6MO.3. At each exposure time, the slope values for the amount in the skin and absorbed systemically were almost the same. Figure 6MO.7 shows that both the percent of applied dose in the skin and absorbed systemically were essentially independent of L_{film}.

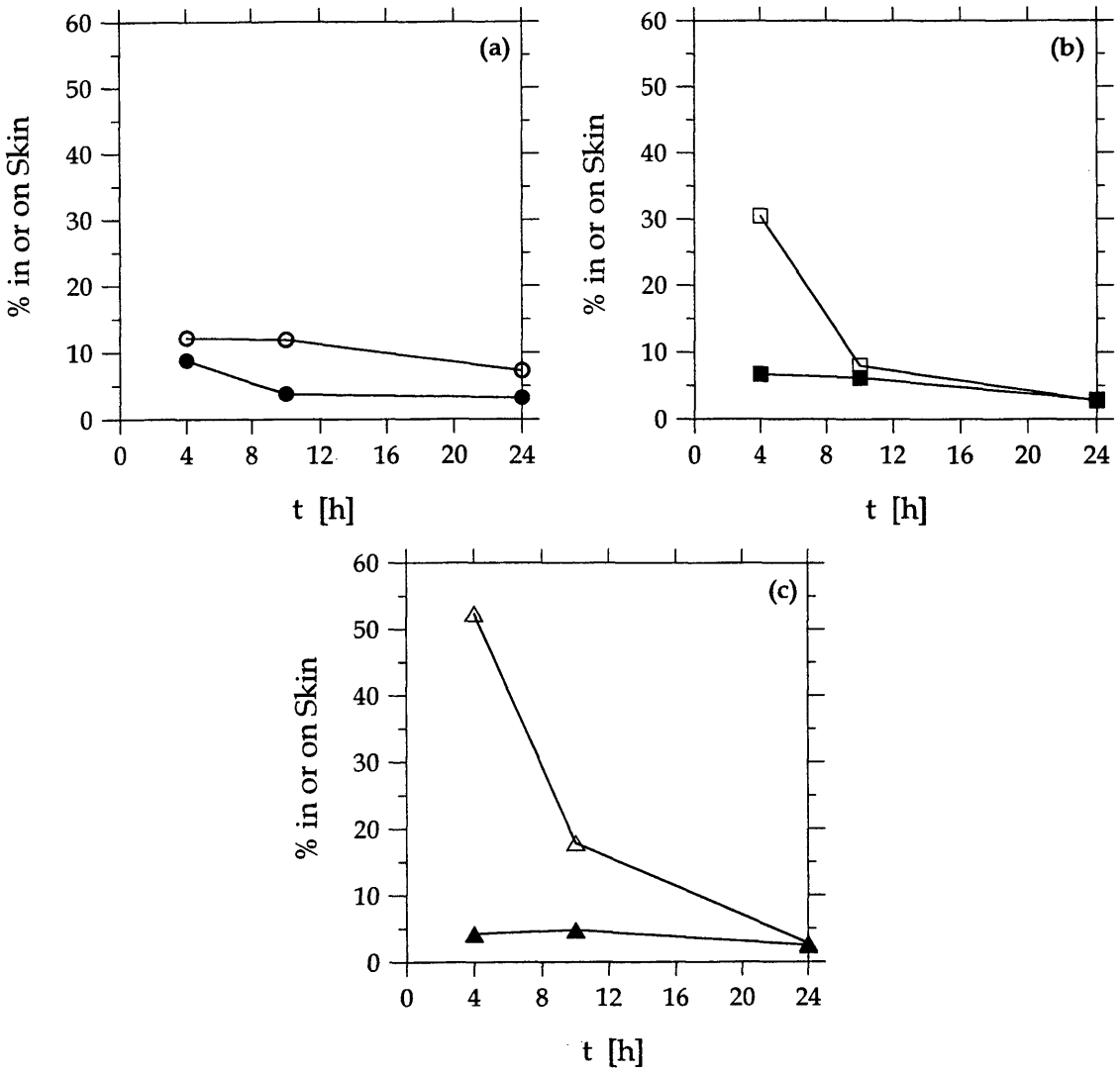

Figure 6MO.4 – Percent of applied dose on (open symbols) and in (closed symbols) the skin as a function of time for all doses: (a) L, (b) M, and (c) H.

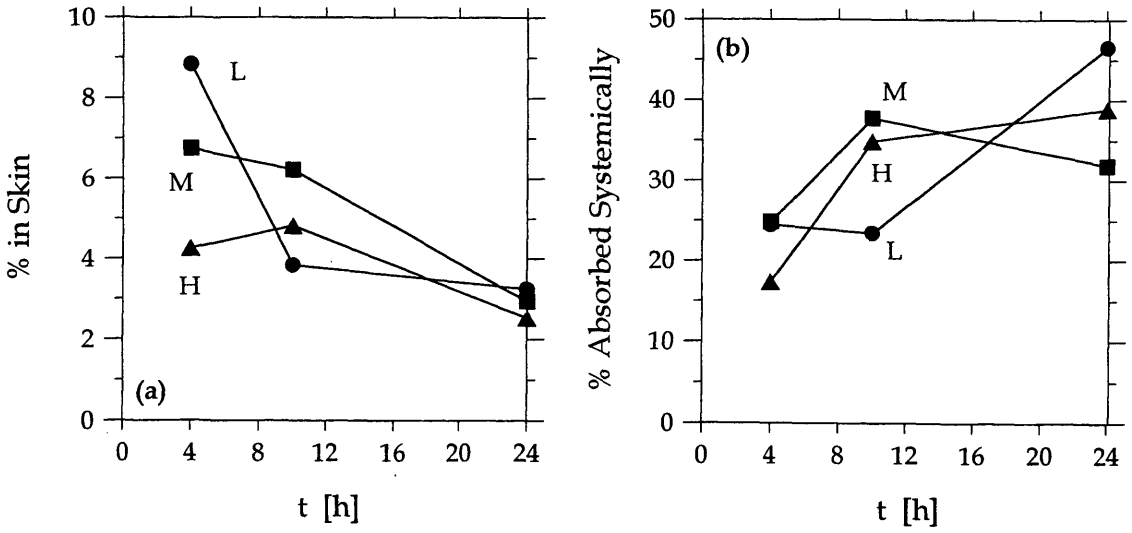

Figure 6MO.5 – Percent of applied dose (a) in the skin and (b) absorbed systemically as a function of time.

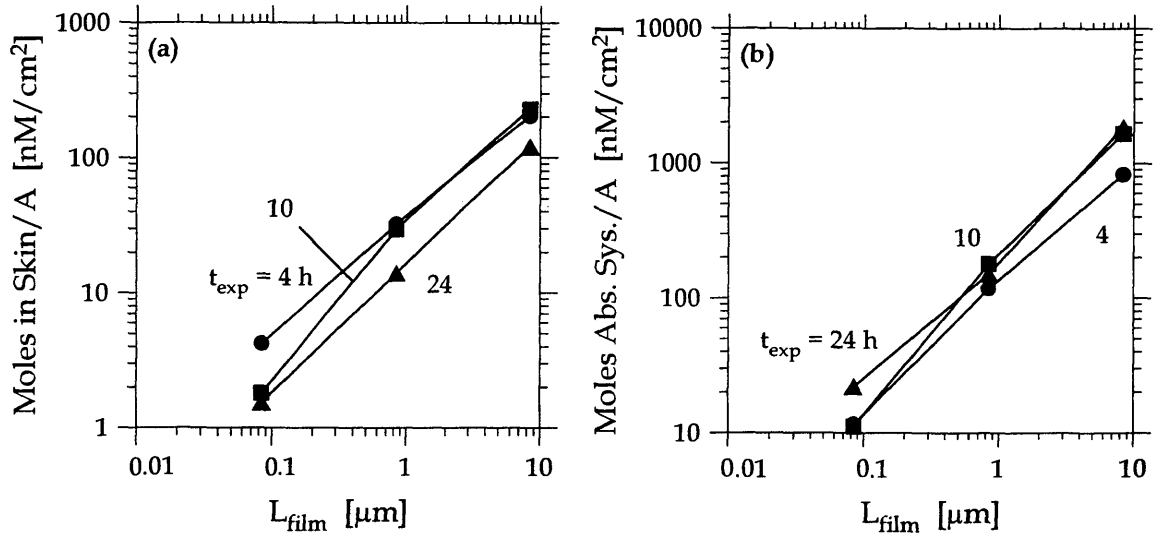

Figure 6MO.6 – Moles of chemical (a) in the skin and (b) absorbed systemically as a function of L_{film}.

Table 6MO.3 – Coefficients for best-fit lines through log-log plots of moles of chemical in the skin and absorbed systemically as a function of dose.

time, h	moles in skin		moles absorbed systemically	
	$\hat{S}$	$\hat{I}$	$\hat{S}$	$\hat{I}$
4	0.84	1.9	0.93	3.1
10	1.1	1.6	1.1	3.5
24	0.95	1.1	0.96	3.7

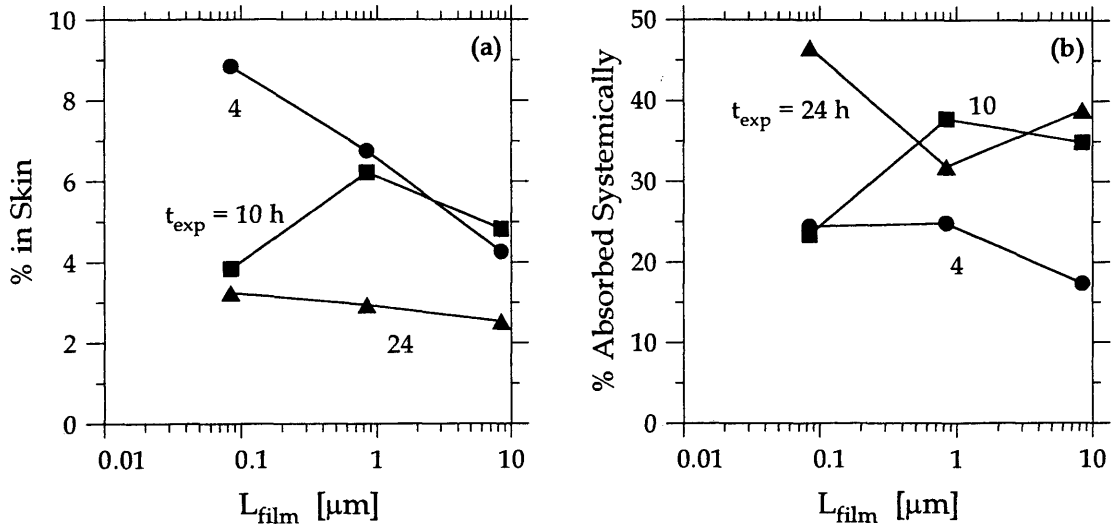

Figure 6MO.7 – Percent of applied dose (a) in the skin and (b) absorbed systemically as a function of L_{film}.

Phosmet (PH)

The molecular structure of phosmet is shown in Figure 6PH.1. Phosmet is an insecticide and acaricide used for control of lepidopterous larvae, aphids, suckers, fruit flies, and spider mites on pome fruit, stone fruit, citrus fruit, ornamentals and vines, and it has many other uses as well. Its tradenames include Cekumet, Fosdan, and Imidan. Phosmet, a solid, lipophilic pesticide ($\log K_{o/w} = 2.95$), is available as wettable and dispersible powders, and as soluble and emulsifiable concentrates (Tomlin, 1997). Table 6PH.1 shows applied doses used in the phosmet study with the results listed in Table 6PH.2.

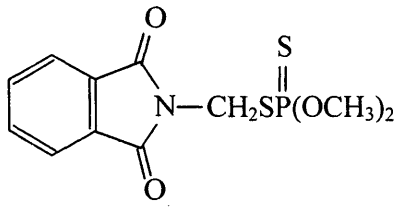

Figure 6PH.1 – Molecular structure of phosmet.

Table 6PH.1 – Applied doses used in phosmet study.

dose	moles /A , nM / cm^2	mass / A, μg / cm^2	L_{film}, μm
L	183	58.0	0.56
M	1640	519.9	5.1
H	8423	2670.	26

Table 6PH.2 – Results of phosmet dermal absorption study (Zendzian, 2000b).[a]

Dose	Exposure	Skin		Absorbed[b]	
	hours	%	nM/cm^2	%	nM/cm^2
L	1	4.07	7.45	0.80	1.46
	2	4.20	7.69	1.33	2.43
	4	4.07	7.45	1.99	3.64
	10	3.34	6.11	5.88	10.76
	24	3.99	7.30	7.82	14.31
M	1	1.74	28.54	0.21	3.44
	2	1.64	26.90	0.24	3.94
	4	1.88	30.83	0.40	6.56
	10	2.54	41.66	0.67	10.99
	24	2.12	36.08	1.68	27.55
H	1	0.84	70.75	0.03	2.53
	2	0.78	65.70	0.09	7.58
	4	0.86	72.44	0.06	5.05
	10	0.97	81.70	0.09	7.58
	24	0.66	55.59	0.23	19.37

[a] Data are from the study of the Imidan formulation with MRID 401222-01 dated 3/5/87. [b] Data include pesticide in blood, urine, feces, carcass.

The summary report of the phosmet study did not include the percent of dose recovered, on the enclosure and cover, or in the skin wash. Phosmet, with the relatively low vapor pressure of 0.065 mPa at 25°C (Tomlin, 1997), probably did not evaporate during the experiment. Also, the maximum amount absorbed into and through the skin for any exposure was 12%, and so the amount on the skin probably did not decrease significantly.

Figure 6PH.2 shows the percent of applied dose in the skin and absorbed systemically as a function of time. If statistical information were available, it would probably be apparent that for all doses the amount in skin was independent of exposure time. The amount absorbed systemically increased with exposure time.

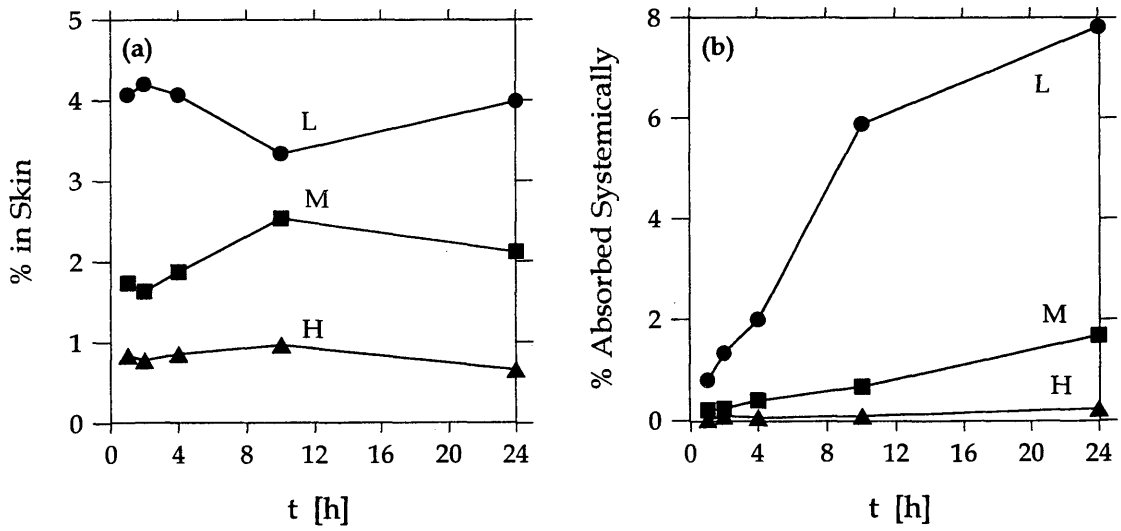

Figure 6PH.2 – Percent of applied dose (a) in the skin and (b) absorbed systemically as a function of time.

Moles of phosmet in the skin and absorbed systemically are shown in Figure 6PH.3 as a function of L_{film}. Coefficients of the best-fit lines for these data are listed in Table 6PH.3. Slope values for the amount absorbed systemically ranged from 0 to 0.3, which were much lower than slope values for the amount in the skin (i.e., 0.5 – 0.7). Figure 6PH.4 shows that both the percent of applied dose in the skin and absorbed systemically decreased significantly as L_{film} increased. For the amount absorbed systemically, the effect of dose increased as the exposure time increased.

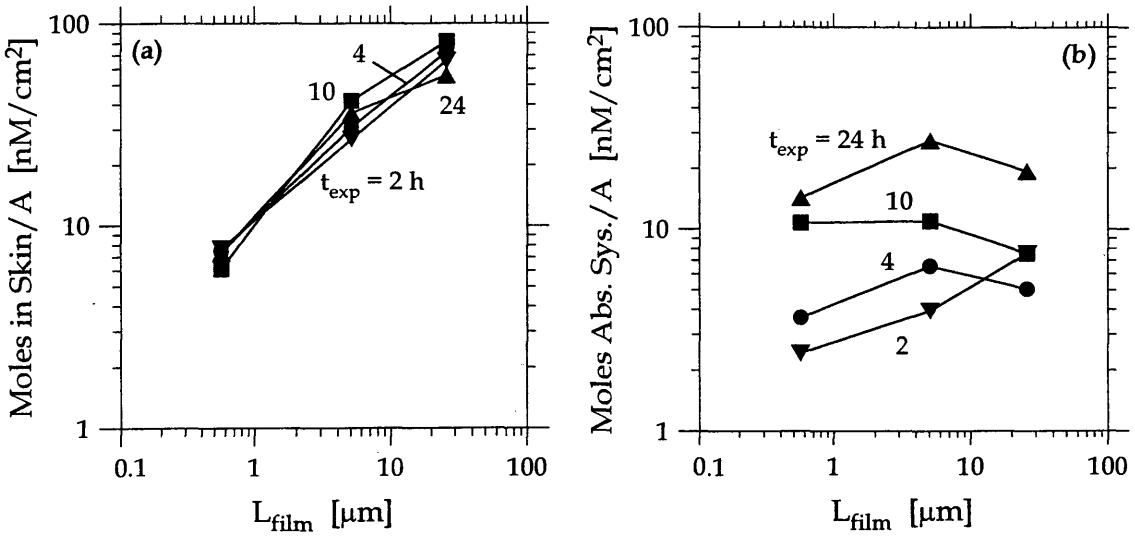

Figure 6PH.3 – Moles of chemical (a) in the skin and (b) absorbed systemically as a function of L_{film}.

Table 6PH.3 – Coefficients for best-fit lines through log-log plots of moles of chemical in the skin and absorbed systemically as a function of dose.

time, h	moles in skin		moles absorbed systemically	
	$\hat{S}$	$\hat{I}$	$\hat{S}$	$\hat{I}$
2	0.56	2.6	0.29	1.1
4	0.60	2.6	0.096	1.5
10	0.69	2.6	-0.086	2.4
24	0.54	2.6	0.091	2.9

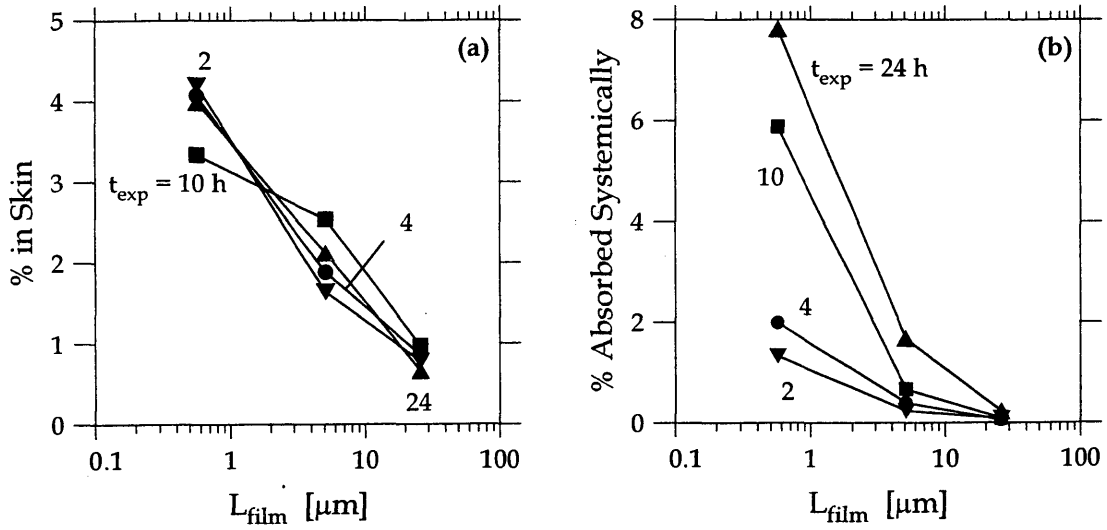

Figure 6PH.4 – Percent of applied dose (a) in the skin and (b) absorbed systemically as a function of L_{film}.

Thiobencarb (TH)

Thiobencarb, with the molecular structure shown in Figure 6TH.1, is an herbicide used for control of several monocotyledonous and annual broad-leaved weeds in direct-seeded and transplanted rice. It is a liquid, lipophilic pesticide ($\log K_{o/w} = 3.42$) available as granules or as an emulsifiable concentrate with tradenames including Saturn, Bigturn, and Bolero (Tomlin, 1997). Table 6TH.1 shows the applied doses in the thiobencarb study with the results listed in Table 6TH.2.

Figure 6TH.1 – Molecular structure of thiobencarb.

Table 6TH.1 – Applied doses used in thiobencarb study.

dose	moles /A , nM / cm^2	mass / A, μg / cm^2	L_{film}, μm
L	20	5.2	0.045
M	194	50.1	0.44
H	1937	499.7	4.3

Table 6TH.2 – Results of thiobencarb dermal absorption study (Zendzian, 2000b).[a]

Dose	Exposure	Enclosure and Cover	Skin Wash	Skin		Absorbed[b]		Total Recovery
	hours	%	%	%	nM/cm^2	%	nM/cm^2	%
L	1	4.3	56.0	14.4	2.88	16.4	3.28	91.0
	2	3.6	45.7	19.0	3.80	19.6	3.92	87.7
	4	2.9	31.0	15.3	3.06	23.6	4.72	82.7
	10	0.8	14.9	5.9	1.18	60.2	12.04	81.6
	24	0.7	4.7	3.7	0.74	71.5	14.30	80.5
M	1	3.3	68.9	12.7	24.64	9.5	18.43	94.3
	2	3.1	52.8	21.4	41.52	12.9	25.03	90.2
	4	1.5	42.1	13.2	25.61	32.6	63.24	89.2
	10	1.5	19.4	8.8	17.07	52.6	102.04	92.2
	24	0.9	6.5	3.1	6.01	72.6	140.84	82.8
H	1	3.8	77.6	10.2	197.6	2.4	46.5	94.1
	2	2.4	73.2	11.2	216.9	6.5	125.9	93.2
	4	2.0	71.0	10.9	211.1	11.0	213.1	94.7
	10	2.8	59.0	11.6	224.7	17.1	331.2	90.4
	24	1.7	37.1	8.5	164.6	41.7	807.8	88.9

[a] Data are from the study of the Bolero 8 emulsifiable concentrate formulation with MRID 412153-11 dated 8/1/89. [b] Data include pesticide in blood, urine, feces, carcass, and cage wash.

Figure 6TH.2 shows that percent recoveries decreased with increasing time and were poorest for dose L. The percent of applied dose found on the enclosure and cover was always less than 5%. It is not known whether the cover included an activated carbon filter. If there was no carbon trap, then evaporated chemical might have been lost, which is consistent with the time dependence of the recoveries reported. Thiobencarb has a vapor pressure (2.93 mPa at 23°C (Tomlin, 1997)) that is similar to other pesticides that evaporated (e.g., lindane with a vapor pressure of 5.6 mPa at 20°C (Tomlin, 1997) is suspected to evaporate because it also had time-dependent percent recoveries).

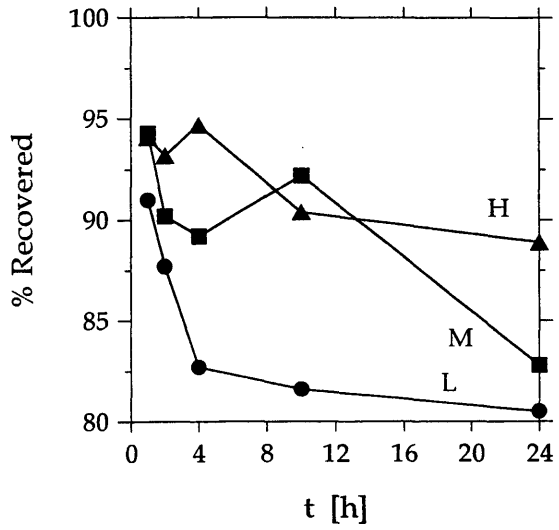

Figure 6TH.2 – Percent of applied dose recovered as a function of time.

The percent of applied dose on and in the skin are shown in Figure 6TH.3 as a function of time. For doses L and M, the amount in the skin decreased with increasing time reflecting the decrease in the amount on the skin surface. For doses L and M, only about 5% of the applied dose was left on the skin at 24 hours. The decreasing amount of thiobencarb may have been partly due to evaporation, but was mainly due to dermal absorption. Even if the unrecovered thiobencarb was lost to evaporation, more chemical was absorbed into and through the skin than was lost to evaporation.

The percent of applied dose in the skin and absorbed systemically are shown in Figure 6TH.4 as a function of time. After two hours, the amount in the skin for dose H was essentially constant. It is expected that thiobencarb, a relatively small molecule (MW = 258), probably has a larger diffusion coefficient than many of the other pesticides studied here. This may explain its rapid absorption into and through skin. Depletion of the chemical from the skin surface is evident in Figure 6TH.4a by the large decrease of the amount in the skin for doses L and M. Despite this, systemic absorption was significant (e.g., almost 75% for doses L and M), and increased with time.

Moles of chemical in the skin and absorbed systemically are shown in Figure 6TH.5 as a function of L_{film}. Coefficients of the best-fit line for these data are listed in Table 6TH.3. For the 2 and 4 hour data, the slope values for amount in the skin were approximately 0.9. For 10 and 24 hours they increased to greater than 1, probably because the amount on the skin decreased more for doses L and M than for dose H. The slope values for amount absorbed systemically (0.7 – 0.9) were less affected by this, and were always less than those for the amount in the skin.

Figure 6TH.6 shows that percent in the skin and absorbed systemically were both relatively independent of dose. At 2 and 4 hours, the percent in the skin was larger for dose L than dose H, but at 10 and 24 hours the percent in skin was larger for dose H than dose L because the amount in skin for dose L dropped significantly for long exposures.

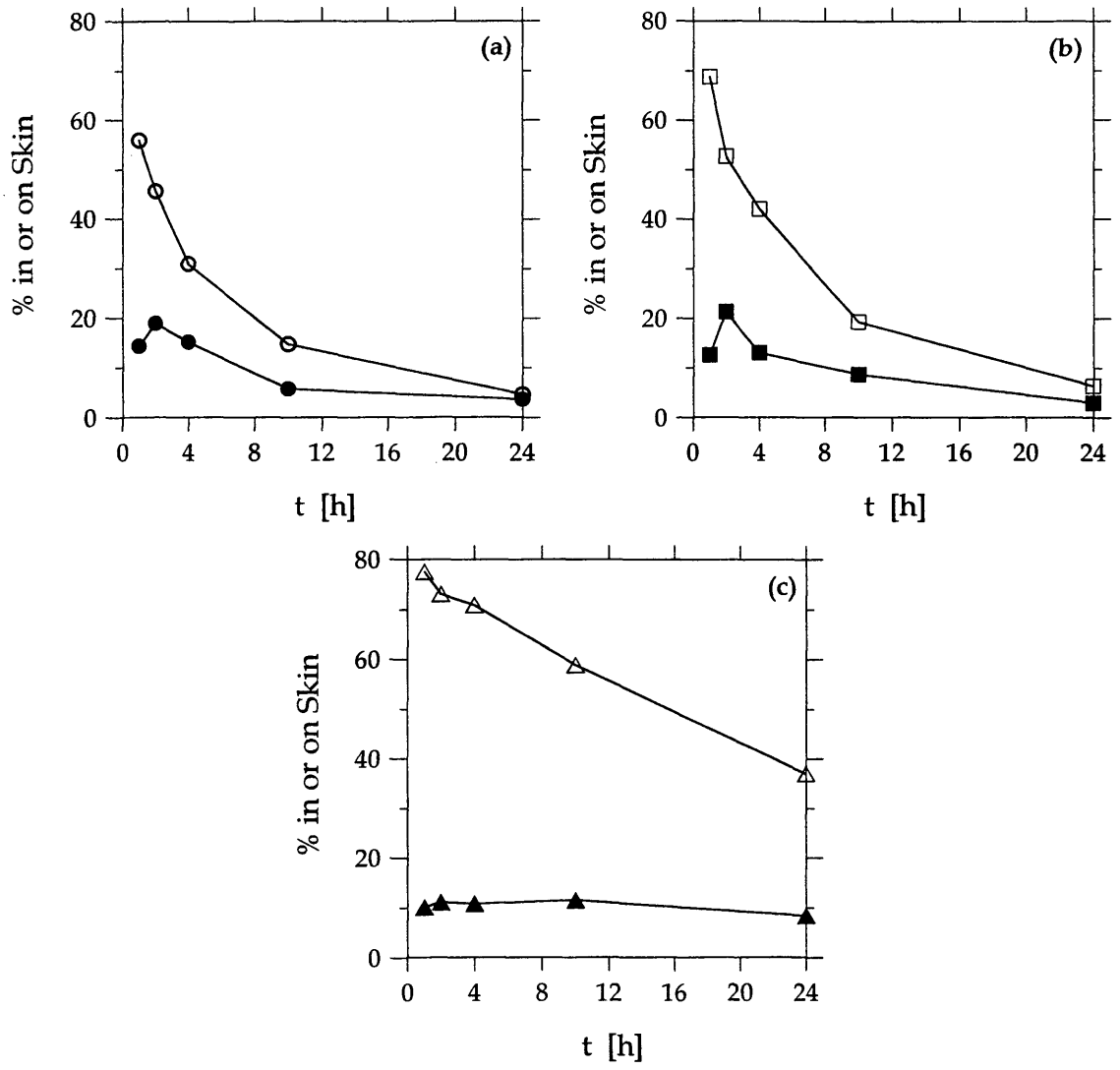

Figure 6TH.3 – Percent of applied dose on (open symbols) and in (closed symbols) the skin as a function of time for all doses: (a) L, (b) M, and (c) H.

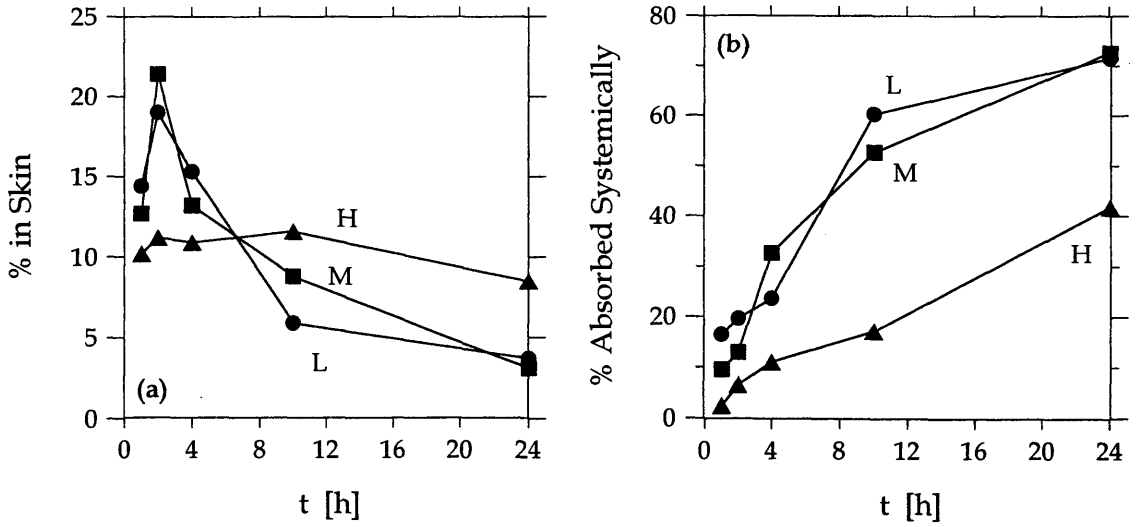

Figure 6TH.4 – Percent of applied dose (a) in the skin and (b) absorbed systemically as a function of time.

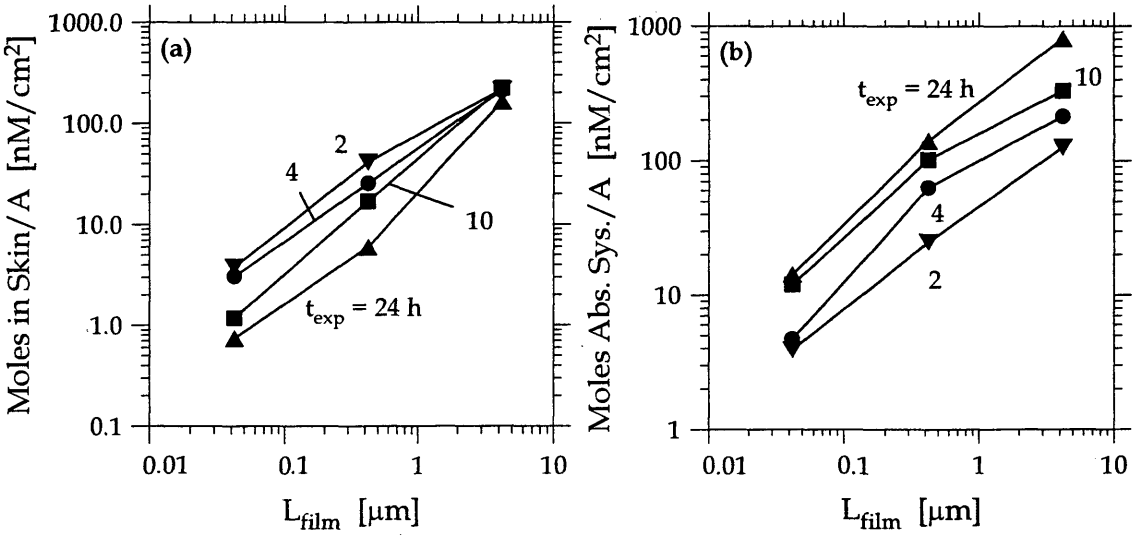

Figure 6TH.5 – Moles of chemical (a) in the skin and (b) absorbed systemically as a function of L_{film}.

Table 6TH.3 – Coefficients for best-fit lines through log-log plots of moles of chemical in the skin and absorbed systemically as a function of dose.

time, h	moles in skin		moles absorbed systemically	
	$\hat{S}$	$\hat{I}$	$\hat{S}$	$\hat{I}$
2	0.89	4.2	0.75	3.8
4	0.92	4.0	0.83	4.4
10	1.1	3.8	0.72	4.9
24	1.2	3.2	0.88	5.5

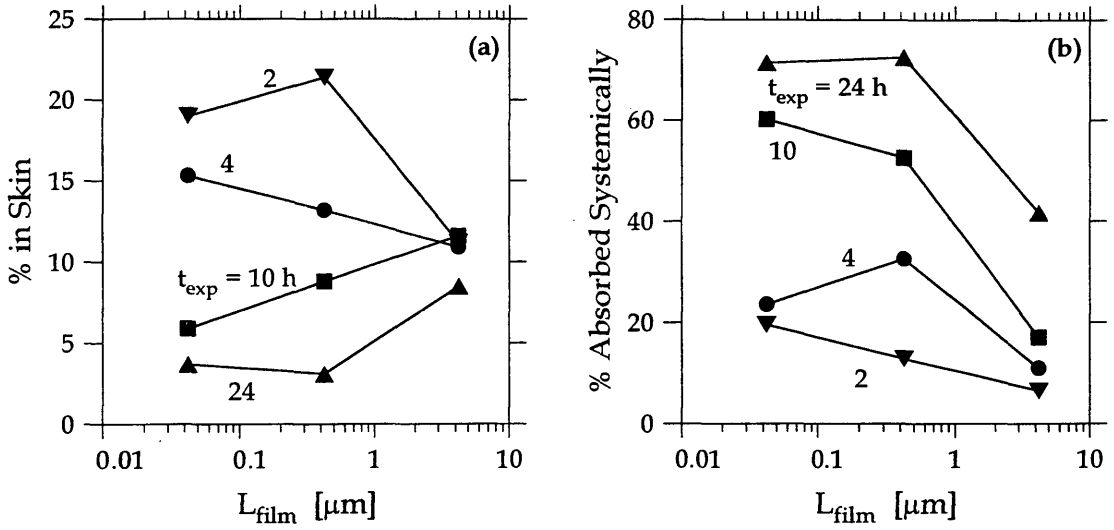

Figure 6TH.6 – Percent of applied dose (a) in the skin and (b) absorbed systemically as a function of L_{film}.

Tribufos (TR)

Tribufos, with the molecular structure shown in Figure 6TR.1, is a plant growth regulator mainly used for defoliation of cotton to facilitate harvesting with tradenames including DEF 6. It is a lipophilic, liquid pesticide ($\log K_{o/w} = 3.23$) available as an emulsifiable concentrate (Tomlin, 1997). Table 6TR.1 shows the applied doses in the tribufos study with the results listed in Table 6TR.2. Percent recoveries ranged from 100 to 106%. Less than 5.3% of the applied dose was found on the enclosure and cover. There is no evidence that tribufos, with a vapor pressure of 0.71 mPa at 25°C (Tomlin, 1997), evaporated significantly.

$[CH_3(CH_2)_3S]_3PO$

Figure 6TR.1 – Molecular structure of tribufos.

Table 6TR.1 – Applied doses used in tribufos study.

dose	moles /A , nM / cm^2	mass / A, µg / cm^2	L_{film}, µm
L	6.42	2.02	0.019
M	32.1	10.1	0.095
H	321	101	0.95

Table 6TR.2 – Results of tribufos dermal absorption study.[a]

Dose	Expo-sure	Enclosure and Cover[b]	Skin Wash	Skin		Absorbed[c]		Total Recovery
	hours	%	%	%	nM/cm^2	%	nM/cm^2	%
L	1	3.80	71.33	32.52	2.09	0.90	0.06	106.08
	4	4.29	55.05	38.05	2.44	7.89	0.51	104.47
	10	5.31	49.32	33.64	2.16	18.68	1.20	103.98
M	1	4.29	64.38	32.24	10.35	0.88	0.28	99.72
	4	4.09	57.07	39.12	12.56	7.20	2.31	105.22
	10	4.13	48.93	36.02	11.56	13.39	4.30	100.48
H	1	2.62	74.42	29.75	95.50	0.92	2.95	106.53
	4	3.20	63.30	34.29	110.07	3.46	11.11	103.08
	10	3.54	59.05	32.53	104.42	12.93	41.51	106.18

[a] Data are from the study of the DEF 6 emulsifiable formulation with MRID 423500-03 dated 5/19/92. [b] Data include pesticide from the application device, protective cover, and ring. [c] Data include pesticide from the blood, urine, feces, carcass, and cage wash.

The percent of applied dose found on and in the skin are shown in Figure 6TR.2 as a function of time. The percent in the skin remained constant even though the percent on the skin decreased with time. Figure 6TR.3 shows the percent of applied dose in the skin and absorbed systemically as a function of time. Statistical information, if it were available, might show that there was no statistical difference between the different doses for the percent in the skin and absorbed systemically.

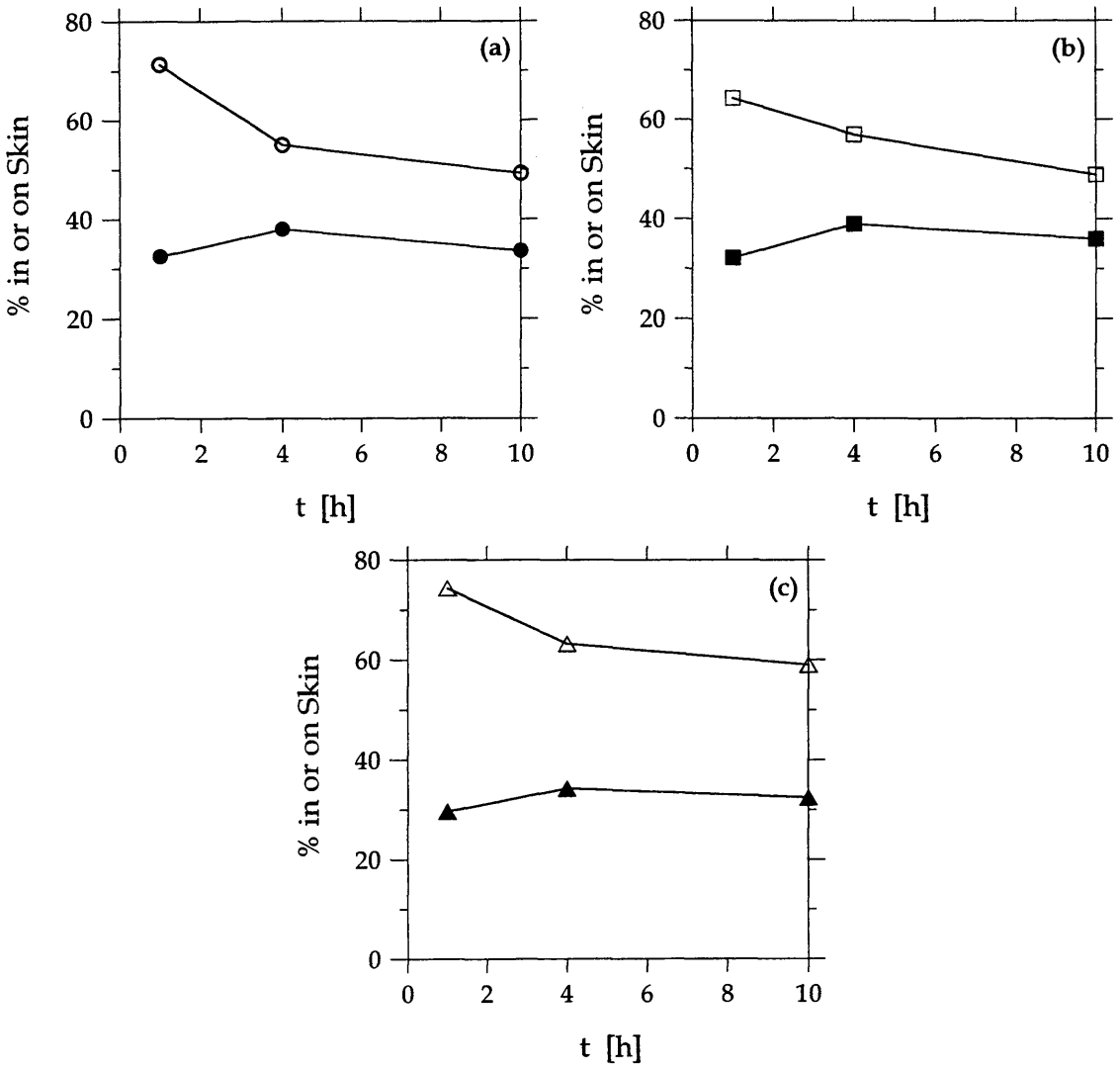

Figure 6TR.2 – Percent of applied dose on (open symbols) and in (closed symbols) the skin as a function of time for all doses: (a) L, (b) M, and (c) H.

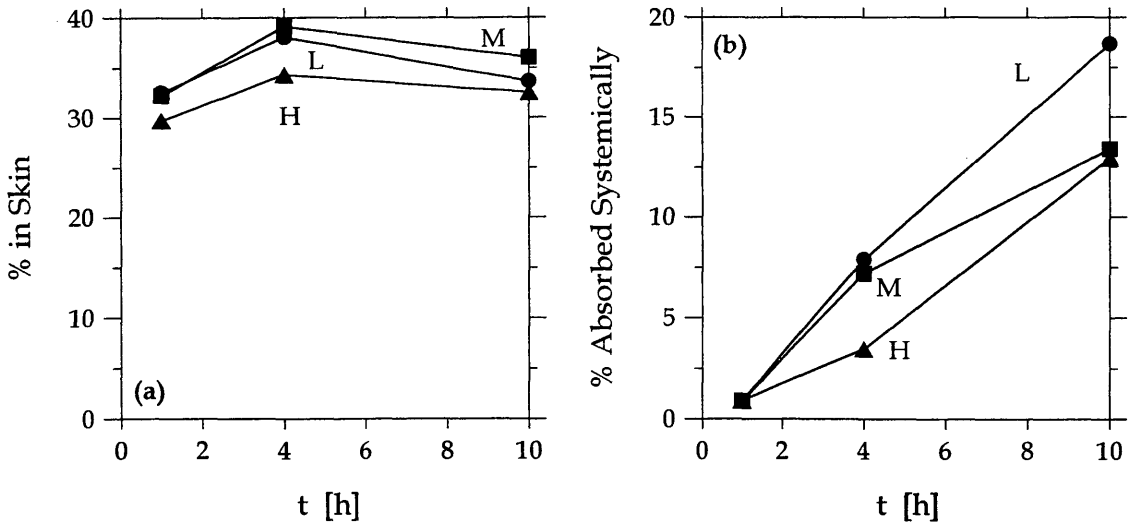

Figure 6TR.3 – Percent of applied dose (a) in the skin and (b) absorbed systemically as a function of time.

Moles in the skin and absorbed systemically are shown in Figure 6TR.4 as a function of L_{film}. Coefficients of the best-fit lines for these data are listed in Table 6TR.3. Slope values for the amount in the skin are approximately 1, while those for the amount absorbed systemically are slightly smaller at approximately 0.8 – 0.9. Figure 6TR.5 shows that the percent of applied dose in the skin is independent of L_{film}, while the percent of applied dose absorbed systemically decreased slightly with increasing L_{film}.

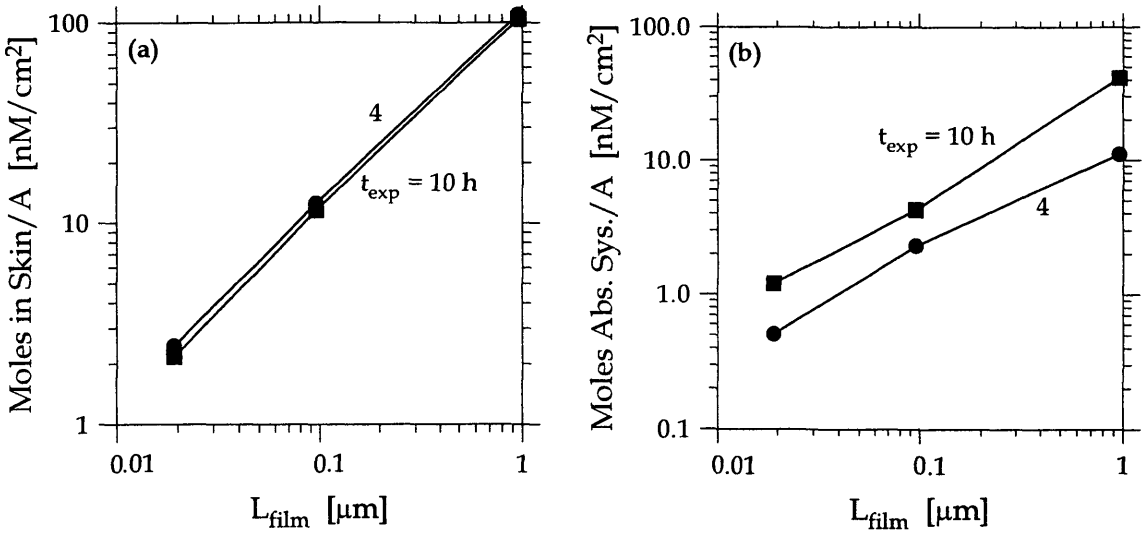

Figure 6TR.4 – Moles of chemical (a) in the skin and (b) absorbed systemically as a function of L_{film}.

Table 6TR.3 – Coefficients for best-fit lines through log-log plots of moles of chemical in the skin and absorbed systemically as a function of dose.

time, h	moles in skin		moles absorbed systemically	
	$\hat{S}$	$\hat{I}$	$\hat{S}$	$\hat{I}$
4	0.99	4.7	0.78	2.5
10	0.97	4.8	0.91	3.7

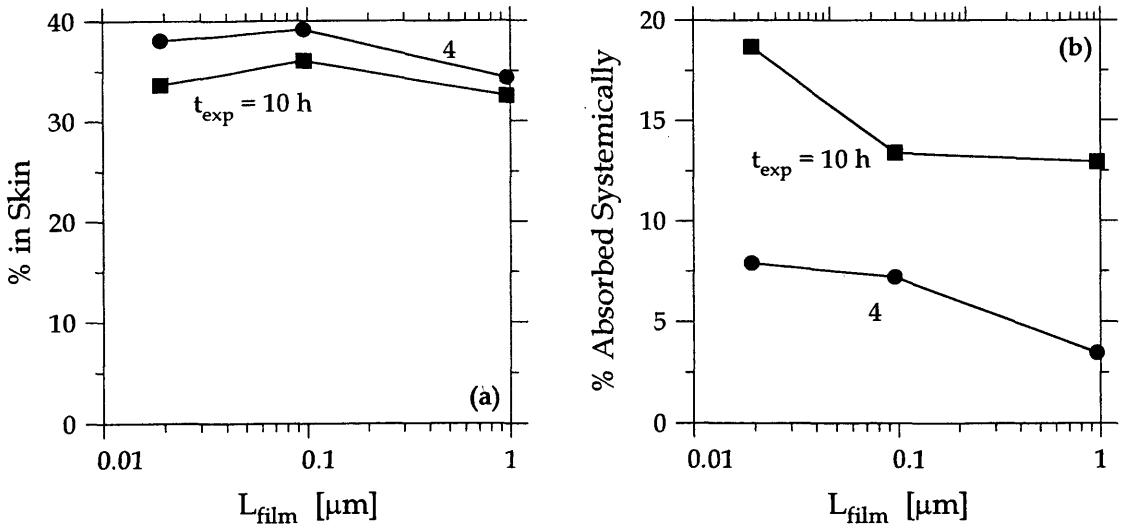

Figure 6TR.5 – Percent of applied dose (a) in the skin and (b) absorbed systemically as a function of L_{film}.

Vinclozlin (VI)

Figure 6VI.1 shows the molecular structure of vinclozlin, a fungicide used for control of Botrytis and Sclerotinia spp. in vines, strawberries, oilseed rape, vegetables, fruit and ornaments, and other purposes. Vinclozlin, a solid, lipophilic pesticide ($logK_{o/w}$ = 3), is available as a suspension concentrate, a wettable powder, as water dispersible granules, and a smoke tin with tradenames such as Ronilan and Flotilla (Tomlin, 1997). Table 6VI.1 shows the applied doses in the vinclozlin study with the results listed in Table 6VI.2. Percent recoveries were greater than 86% and were independent of exposure time. The percent of applied dose on the enclosure and cover were not reported. However, based on the high recoveries and a relatively low vapor pressure of 0.13 mPa at 20°C (Tomlin, 1997), vinclozlin probably did not evaporate significantly.

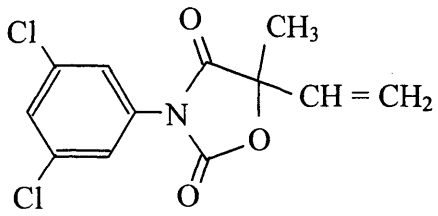

Figure 6VI.1 – Molecular structure of vinclozlin.

Table 6VI.1 – Applied doses used in vinclozlin study.

dose	moles /A , nM / cm^2	mass / A, μg / cm^2	L_{film}, μm
LL	7	2	0.013
L	70	20	0.13
M	699	200	1.3
H	6990	2000	13

Table 6VI.2 – Results of vinclozlin dermal absorption study.[a]

Dose	Exposure	Skin Wash	Skin		Absorbed[b]		Total Recovery
	hours	%	%	nM/cm^{2} [c]	%	nM/cm^{2} [c]	%
LL	0.5	81.7	8.87	0.62	0.44	0.031	91.0
	1	77.4	11.3	0.80	1.80	0.13	91.4
	2	76.7	10.8	0.79	2.55	0.18	90.1
	4	70.2	12.1	0.85	5.51	0.39	87.8
	10	61.5	11.9	0.83	13.3	0.93	86.7
L	0.5	81.3	16.3	11.4	<0.38	<0.27	97.6
	1	71.9	16.1	11.3	0.52	0.36	88.3
	2	75.8	23.3	16.3	0.97	0.68	100
	4	74.4	16.5	11.5	1.84	1.3	92.7
	10	67.5	15.2	10.6	4.29	3.0	86.9
M	0.5	82.9	15.0	105	<0.17	<1.2	97.9
	1	79.4	18.0	126	<0.16	<1.1	97.4
	2	78.2	18.0	126	0.18	1.3	96.4
	4	78.6	18.4	129	0.27	1.9	97.2
	10	85.7	5.65	39.5	0.51	3.6	91.9
H	0.5	89.5	9.78	684	<0.19	<13.3	99.3
	1	96.1	3.91	273	1.07	74.8	101
	2	99.2	4.36	305	<0.22	<15.4	104
	4	88.6	11.0	769	<0.23	<16.1	99.7
	10	93.9	4.20	294	<0.22	<15.4	98.1

[a] Data are from the study with MRID 418243-09 dated 1/3/91. [b] Data include pesticide in tissues, urine, feces, carcass, and cage wash. [c] Calculated using reported data (i.e., the percent of applied dose in the skin and absorbed systemically).

Figure 6VI.2 shows the percent of applied dose on and in the skin as a function of time. For doses L and LL, the percent on the skin does not decreased more than 30% by 10 hours. The amount in the skin, however, did not decrease in response to that. The percent of applied dose in the skin and absorbed systemically are shown in Figure 6VI.3 as a function of time. It is likely that with more statistical information, the percent in the skin would be found to be relatively independent of time. The percent of dose absorbed systemically increased with time and was larger for small doses than for large ones. In Figure 6VI.3, the symbol "D" (for detection limit) marks the value that systemic absorption was reported as being less than for several data points. For each of these data points, at least one animal had an undetectable amount of systemic absorption.

Moles in the skin and absorbed systemically are shown in Figure 6VI.4 as a function of L_{film}. Coefficients for the best-fit lines of the data in Figure 6VI.4 are listed in Table 6VI.3. Coefficients for the amount absorbed systemically were based on data from doses LL, L, and M, while coefficients for amount in the skin were calculated using all doses and also using only LL, L and M data. Slopes values for amount in the skin were essentially the same for all doses (0.8 – 1) and without dose H (0.8 – 1.1). At 0.3 to 0.4, the slope values for the amount absorbed systemically were much smaller than slope values for the amount in skin.

Figure 6VI.5 shows that the percent of applied dose in the skin might have been independent of L_{film}, depending on the size of the variance. The percent of applied dose absorbed systemically, however, decreased with applied dose and the effect of increasing dose was magnified for longer exposure times.

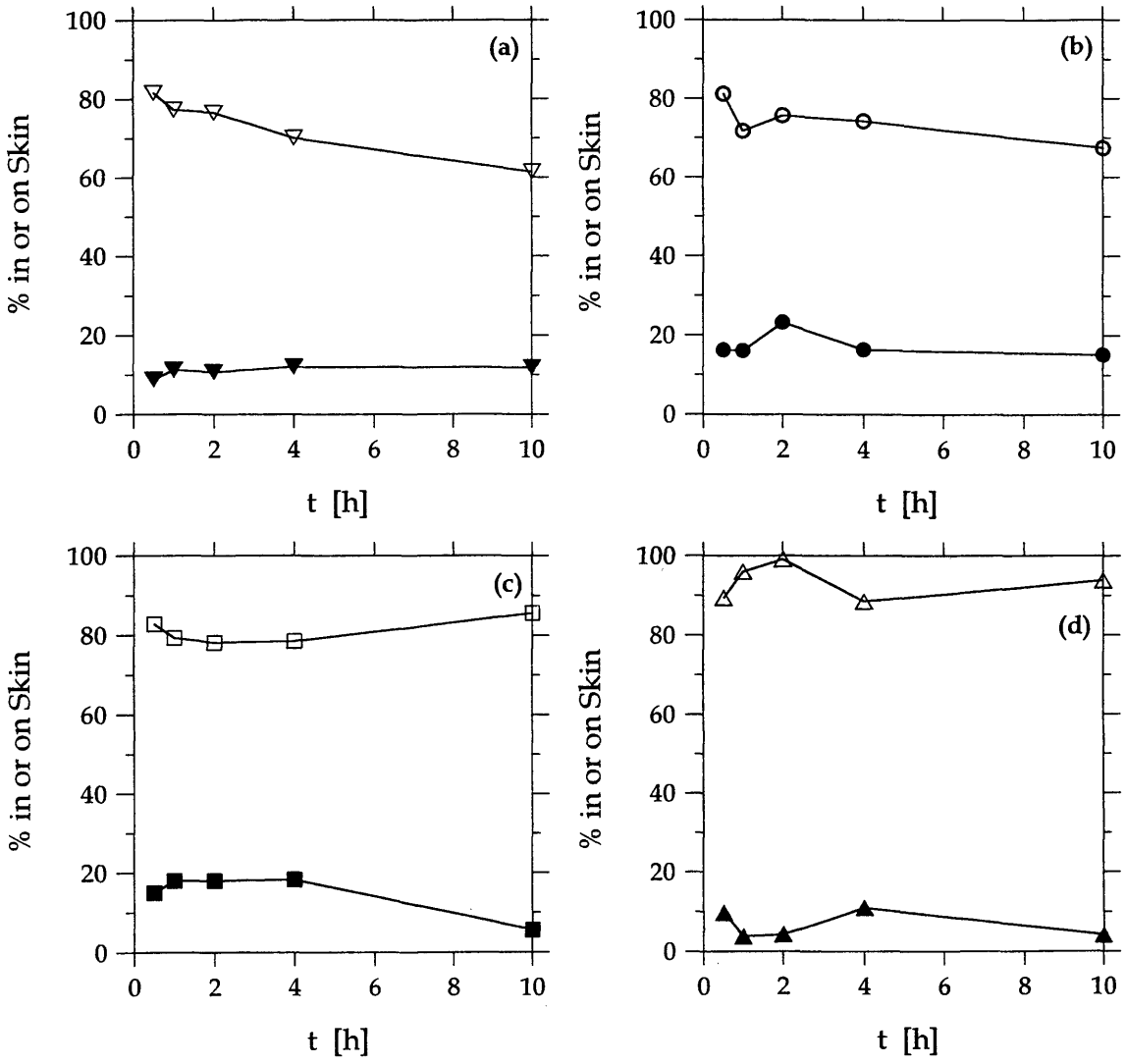

Figure 6VI.2 – Percent of applied dose on (open symbols) and in (closed symbols) the skin as a function of time for all doses: (a) LL, (b) L, (c) M, and (d) H.

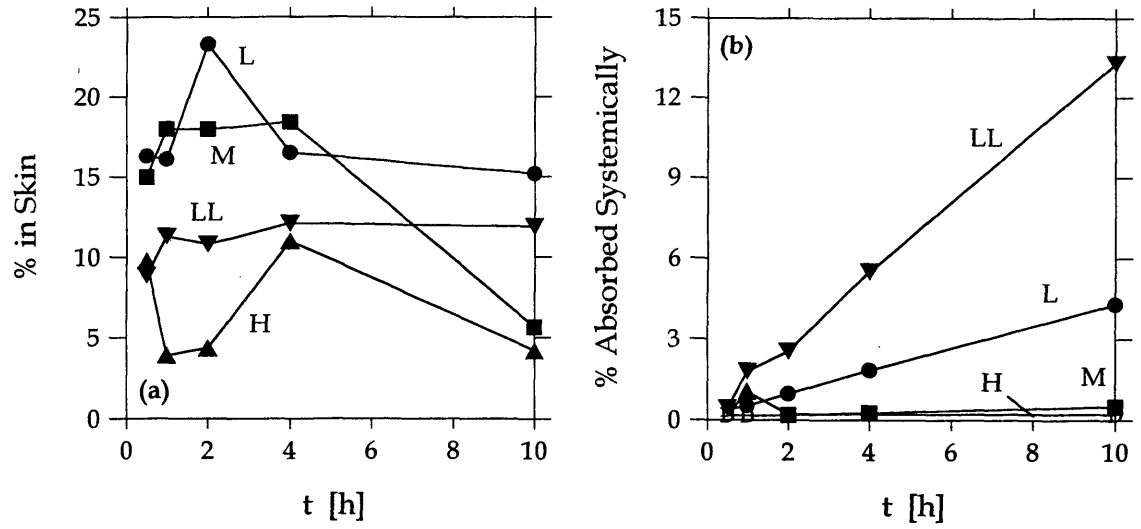

Figure 6VI.3 – Percent of applied dose (a) in the skin and (b) absorbed systemically as a function of time.

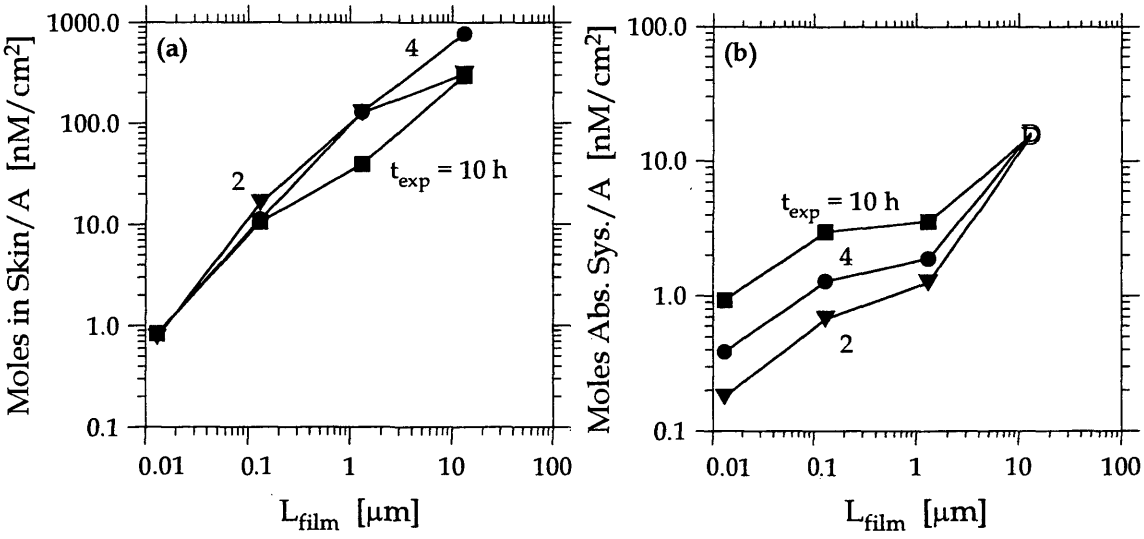

Figure 6VI.4 – Moles of chemical (a) in the skin and (b) absorbed systemically as a function of L_{film}.

Table 6VI.3 – Coefficients for best-fit lines through log-log plots of moles of chemical in the skin and absorbed systemically as a function of dose.

time, h	moles in skin		moles in skin[a]		moles abs. sys.[a]	
	$\hat{S}$	$\hat{I}$	$\hat{S}$	$\hat{I}$	$\hat{S}$	$\hat{I}$
2	0.87	4.0	1.1	4.7	0.42	0.24
4	0.99	4.3	1.1	4.6	0.35	0.68
10	0.82	3.6	0.84	3.7	0.29	1.4

[a] Calculation did not use data for dose H.

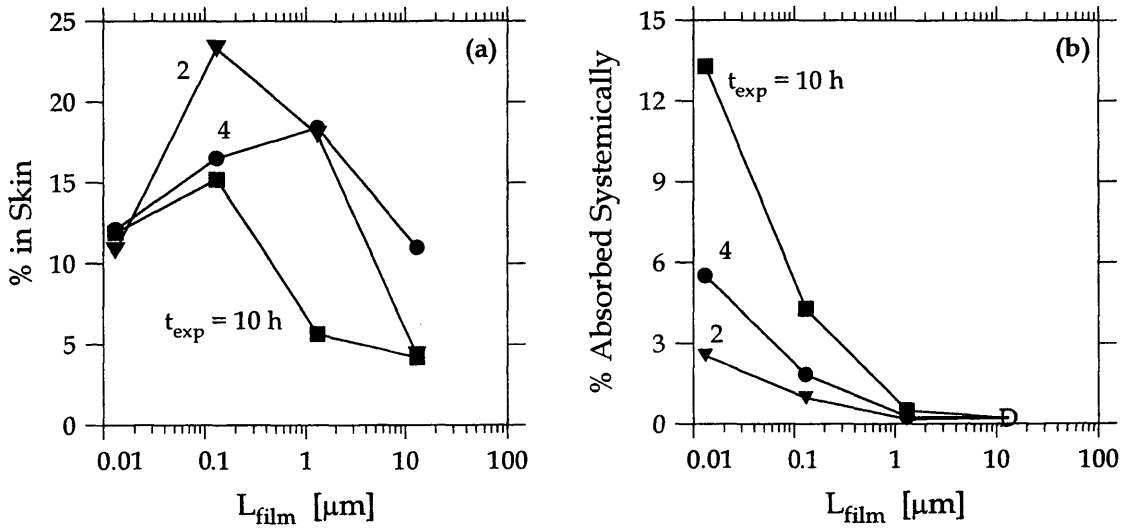

Figure 6VI.5 – Percent of applied dose (a) in the skin and (b) absorbed systemically as a function of L_{film}.

DERMAL ABSORPTION OF CHEMICAL RESIDUES DISTRIBUTED SPATIALLY ON SKIN

Introduction

In many dermal exposures, the amount of chemical deposited on the skin surface is insufficient to completely cover the exposed area. Experiments in which chemicals are applied to skin in a small amount of volatile solvent are meant to simulate this type of exposure. Almost certainly, deposited chemical residues are distributed non-uniformly on the exposed surface with chemical-free regions separating regions covered with chemical. Figure 7.1 shows an Environmental Scanning Electron Micrograph (ESEM) of the skin surface magnified 200 times. It shows human skin *in vivo* with 0.0106 mg/cm^2 4-cyanophenol applied in acetone after the acetone evaporated. This applied dose is in the middle of the range found in Chapter 6 (i.e., ~ 0.0001 to 10 mg /cm^2). Chemical-free areas of skin are apparent.

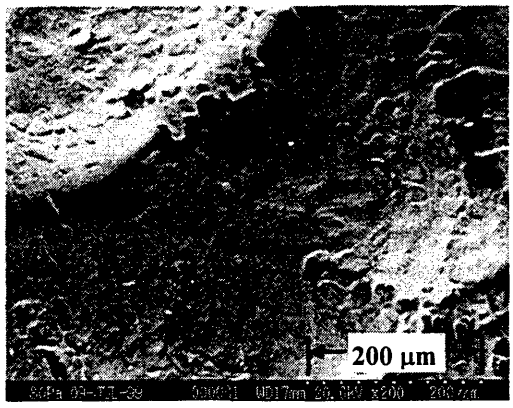

Figure 7.1 – ESEM of human skin contaminated with 0.0106 mg/cm^2 4-cyanophenol.

The amount of chemical absorbed in such situations should depend on the chemical's concentration (a constant for deposited residues of almost pure chemical), the skin area that is actually covered by the deposited residue (i.e., the contact area), and the exposure time. The contact area increases as the applied dose increases until the entire exposed area is covered by chemical.

Physiologically, skin is a multi-layered membrane. For many chemicals the outer layer (the stratum corneum, sc) is the rate-limiting barrier to dermal absorption, but for lipophilic chemicals the second layer (the viable epidermis, ve) also contributes a significant mass transfer resistance. Together, the sc and ve form the epidermis (epi). Below the epi is the dermis, a highly vascularized tissue that typically has adequate blood flow to clear away all chemical passing through the epi (Scheuplein and Bronaugh, 1983).

Often, dermal absorption of chemical is represented mathematically as one-dimensional passive diffusion through one or more membranes in series. For describing dermal absorption of chemicals with a range of lipophilic properties, the sc and ve are included as separate membranes with distinct properties. One-dimensional models are reasonable when the skin is completely covered with chemical, as shown in Figure 7.2a, which indicates thermodynamic activity (or concentration, if the partition coefficient between the sc and ve is unity) of the absorbing chemical from large (the darkest region) to small (the lightest region). However, when chemical incompletely covers the skin surface, as illustrated in Figure 7.2b, c and d, diffusion will proceed horizontally within each membrane as well as vertically through the membrane. Figure 7.3 schematically portrays the exposure from Figures 7.2b assuming no horizontal diffusion occurs (i.e., using a one-dimensional model). By comparing Figures 7.2b and 7.3, it is evident that horizontal diffusion within the sc and ve can contribute significantly to dermal absorption within and through the skin barrier when the surface is partly covered by chemical.

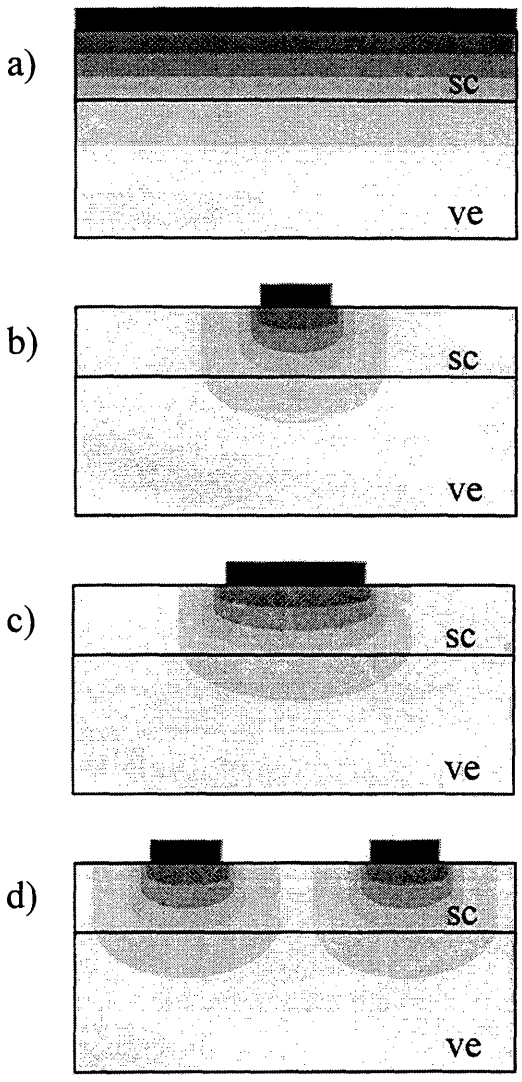

Figure 7.2 – Schematic illustration of dermal absorption from deposited chemical including horizontal and vertical diffusion when the exposed surface area is (a) completely, (b) 1/6th and (c and d) 1/3rd covered.

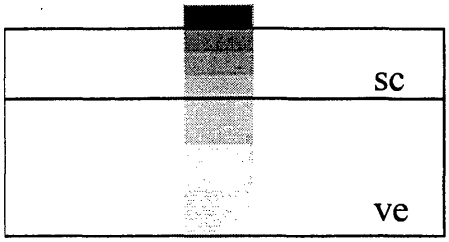

Figure 7.3 – Schematic illustration of dermal absorption from deposited chemical covering 1/6th of the surface area with vertical diffusion but no horizontal diffusion.

Several authors have described mathematical models of dermal absorption from finite dose exposures (i.e., as dermal absorption occurs, the mass of chemical on the skin decreases). Kasting (J. Pharm. Sci, submitted 2000) reported a set of dermal absorption data for vanillylnonamide (VN) applied to split-thickness (i.e., 150 μm thick) human cadaver skin in a propylene glycol vehicle with applied doses ranging from 1.4 to 4228 μg/cm^2. McCarley and Bunge (J. Pharm. Sci., submitted 2000) presented a model with one-dimensional diffusion through one skin layer (i.e., only accounting for the resistance of the sc) to describe these data. This model was developed assuming that uniformly distributed, equally sized piles of chemical decreased in size as dermal absorption proceeded. Kasting (J. Pharm. Sci, submitted 2000) proposed a different model of one-dimensional diffusion through a single skin layer to describe VN dermal absorption. Specifically, Kasting assumed that a finite chemical dose quickly distributes uniformly as a mixture with the outermost layer of the sc that can saturate.

Manitz *et al.* (1998) proposed a dermal absorption model with two-dimensional diffusion through three skin layers (i.e., the sc, ve, and dermis) from a vehicle that partially covers the skin surface. This model allowed for exposure to vehicles that included a penetration enhancer or reducer, either of which could alter the diffusion coefficient of the absorbing chemical in a skin layer. However, Manitz *et al.* (1998) only

considered the situation in which the space between chemical piles is large enough that there is no interference between adjacent piles.

Given the present understanding of non-uniformly distributed chemicals on the skin, a general mathematical description would be unjustifiably complicated. To focus specifically on the contribution of two-dimensional diffusion, certain simplifications have been included in our model development. Chemical residues on the skin surface may have irregular shapes, and these may shrink if sufficient chemical absorbs into the skin. To produce a mathematically manageable model, we have assumed that piles of chemical on the skin surface are identical, uniformly spaced rectangles of constant size (i.e., the dose is infinite). Similarly, while electron micrographs of skin show that the surface topography is irregular, we have treated the sc as a flat surface.

Increasing exposure time and increasing amount of chemical on the skin surface (i.e., applied dose) both cause increases in the mass of chemical in the epi and the rate of systemic absorption until saturation occurs and the rate of dermal absorption reaches a maximum. To remove the contribution of the exposure time, the results presented here were all calculated for steady state. The effects of two-dimensional diffusion and changes in applied dose at steady state should reasonably represent these effects before steady state is established. In addition, for situations in which chemicals are deposited using evaporating solvents, it is likely that solvent effects will have disappeared by the time steady state is reached.

Theory

The model system is depicted schematically in Figure 7.4. A three-dimensional view showing rectangular piles of chemical of width 2a, depth d, and height h distributed uniformly across the entire area exposed to chemical is shown in Figure 7.4a. The

exposed area is assumed to be large enough that its edges have little effect on dermal absorption. Furthermore, we assume that pile depth is much larger than pile width (i.e., a/d << 1) and that the distance between the center axis of adjacent piles is 2b, a constant. These assumptions allow for the simplified two-dimensional view of the system shown in Figure 7.4b. Two-dimensional, steady-state passive diffusion through the sc and ve, treated as two pseudo-homogenous membranes in series, is mathematically represented as follows:

$$\frac{\partial^2 C_{sc}}{\partial x^2} + \frac{\partial^2 C_{sc}}{\partial y^2} = 0 \qquad \text{for } 0 < x < L_{sc} \text{ and } 0 < y < b \qquad (7\text{-}1)$$

$$\frac{\partial^2 C_{ve}}{\partial x^2} + \frac{\partial^2 C_{ve}}{\partial y^2} = 0 \qquad \text{for } L_{sc} < x < L_{sc} + L_{ve} \text{ and } 0 < y < b \qquad (7\text{-}2)$$

in which x and y are vertical and horizontal position coordinates, respectively, and in membrane j with j designating either the sc or the ve, C_j is the concentration of the absorbing chemical and L_j is the apparent thickness.

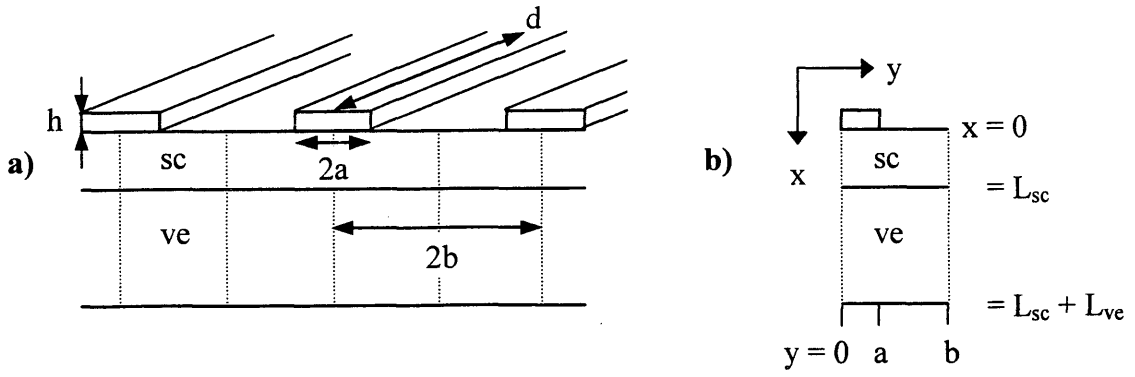

Figure 7.4 – Schematic diagrams, (a) three-dimensional and (b) two-dimensional, of the model coordinate system and variables.

Eqs 7-1 and 7-2 were solved subject to conditions at the boundaries of the sc and ve and between the piles of chemical. The skin surface (i.e., at x = 0) includes regions covered with chemical (i.e., for $0 < y < a$) separated by regions that are chemical free (i.e., $a < y < b$). Stated mathematically,

$$\text{at } x = 0 \qquad C_{sc} = C_{sc}^{o} \qquad \text{for } 0 < y < a \tag{7-3}$$

$$\text{and} \qquad \frac{\partial C_{sc}}{\partial x} = 0 \qquad \text{for } a < y < b \tag{7-4}$$

where eq 7-4 contains the assumption that that the absorbing chemical is not volatile. In eq 7-3, C_{sc}^{o} is the concentration of chemical in the outermost layer of the sc in direct contact with the applied material. If there is local equilibrium between the sc and the applied material, C_{sc}^{o} is the solubility limit in the sc if the applied material is neat chemical. However, if the applied material is a vehicle (v) containing non-evaporating components and the absorbing chemical at the concentration C_{v}^{o}, $C_{sc}^{o} = K_{sc/v} C_{v}^{o}$ where $K_{sc/v}$ is the partition coefficient between the sc and the vehicle. The remaining boundary conditions are:

$$\text{at } x = L_{sc} \qquad C_{sc} = K_{sc/ve}\, C_{ve} \tag{7-5}$$

$$\text{and} \qquad D_{sc} \frac{\partial C_{sc}}{\partial x} = D_{ve} \frac{\partial C_{ve}}{\partial x} \qquad \text{for } 0 < y < b \tag{7-6}$$

$$\text{at } x = L_{sc} + L_{ve} \qquad C_{ve} = 0 \qquad \text{for } 0 < y < b \tag{7-7}$$

$$\text{at } y = 0 \text{ and } y = b \qquad \frac{\partial C_{sc}}{\partial y} = 0 \qquad \text{for } 0 < x < L_{sc} \tag{7-8}$$

$$\text{and} \qquad \frac{\partial C_{ve}}{\partial y} = 0 \qquad \text{for } L_{sc} < x < L_{sc} + L_{ve} \tag{7-9}$$

where D_j is the effective diffusion coefficient of membrane j with j designating either the sc or the ve and $K_{sc/ve}$ is the equilibrium partition coefficient of absorbing chemical between the sc and ve. Eqs 7-5 and 7-6 stipulate local equilibrium and continuity of flux

at the sc-ve interface, and eq 7-7 specifies that the absorbing chemical concentration is zero (i.e., sink conditions are maintained) at the innermost boundary of the ve. Eqs 7-8 and 7-9 represent mathematically the symmetry depicted in Figure 7.4b.

Eqs 7-1 and 7-2 were solved subject to the conditions in eqs 7-3 through 7-9 to obtain C_{sc} and C_{ve} as functions of x and y. Since experimental determinations of these are practically impossible, they were converted into variables that can be measured experimentally, namely the steady-state mass of chemical in the epi (M_{epi}^{ss}) and the average steady-state flux of chemical across the epi (J^{ss}) defined as follows:

$$M_{epi}^{ss} = \frac{A}{b}\int_0^b \left[\int_0^{L_{sc}} C_{sc}dx + \int_{L_{sc}}^{L_{sc}+L_{ve}} C_{ve}dx\right] dy \tag{7-10}$$

$$J^{ss} = \frac{1}{b}\int_0^b -D_j \left.\frac{\partial C_j}{\partial x}\right|_x dy \tag{7-11}$$

where A is the total area of exposed skin and j = sc or ve depending on the position x at which the derivative is evaluated. At steady state, the average flux is the same at any position x within the sc or ve. Because M_{epi}^{ss} and J^{ss} are maximized when chemical completely covers the sc surface (i.e., when a/b = 1) it is convenient to define $\tilde{M}_{epi}^{ss} = M_{epi}^{ss} / (M_{epi}^{ss}$ when a/b = 1) and $\tilde{J}^{ss} = J^{ss} / (J^{ss}$ when a/b = 1).

Methods

Eqs 7-1 and 7-2 were solved subject to the conditions in eqs 7-3 through 7-9 using the finite difference scheme described in Appendix 7A. Each calculation required that four parameters be specified. Two parameters designate the amount and distribution of the applied chemical (i.e., a/b and either a/L_{sc} or b/L_{sc}). The remaining two parameters

are ratios of the dermal absorption properties of the sc and ve. These are thicknesses (L_{sc} / L_{ve} ~ 0.1 based on L_{sc} ~ 15 μm and L_{ve} ~ 100 – 200 μm (Scheuplein, 1972)) and the permeability coefficients (B) defined as follows:

$$B = K_{sc/ve}\frac{D_{sc}L_{ve}}{D_{ve}L_{sc}} \tag{7-12}$$

Since permeability coefficients through the ve have been measured infrequently, few experimental values of B are available. Bunge and Cleek (1995) proposed estimating B using the formula:

$$B = 0.00061\sqrt{MW}10^{-0.006MW}K_{o/w}^{0.74} \tag{7-13}$$

where MW is molecular weight and $K_{o/w}$ is the octanol – water partition coefficient. Vecchia (1997) was able to estimate B values from experimental measurements for a few chemicals, which were generally consistent with eq 7-13. This equation indicates that B can range from nearly zero for highly hydrophilic chemicals to 10 for highly lipophilic chemicals of small molecular size.

The calculation of M_{epi}^{ss} requires the specification of one more parameter, the ratio of the sc to the ve lag times (G) defined as:

$$G = \frac{D_{ve}L_{sc}^2}{D_{sc}L_{ve}^2} \tag{7-14}$$

Typically, G > 10 because D_{ve} / D_{sc} > 1000 (Scheuplein, 1972). When G > 10, M_{epi}^{ss} is essentially independent of G. However, if the applied dose is small (i.e., a/b < 0.3) and the chemical is not extremely lipophilic (i.e., B < 1), M_{epi}^{ss} does vary slightly with G. For all calculations in this study, G = 10.

Assuming the height of the chemical piles (h) is constant as long as the exposed surface is partly covered, defining two of the specified ratios (a/b, a/L_{sc} and b/L_{sc}) specifies the applied dose (i.e., the mass of chemical applied per area exposed) and the

distribution of chemical on the skin surface. As the applied dose increases, a/b increases to a maximum value of 1, when the entire exposed area is in direct contact with chemical. Further increases in applied dose increase the pile height.

An applied dose of chemical can be distributed as a few large piles or many small piles as illustrated in Figures 7.2c and d. In these diagrams, the amount of chemical applied is identical (i.e., a/b = 1/3) but the piles in Figure 7.2d are half as wide as the piles in Figure 7.2c (i.e., both a/L_{sc} and b/L_{sc} are half as big). Similarly, increasing the applied dose can be modeled using two distinct mechanisms, referred to here as dose effect one (DE1) and two (DE2). For DE1, increasing the applied dose is modeled as a finite number of piles of chemical on the skin increasing in size, as illustrated by Figure 7.2b and c. The applied dose per area is two times larger in Figure 7.2c because it is twice as wide (i.e., a/b doubled because a/L_{sc} doubled while b/L_{sc} remained constant). For DE2, as the applied dose increases more identically sized piles are deposited on the skin as illustrated by Figures 7.2b and d. The applied dose is doubled in Figure 7.2d because there are twice as many piles of identical size (i.e., a/b doubled because b/L_{sc} are half as big while a/L_{sc} remained constant).

Results and Discussion

Figures 7.5 and 7.6 present $\tilde{M}^{ss}_{epi}$ and $\tilde{J}^{ss}$ respectively for DE1 (i.e., the applied dose is increased by increasing the pile size) for B = 0.1, 1, and 10. For DE1, small values of a/b correspond to piles of small width. Figures 7.7 and 7.8 present the same information for DE2 (i.e., the applied dose is increased by increasing the number of piles). In Figures 7.7 and 7.8, small values of a/b represent a small number of piles.

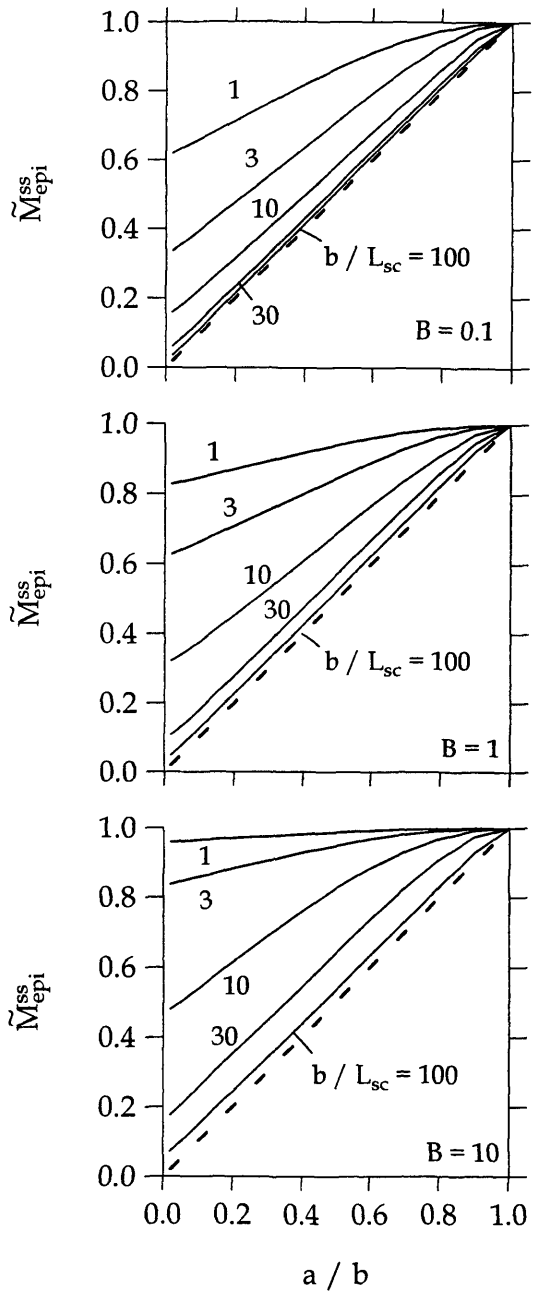

Figure 7.5 – $\tilde{M}^{ss}_{epi}$ as a function of the area fraction covered (a/b) for constant spacing between piles (i.e., constant b/L_{sc}) when B = 0.1, 1, and 10. As the applied dose increases, piles get wider (DE1).

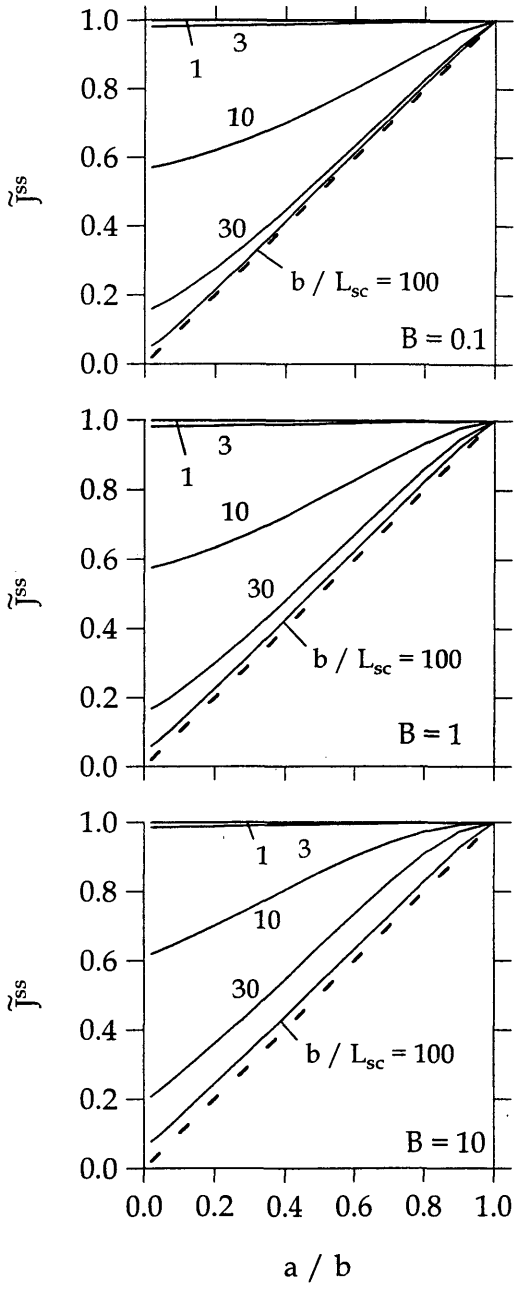

Figure 7.6 – $\tilde{J}^{ss}$ as a function of the area fraction covered (a/b) for constant spacing between piles (i.e., constant b/L_{sc}) when B = 0.1, 1, and 10. As the applied dose increases, piles get wider (DE1).

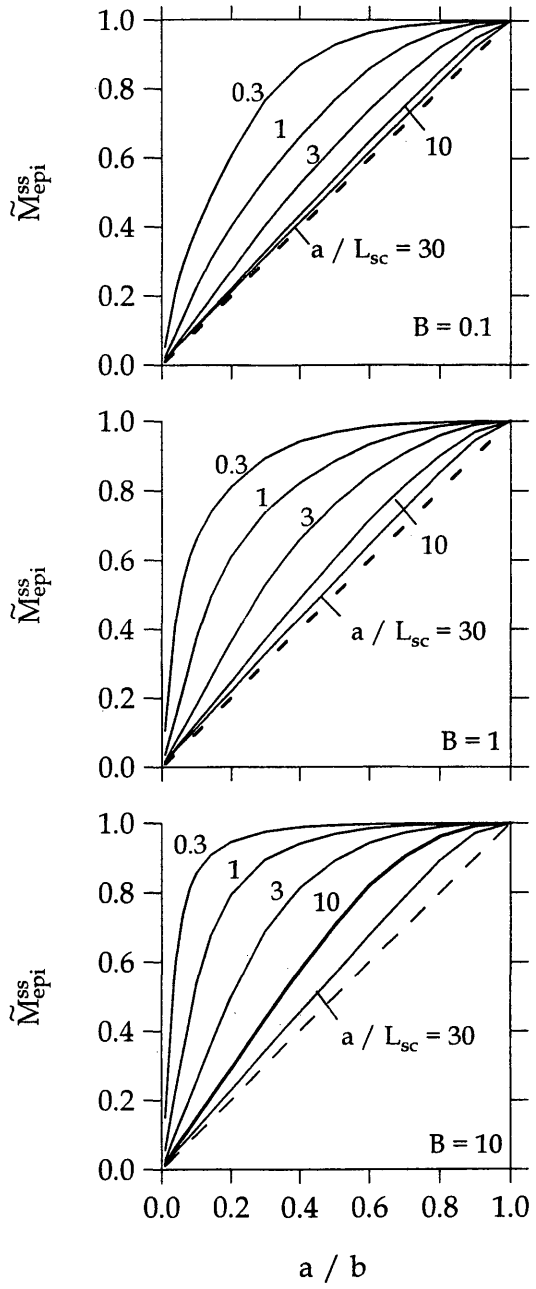

Figure 7.7 – $\tilde{M}^{ss}_{epi}$ as a function of the area fraction covered (a/b) for piles of constant width (i.e., constant a/L_{sc}) when B = 0.1, 1, and 10. As the applied dose increases, more piles are deposited on the skin (DE2).

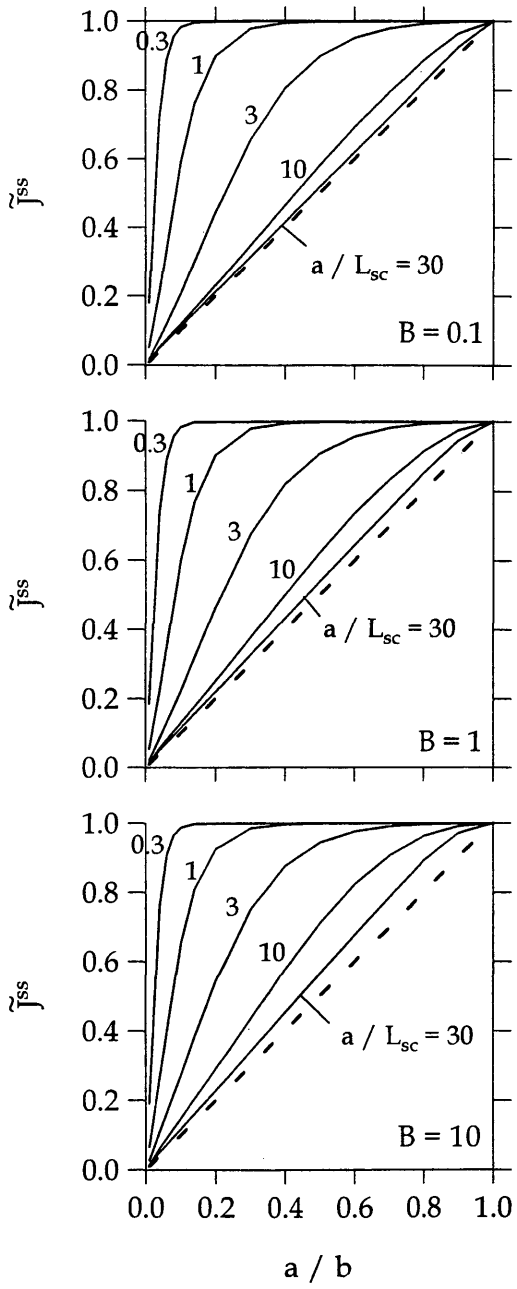

Figure 7.8 – $\tilde{J}^{ss}$ as a function of the area fraction covered (a/b) for piles of constant width (i.e., constant a/L_{sc}) when B = 0.1, 1, and 10. As the applied dose increases, more piles are deposited on the skin (DE2).

Plotting $\tilde{M}_{epi}^{ss}$ and $\tilde{J}^{ss}$ instead of M_{epi}^{ss} and J^{ss} allows comparison of results for exposures to chemicals with different lipophilicities (i.e., values of B). The dashed lines in Figures 7.5-7.8 indicate results if horizontal diffusion does not occur (i.e., assuming one-dimensional diffusion as illustrated in Figure 7.3). The dashed lines are calculated by multiplying $\tilde{M}_{epi}^{ss}$ and $\tilde{J}^{ss}$ when the skin is completely covered by a/b. Because horizontal diffusion causes chemical to move into areas of the skin uncovered by chemical, $\tilde{M}_{epi}^{ss}$ and $\tilde{J}^{ss}$ calculated with horizontal diffusion are always larger than when calculated without horizontal diffusion.

For constant applied dose (i.e., constant a/b), the chemical pile width decreases as b/L_{sc} decreases in Figures 7.5 and 7.6, and as a/L_{sc} decreases in Figures 7.7 and 7.8. Smaller values of a/L_{sc} than b/L_{sc} are considered because a is always $\leq$ b, as shown in Figure 7.4. For both DE1 and DE2, the effect of horizontal diffusion increases (i.e., the solid curves deviate more from the dashed line) as the width of the chemical pile decreases. This situation is illustrated in Figures 7.2c and d. When the pile width is large relative to the sc thickness, horizontal diffusion has almost no effect and $\tilde{M}_{epi}^{ss}$ and $\tilde{J}^{ss}$ increase proportionally with applied dose, as predicted by the one-dimensional model. Based on results in Figures 7.7 and 7.8, horizontal diffusion contributes noticeably if the pile width, 2a, is less than ~ 60 L_{sc} (i.e., $a/L_{sc} < 30$). For typical human sc, this corresponds to a pile width of about 600 – 1200 μm, which is large enough to be visible. Commonly, skin contamination is present with no visible evidence, indicating that pile sizes are small enough that horizontal diffusion could be important for typical exposures.

Whether chemicals deposit by DE1 or DE2 does affect results. Unless the piles are much farther apart than the sc thickness (i.e., $b/L_{sc} > 100$), increasing the applied dose by increasing the pile size (i.e., DE1) affects dermal absorption differently than increasing the number of piles (i.e., DE2). For example, when the area fraction covered is small

(i.e., a/b ~ 0), DE1 does not predict negligible $\tilde{M}_{epi}^{ss}$ and $\tilde{J}^{ss}$, but DE2 does. For DE1, a/b ~ 0 represents a finite number of extremely narrow piles of chemical on the skin at a specified distance apart (i.e., at a given b/L_{sc}). In contrast, when a/b ~ 0 for DE2 the number of piles of specified width (i.e., at a given a/L_{sc}) has shrunk to zero.

Examination of Figures 7.5 to 7.8 shows that $\tilde{J}^{ss}$ is nearly independent of B, but $\tilde{M}_{epi}^{ss}$ is not. As a result, $\tilde{J}^{ss}$ can appear to be saturated (i.e., $\tilde{J}^{ss} \sim 1$) at an applied dose smaller than required to completely cover the sc (i.e., a/b < 1), while $\tilde{M}_{epi}^{ss}$ still increases with applied dose. The values of a/b causing $\tilde{J}^{ss} \sim 1$ and $\tilde{M}_{epi}^{ss} \sim 1$ are most different when B is small. At larger values of B, the ve presents a significant mass transfer barrier and restricts flux, causing $\tilde{J}^{ss}$ and $\tilde{M}_{epi}^{ss}$ to appear saturated at similar values of a/b.

To examine saturation, we define $(a/b)_{90\%}$ as the fraction of the exposed area covered by chemical at which M_{epi}^{ss} and J^{ss} reach 90% of their maximum values (i.e., $\tilde{J}^{ss}$ or $\tilde{M}_{epi}^{ss} = 0.9$) because at the applied dose of $(a/b)_{90\%}$, M_{epi}^{ss} or J^{ss} would appear to be saturated. Figure 7.9 presents $(a/b)_{90\%}$ plotted as a function of surface distribution (i.e., a/L_{sc} for DE1 and b/L_{sc} for DE2) for three values of B. As already discussed, $\tilde{J}^{ss}$ saturates at smaller applied doses than $\tilde{M}_{epi}^{ss}$. This observation is consistent with results described in Chapter 6 of dermal absorption from small doses of pesticide, in which the mass in the skin increased proportionally to applied dose while the flux through the skin was almost independent of applied dose. Also, $\tilde{J}^{ss}$ is less dependent on B than $\tilde{M}_{epi}^{ss}$ for both DE1 and DE2. Significantly, as long as b/L_{sc} or a/L_{sc} is smaller than ~ 20, both $\tilde{J}^{ss}$ and $\tilde{M}_{epi}^{ss}$ are 90% saturated even for a/b < 0.9. As illustrated in Figure 7.2, this occurs because the ve is thicker and has a larger diffusion coefficient than the sc, while the sc holds more chemical than the ve. Thus, several small piles (e.g., Figure 7.2d) can

produce a concentration profile in the ve that is similar to that from a completely covered surface (e.g., Figure 7.2a). At the same time, the concentration profile in the sc for the partly covered and completely covered surfaces are quite different (e.g., compare Figures 7.2d and a).

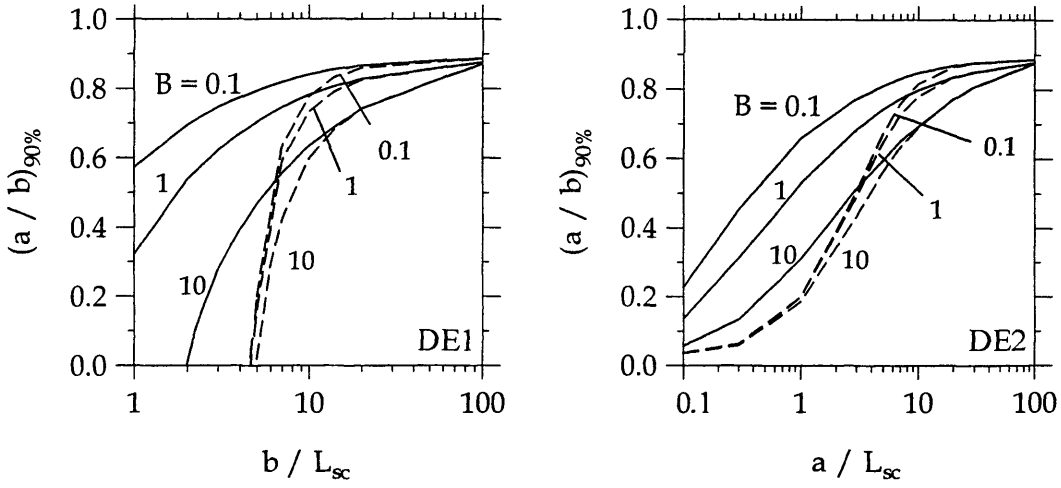

Figure 7.9 – The value of a/b at which $\tilde{M}_{epi}^{ss}$ (solid curves) and $\tilde{J}^{ss}$ (dashed curves) = 0.9 as a function of distance between piles (b/L_{sc}) for DE1 and pile size (a/L_{sc}) for DE2.

Because many deposition studies of dermal absorption have applied doses in log-intervals (i.e., 10-fold dilutions) (Zendzian, 1994), log-log plots of selected results for DE1 and DE2 are shown in Figures 7.10 and 7.11, respectively. At a given a/b and either b/L_{sc} (for DE1) or a/L_{sc} (for DE2), the fact that the slope of $\tilde{J}^{ss}$ is always less than or equal to the slope of $\tilde{M}_{epi}^{ss}$ is consistent with $\tilde{J}^{ss}$ saturating at much smaller values of a/b than $\tilde{M}_{epi}^{ss}$.

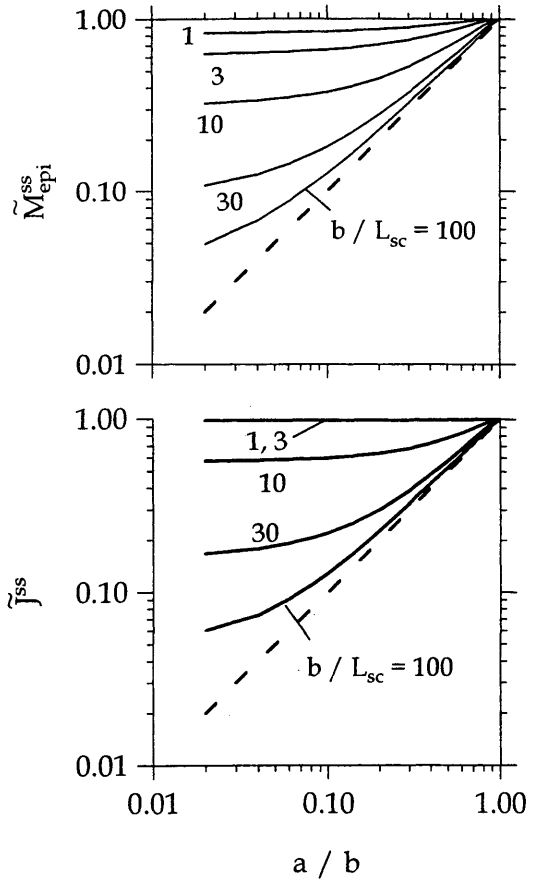

Figure 7.10 – $\tilde{M}^{ss}_{epi}$ and $\tilde{J}^{ss}$ as a function of the area fraction covered (a/b) for constant spacing between piles (i.e., constant b/L_{sc}) for DE1 when B = 1.

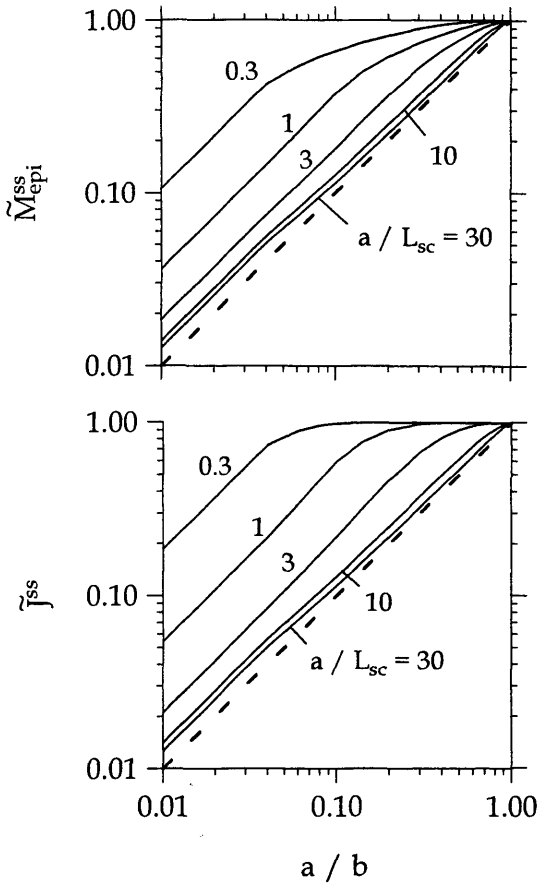

Figure 7.11 – $\tilde{M}^{ss}_{epi}$ and $\tilde{J}^{ss}$ as a function of the area fraction covered (a/b) for piles of constant width (i.e., constant a/L_{sc}) for DE2 when B = 1.

Figures 7.10 and 7.11 also demonstrate that varying the spatial distribution of chemical on the skin surface can dramatically affect both the amount of chemical in the skin and the flux through the skin. For example, results in Figure 7.10 indicate that when 2% of the surface is covered with absorbing chemical (i.e., a/b = 0.02), $\tilde{J}^{ss}$ is 16-fold larger if $b/L_{sc} = 3$ (i.e., many small piles) than if $b/L_{sc} = 100$ (i.e., few large piles). Specifically, $\tilde{J}^{ss} \sim 1$ when $b/L_{sc} = 3$ and $\tilde{J}^{ss} \sim 0.06$ when $b/L_{sc} = 100$. For a typical L_{sc} value of 20 μm, when a/b = 0.02, the b/L_{sc} values of 3 and 100 correspond to pile widths of 1.2 and 40 μm, respectively. Pile widths of 1.2 and 40 μm both seem plausible. Thus, without experimental measurements of spatial distribution, it is impossible to know if differences in the amount absorbed for two different chemicals arise from differences in chemical activity or from differences in spatial distribution on the skin surface.

Comparing Figures 7.10 and 7.11, distinctive differences between DE1 and DE2 are evident. For DE1, Figure 7.10 slopes are smaller for low applied doses (i.e., small a/b) and larger (i.e., approaching 1) for higher doses. In contrast, for DE2 (Figure 7.11) the slopes are ~ 1 at small values of a/b and decrease to zero as a/b increases. If increases in applied dose proceed by DE1, M_{epi}^{ss} and J^{ss} would appear to be independent of dose at low doses which could be incorrectly interpreted as evidence that M_{epi}^{ss} and J^{ss} are saturated. This confusion will not occur if increases in applied dose occur by DE2.

In an actual dermal exposure, it is unknown whether increases in applied doses proceed by DE1, DE2, or a combination of the two. Both mechanisms may occur to varying extents depending on a range of variables including the size of the applied dose and the composition of the formulation applied to the skin. One mechanism (perhaps DE2) may dominate at low applied doses, and the other (perhaps DE1) might dominate at high applied doses. Also, the spatial distribution of deposited chemicals may be different for rapidly and slowly evaporating solvents. Finally, surfactants and spreading agents, if present, almost certainly would affect distribution.

The potential effects of surface distribution on dermal absorption experiments are explored in Figure 7.12, which shows mathematically simulated results for a chemical with B = 0.1 for the five *hypothetical experiments* described in Table 7.1. The curves represent results for all values of $(a\ h^*)/(b\ h)$ between 0.01 and 10, in which $h^* = h$ for $a/b < 1$ and $h^* \geq h$ for $a/b = 1$ (i.e., applied doses large enough to completely cover the skin result in a thicker layer of chemical). Once the surface is completely covered by chemical, further increasing dose (i.e., for $(a\ h^*)/(b\ h) \geq 1$) has no effect on M_{epi}^{ss} and J^{ss}.

A typical deposition experiment (e.g., data collected using the Zendzian protocol (Zendzian, 1994)) might have data for three or four applied doses at 10-fold dilutions of a concentrated formulation. This situation is illustrated by three *data points* marked on each curve at $(a\ h^*)/(b\ h) = 0.04$, 0.4, and 4. In these hypothetical experiments, only the highest applied dose of chemical completely covers the skin. A chemical applied in different formulations might distribute on the skin by different mechanisms. Significantly, different mechanisms could produce widely varying results as shown in Figure 7.12 for the experiments listed in Table 7.1.

Experimentally, M_{epi}^{ss} and J^{ss} at $a/b = 1$ are usually unknown, and consequently saturation (i.e., $\tilde{M}_{epi}^{ss}$ and $\tilde{J}^{ss} \sim 1$) can only be recognized when M_{epi}^{ss} and J^{ss} are the same for at least two applied doses. Looking at the three data points for each of the hypothetical experiments, none appear to be saturated based on $\tilde{M}_{epi}^{ss}$ (i.e., $\tilde{M}_{epi}^{ss}$ increases as applied dose increases for all three data points), although $\tilde{M}_{epi}^{ss}$ is saturated at the highest applied dose. To experimentally demonstrate that $\tilde{M}_{epi}^{ss}$ is saturated at the highest dose would require data for an even higher dose. When looking at $\tilde{J}^{ss}$, experiments 2, 4 and 5 do not appear to reach saturation, but experiments 1 and 3 appear to be saturated at all three applied doses. Thus, consistent with previous discussion, J^{ss}

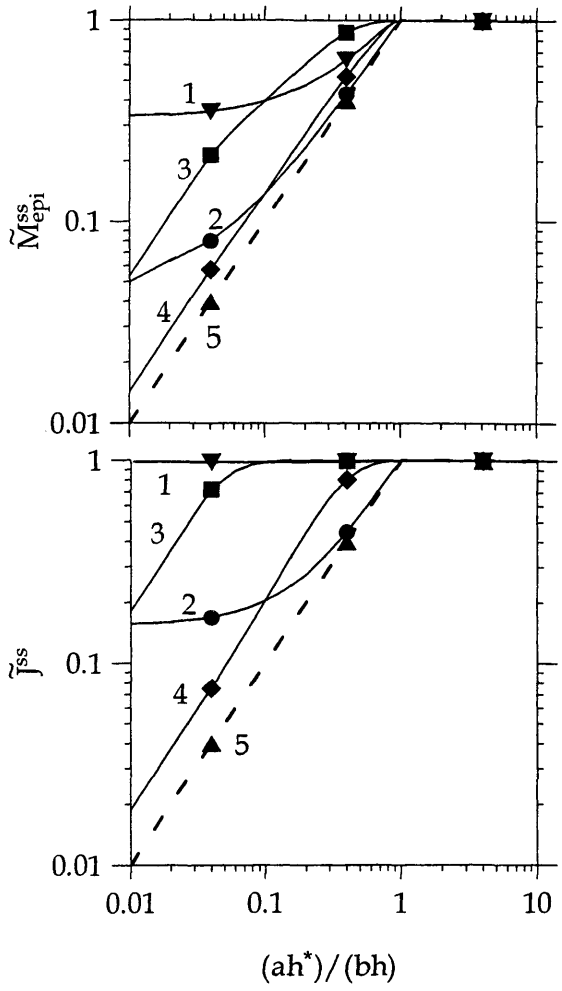

Figure 7.12 – $\tilde{M}_{epi}^{ss}$ and $\tilde{J}^{ss}$ as a function of applied dose for B = 0.1 for simulated dermal exposures with the distributions of chemical on the skin described in Table 7.1.

Table 7.1 – Summary of dermal exposure scenarios simulated in Figure 7.12.

experiment	increase dose by increasing	distribution	symbol in Figure 7.12
1	pile size (DE1)	$b/L_{sc} = 3$	▼
2	pile size (DE1)	$b/L_{sc} = 30$	●
3	number of piles (DE2)	$a/L_{sc} = 0.3$	■
4	number of piles (DE2)	$a/L_{sc} = 3$	◆
5	one-dimensional model	NA	▲

can appear to be saturated at applied doses that do not completely cover the skin (i.e., $(a\ h^*)/(b\ h) < 1$). In addition, experiments 1 and 3 show that when horizontal diffusion is important as it is for the small piles in Experiments 1 and 3, $\tilde{M}_{epi}^{ss}$ can continue to increase with increasing applied dose even when $\tilde{J}^{ss}$ is saturated. If data are collected for several applied doses over a wide enough range of values, it is experimentally possible to determine the minimum applied dose producing dose-independent values for both M_{epi}^{ss} and J^{ss}. However, it is impossible to know whether or not the saturating dose completely covers the skin.

Conclusions

For a dermal exposure to chemical deposited on the skin surface, the distribution of chemical as either many small piles or few large piles can significantly affect dermal absorption. Horizontal diffusion into uncovered regions of the skin can increase the mass of chemical in the epi and the flux through the skin. This is most pronounced when the width of the chemical piles is small relative to the thickness of the sc. For small piles of

chemical, applied doses covering only a fraction of the exposed skin can produce as much dermal absorption as occurs with completely covered skin. For small piles of chemical with up to moderate lipophilicity (i.e., small values of B), flux from the epi can appear to be saturated at much smaller applied doses than required to saturate the epi with chemical. Significantly, it is impossible to know whether chemical completely covers the skin at the applied dose at which both M_{epi}^{ss} and J^{ss} appear saturated.

Notation

a	half the thickness of a pile of deposited chemical
A	total surface area exposed to chemical
b	half the distance from the center of one pile of deposited chemical to another
B	ratio of the permeability coefficient of the absorbing chemical in the sc to the permeability coefficient in the ve from the same vehicle
C_j	concentration of the absorbing chemical in membrane layer j
C_{sc}^o	concentration of chemical in the outermost layer of the sc in direct contact with the applied material (e.g., the solubility limit if pure chemical is applied)
C_v^o	constant concentration of the absorbing chemical in the vehicle
d	depth of the deposited pile
D_j	effective diffusion coefficient of the absorbing chemical in membrane layer j
epi	epidermis
G	ratio of lag times in the sc and ve, $D_{ve}L_{sc}^2/\left(D_{sc}L_{ve}^2\right)$
h	height of the deposited piles of chemical when $a/b \leq 1$
h^*	height of the deposited piles of chemical (i.e., $h^* = h$ for $a/b < 1$, $h^* \geq h$ for $a/b = 1$)
j	designates either the sc or ve
J^{ss}	average flux of absorbing chemical through the epi at steady state
$\tilde{J}^{ss}$	average steady-state flux through the membrane divided by the steady-state flux when $a/b = 1$
$K_{o/w}$	octanol – water partition coefficient

$K_{sc/v}$	equilibrium partition coefficient of the absorbing chemical between the sc and the vehicle
$K_{sc/ve}$	equilibrium partition coefficient of the absorbing chemical between the sc and ve
L_j	apparent thickness of membrane layer j
M_{epi}^{ss}	mass of absorbing chemical in the epi at steady state
$\tilde{M}_{epi}^{ss}$	steady-state mass of chemical in the epi divided by the steady-state mass of chemical in the epi when a/b = 1
MW	molecular weight
N_b	number of nodes in the y-direction for the finite difference solution
N_j	number of nodes in the x-direction of membrane layer j for the finite difference solution
sc	stratum corneum
ve	viable epidermis
x	vertical position in the epi
Δx_j	distance between finite difference nodes in membrane layer j in the x-direction
y	horizontal position in the epi
Δy	distance between finite difference nodes in the y-direction

References

Bunge, A. L. and R. L. Cleek (1995). "A new method for estimating dermal absorption from chemical exposure. 2. Effect of molecular weight and octanol-water partitioning." Pharmaceutical Research **12**:88-95.

Kasting, G. B. (submitted 2000). "Kinetics of finite dose absorption through skin. 1. Vanillylnonamide." Journal of Pharmaceutical Sciences.

Manitz, R., W. Lucht, K. Strehmel, R. Weiner and R. Neubert (1998). "On mathematical modeling of dermal and transdermal drug delivery." Journal of Pharmaceutical Sciences **87**:873-879.

McCarley, K. D. and A. L. Bunge (submitted 2000). "Dermal absorption of solvent deposited chemicals." Journal of Pharmaceutical Sciences.

Scheuplein, R. J. (1972). "Properties of the skin as a membrane." Advances in Biology of Skin (New York) **12**:125-152.

Scheuplein, R. J. and R. L. Bronaugh (1983). Percutaneous absorption. Biochemistry and Physiology of the Skin, vol. II. L. A. Goldsmith, ed. New York, Oxford University Press. 1255-1295.

Vecchia, B. (1997). Estimating the Dermally Absorbed Dose from Chemical Exposure: Data Analysis, Parameter Estimation, and Sensitivity to Parameter Uncertainties. M.S. thesis, Department of Chemical Engineering and Petrolium Refining, Colorado School of Mines, Golden, CO.

Zendzian, R. P. (1994). Pesticide Assessment Guidelines. Subdivision F, Hazard Evaluation, Human and Domestic Animals: Dermal Absorption of Pesticides. Office of Pesticide Programs, US Environmental Protection Agency, Washington, DC.

Appendix 7A – Numerical Solution

For the finite difference solution, the sc, ve and length between piles (i.e., b) were split into N_{sc}, N_{ve} and N_b nodes, respectively. The spatial derivatives were calculated using the following finite difference formulas:

$$\left.\frac{\partial^2 C_j}{\partial k^2}\right|_i = \frac{C_{j,i-1} - C_{j,i} + C_{j,i+1}}{(\Delta k)^2} \tag{7A-1}$$

$$\left.\frac{\partial C_j}{\partial k}\right|_i = \frac{-3C_{j,i} + 4C_{j,i+1} - C_{j,i+2}}{2\Delta k} \tag{7A-2}$$

$$\left.\frac{\partial C_j}{\partial k}\right|_i = \frac{C_{j,i-2} - 4C_{j,i-1} + 3C_{j,i}}{2\Delta k} \tag{7A-3}$$

where j designates either the sc or ve, k can be x or y, and i represents the position of the nodes in the direction of k. Eq 7A-1 was used for eqs 7-1 and 7-2. Eq 7A-2 is a forward difference equation (e.g., it can be used for eq 7-4), and eq 7A-3 is a backwards difference equation (e.g., it can be used for eq 7-8 at y = b). When k = x, $\Delta k = \Delta x_j$ defined as

$$\Delta x_j = L_j / (N_j - 1) \tag{7A-4}$$

and when k = y, $\Delta k = \Delta y$ defined as

$$\Delta y = b / (N_b - 1) \tag{7A-5}$$

Eqs 7A-1 through 7A-3 are second-order accurate in x. Calculations were typically performed with $N_{sc} = 51$, $N_{ve} = 31$, and $N_b = 51$. N_{ve} was smaller because the ve contains less chemical than the sc and the concentration gradient across it is smaller. The resulting system of ordinary differential equations was solved using the FORTRAN computer program found in Appendix B.

The numerical solution was checked for stability with respect to the number of nodes by increasing the number of nodes with no change in the answer. Also, the solution when a/b = 1 was compared to the solution for a one-dimensional model.

Appendix 7B – FORTRAN Program

Table 7B.1 – Variable names in the FORTRAN program.

variable in program	variable in chapter
X(N1,ND)	Array containing $C_{sc}/\left(K_{sc/v}C_v^o\right)$ at various nodes
Y(N2,ND)	Array containing $C_{ve}/\left(K_{ve/v}C_v^o\right)$ at various nodes
B	B
G	G
EVE	η_{ve}
ED	b/L_{sc}
N1	N_{sc}
N2	N_{ve}
ND	N_b
DSC	$\Delta x_{sc} / L_{sc}$
DVE	$\Delta x_{ve} / L_{sc}$
DY	$\Delta y / b$
MG	$M_{epi}^{ss}/\left(AL_{sc}K_{sc/v}C_v^o\right)$ calculated assuming G = 10
MGG	$M_{epi}^{ss}/\left(AL_{sc}K_{sc/v}C_v^o\right)$ calculated assuming G = 100
FSS	$J^{ss}/\left(P_{sc,v}C_v^o\right)$
DDD	a/b
ED	b/L_{sc}

```
      PROGRAM PESTCALC
C 2-D model to calculate dermal absorption from an incomplete
C film through a 2-layer membrane into an infinite sink

      INTEGER N,ND
      PARAMETER(N1 = 51, N2 = 31, ND = 51)
      INTEGER I1,I2,I3,IC3,IC,IC2,DD,I,J,M,I7
      REAL X(N1,ND),XD(N1,ND),Y(N2,ND),YD(N2,ND)
      REAL DSC,DVE,DY,RC(6),RN,DDD,FSSD,REAL B,EVE,ED,Z,FSS
      REAL MVE,MSC,DUM1,SSC,MVED,SSC2,XL,MG,MGG

C The file input.dat contains an integer with the number of solutions
C you want the program to complete, and then a list which contains (for
C each solution) b/Lsc, B, and the number of nodes covered by chemical.
      OPEN(1, FILE='input.dat', STATUS='OLD')
      OPEN(4, FILE='data.dat', STATUS='NEW')

      EVE = 10.
      G = 10.
      DSC = 1./REAL(N1-1)
      DVE = EVE/REAL(N2-1)
      DY = 1./REAL(ND-1)

      READ(1,*) IC
      DO 91,I1 = 1,IC
      READ(1,*) ED, B, DD

      DDD = REAL(DD-1)/REAL(ND-1)
      FSSD = 0.
      MVED = 0.

C Setting Initial Condition
      DO 1, J=2,ND
      DO 2, I=1,N1
      X(I,J) = 0.
 2    XD(I,J) = 0.
      DO 3, I=1,N2
      Y(I,J) = 0.
 3    YD(I,J) = 0.
 1    CONTINUE

      DO 4,J=1,DD
      XD(1,J) = 1.
 4    X(1,J) = 1.
      IF (DD .NE. ND) THEN
      XD(1,DD) = 0.5
      X(1,DD) = 0.5
      END IF

C BC is no-flux, but I set it to the known solution concentration
C profile every 20 iterations to speed convergence to the solution.
      DO 5,I=2,N1
      XL = REAL(I-1)/REAL(N1-1)
 5    X(I,1) = (1.+B-XL)/(1.+B)
```

```
      DO 6,I=1,N2-1
      XL = REAL(I-1)/REAL(N2-1)
 6    Y(I,1) = B*(1.-XL)/(1.+B)

      IC2 = 2000
      IC3 = 200
      I7 = 0
      DO 922,I3 = 1,IC3
      DO 92,I2 = 1,IC2

C Calculating middle values
      DO 7,J=2,ND-1

      DO 8,I=2,N1-1
      RC(1) = X(I+1,J)
      RC(2) = X(I-1,J)
      RC(3) = X(I,J+1)
      RC(4) = X(I,J-1)
 8    XD(I,J) = RN1(RC,DSC,DY,ED)

      DO 7,I=2,N2-1
      RC(1) = Y(I+1,J)
      RC(2) = Y(I-1,J)
      RC(3) = Y(I,J+1)
      RC(4) = Y(I,J-1)
 7    YD(I,J) = RN1(RC,DVE,DY,ED)

      DO 623,J=2,ND-1
      DO 624,I=2,N1-1
 624  X(I,J) = XD(I,J)
      DO 623,I=2,N2-1
 623  Y(I,J) = YD(I,J)

C Calculating BCs
      DO 11,J=2,ND
      DO 12,M=1,3
      RC(M)=X(N1-M,J)
 12   RC(3+M)=Y(1+M,J)
      Y(1,J)=RN3(RC,DSC,DVE,EVE,B)
 11   X(N1,J)=Y(1,J)

      DO 13,I=2,N1
      DO 14,M=1,3
 14   RC(M)=X(I,ND-M)
      X(I,ND) = RN2(RC)
      DO 1444,M=1,3
 1444 RC(M)=X(I,1+M)
 13   X(I,1) = RN2(RC)

      DO 15,I=2,N2-1
      DO 16,M=1,3
 16   RC(M)=Y(I,ND-M)
      Y(I,ND) = RN2(RC)
      DO 1666,M=1,3
```

```
 1666  RC(M)=Y(I,1+M)
 15    Y(I,1) = RN2(RC)

       Y(1,ND)=X(N1,ND)
       Y(1,1)=X(N1,1)

       DO 17,J=DD,ND
       DO 18,M=1,3
 18    RC(M)=X(1+M,J)
 17    X(1,J) = RN2(RC)
       DO 19,M=1,3
 19    RC(M)=X(1,ND-M)
       X(1,ND) = X(1,ND)/2. + RN2(RC)/2.
       X(1,DD) = X(1,DD)/2.+0.5
       IF (DD .EQ. ND) XD(1,DD) = 1.

C BC is no-flux, but I set it to the known solution concentration
C profile every 20 iterations to speed convergence to the solution.
       I7 = I7 + 1
       IF (I7 .EQ. 20) THEN
       DO 1112, I = 1,N1
       XL = REAL(I-1)/REAL(N1-1)
 1112  X(I,1) = (B+1.-XL)/(B+1.)
       DO 1113, I = 1,N2-1
       XL = REAL(I-1)/REAL(N2-1)
 1113  Y(I,1) = B*(1.-XL)/(B+1.)
       I7 = 0
       END IF

 92    CONTINUE

C Calculating masses of chemical in the SC and VE and SS flux
       MSC = 0.
       MVE = 0.
       DO 20,J=1,ND-1
       DO 625,I=1,N1-1
       DUM1 = X(I,J)+X(I+1,J)+X(I,J+1)+X(I+1,J+1)
 625   MSC = MSC + DUM1/4.*DSC*DY
       DO 20,I=1,N2-1
       DUM1 = Y(I,J)+Y(I+1,J)+Y(I,J+1)+Y(I+1,J+1)
 20    MVE = MVE + DUM1/4.*DVE*DY/EVE

       FSS = 0.
       DO 21,J=1,ND-1
       DUM1 = 2.*(Y(N2-3,J)+Y(N2-3,J+1)) - 9.*Y(N2-2,J)
       DUM1 = DUM1 - 9.*Y(N2-2,J+1) + 18.*(Y(N2-1,J)+Y(N2-1,J+1))
 21    FSS = FSS + DUM1/2./6./DVE*DY*EVE/B

C 92    CONTINUE

C Convergence criteria:  If FSS and MVE change by < 0.2%in 2000
C iterations, answer ok
       SSC = (FSS - FSSD)/FSS*100.
       FSSD = FSS
```

```
      SSC2 = (MVE - MVED)/MVE*100.
      MVED = MVE
      MG = MSC + MVE/B/G
      MGG = MSC + MVE/B/G/10.

      IF ((SSC .LT. 0.2) .AND. (SSC2 .LT. 0.2)) GOTO 995

 922  CONTINUE
 995  CONTINUE
      WRITE(4,997) DDD,B,ED,MSC,MG,MGG,FSS,I3
 91   CONTINUE

 997  FORMAT(2F6.2,F5.1,4E10.4,I4)
 999  FORMAT(30E11.5)
 998  FORMAT(2F5.2,2E8.2,4E10.4,I4)
      END

C RN1 calculates the values for the middle nodes.
      FUNCTION RN1(RC,DX,DY,ED)
      REAL RC(6)
      REAL DX,DY,TT,ED
      RN1 = (RC(1)+RC(2))/DX/DX
      RN1 = RN1 + (RC(3)+RC(4))/DY/DY/ED/ED
      RN1 = RN1 / (2./DX/DX+2./ED/ED/DY/DY)
      RETURN
      END

      FUNCTION RN2(RC)
      REAL RC(6)
      RN2 = (18.*RC(1)-9.*RC(2)+2.*RC(3))/11.
      RETURN
      END

      FUNCTION RN3(RC,DSC,DVE,EVE,B)
      REAL RC(6),DSC,DVE,EVE,B
      RN3 = (18.*RC(1)-9.*RC(2)+2.*RC(3))/DSC
      RN3 = RN3 + (18.*RC(4)-9.*RC(5)+2.*RC(6))*EVE/B/DVE
      RN3 = RN3/(11./DSC+11.*EVE/B/DVE)
      RETURN
      END
```

Chapter 8. SUMMARY AND RECOMMENDATIONS FOR FUTURE WORK

The overall goal of this research was to expand the general mechanistic understanding of the percutaneous penetration process through detailed studies of several factors affecting dermal uptake and its measurement. To accomplish this goal, various mathematical models were developed describing human skin as a one or two-layer membrane through which chemical passively diffused. These conceptualizations were then used to examine the six issues described in Chapters 2 through 7. Here the key findings from each of these six studies are summarized and recommendations for future work are presented.

The specific aim of the work described in Chapter 2 was to assess whether simple one-compartment models of skin can reasonably represent the membrane characteristics of mammalian skin. This question was addressed by comparing four different one-compartment mathematical models of dermal absorption taken from the literature to a one-layer membrane model, all in combination with a one-compartment pharmacokinetic model representing the body. All of the compartment models were originally developed assuming that blood and vehicle concentrations were constant. Despite this, in many cases compartment models can reasonably represent membrane model results for time-variations in blood concentrations and in the percent of dose absorbed and eliminated. The largest deviations between compartment and membrane model calculations arose during short exposures relative to a chemical's lag time for diffusion through the stratum corneum (sc), $t_{lag,sc}$. As time increased, differences between the membrane model and all of the compartment models decreased. Compartment models provide acceptable results for exposure times that are long relative to $t_{lag,sc}$. Also, the four compartment models

predicted different results. Significantly, a model commonly described in the literature was not the most representative of the membrane model in any of the exposure scenarios studied, but typically predicted the correct long time (relative to $t_{lag,sc}$) rate of dermal absorption.

Compartment models have been used to estimate dermal absorption parameters from *in vivo* experimental data. Parameters that have been estimated in this way include the permeability coefficient, $P_{sc,v}$, partition coefficient, $K_{sc/v}$, and $t_{lag,sc}$. As shown in Chapter 2, parameters estimated using different compartment models will be different. The magnitude of the differences between the membrane model and the various compartment models has not yet been quantified. An important question left for future research is whether the reported differences between *in vivo* and *in vitro* experiments might be an artifact of the model used to analyze the *in vivo* data. One strategy for investigating this question would be to use the membrane model to simulate experimental data, which could then be analyzed using various compartment models to obtain values for the dermal absorption parameters. By comparing the model estimates with the known values used to simulate the data, estimation errors introduced by various models could be quantitatively assessed.

In Chapter 3, a one-layer membrane model was used to examine procedural aspects of the tape strip (TS) experiment. In the TS experiment, adhesive tape is used to sequentially remove layers of the sc after it has been exposed to a chemical. Because chemical in the sc continues to diffuse after an exposure ends, the concentration measured in each TS will be different than the concentration at that location in the sc when the chemical exposure ended. Stinchcomb (1999) provided human, *in vivo* data from TS's collected after an exposure for one-hour to aqueous solutions saturated with 4-cyanophenol (4CP). Concentrations in the TS's collected rapidly after a one-hour delay following the exposure and in TS's collected slowly over an hour were smaller than in TS's collected in less than 6 min directly after the exposure ended. Dermal absorption

parameters for 4CP were determined by comparing the TS data from the various procedures to the mathematical model. Specifically, $t_{lag,sc}$ was determined to be 26 to 40 min, $K_{sc/v}$ was 8.2 to 9.5 and $P_{sc,v}$ was 0.0019 to 0.0032 cm/hr. These results are consistent with values reported previously in the literature by Pirot *et al.* (1997) ($t_{lag,sc}$ = 32.5 min, $K_{sc/v}$ = 8.4, and $P_{sc,v}$ = 0.0037 cm/h). Using the mathematical model, we showed that if the time required to complete the tape strip procedure, t_{TS}, is less than 0.2 $t_{lag,sc}$, and the exposure time, t_{exp}, is greater than 0.3 $t_{lag,sc}$ then diffusion during the TS procedure will not significantly affect the TS data.

The experiment in Chapter 3 where skin was exposed until steady state was reached and then tape stripped rapidly after a period of clearance provided results that allowed for consistent parameter estimation. However, the experiment only works for chemicals with small enough values of $t_{lag,sc}$ to reach steady state within a few hours. An alternative experiment could also be done with an exposure time less than required to reach steady state to determine if consistent parameter estimation still results. A mathematical model for this case would need to be developed for data analysis.

Touraille (1998) used a TS technique to measure *in vivo* dermal absorption of 4CP on soil by humans exposed for 45 and 180 minutes on each forearm. Because Touraille determined transepidermal water loss (TEWL) after every fourth TS, the TS procedure took about 35 minutes to complete. Based on Chapter 3 results, this was long enough that diffusion during the TS procedure did affect the TS data. In Chapter 4, these TS data were analyzed using two different models. First, a one-layer membrane model that accounted for the additional resistance to mass transport provided by the soil vehicle was used to analyze the data and no constraints were placed upon the value of $t_{lag,sc}$. The resulting regressed values of $t_{lag,sc}$ (130, 430 and 280 min for subjects A, B and C, respectively) were much higher than values calculated in Chapter 3, but should have been similar. For the second method, the data were analyzed with a model that accounted for diffusion during the tape strip procedure. The value of $t_{lag,sc}$ was restricted to a reasonable

value (i.e., less than 45 min) and forced to be the same for all subjects. The resulting regressed value, $t_{lag,sc}$ = 35 min, was consistent with parameter estimation results from Chapter 3. The residuals were slightly larger for the second method than for the first (%30%), but the estimated parameters were consistent with other published values.

Further studies of *in vivo* human absorption from contaminated soils are needed, particularly in view of the data limitations of the study by Touraille (1998). In future TS experiments, either TEWL measurements should not be made or the TEWL measurements should follow the method proposed by Pirot *et al.* (1998), which requires one TEWL measurement directly after the skin is cleaned and a second after half the sc has been stripped.

Skin is continuously replaced through epidermal turnover, the process by which new cells are generated at the base of the epidermis (epi) while the outermost surface flakes off (i.e., desquamates) at the same rate. In Chapter 5, an unsteady two-layer membrane model of skin that included epi turnover and penetrant lipophilicity was used to quantitatively assess the extent that epi turnover could reduce percutaneous penetration. Model calculations showed that for most chemicals nearly all of the chemical in the skin at the end of an exposure will ultimately absorb into the body. Highly lipophilic or large molecular weight chemicals are the notable exceptions to this rule. When the sc is the primary barrier to dermal absorption, more than 80% of the chemical in the skin at the end of an exposure will be systemically absorbed if $t_{lag,sc}$ is less than 5% of the time for the sc to be completely replaced. For normal human skin, this corresponds to chemicals with an octanol – water partition coefficient, $K_{o/w}$, less than about 10,000 and a molecular weight was less than about 340.

Appropriate experimental evidence for the theoretical predictions presented in Chapter 5 do not currently exist. Experimental studies that could be compared with mathematical theory are needed. Excised skin is not continuously regenerated and consequently, studies of epidermal turnover must necessarily involve live animals. An

animal model such as the rat could be exposed to a series of radiolabeled chemicals with molecular weights less than about 200 selected to provide a range in lipophilic character (e.g., $\log K_{o/w}$ of about 2, 4 and 6). The shaved skin would be exposed to the chemical for a fixed period of time. After that the skin surface would be washed and then covered with a non-occlusive protective dressing that would trap desquamating sc. If the model chemicals have high solubility in the sc and the exposure time is short, the difference between the amount applied to the skin and recovered from the skin wash would reasonably approximate the amount of chemical in the skin at the end of the exposure. The dressing would be periodically removed and analyzed for chemical. Percutaneous penetration during and following the chemical exposure would be measured by liquid scintillation. When insignificant amounts of chemical are recovered from the cover, the animal could be humanely sacrificed and the carcass analyzed for chemical. By comparing the amount of chemical from the cover with the amount from the cage washes and carcass (i.e., the amount that was systemically absorbed), the effects of desquamation on percutaneous penetration could be examined.

Chapter 6 presented *in vivo* dermal absorption data of 18 pesticides measured in young, adult rats following the Zendzian protocol. These data were collected for exposure times up to 24 hours and for 3 or 4 different applied doses. For all 18 pesticides, systemic absorption increased during the entire exposure up to 24 hours, including the time after liquid components of the applied solution had evaporated. For most of the pesticides, the amount of chemical in the skin reached a maximum before 4 hours of exposure. The effect of applied dose was more complicated when the amount of pesticide on the skin surface decreased significantly during the exposure from either evaporation or dermal absorption. Consequently, we examined the effect of applied dose on data for 12 of the 18 pesticides, leaving out pesticides for which the amount on skin had decreased to less than 50% of the applied dose for all dose levels at 10 hours. This analysis showed a possible difference between solid and liquid pesticides. For pesticides

with melting points below skin temperature (i.e., liquids), both the amount of pesticide in the skin and the amount absorbed systemically increased proportionally with applied dose. For pesticides with melting points above skin temperature (i.e., solids), the amount in the skin increased almost proportionally to the applied dose, but the amount absorbed systemically was less than proportional to applied dose and sometimes was independent of applied dose.

The U.S. EPA has data for many more pesticide studies than examined here, and examination of these other studies should be emphasized in future research. A logical strategy is to divide the acceptable studies in the EPA database (i.e. complete studies with no apparent flaws) into two groups. One group would be used for formulating hypotheses, and the other would be used for testing hypotheses. Except for acetochlor, we were provided with no statistical information for the pesticides examined in Chapter 6. With no information on data variability, it is difficult to make judgments regarding similarities or differences between results. Future investigations of the pesticide data should include analysis of measurements from individual animals. Data from the individual animals should be analyzed to determine whether variance pooling could be justified in some cases. For example, in some cases, it might be appropriate to pool variances from different exposure times for the same applied dose. If so, this pooled variance would have a much greater statistical power and meaning than the standard deviations of measurements from only 4 animals (i.e., the number of samples upon which it is based is much larger).

Chapter 7 presented a steady-state, two-dimensional mathematical model representing skin as a two-layer membrane with uniformly spaced lines (or piles) of chemical with constant width and height on the skin surface. When the fraction of the exposed skin in contact with chemical is held constant, the amount of chemical in the epi at steady state (M_{epi}^{ss}) and the average flux through the epi at steady state (J^{ss}) were

larger from many small piles than from a few large piles. Both M_{epi}^{ss} and J^{ss} reached their maximum values when the skin was only partly covered by chemical if the piles of chemical were small enough. Significantly, and consistent with observations from the results for solid pesticides described in Chapter 6, systemic absorption as represented by J^{ss} can reach its maximum value at a smaller applied dose than is required to maximize the amount in the skin (i.e., M_{epi}^{ss}).

The calculations in Chapter 7, while interesting, are only a beginning. Future work should examine dermal absorption of two-dimensional piles on the skin surface. This will require a three-dimensional membrane model of the skin. Also, the effects of exposure time should be studied. This would include investigating the time required for dermal absorption to reach steady state when the skin is not completely covered. Finally, dermal absorption from two-dimensional piles that do not have a constant size could be examined with a two-dimensional model. This more complicated analysis allowing for the amount of chemical on the surface to change is needed to interpret experimental measurements of pesticides that evaporate or dermally absorb to a large extent.

Notation

epi	epidermis
J^{ss}	average flux of absorbing chemical through the epi at steady state
$K_{o/w}$	octanol – water partition coefficient
$K_{sc/v}$	partition coefficient of the absorbing chemical between the sc and the vehicle
L_{sc}	apparent thickness of the sc
M_{epi}^{ss}	mass of absorbing chemical in the epi at steady state
$P_{sc,v}$	permeability coefficient of the absorbing chemical through the sc from the vehicle
sc	stratum corneum
$t_{lag,sc}$	lag time for chemical penetrating through the sc
t_{TS}	the time required to complete the TS procedure

References

Pirot, F., E. Berardesca, Y. N. Kalia, M. Singh, H. I. Maibach and R. H. Guy (1998). "Stratum corneum thickness and apparent water diffusivity: facile and noninvasive quantitation *in vivo*." Pharmaceutical Research **15**:492-494.

Pirot, F., Y. N. Kalia, A. L. Stinchcomb, G. Keating, A. L. Bunge and R. H. Guy (1997). "Characterization of the permeability barrier of human skin *in vivo*." Proceedings of the National Academy of Sciences of the United States of America **94**:1562-1567.

Stinchcomb, A. L. (1999). Unpublished data, Personal communication.

Touraille, G. D. (1998). Unpublished data, Personal communication.